

CENTER FOR IMAGING SCIENCE  
ROCHESTER INSTITUTE OF TECHNOLOGY

ROCHESTER, NY

CERTIFICATE OF APPROVAL

---

M.S. DEGREE THESIS

---

The M.S. Degree Thesis of Erin P. Murphy  
has been examined and approved by two members of the  
Color Science faculty as satisfactory for the thesis  
requirement for the Master of Science degree

---

Dr. Roy S. Berns, Thesis Advisor

---

Dr. Mitchell R. Rosen

**A Testing Procedure to Characterize Color  
and Spatial Quality of Digital Cameras  
Used to Image Cultural Heritage**

Erin P. Murphy

B.S. Rochester Institute of Technology (2002)

A thesis submitted in partial fulfillment of the requirements  
for the degree of Master of Science in Color Science  
in the Center for Imaging Science,  
Rochester Institute of Technology

February 2005

---

Signature of the Author

---

Accepted by Dr. Roy S. Berns,  
Coordinator, M.S. Degree Program

## THESIS RELEASE PERMISSION FORM

ROCHESTER INSTITUTE OF TECHNOLOGY  
CENTER FOR IMAGING SCIENCE

***Title of Thesis***

A Testing Procedure to Characterize Color and Spatial Quality of Digital Cameras Used  
to Image Cultural Heritage

I, **Erin P. Murphy**, hereby grant permission to the Wallace Memorial Library of R.I.T.  
to reproduce my thesis in whole or part. Any reproduction will not be for commercial  
use or profit.

---

Signature of the Author

---

Date

# **A Testing Procedure to Characterize Color and Spatial Quality of Digital Cameras Used to Image Cultural Heritage**

Erin P. Murphy

A thesis submitted in partial fulfillment of the requirements  
For the degree of Master of Science in Color Science  
In the Center for Imaging Science,  
Rochester Institute of Technology

## ***Abstract***

*A testing procedure for characterizing both the color and spatial image quality of trichromatic digital cameras, which are used to photograph paintings in cultural heritage institutions, is described. This testing procedure is target-based, thus providing objective measures of quality. The majority of the testing procedure followed current standards from national and international organizations such as ANSI, ISO, and IEC. The procedure was developed in an academic research laboratory and used to benchmark four representative American museum's digital-camera systems and workflows. The quality parameters tested included system spatial uniformity, tone reproduction, color reproduction accuracy, noise, dynamic range, spatial cross-talk, spatial frequency response, color-channel registration, and depth of field. In addition, two paintings were imaged and processed through each museum's normal digital workflow. The results of the four case studies showed many dissimilarities among the digital-camera systems and workflows of American museums, which causes a significant range in the archival quality of their digital masters.*

## ***Acknowledgements***

I would like to thank the following people for their help with and support of my thesis:

Roy S. Berns, my thesis advisor, for his guidance and kindness,

Lawrence Taplin, for his help with numerous aspects of my thesis, especially with programming and performing three of the case studies,

Mitch Rosen, for sharing his knowledge and helping me with performing case study three,

Franziska Frey, for sharing her knowledge and painting the flower painting used in my thesis research,

Josi Etter, for painting the fish painting used in my thesis research,

Peter Burns, for volunteering his time and sharing his knowledge,

Bob Hashimoto, Katya Kallsen, Allen MacIntyre, Juan Trujillo, and John Wronn, the photographers at the museums, for volunteering many hours of their time and sharing their experiences,

Barbara Bridgers, Chris Gallagher, Andrew Gunther, and Erik Landsberg, the digital studio managers at the museums, for their generosity of allowing me the opportunity to apply my research and benchmark their equipment and procedures,

the Andrew W. Mellon Foundation for its financial support of my research,

the Munsell Color Science Laboratory faculty and staff, for the use of the laboratory and equipment and for teaching me a lot about color science and other interesting things,

Val Hemink, for her hospitality and superb organizational skills,

my fellow classmates, for our great office conversations,

my friends and family, for their support,

and Dan Smoyer, for his love and patience.

## ***Table of Contents***

Table of Contents.....	vi
List of Tables.....	viii
List of Figures.....	xi
List of Equations.....	xv
1. Introduction.....	1
2. Standards Review.....	8
2.1 ISO.....	16
2.2 IEC.....	51
2.3 ANSI.....	61
2.4 CIE.....	65
2.5 NISO.....	69
3. Testing Procedure and Targets.....	73
3.1 Case Study Zero: Camera Description and Set-up.....	74
3.2 System Spatial Uniformity.....	79
3.3 Tone Reproduction.....	84
3.4 Color Reproduction Accuracy.....	89
3.4.1 Spectral Sensitivity.....	90
3.4.2 Target-based Color Reproduction Accuracy.....	98
3.4.3 Metamerism.....	113
3.5 Noise.....	119
3.5.1 Image Noise.....	120
3.5.2 Color Noise.....	126
3.6 Dynamic Range.....	127
3.7 Spatial Cross-talk.....	130
3.8 Spatial Frequency Response (SFR).....	133
3.9 Color Channel Registration.....	138
3.10 Depth of Field.....	141
3.11 Case Study Zero Summary.....	144
4. Case Studies.....	146
4.1 Procedure Used to Analyze the Colorimetric Accuracy of Case Study Digital Imaging Workflows.....	146
4.2 Differences Between the CS0 Testing Procedure and the Museum Case Study Procedures.....	151
4.3 Case Study One.....	152
4.3.1 Case Study One: Digital Imaging System Description.....	152
4.3.2 Case Study One: Imaging Procedure.....	154
4.3.3 Case Study One: Results and Discussion.....	163
4.4 Case Study Two.....	182
4.4.1 Case Study Two: Digital Imaging System Description.....	182
4.4.2 Case Study Two: Imaging Procedure.....	184
4.4.3 Case Study Two: Results and Discussion.....	196
4.5 Case Study Three.....	216
4.5.1 Case Study Three: Digital Imaging System Description.....	216
4.5.2 Case Study Three: Imaging Procedure.....	218

4.5.3 Case Study Three: Results and Discussion.....	230
4.6 Case Study Four.....	250
4.6.1 Case Study Four: Digital Imaging System Description.....	251
4.6.2 Case Study Four: Imaging Procedure.....	253
4.6.3 Case Study Four: Results and Discussion.....	263
4.7 Case Study Comparison.....	281
4.7.1 Paintings Comparison.....	282
4.7.2 Characterization Comparison.....	287
5. Conclusions.....	306
6. References.....	307
7. Appendices.....	313
Appendix 7.1: System Spatial Uniformity Supplemental Data.....	313
Appendix 7.2: Tone Reproduction Supplemental Data.....	318
Appendix 7.3: Spatial Cross-talk Supplemental Data.....	321
Appendix 7.4: Depth of Field Supplemental Data.....	325

## *List of Tables*

Table I:	List of standards that are summarized in the standards review.....	12
Table II:	Digital image quality parameters discussed in each standard.....	14
Table III:	ANSI IT8.7/2 standard test target CIELAB hue, lightness and chroma.	62
Table IV:	CS0 taking illuminant characteristics.....	75
Table V:	CS0 $\mu$ -factor results.....	96
Table VI:	CS0 color reproduction accuracy results.....	111
Table VII:	CS0 D&H Color Rule metameristic matches.....	118
Table VIII:	CS0 image total, fixed pattern and temporal noise results.....	125
Table IX:	CS0 color noise results.....	127
Table X:	CS0 dynamic range results.....	129
Table XI:	CS0 summary of spatial cross-talk results.....	132
Table XII:	CS0 SFR area results.....	137
Table XIII:	CS0 color channel registration results.....	140
Table XIV:	Summarization of CS0 characterization results.....	145
Table XV:	CS1 taking illuminant characteristics.....	153
Table XVI:	CS1 paintings color difference results.....	164
Table XVII:	CS1 $\mu$ -factor results.....	169
Table XVIII:	CS1 color reproduction accuracy results.....	172
Table XIX:	CS1 color reproduction accuracy results compared to results found using a simplified color transformation.....	173
Table XX:	CS1 D&H Color Rule metameristic matches.....	174
Table XXI:	CS1 image total, fixed pattern and temporal noise results.....	175
Table XXII:	CS1 color noise results.....	176
Table XXIII:	CS1 dynamic range results.....	177
Table XXIV:	CS1 summary of spatial cross-talk results.....	178
Table XXV:	CS1 SFR area results.....	179
Table XXVI:	CS1 color channel registration results.....	180
Table XXVII:	CS2 taking illuminant characteristics.....	183
Table XXVIII:	CS2 viewing illuminant characteristics.....	192
Table XXIX:	CS2 paintings color difference results.....	198
Table XXX:	CS2 $\mu$ -factor results.....	202
Table XXXI:	CS2 color reproduction accuracy results.....	205
Table XXXII:	CS2 color reproduction accuracy results compared to results found using a simplified color transformation.....	206
Table XXXIII:	CS2 D&H Color Rule metameristic matches.....	207
Table XXXIV:	CS2 image total, fixed pattern and temporal noise results.....	208
Table XXXV:	CS2 color noise results.....	209
Table XXXVI:	CS2 dynamic range results.....	210
Table XXXVII:	CS2 summary of spatial cross-talk results.....	210
Table XXXVIII:	CS2 SFR area results.....	212
Table XXXIX:	CS2 color channel registration results.....	213
Table XL:	CS3 taking illuminant characteristics.....	217
Table XLI:	CS3 viewing illuminant characteristics.....	223
Table XLII:	CS3 paintings color difference results.....	231

Table XLIII:	CS3 $\mu$ -factor results.....	237
Table XLIV:	CS3 color reproduction accuracy results.....	240
Table XLV:	CS3 color reproduction accuracy results compared to results found using a simplified color transformation.....	241
Table XLVI:	CS3 D&H Color Rule metameric matches.....	242
Table XLVII:	CS3 image total, fixed pattern and temporal noise results.....	244
Table XLVIII:	CS3 color noise results.....	245
Table XLIX:	CS3 dynamic range results.....	246
Table L:	CS3 summary of spatial cross-talk results.....	246
Table LI:	CS3 SFR area results.....	248
Table LII:	CS3 color channel registration results.....	249
Table LIII:	CS4 taking illuminant characteristics.....	252
Table LIV:	CS4 paintings color difference results.....	265
Table LV:	CS4 $\mu$ -factor results.....	269
Table LVI:	CS4 color reproduction accuracy results.....	272
Table LVII:	CS4 color reproduction accuracy results compared to results found using a simplified color transformation.....	273
Table LVIII:	CS4 D&H Color Rule metameric matches.....	274
Table LIX:	CS4 image total, fixed pattern and temporal noise results.....	275
Table LX:	CS4 color noise results.....	276
Table LXI:	CS4 dynamic range results.....	277
Table LXII:	CS4 summary of spatial cross-talk results.....	277
Table LXIII:	CS4 SFR area results.....	279
Table LXIV:	CS4 color channel registration results.....	279
Table LXV:	CS1 – CS4 comparison of paintings color difference results.....	284
Table LXVI:	CS2 – CS4 monitor calibration accuracy.....	285
Table LXVII:	CS2 – CS4 parameters of viewing illumination and monitor.....	286
Table LXVIII:	CS1 – CS4 summary of characterization mono-numeric metrics.....	288
Table LXIX:	CS1 – CS4 factors that influenced the depth of field results.....	305
Table 7-I:	CS1 system spatial uniformity supplemental data.....	314
Table 7-II:	CS2 system spatial uniformity supplemental data.....	315
Table 7-III:	CS3 system spatial uniformity supplemental data.....	316
Table 7-IV:	CS4 system spatial uniformity supplemental data.....	317
Table 7-V:	CS0 tone reproduction supplemental data.....	318
Table 7-VI:	CS1 tone reproduction supplemental data.....	319
Table 7-VII:	CS2 tone reproduction supplemental data.....	319
Table 7-VIII:	CS3 tone reproduction supplemental data.....	320
Table 7-IX:	CS4 tone reproduction supplemental data.....	320
Table 7-X:	CS0 spatial cross-talk supplemental data.....	322
Table 7-XI:	CS1 spatial cross-talk supplemental data.....	322
Table 7-XII:	CS2 spatial cross-talk supplemental data.....	323
Table 7-XIII:	CS3 spatial cross-talk supplemental data.....	323
Table 7-XIV:	CS4 spatial cross-talk supplemental data.....	324
Table 7-XV:	CS0 depth of field areas under the SFR curves supplemental data...326	
Table 7-XVI:	CS1 depth of field areas under the SFR curves supplemental data...327	
Table 7-XVII:	CS2 depth of field areas under the SFR curves supplemental data...328	

Table 7-XVIII: CS3 depth of field areas under the SFR curves supplemental data...329

Table 7-XIX: CS4 depth of field areas under the SFR curves supplemental data...330

## ***List of Figures***

Figure 1:	Flowchart of how a standard evolves in the ISO.....	9
Figure 2:	ISO Resolution Chart.....	26
Figure 3:	ISO display resolution, uniformity, convergence and geometric accuracy test targets.....	31
Figure 4:	ISO Camera OECF Test Chart.....	37
Figure 5:	ISO Camera Noise Test Chart.....	40
Figure 6:	IEC 61966-8 color and grayscale and spatial cross-talk targets.....	54
Figure 7:	IEC 61966-9 equipment arrangement and test charts.....	57
Figure 8:	IT8.7/2 color reflection input calibration target.....	63
Figure 9:	CS0 relative spectral power distribution of the taking illumination.....	75
Figure 10:	Schematic of CS0 imaging set-up.....	76
Figure 11:	Schematic of CS0 set-up for the depth of field target imaging.....	77
Figure 12:	Schematic of CS0 set-up for the monochromator instrument imaging.....	77
Figure 13:	System spatial uniformity and flat-fielding gray card target.....	79
Figure 14:	CS0 system spatial uniformity surface plot.....	82
Figure 15:	Flowchart of the system spatial uniformity analysis.....	84
Figure 16:	ISO OECF Chart target used to evaluate tone reproduction.....	85
Figure 17:	CS0 OECF curves.....	88
Figure 18:	Flowchart of the tone reproduction analysis.....	89
Figure 19:	Monochromator instrument used to evaluate spectral sensitivity.....	90
Figure 20:	Schematic of how a monochromator works and a its resulting image.....	91
Figure 21:	CS0 $\lambda$ vs. RGB linearized DC from monochromator images and $\lambda$ vs. the sum of the measured spectral radiances.....	93
Figure 22:	CS0 relative spectral sensitivities and rotated to fit the CIE 2° observer.....	94
Figure 23:	Relationship between $\mu$ -factor and average $\Delta E^*$ <sub>94</sub> color difference.....	97
Figure 24:	Flowchart of the spectral sensitivity analysis.....	98
Figure 25:	Cobalt Blue Pigments, Esser, Macbeth ColorChecker, D&H Color Rule, and Pigment charts.....	100
Figure 26:	Macbeth ColorChecker DC, Kodak Color Separation & Grayscale, and IT8 charts.....	101
Figure 27:	BCRA target.....	102
Figure 28:	Flowchart of the target-based color reproduction accuracy first evaluation method.....	105
Figure 29:	Flowchart of the target-based color reproduction accuracy second evaluation method.....	108
Figure 30:	CS0 CIELAB a* vs. b* and C* <sub>ab</sub> vs. L* error vector plots.....	109
Figure 31:	CS0 histogram of $\Delta E_{00}$ error distributions of the Macbeth CC.....	110
Figure 32:	Image of Davidson & Hemmendinger (D&H) Color Rule.....	114
Figure 33:	Percent reflectance of the Davidson & Hemmendinger Color Rule.....	114
Figure 34:	Flowchart of the camera metameric match determination procedure.....	116
Figure 35:	CS0 D&H Color Rule camera metameric match.....	117
Figure 36:	CS0 % reflectance curves of CIE 2° observer D&H Color Rule metameric match.....	118
Figure 37:	Image noise and dynamic range ISO Noise Chart target.....	121

Figure 38:	IEC Large Area Spatial Cross-talk Chart.....	131
Figure 39:	ISO Resolution Chart target used to evaluate spatial frequency response (SFR) and color channel registration.....	134
Figure 40:	Flowchart of the ISO 12233 spatial frequency response evaluation.....	135
Figure 41:	CS0 SFR of four knife edges.....	136
Figure 42:	Flowchart of the color channel misregistration error evaluation.....	139
Figure 43:	Depth of field target.....	141
Figure 44:	CS0 depth of field distance vs. area under SFR plot.....	143
Figure 45:	Flower and fish paintings used to analyze CS workflows.....	148
Figure 46:	Percent reflectance of 11 Gamblin Artist's Oil Colors.....	149
Figure 47:	CS1 relative spectral power distribution of the taking illumination.....	154
Figure 48:	Schematic and image of CS1 imaging set-up.....	155
Figure 49:	CS1 native resolution and cropped painting image area.....	156
Figure 50:	Flowchart of CS1 digital imaging workflow.....	157
Figure 51:	Screen shot of the tone curve applied by the CS1 capture software.....	158
Figure 52:	Placement of the SFR target in the CS1 cropped image area.....	160
Figure 53:	CS1 set-up for the depth of field target imaging.....	161
Figure 54:	CS1 set-up for the monochromator instrument imaging.....	162
Figure 55:	CS1 CIELAB a* vs. b* and C* <sub>ab</sub> vs. L* error vector plots of the fish painting.....	164
Figure 56:	CS1 system spatial uniformity surface plot.....	165
Figure 57:	CS1 OECF curves.....	166
Figure 58:	CS1 relative spectral sensitivities and rotated to fit CIE 2° observer.....	168
Figure 59:	CS1 CIELAB a* vs. b* and C* <sub>ab</sub> vs. L* error vector plots.....	170
Figure 60:	CS1 histogram of ΔE <sub>00</sub> error distributions of the Macbeth CC.....	171
Figure 61:	CS1 SFR of four knife edges.....	179
Figure 62:	CS1 depth of field distance vs. area under SFR plot.....	181
Figure 63:	CS2 relative spectral power distribution of the taking illumination.....	184
Figure 64:	CS2 set-up for the monochromator instrument imaging.....	185
Figure 65:	Schematic and image of CS2 imaging set-up.....	187
Figure 66:	Flowchart of CS2 digital imaging workflow.....	189
Figure 67:	Screen shot of the tone curve applied by the CS2 capture software.....	190
Figure 68:	Image of CS2 photographer making visual corrections to an image.....	191
Figure 69:	CS2 relative spectral power distribution of the viewing illumination....	192
Figure 70:	Placement of the SFR target in the CS2 uncropped image area.....	194
Figure 71:	CS2 set-up for the depth of field target imaging.....	195
Figure 72:	CS2 CIELAB a* vs. b* and C* <sub>ab</sub> vs. L* error vector plots of the fish painting.....	197
Figure 73:	CS2 system spatial uniformity surface plot.....	199
Figure 74:	CS2 OECF curves.....	200
Figure 75:	CS2 relative spectral sensitivities and rotated to fit CIE 2° observer....	201
Figure 76:	CS2 CIELAB a* vs. b* and C* <sub>ab</sub> vs. L* error vector plots.....	203
Figure 77:	CS2 histogram of ΔE <sub>00</sub> error distributions of the Macbeth CC.....	204
Figure 78:	CS2 SFR of four knife edges.....	212
Figure 79:	CS2 depth of field distance vs. area under SFR plot.....	214

Figure 80:	CS3 relative spectral power distribution of the taking illumination.....	217
Figure 81:	Schematic of CS3 imaging set-up.....	219
Figure 82:	Flowchart of CS3 digital imaging workflow.....	221
Figure 83:	Image of CS3 viewing illumination.....	223
Figure 84:	CS3 relative spectral power distribution of the viewing illumination....	224
Figure 85:	Placement of the SFR target in the CS3 uncropped image area.....	225
Figure 86:	CS3 set-up for the depth of field target imaging.....	227
Figure 87:	CS3 set-up for the monochromator instrument imaging.....	228
Figure 88:	CS3 CIELAB a* vs. b* and C* <sub>ab</sub> vs. L* error vector plots of the fish painting.....	231
Figure 89:	CS3 system spatial uniformity surface plot.....	233
Figure 90:	CS3 OECF curves.....	235
Figure 91:	CS3 relative spectral sensitivities and rotated to fit CIE 2° observer.....	236
Figure 92:	CS3 CIELAB a* vs. b* and C* <sub>ab</sub> vs. L* error vector plots.....	238
Figure 93:	CS3 histogram of ΔE <sub>00</sub> error distributions of the Macbeth CC.....	239
Figure 94:	CS3 SFR of four knife edges.....	247
Figure 95:	CS3 depth of field distance vs. area under SFR plot.....	250
Figure 96:	CS4 relative spectral power distribution of the taking illumination.....	252
Figure 97:	Schematic and image of CS3 imaging set-up.....	254
Figure 98:	CS4 native resolution and cropped painting image area.....	255
Figure 99:	Screen shot of the tone curve applied by the CS4 capture software.....	256
Figure 100:	Flowchart of CS4 digital imaging workflow.....	257
Figure 101:	Image of CS4 photographer making visual corrections to an image.....	258
Figure 102:	Placement of the SFR target in the CS4 cropped image area.....	260
Figure 103:	CS4 set-up for the monochromator instrument imaging.....	262
Figure 104:	CS4 CIELAB a* vs. b* and C* <sub>ab</sub> vs. L* error vector plots of the fish painting.....	264
Figure 105:	CS4 system spatial uniformity surface plot.....	267
Figure 106:	CS4 OECF curves.....	268
Figure 107:	CS4 relative spectral sensitivities and rotated to fit CIE 2° observer.....	269
Figure 108:	CS4 CIELAB a* vs. b* and C* <sub>ab</sub> vs. L* error vector plots.....	270
Figure 109:	CS4 histogram of ΔE <sub>00</sub> error distributions of the Macbeth CC.....	271
Figure 110:	CS4 SFR of four knife edges.....	278
Figure 111:	CS4 depth of field distance vs. area under SFR plot.....	280
Figure 112:	CS1 – CS4 comparison of digital master painting Lab images.....	282
Figure 113:	CS1 – CS4 comparison of visually corrected painting Lab images.....	283
Figure 114:	CS1 – CS4 comparison of system spatial uniformity surface plots.....	289
Figure 115:	CS1 – CS4 color reproduction accuracy targets' mean ΔE <sub>00</sub> .....	292
Figure 116:	CS1 – CS4 color reproduction accuracy targets' 90 <sup>th</sup> percentile ΔE <sub>00</sub> ....	292
Figure 117:	CS1 – CS4 comparison of digital master Macbeth ColorChecker images to the spectrophotometrically measured data.....	294
Figure 118:	CS1 – CS4 mean ΔE <sub>00</sub> color reproduction accuracy results compared to results found using a simplified color transformation of the Macbeth ColorChecker.....	295
Figure 119:	CS1 – CS4 90 <sup>th</sup> percentile ΔE <sub>00</sub> color reproduction accuracy results	

compared to results found using a simplified color transformation of the Macbeth ColorChecker.....	296
<b>Figure 120:</b> CS1 – CS4 D & H Color Rule metameric matches made by photographer and camera.....	297
<b>Figure 121:</b> CS1 – CS4 depth of field distance vs. area under SFR plots.....	304
<b>Figure 7-1:</b> Spatial cross-talk target with gray squares labeled.....	321
<b>Figure 7-2:</b> CS0 depth of field SFR plots of horizontal edges.....	326
<b>Figure 7-3:</b> CS1 depth of field SFR plots of vertical edges.....	327
<b>Figure 7-4:</b> CS2 depth of field SFR plots of horizontal edges.....	328
<b>Figure 7-5:</b> CS3 depth of field SFR plots of horizontal edges.....	329
<b>Figure 7-6:</b> CS4 depth of field SFR plots of horizontal edges.....	330

## *List of Equations*

Equation 1:	sRGB to CIE 1931 XYZ tristimulus values linear transformation matrix.	52
Equation 2:	CIE 1931 XYZ tristimulus values to sRGB linear transformation matrix.	52
Equation 3:	X tristimulus value calculation from CIELAB units.....	80
Equation 4:	Y tristimulus value calculation from CIELAB units.....	81
Equation 5:	Z tristimulus value calculation from CIELAB units.....	81
Equation 6:	X tristimulus value calculation.....	81
Equation 7:	Y tristimulus value calculation.....	81
Equation 8:	Z tristimulus value calculation.....	81
Equation 9:	Normalizing constant used in XYZ tristimulus value calculations.....	81
Equation 10:	% difference calculation used in system spatial uniformity analysis.....	82
Equation 11:	CIELAB L* equation.....	83
Equation 12:	CIELAB a* equation.....	83
Equation 13:	CIELAB b* equation.....	83
Equation 14:	CIELAB C* <sub>ab</sub> equation.....	83
Equation 15:	ΔE* <sub>ab</sub> equation.....	83
Equation 16:	Luminance correction factor equation.....	86
Equation 17:	Gamma equation.....	87
Equation 18:	Color-matching function estimation calculation.....	94
Equation 19:	Pseudoinverse equation.....	94
Equation 20:	μ-factor equation.....	95
Equation 21:	S used in μ-factor equation.....	95
Equation 22:	A used in μ-factor equation.....	95
Equation 23:	Flat-field calculation.....	106
Equation 24:	3x3 transformation used to convert from RGB to XYZ.....	106
Equation 25:	XYZ tristimulus value estimation when converting from RGB.....	106
Equation 26:	XYZ tristimulus value flat-field calculation.....	116
Equation 27:	Incremental gain equation.....	122
Equation 28:	Average total noise equation.....	122
Equation 29:	Total noise signal-to-noise ratio.....	123
Equation 30:	Average fixed pattern noise.....	123
Equation 31:	Variance used in average fixed pattern noise calculation.....	123
Equation 32:	Average temporal noise.....	124
Equation 33:	Black incremental gain.....	128
Equation 34:	ISO digital still camera dynamic range as a luminance ratio equation...	128
Equation 35:	Theoretical dynamic range calculation.....	129
Equation 36:	Percent relative differences calculation of spatial cross-talk.....	132
Equation 37:	Percent relative standard deviation calculation of spatial cross-talk.....	132
Equation 38:	Linear equation used to determine an edge location for a color channel.	140
Equation 39:	Relative luminance calculation.....	167

## ***1. Introduction***

For decades, museums, libraries, and other cultural-heritage institutions have been using analog photography as a means for documenting their collections and producing reproductions of their artifacts. Through the years, these institutions developed “best practices” for the process of documentation and reproduction, which included photographing the object, storing the image, and cataloging, so that a high quality image archive could be obtained and maintained for many years.

Now that digital photography is well established and comparable to analog photography both in price and image quality, these cultural-heritage institutions have a choice of whether to continue imaging the traditional way or start imaging using digital technology. Those institutions who have chosen to continue documenting using traditional methods either do not have the funds to move into the digital realm or admit that they do not have the knowledge and argue that there has not yet been a standardized method or “best practices” developed for digital-image capture and digital preservation of the files produced. This thesis will attempt to aid the community in addressing the latter concern, with a focus on the direct-digital-capture component of the documentation and reproduction of paintings. The cultural-heritage institutions that have chosen to begin using digital capture realize that imaging their collections digitally satisfies their two main objectives: to document and to present cultural-heritage materials. By digitizing their artifacts, museums can show more of their collections to more people all over the world and can simultaneously build an archive of digital files with an estimated lifespan of about 50 years (Waibel, 2000). The photographers at these museums prefer digital capture to analog photography because they can instantly see whether the image is

acceptable and do not have to wait for the film to be processed. The following is a quote by a scholar-teacher who depends greatly on information from libraries, archives, and museums in his everyday life.

“I have no doubt that the digital revolution is one of the great information revolutions in the history of humankind, fully comparable to the invention of printing and the invention of photography, but taking place at dramatic speed. We are privileged to be alive with the opportunity to witness this transformation, to experience it, and even to participate in its development. Indeed, only if all elements of society do participate in its development will it fulfill its immense potential. In deciding what materials to digitize, how to preserve them, and how to make them available, let us recognize the serious interest of the public in all areas of human knowledge, the public’s right to know, and the great untapped resource that these materials provide. The digital revolution offers us our first opportunity for a fully participatory society” (Rhyne, 2000).

Using digital technology in the cultural-heritage environment requires a shared vocabulary and standardized evaluation of system performance and digital output (Kenney, 2000). A research project, of which this thesis is a part, entitled “Direct Digital Image Capture of Cultural Heritage – Benchmarking American Museum Practices and Defining Future Needs,” surveyed American museums about their involvement with digital photography and performed six American museum on-site case study interviews to document their current digital-imaging workflows (Rosen, 2005).

The purpose of this thesis is to provide a testing procedure, including test targets, or test charts, for characterizing trichromatic digital cameras used to digitally capture cultural-heritage collections, and in particular, paintings. A number of procedures for testing the quality of digital cameras have been established in the recent past (see the Standards Review in Part 2). Unfortunately, there has been no unifying attempt to collect

them into a cohesive package for the purposes of comprehensive evaluation of studio imaging environments, particularly those used in museums for the direct digital capture of artwork. The ultimate goals of this thesis are twofold. First, as mentioned above, this research will be beneficial to the cultural-heritage community because it might provide a possible guideline for high-quality-digital imaging in a museum setting and second, it will benchmark camera systems and procedures currently used for digital imaging by the cultural-heritage community. The benchmarking of camera systems is performed by relating the quality of the digital reproduction to the physical characteristics of the original. Although the saying, “You get what you pay for” typically applies in the acquisition of imaging systems, there is no substitute for the careful and thorough testing and benchmarking of digital-imaging systems (Conway, 2000). Benchmarking systems will help to compare different camera systems, giving better information than the manufacturers provide, and should lead to a better understanding of the whole imaging process (Kenney, 2000).

The aims of the testing procedure are to follow current digital-photography standards to the greatest extent possible, provide only objective measures of image quality, and be as automated as possible with the use of analysis software. Frey and Reilly recognized that “all of the chosen image quality parameters should be tied to well-documented standards to make it possible to take images safely into the future” (Frey, 2000) and that “for objective image quality measurements, software should be available which is designed to locate and evaluate specific targets and then report numbers or graphs describing key image quality parameters” (Frey, 1999) along with their tolerance

limits (D'Amato, 2000). Simplification of the characterization process makes it more practical for future use by photographers in the museum environment.

Production projects that capture high-quality images using a digital camera are still rare (Besser, 1996). Vogt-O'Connor advises that "if you can't capture the image accurately, don't digitize the materials" (Vogt-O'Connor, 2000). The main objective of the camera characterization testing procedure contained in this thesis is to determine whether the digital equipment can produce images that meet the needs for image quality. It is important that the digital image is a "replacement" of the original. Therefore, the digital data have to be captured and archived, along with technical metadata, in such a manner that the original can be reconstructed (Frey, 1996). Since digitization is both labor intensive and expensive, it is important to capture an image in a way and at a quality level that makes it possible to use it to serve several needs (IFLA/ICA Working Group, 2002). The digitally captured image with the highest quality (with minimal to no adjustments) that is archived is termed the "digital master." Images possibly of lower quality, which can be derived (through image processing, compression, etc.) from the digital master for future use in applications such as the Internet or publication, are termed "derivatives." The richness of the digital master affects the quality and processibility of subsequent files derived from it, determining whether derivatives can be used for enhanced access (Price-Wilkin, 2000). In order to prevent excessive handling of and light exposure to an original, which impacts its lifetime, the digital master needs to be optimized during the capture process. The availability of accurate digital surrogates cuts down on the handling of original objects by both staff and researchers; digital images answer most needs (Waibel, 2000).

The testing procedure and accompanying test targets described in this thesis, if used correctly, can quickly inform the photographer of the maximum level of objective image quality achievable by his imaging system before he even takes his first digital photograph of a piece of artwork. The outcome of this procedure is an extensive quantitative description of the digital-image-quality parameters, which characterize a camera used for the direct-digital capture of cultural heritage. Currently, a digital image's quality is often theoretically based on its pixels per inch and bits per pixel. There is a lack of usage of quantitative metrics to define image quality. Spatial frequency response, spectral sensitivity and relating the digital data back to physical features of the art are examples of phrases that are seldom heard in the cultural-heritage community, but will be mentioned here.

The digital-image-quality parameters and metrics, which will be encompassed in the testing procedure and test targets, are as follows. Tone reproduction is the most important aspect of image quality. If the tone reproduction of an image is correct, users will generally accept it, even if the other attributes are not ideal (Frey, 2000). Tone reproduction is affected by three mutually dependent attributes: the opto-electronic conversion function (OECF), dynamic range, and spatial cross-talk. Resolution, or image detail, is another image quality parameter best described by a metric, the spatial frequency response (SFR). Other image-quality parameters include system spatial uniformity, color reproduction, depth of field/texture-reproduction, and artifacts such as misregistration of the color channels, and noise. There are many metrics that, in combination, can be used to specify a desired level of image quality (D'Amato, 2000). Physical features of the original object can be characterized numerically and matched up

with digital equivalencies (Kenney, 2000). Thus, if the original objects to be digitized are first characterized through measurements of their reflectances, colors, and levels of detail, it is then possible to select image-quality test targets and testing procedures to ensure that these characteristics are faithfully captured in the images (D'Amato, 2000).

Targets, or charts, are vital parts of the image-quality framework in order for one to be able to make objective measurements. Targets can be incorporated into the workflow in various ways. Full versions of the targets might be digitally captured every few hundred images and then linked to specific batches of production files, or smaller versions of the targets might be included with every image (Frey, 1999). In this thesis, several test targets, each consisting of a combination of various elements, will be used, which will require several digital photographs to be taken within the testing procedure. Properly designed targets can be imaged and analyzed to predict image quality, and help ensure that the camera system produces the best quality image it can and operates at a consistent level of quality over time (Rhodes, 1999). If test patterns are periodically interspersed in the imaging workflow and substandard image quality is detected, all images generated after the last above-standard test pattern must be considered substandard (D'Amato, 2000).

The testing procedure and test targets in this thesis were developed through research that consisted of both a literature review and experimentation in the Munsell Color Science Laboratory. The results were reviewed by representatives of camera manufacturers, standards committees, and museums, who, in their joint expertise agreed that this was a reasonable first step toward the standardization of practices for digital archiving of direct digital capture. Four American museum case studies were carried out

to analyze how the testing procedure and test targets performed in the environment where their use is intended. In these case studies, the test targets were imaged using both the testing procedure described here and each museum's usual digital imaging workflow. As a part of the "Direct Digital Image Capture of Cultural Heritage – Benchmarking American Museum Practices and Defining Future Needs" project, the results of this research thesis were disseminated through a conference and will be available on-line (see <http://www.art-si.org>).

## ***2. Standards Review***

There are many standards provided by both national and international standards bodies for businesses, the government and society in order to allow for agreement on specifications, criteria and terminology. The major roles played by standards are that they raise levels of quality, safety, reliability, efficiency and interchangeability, as well as provide these benefits at an economical cost. Only a few of these standards bodies provide standards that apply directly to this research thesis topic. The standards that will be described here are provided by the ISO (International Organization for Standardization), IEC (International Electrotechnical Commission), ANSI (American National Standards Institute), CIE (International Commission on Illumination) and NISO (National Information Standards Organization), each of which is related to each other in some way.

McDowell describes standards and specifications that apply to digital imaging as “nothing more than written agreements that describe how something should be done or the agreed upon characteristics of, or interfaces between, devices or software” (McDowell, 2002). The standards developed by the five standards bodies listed above are used in this research thesis because they are developed by a consensus. Participation in the decision making process to develop these standards is completely open, which means that the expertise that goes into the development of these standards is widespread (McDowell, 2002).<sup>1</sup>

As an example, the following is a brief summary of who develops standards and how they are developed in the ISO. There are similarities in most other standards bodies.

---

<sup>1</sup> Some other specifications, which also apply to this research and will be mentioned later in this thesis, are developed solely within an industry trade group, such as the ICC (International Color Consortium), or within a single company or group of companies as “de facto” or private specifications, such as TIFF (Tag Image File Format).

The ISO has a Technical Committee, or TC, for each different area of research, which is ultimately responsible for developing the standards. A Sub-Committee (SC), a subgroup within a TC, a Working Group (WG), a subgroup within a SC or TC, or a Task Force (TF), a subgroup within a WG or SC, is formed to be directly involved in the creation process of a standard. Sometimes a Joint Working Group (JWG), which involves participants from multiple TCs, is needed for developing standards that overlap two or more areas of research. Figure 1 is a flowchart showing how a standard evolves from a New Work Item proposal into a Final Draft International Standard (FDIS).

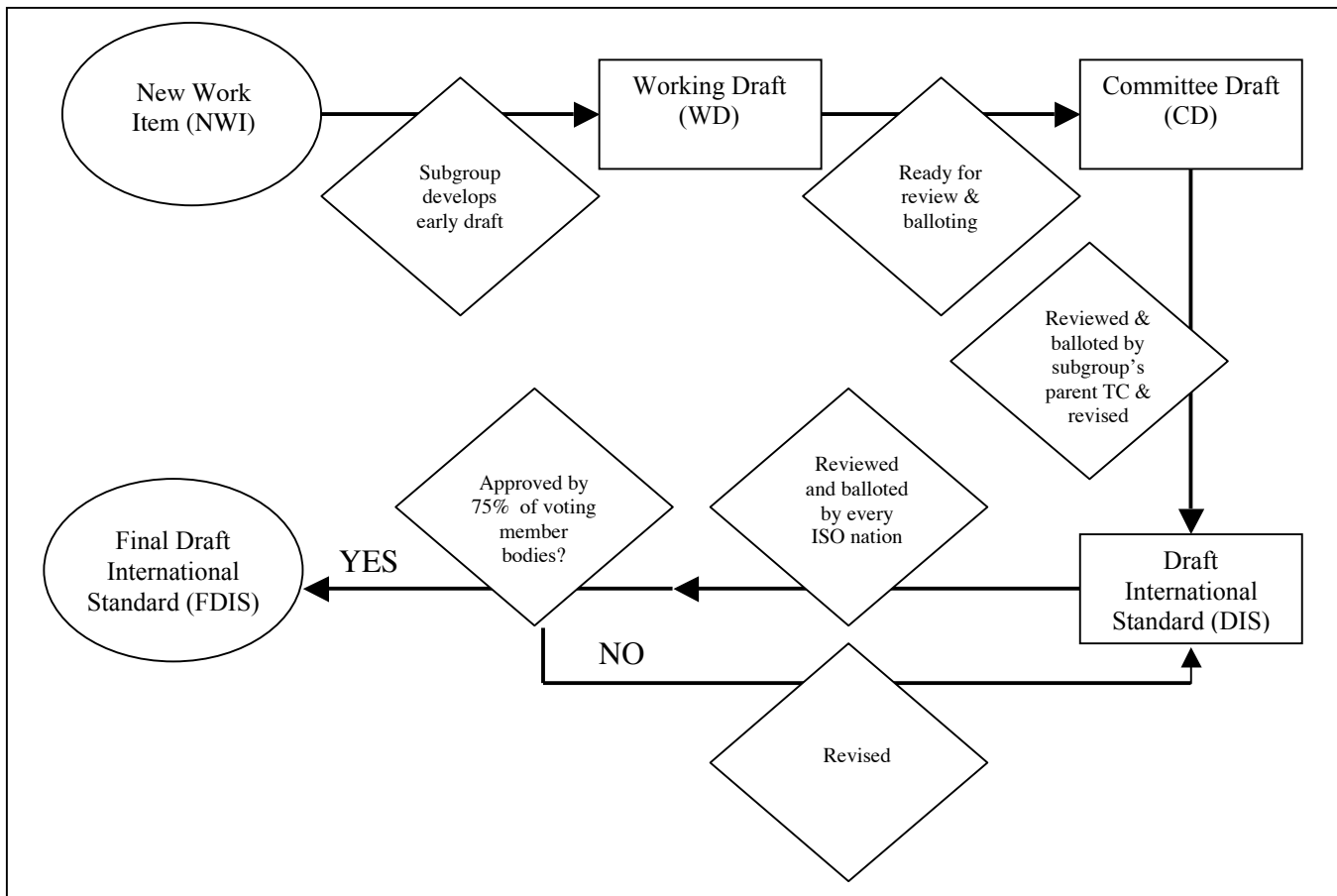


Figure 1. Flowchart of how a standard evolves in the ISO (McDowell, 2002).

Once a standard is published, it must be reviewed on a periodic basis to be sure that it is still applicable, but a revision can be produced at any time by the committee responsible for the standard (McDowell, 2002).

One clarification that should be noted about the standards language is that the words "shall" and "should", which are contained in some of the standards described below, have specific meanings. "Shall" means that you must do something in order to comply with the standard. "Should" means that it is really preferable to do something and you should try very hard to do it (Harold, 1999).

The purpose of this standards review is to summarize<sup>2</sup> the most current standards, which relate the closest to this thesis topic. Not all of the standards described below were in their published FDIS form at the time in which this thesis was written. Even though some of the standards were in their intermediate form, they were still useful tools needed for the development of the testing procedure for characterizing trichromatic digital cameras used to digitally archive cultural heritage collections. The form that each standard was in at the time that this was written is listed in Table I. The standards that are described below, which were developed by the ISO, IEC and ANSI standards bodies pertain to the areas of photography, which includes the use of both digital still cameras and scanners, and graphic technology. The CIE publications<sup>3</sup> pertain to light sources and colorimetry, and the NISO standard pertains to the technical metadata of digital still images. The descriptions of the standards below will focus on information contained in the standards, which applies directly to this research thesis. Because the information in this standards review is in the form of a summation, anyone wishing to use these

---

<sup>2</sup> Most of the wording used in the summaries is taken directly from the standards themselves so that the meaning of the standard is not lost.

<sup>3</sup> Most CIE documents are technical publications or recommended practices. Only those labeled ISO/CIE are standards.

standards should refer to the standard itself for detailed information. Table I lists the standards in the order that they will be reviewed here. Table II can be used as a reference for the digital image quality parameters discussed in each standard. A brief explanation about each standards body and a summary of each standard listed in Tables I and II will be given next.

Table I. List of standards that are summarized in this standards review.

<u>Title</u>	<u>No.</u>	<u>Date</u>	<u>Organization</u>	<u>Form (in ISO terms)</u>	<u>Edition</u>	<u>TCs</u>	<u>Page #</u>
Viewing conditions - Graphic technology and photography	3664	02/01/2002	ISO	FDIS	2nd	ISO/TC 42 (Photography), ISO/TC 130 (Graphic Technology)	16
Photography - Illuminants for sensitometry - Specifications for daylight, incandescent tungsten and printer	7589	09/01/2000	ISO	FDIS	2nd	ISO/TC 42 (Photography)	18
Photography -- Electronic still-picture cameras -- Terminology	12231	06/15/1997	ISO	FDIS	1st	ISO/TC 42 (Photography)	21
Photography -- Electronic still-picture cameras -- Determination of ISO speed	12232	08/01/1998	ISO	FDIS	1st	ISO/TC 42 (Photography)	21
Photography -- Electronic still-picture cameras -- Resolution measurements	12233	09/01/2000	ISO	FDIS	1st	ISO/TC 42 (Photography)	25
Graphic Technology - Displays for color proofing - Characteristics and viewing conditions	12646	05/30/2002	ISO	DIS	N/A	ISO/TC 130 (Graphic Technology)	30
Photography -- Electronic still-picture cameras -- Methods for measuring opto-electronic conversion functions (OECFs)	14524	12/15/1999	ISO	FDIS	1st	ISO/TC 42 (Photography)	34
Photography -- Electronic still-picture imaging -- Noise measurements	15739	05/01/2003	ISO	FDIS	1st	ISO/TC 42 (Photography)	38
Graphic technology and photography — Colour characterisation of digital still cameras (DSCs) — Part 1: Stimuli, metrology, and test procedures	17321-1	09/17/2003	ISO	WD	N/A	ISO/TC 42 (Photography), ISO/TC 130 (Graphic Technology)	41
Graphic technology and photography - Colour characterization of digital still cameras (DSCs) - Part 2: Methods for determining transforms from raw DSC to scene-referred data	17321-2	10/10/2003	ISO	WD	N/A	ISO/TC 42 (Photography), ISO/TC 130 (Graphic Technology)	45
Photography and Graphic Technology - Extended color encodings for digital image storage, manipulation and interchange - Part 1: Architecture and requirements	22028-1	08/30/2002	ISO	DIS	N/A	ISO/TC 42 (Photography), ISO/TC 130 (Graphic Technology)	48

<u>Title</u>	<u>No.</u>	<u>Date</u>	<u>Organization</u>	<u>Form (in ISO terms)</u>	<u>Edition</u>	<u>TCs</u>	<u>Page #</u>
Multimedia systems and equipment - Colour measurement and management - Part 2-1: Colour management - Default RGB colour space - sRGB	61966-2-1	10/1999 + 01/2003	IEC	FDIS	1st + Amd 1	IEC/TC 100 (Audio,video and multimedia systems and equipment)	51
Multimedia systems and equipment - Colour measurement and management - Part 8: Multimedia colour scanners	61966-8	02/2001	IEC	FDIS	1st	IEC/TC 100 (Audio,video and multimedia systems and equipment)	53
Multimedia systems and equipment - Colour measurement and management - Part 9: Digital cameras	61966-9	06/2000	IEC	FDIS	1st	IEC/TC 100 (Audio,video and multimedia systems and equipment)	57
Graphic Technology - Color reflection target for input scanner calibration	IT8.7/2	06/21/1993	ANSI	FDIS	1st	IT8 Subcommittee 4	61
Colorimetry	15.2	1986	CIE	N/A	2nd	CIE/TC 1.3 (Colorimetry)	64
A method for assessing the quality of daylight simulators for colorimetry	51	1981	CIE	N/A	1st	CIE/TC 1.3 (Colorimetry)	66
Data Dictionary - Technical Metadata for Digital Still Images	N/A	06/01/2002	NISO	DIS	N/A	N/A	68

Table II. A reference for the digital image quality parameters discussed in each standard.

Title	No.	Organization	Page #	Digital Image Quality Parameter							
				Spatial Uniformity	Tone Reproduction	Color Reproduction Accuracy	Noise	Dynamic Range	Spatial Cross-talk	Resolution	Non-Image Quality
Viewing conditions -- Graphic technology and photography	3664	ISO	16								X
Photography - Illuminants for sensitometry - Specifications for daylight, incandescent tungsten and printer	7589	ISO	18								X
Photography -- Electronic still-picture cameras - - Terminology	12231	ISO	21								X
Photography -- Electronic still-picture cameras - - Determination of ISO speed	12232	ISO	21								X
Photography -- Electronic still-picture cameras - - Resolution measurements	12233	ISO	25							X	
Graphic Technology - Displays for color proofing - characteristics and viewing conditions	12646	ISO	30								X
Photography -- Electronic still-picture cameras - - Methods for measuring opto-electronic conversion functions (OECFs)	14524	ISO	34		X						
Photography -- Electronic still-picture imaging - - Noise measurements	15739	ISO	38				X	X			

<b>Digital Image Quality Parameter</b>											
<b><u>Title</u></b>	<b><u>No.</u></b>	<b><u>Organization</u></b>	<b><u>Page #</u></b>	<b><u>Spatial Uniformity</u></b>	<b><u>Tone Reproduction</u></b>	<b><u>Color Reproduction Accuracy</u></b>	<b><u>Noise</u></b>	<b><u>Dynamic Range</u></b>	<b><u>Spatial Cross-talk</u></b>	<b><u>Resolution</u></b>	<b><u>Non-Image Quality</u></b>
Graphic technology and photography — Colour characterisation of digital still cameras (DSCs) — Part 1: Stimuli, metrology, and test procedures	17321-1	ISO	41			X					
Graphic technology and photography - Colour characterization of digital still cameras (DSCs) - Part 2: Methods for determining transforms from raw DSC to scene-referred data	17321-2	ISO	45			X					
Photography and Graphic Technology - extended color encodings for digital image storage, manipulation and interchange - Part 1: architecture and requirements	22028-1	ISO	48			X					
Multimedia systems and equipment - Colour measurement and management - Part 2-1: Colour management - Default RGB colour space - sRGB	61966-2-1	IEC	51			X					
Multimedia systems and equipment - Colour measurement and management - Part 8: Multimedia colour scanners	61966-8	IEC	53	X	X	X			X		

<b>Digital Image Quality Parameter</b>											
<b>Title</b>	<b>No.</b>	<b>Organization</b>	<b>Page #</b>	<b>Spatial Uniformity</b>	<b>Tone Reproduction</b>	<b>Color Reproduction Accuracy</b>	<b>Noise</b>	<b>Dynamic Range</b>	<b>Spatial Cross-talk</b>	<b>Resolution</b>	<b>Non-Image Quality</b>
Multimedia systems and equipment - Colour measurement and management - Part 9: Digital cameras	61966-9	IEC	57	X	X	X					
Graphic Technology - Color reflection target for input scanner calibration	IT8.7/2	ANSI	61			X					
Colorimetry	15.2	CIE	64								X
A method for assessing the quality of daylight simulators for colorimetry	51	CIE	66								X
Data Dictionary - Technical Metadata for Digital Still Images	N/A	NISO	68								X

## 2.1 ISO

The ISO is a non-governmental international standards body made up of a network of national standards institutes from 147 countries working in partnership with international organizations, governments, industry, businesses, and consumer representatives. The ISO collaborates closely with the IEC and is responsible for all standards areas not specifically assigned to the IEC.

### ISO 3664, Viewing conditions – Graphic technology and photography

This standard specifies illumination and viewing conditions for reflective media, such as prints, transmissive media, such as transparencies, and images displayed on a

color monitor, which are not viewed in comparison to any form of hardcopy simultaneously. The viewing conditions described in the standard for the third case are what are pertinent to this research. When a monitor viewing condition is standardized and properly implemented by various people in a production chain, then errors and misunderstandings about color reproduction and processing will be minimized. The standard does not, however, dismiss the fact that the best viewing condition for the visual assessment of color is that in which the product will be finally seen, but it stresses that this viewing condition must be well specified and agreed upon by everyone in the production chain for it to be effective.

As mentioned above, the specifications provided by the standard are only relevant to images viewed successively, not simultaneously, with a hardcopy. The standard recommends the unpublished standard *ISO 12646, Graphic Technology – Displays for color proofing – Characteristics and viewing conditions* for the direct comparison of softcopy and hardcopy. That standard is summarized on page 30.

The color monitor viewing conditions specified in the standard are as follows. The chromaticity of the white displayed on the monitor should be approximately D<sub>65</sub>. The standard refers to *CIE Publication No. 51, A method for assessing the quality of daylight simulators for colorimetry*, which is summarized on page 66, for evaluating whether a particular light source is considered to be a D<sub>65</sub> illuminant. The white point of the monitor should have u'₁₀, v'₁₀ coordinates within the radius of 0.025 of u'₁₀ = 0.1979 and v'₁₀ = 0.4695 in the CIE 1976 Uniform Chromaticity Scale (UCS) Diagram. The luminance level of the white displayed on the monitor shall be greater than 75 cd/m<sup>2</sup> and should be greater than 100 cd/m<sup>2</sup>. The level of ambient illumination, when measured at

the face of the monitor or in any plane between the monitor and the observer with a cosine corrected photometer and with the monitor switched off, shall be less than, or equal to, 64 lux and should be less than, or equal to, 32 lux. The correlated color temperature of the ambient illumination shall be less than, or equal to, that of the monitor white point. If the ambient illumination approaches the maximum illumination levels above, then the chromaticity of the ambient illumination should be approximately the same as the white point of the monitor, so that chromatic adaptation complications are minimized. The area immediately surrounding the displayed image and its border shall be neutral, preferably dark gray or black to minimize flare, and of approximately the same chromaticity of the white point of the monitor. The luminance of the border of the image should be 20% of the white point luminance, or less, and preferably 3% of the white point luminance, or less. There should be no strongly colored areas, including clothing, directly in the field of view of the monitor or which may cause reflections in the monitor screen. Ideally, the walls, floors, and furniture in the field of view should be gray and free of any objects, which may affect the vision of the viewer. All sources of glare, such as from unshielded lamps or windows, which are directly in the field of view or are causing reflections from the surface of the monitor, should be avoided.

*ISO 7589, Photography – Illuminants for sensitometry – Specifications for daylight,*

*incandescent tungsten and printer*

This standard specifies the spectral characteristics of three corresponding illuminants for film sensitometry (daylight, studio tungsten, and photoflood) and one for black-and-white paper sensitometry (incandescent tungsten). It also describes methods

for evaluating the acceptability of illuminants for sensitometry and specifies tolerances. Since the standard is referenced in some of the standards summarized below to determine whether an illuminant is an acceptable match to a defined ISO illuminant, it is an important standard to include in this review. The relative spectral power distributions of the four ISO sensitometric illuminants described in the standard were obtained by operating a lamp at a specified condition and modulating the flux with selectively absorbing filters of suitable spectral transmittance, and are presented in tables at 10nm intervals.

The “ISO sensitometric daylight illuminant” spectral power distribution data, listed in the standard from 350nm to 690nm, correspond to a correlated color temperature of 5500K designated as D<sub>55</sub> and was obtained from *CIE Publication No. 15.2, Colorimetry*, summarized on page 64. This illuminant is defined as the product of the spectral power distribution of photographic daylight (D<sub>55</sub>) and the spectral transmittance of the ISO standard camera lens. The “ISO sensitometric studio tungsten illuminant” spectral power distribution data, also listed in the standard from 350nm to 690nm, correspond to a correlated color temperature of about 3050K. It is defined in the same way as the daylight illuminant in the standard. The “ISO sensitometric photoflood illuminant” is similarly defined, but with a correlated color temperature of 3400K. Details about the “ISO sensitometric printer illuminant” are not necessary to mention here, but are explained in the standard.

The spectral distribution index (ISO/SDI) is a three-number designation which describes how well a test illuminant matches a specified spectral power distribution in terms of the total photographic responses of the three component emulsions of average

color films. Weighted spectral sensitivity values, which were derived from average color film relative sensitivities for each film layer produced by several manufacturers worldwide, used to evaluate candidate illuminants for acceptability are listed in the standard for the ISO daylight, studio tungsten, and photoflood illuminants described above. They are weighted so that the aim relative spectral power values for the ISO illuminant will yield an ISO/SDI of 0/0/0.

The process of calculating an ISO/SDI designation is as follows. First, the relative spectral power values of a candidate illuminant are determined at 10nm intervals. These values are multiplied by each of the appropriate blue, green and red weighted spectral sensitivity values. The total responses are obtained by summing each result. Then, the logarithms to the base 10 of the total response values are determined to two decimal places. The smallest element of the three-number designation is subtracted from all three  $\log_{10}$  values, making the smallest element equal to zero. Finally, all three designations are multiplied by 100. The resulting numbers are the ISO/SDI for the candidate illuminant. An example of this calculation is given in an annex in the standard. To meet the requirements of the standard, the red index shall not differ from the green index by more than  $\pm 3$ , and the blue index shall not differ from the green index by more than  $\pm 4$ . A trilinear diagram is used in the standard to show these tolerances. Examples of actual lamp-filter combinations that meet these requirements are listed in an annex in the standard.

*ISO 12231, Photography – Electronic still-picture cameras – Terminology*

The purpose of this standard is to standardize the use and meaning of terms associated with electronic still-picture cameras. Even though electronic photography concepts are drawn from traditional photography, electronics, video and information technology, some of these concepts need to be redefined to apply to electronic photography. The source of most of the terms listed in the standard are the standards *ISO 12232, Photography – Electronic still-picture cameras – Determination of ISO speed*, *ISO 12233, Photography – Electronic still-picture cameras – Resolution measurements*, and *ISO 12234, Photography – Electronic still-picture cameras – Removable memory*, which is the only standard, out of the three, that will not be summarized in this standards review because it is not considered directly relevant to this research.

*ISO 12232, Photography – Electronic still-picture cameras – Determination of ISO speed*

This standard specifies a method for assigning exposure index values, ISO speed ratings, and ISO speed latitude ratings to electronic still-picture cameras, so that they relate, as much as possible, to current traditional photography standards. ISO speed is defined in the standard as the numerical value calculated from the exposure provided at the focal plane of an electronic camera to produce specified camera output signal characteristics using the methods described in the standard. It should correlate with the highest exposure index value that provides peak image quality for normal scenes. The exposure index is defined in the standard as the numerical value that is inversely proportional to the exposure provided to an image sensor to obtain an image.

Standardization of the ISO speed rating is useful for electronic camera users and manufacturers, because it assists them in obtaining proper exposures and in determining the low light capability of electronic still cameras. The exposure time, lens aperture, lens transmittance, level and color temperature of the scene illumination, and scene reflectance determine the camera exposure. When an image from an electronic still-picture camera is captured using an insufficient exposure, proper tone reproduction can generally be maintained by increasing the electronic gain, but the image will contain an unacceptable amount of noise. As the exposure is increased, the gain can be decreased, and therefore the image noise can normally be reduced to an acceptable level. If the exposure is increased excessively, the resulting signal in bright areas of the image may exceed the maximum signal level capacity of the image sensor of camera signal processing. Cameras with variable gain, and digital processing after the data has been captured, allow desired tone reproduction to be achieved over a range of camera exposures and speed ranges. The ISO speed latitude is defined as this range of speed ratings.

The standard explains how to calculate the following metrics. Exposure index, saturation-based speed, and noise-based speed can all be calculated using either the focal plane exposure measurement or the scene luminance measurement. The two ISO speed ratings above should indicate, when reported, whether daylight or tungsten illumination was used. The standard references the ISO standard 7589, *Photography – Illuminants for sensitometry – Specifications for daylight and incandescent tungsten*, which was described on page 18, for the determination of whether an illuminant is an acceptable match to either of these two illuminants. The standard also specifies that for the

determination of ISO speed, the temperature during the acquisition of the test data shall be  $23^{\circ}\text{C} \pm 2^{\circ}\text{C}$ , the relative humidity should be  $50\% \pm 20\%$ , the camera white balance should be adjusted to provide proper white balance for the illumination light source, an IR blocking filter shall be used, if required, and the photosite integration time, which is defined as the total time period during which the photosites of an image sensor are able to integrate the light from the scene to form an image, should not be longer than 1/30s.

The maximum exposure level is the exposure level where typical picture highlights will be clipped as a result of saturating the image sensor capacity or reaching the maximum signal level for camera signal processing. The minimum exposure level depends on the amount of noise that can be tolerated in the image. The saturation-based speed values describe the former case, and the noise-based speed values describe the latter case. The camera ISO speed is preferably determined using the noise-based speed value,  $S_{\text{noise}40}$ , method. The saturation-based speed value is preferably used to indicate the camera's overexposure speed latitude, and a second noise-based speed value,  $S_{\text{noise}10}$ , is preferably used to indicate the camera's underexposure speed latitude. The visibility of noise to human observers depends on the magnitude of the noise, the apparent tone of the area containing the noise, and the spatial frequency of the noise. The noise visibility is different for the luminance channel and the color channels, so the standard accounts for these factors in measuring the noise-based speed and speed latitude values.

The saturation-based speed rating is appropriate to use as the ISO speed of the electronic camera in photographic situations where the scene illumination level can be controlled, because the photographer wants a camera exposure index setting that provides the best possible image quality. Using the saturation-based speed rating, the

photographer can set the camera exposure so that the image highlights are just below the maximum possible camera signal value.

The noise-based speed rating is most appropriately used as the ISO speed of the electronic camera in photographic applications where it is desirable to have the highest exposure index, or lowest exposure, possible in order to maximize the depth of field, minimize the exposure time, and offer the maximum acceptable speed latitude for exposure of image highlights. Two different noise-based speeds are determined, one that provides the “first excellent” image,  $S_{noise40}$ , and a second that provides the “first acceptable” image,  $S_{noise10}$ .  $S_{noise40}$  and  $S_{noise10}$  have signal-to-noise, S/N, ratios of 40 and 10, respectively. If the electronic still-picture camera is too noisy to meet the S/N = 40 criterion, then the noise-based speed values shall not be reported and the saturation-based speed value shall be reported as the ISO speed of the camera. If the electronic still-picture camera includes any form of lossy compression, it shall be disabled, otherwise the noise-based speed values cannot be properly determined, and shall not be reported.

At the end of the standard, the method of reporting the ISO speed values is explained and a table is given for the value that should be reported when the saturation-based or noise-based speed ratings are between certain ranges of values. The standard also mentions that for electronic still-picture cameras that form a color image using a monochrome image sensor and a color-filter wheel, the ISO speed and speed latitude of each color should be measured and reported separately. In an informative appendix, the standard gives an equation for converting a  $S_{noise10}$  value to a minimum scene illumination level for consumer electronic still-picture cameras that use a minimum scene illumination level rating to define their sensitivity.

*ISO 12233, Photography – Electronic still-picture cameras – Resolution measurements*

This standard defines terminology, test charts and test methods for performing resolution measurements for analog and digital electronic still-picture cameras. The standard summary will focus on the latter type of camera. The ability to resolve detail is determined by the performance of the camera lens, the number of addressable photoelements in the optical imaging device, and the electrical circuits in the camera, which may include image compression and gamma correction functions. Different metrics result from different measurement methods for quantifying the resolution of an imaging system. Resolution metrics include resolving power, limiting resolution at some specified contrast, spatial frequency response, or SFR, which is the measured amplitude response of an imaging system as a function of relative spatial frequency, optical transfer function, or OTF, which is the two-dimensional Fourier transform of the imaging system's point spread function, a normalized spatial signal distribution in the linearized output of an imaging system resulting from imaging a theoretical infinitely small point source, and modulation transfer function, or MTF, which is the modulus of the OTF.

The first step in measuring resolution is to capture an image of a suitable test chart with the electronic camera being tested. This chart should include patterns with sufficiently fine detail, such as edges, lines, square waves, or sine wave patterns. A resolution test chart is defined in the standard. The SFR measurement method described in the standard uses a computer algorithm, which is available in both the C programming language and in an Adobe Photoshop® plug-in, to analyze digital data from the electronic still-picture camera. Digitized image values near slanted vertical and horizontal black to white edges are digitized and used to compute the SFR values. Using

a slanted edge for the SFR measurement allow the edge gradient to be measured at many phases relative to the image sensor photoelements, in order to eliminate the effects of aliasing, which is defined in the standard as output image artifacts that occur in a sampled imaging system for input images having significant energy at frequencies higher than the Nyquist frequency, or the spatial frequency equal to 0.5 times the inverse of the sampling period, of the system.

The resolution test chart defined in the standard is shown in Figure 2.

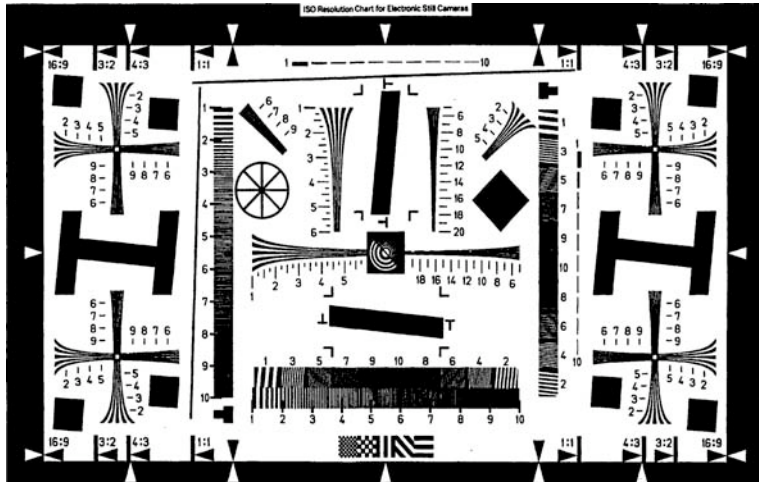


Figure 2. ISO Resolution Chart for electronic still cameras.

The test patterns in this test chart can be separated and rearranged and the framing and reproduction scale of the patterns can also be varied. This test chart is designed for cameras having a limiting resolution of less than 2000 line widths per picture height (LW/PH), but it can be used for electronic cameras having a limiting resolution greater than 2000 LW/PH by adjusting the camera to target distance, or focal length of the camera lens, so that the test chart active area fills only a fraction of the vertical image

height of the camera and then multiplying the test chart features by this fraction to obtain correct values. The test patterns on this test chart are bi-tonal patterns, which are spectrally neutral. The characteristics of the test chart such as the material, size, test-pattern modulation, units, features, and the positional tolerance of any test chart feature are all specified in the standard. A description of the purpose of each test pattern on the chart is also given in the standard.

The conditions under which the test chart should be digitally photographed are as follows. The luminance of the test chart shall be sufficient to provide an acceptable camera output signal level. It shall be uniformly illuminated and the illumination sources should be baffled to prevent direct illumination of the camera lens by the illumination sources. The area surrounding the chart should be of low reflectance, to minimize spatial cross-talk, and the chart should be shielded from any reflected light. The approximate distance between the camera and the test chart should be reported along with the measurement results. The camera focus should be determined by capturing the chart at a variety of focus settings and selecting the focus setting that provides the highest average modulation level at a spatial frequency of about 0.25 the camera Nyquist frequency. The camera focus can alternatively be determined so that the zone plate in the center of the chart exhibits the maximum aliasing possible. The camera exposure should be adjusted so that a near maximum signal level from the white test target areas is achieved. This exposure setting shall not have signal clipping in either the white or black areas of the test chart. All camera-setting values shall be reported along with the measurements. Multiple SFR measurements may be reported for different camera settings. The camera white balance should be adjusted so that proper white balance is provided for the

illumination light source. The resolution measurements should be performed on the camera luminance channel only. Also, the signal shall be linearized before the data analysis is performed, by applying the inverse of the camera opto-electronic conversion function, or OECF, because a non-linear response will affect the SFR values, since they are defined on a linearized output signal.

The test chart in Figure 2 can be used to determine the visual resolution, limiting resolution, spatial frequency response, and aliasing ratio. The visual resolution is the lowest value of the hyperbolic wedge test pattern, in LW/PH, where the individual black and white lines can no longer be distinguished, or are reproduced at a spatial frequency lower than the spatial frequency of the corresponding area of the test chart, which results from aliasing. In order to determine the visual resolution, the image of the test chart is reproduced on a monitor or hard-copy print, and the visual resolution is subjectively judged. The visual resolution value shall not exceed the Nyquist frequency limit. The limiting resolution is the value, in LW/PH, of that portion of the black and white vertical or horizontal square wave sweep where the resolution response (average depth of modulation value) equals 5% of the reference response, which is defined as the difference between the signal values from the slanted black bar and the white region just below the bar. If necessary, multiple images should be averaged to reduce the influence of noise in the determination of the 5% level.

The spatial frequency response, or SFR, of an electronic still-picture camera is measured by analyzing the electronic camera data near a slanted black to white edge. The test chart shown in Figure 2 allows the SFR to be measured horizontally, vertically, and diagonally in the center, corners, and sides of the captured image. The standard

provides a workflow diagram and the C-code of an algorithm used to compute SFR. A vertically oriented black to white slanted edge is used to measure the horizontal SFR and a horizontally oriented slanted edge is used to measure the vertical SFR in the algorithm. The aliasing level is measured using the horizontal and vertical 100 LW/PH to 1000 LW/PH slanted burst patterns in the test chart shown in Figure 2. When aliasing does not occur, the signal level from each black bar, or each white bar, should be identical for each bar in the burst. When aliasing does occur, the signal responses of the camera to the white bars of a particular burst may not be identical, but instead, the response may have a maximum signal value for some white bars, and a minimum signal value for other white bars. The aliasing ratio is the ratio of the *maximum minus the minimum response* for the white bars within a burst to the *average white-bar signal minus the average black-bar signal* within the burst for a particular spatial frequency burst.

The visual resolution values shall be reported as spatial frequency values, in LW/PH, for the horizontal, vertical, and diagonal directions. The limiting resolution values shall be reported the same way, but only for the horizontal and diagonal directions. The SFR values reported shall be the average of four SFR measurements of a black to white edge and four SFR measurements of a white to black edge taken in the middle of the slanted bars. The average SFR results should be reported separately for each direction measured using a graph plotting the modulation level versus spatial frequency where the modulation has a value of 1 at 0 spatial frequency, or by listing the SFR values versus spatial frequency. The spatial frequency axis should range from 0 to the sensor sampling frequency, where the camera Nyquist frequency is labeled and the values between 0.5 and 1 times the sensor sampling frequency is marked to indicate that these

spatial frequencies lead to aliasing. This axis should be labeled with three units: frequency relative to the sensor sampling frequency, LW/PH, and cycles/mm on the sensor, or with equations that represent the relationships between these units. The aliasing ratio values should be reported in a list that indicates the frequency in LW/PH, from 100 LW/PH up to the camera Nyquist frequency, and the aliasing ratios in both the horizontal and vertical directions for each frequency. An informative annex at the end of the standard lists a few relationships between resolution metrics for sine and square waves.

*ISO 12646, Graphic Technology – Displays for colour proofing – Characteristics and viewing conditions*

This unpublished standard specifies requirements for uniformity, size, resolution, convergence, refresh rate, luminance levels and viewing conditions for a color display used to simulate a hard copy proofing system. Because the standard was developed by the Graphic Technology technical committee, it is geared toward matching color images displayed on color monitors to the images produced when the same digital file is rendered by proofing and printing systems. Even though, in this research thesis, the images, which will be displayed on the monitor, will not be visually matched with a proof or printed reproduction, they will, however, be visually matched with the original, or source. Therefore, the information contained in the standard will be useful in defining viewing conditions for this purpose. This summarization will focus on information pertaining to this particular application. The standard is primarily based on CRT display technology, but its recommendations might be appropriate for newer display technologies. The

requirements and test methods of the display are described in the paragraphs that follow.

Figures 3 a, b, and c show the test images used in the test methods described below.

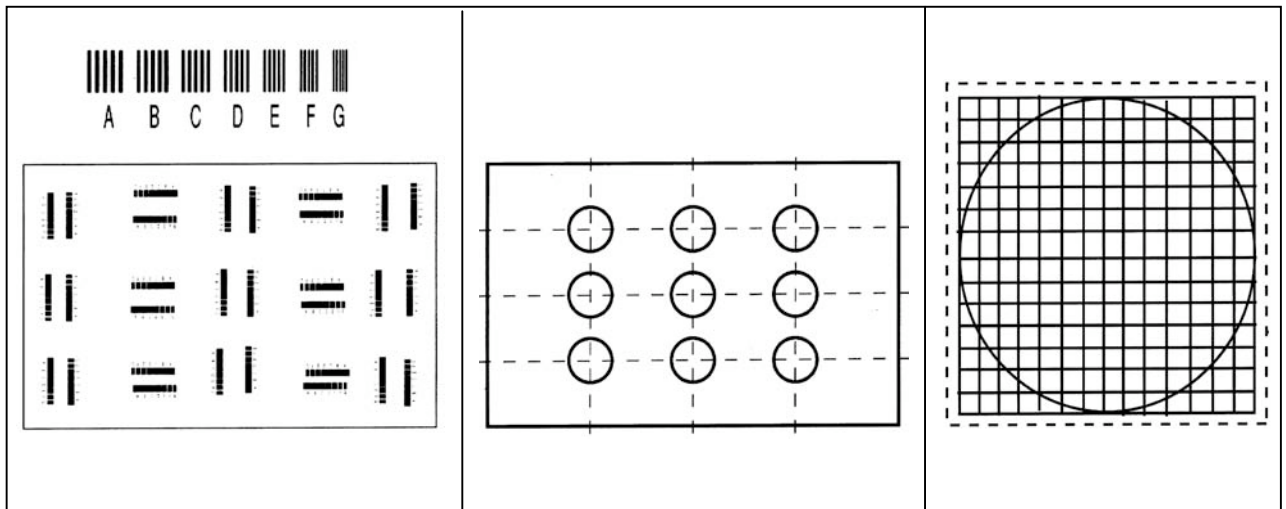


Figure 3 a, b, c. a) Resolution target (above) and its layout (below), b) Positions for measurement of uniformity, c) Grid pattern for assessment of convergence and geometric accuracy.

The display resolution shall be sufficient to display an image of 1280 x 1024 pixels without interpolation. The test image in Figure 3a, with lines and spaces that are equal in width for each field and that range from 0.5mm to 0.2mm in intervals of 0.05mm, shall be used. When viewed normally, and at a typical viewing distance (approximately 0.5m), the lines labeled D shall be clearly distinguishable and those labeled F should be clearly distinguishable, for all images within the central region (defined as that within half the linear diagonal distance) of the display. Any images outside this region may have a resolution poorer by 0.05mm.

The display shall be capable of displaying an image having a diagonal measurement of at least 17" and a height of at least 8.5". The CRT display shall have a refresh rate of at least 80Hz, non-interlaced.

The display should be visually uniform when displaying flat white, gray and black images that each fills the screen. The white image shall consist of the maximum value of the red, green, and blue channels (255 for an 8-bit display). The neutrality and luminance level of the gray and black images is not critical. However, the gray image should consist of approximately half of the maximum value in each channel (127 for an 8-bit display), and the black image should consist of approximately a quarter of the maximum value in each channel (63 for an 8-bit display). For each level, 9 points of the image area of the screen shall be measured, as shown in Figure 3b, using a photometer or radiometer. All luminance values should be within 5% of the luminance of the center and shall be within 10% of it, however, there should not be areas of significant visual non-uniformity between these areas.

When the grid pattern, shown in Figure 3c is displayed, geometric accuracy should be visually assessed by ensuring that the boundary pattern is all present, and that there is negligible distortion of the circle. The lengths of the lines should also be measured. The length of adjacent lines of the grid pattern shall be within 2mm of each other and no line length shall deviate by more than 2.5mm from the mean length. Convergence, which is the ability of the three electron beams to come together at a single spot on the surface of the CRT, shall be evaluated using the grid pattern in Figure 3c, by visually assessing whether all lines are wholly free of color fringing within the central

region. A small amount of fringing may be accepted outside this area, but is not recommended.

The ambient illumination conditions defined in the standard are more restrictive than those defined in ISO standard 3664, *Viewing conditions – Graphic Technology and photography*. An additional constraint beyond ISO 3664 is added to ensure that any reflected glare from the front surface of the display does not significantly reduce the perceived contrast. The requirements set forth in the standard are as follows. The level of illumination shall be less than 32 lux. The surround shall be no more than 10% of the maximum luminance of the screen. The color temperature of the ambient illumination shall approximate D<sub>50</sub>. The level of illumination when viewing a black screen (R=G=B=0) shall be less than 5% of that obtained when viewing a white screen (R=G=B=255) when measured at the plane of the observer.

The white and black images, defined above, should be measured using a spectroradiometer or shall be measured using a tristimulus colorimeter, if no spectroradiometer is available, in contact with the display, in order to determine the chromaticity and luminance of the white and black points of the display. At the center of the white image, the chromaticity of the display should be set to that of D<sub>50</sub> ( $u'=0.2092$ ,  $v'=0.4881$ ). The chromaticity obtained shall be within a circle of radius 0.005 (in  $u'$ ,  $v'$ ) from this point. This chromaticity shall be measured at the other points shown in Figure 3b and must be within 0.01 of the chromaticity of D<sub>50</sub>. The luminance level should be as high as practical, but shall be at least 80cd/m<sup>2</sup> and should be at least 120cd/m<sup>2</sup>. The black point shall have a luminance that is less than 1% of the maximum luminance. The black point chromaticity shall be measured at a luminance level of 10% of the maximum

luminance and shall be within a circle of radius 0.03 of the chromaticity of the white point. The gain of the individual channel amplifiers shall be adjusted to achieve these white and black point settings. After they are set, the gain, offset, and gamma shall be determined from the chromaticities measured for at least 10 neutral colors (R=G=B) at levels of luminance spanning white to full black, which are approximately equally spaced in lightness ( $L^*$ ). The gamma of the CRT display should be in the range 2 to 2.4 for each channel.

Even when the display meets the requirements, described above, of the standard, it does not guarantee that a displayed image will match the color of the hardcopy. To achieve a color match, it is necessary to provide a color transformation such that the color data format, in which the image is encoded, can be transformed into that required by the color display. An annex in the standard makes some recommendations for achieving an acceptable color transformation. The annex also states that in order to retain the validity of a characterization of the monitor, it should be calibrated at regular intervals by measuring the white point and opto-electronic transfer function to ensure that they are consistent with those obtained at the time of the characterization.

*ISO 14524, Photography – Electronic still-picture cameras – Methods for measuring opto-electronic conversion functions (OECFs)*

This standard describes methods for measuring the functional relationship between the focal-plane log exposures or scene luminances, and the digital output levels of a digital camera. It accounts for the variables caused by the flexibility of digital cameras in determining this functional relationship. The OECF shows the relation

between a physical input and digital code values assigned to this physical input. Digital values are assigned arbitrarily and do not have physical meaning or units. The standard applies to both monochrome and color electronic still-picture cameras.

Test methods for measuring both camera OECFs and focal plane OECFs are described in the standard. Camera OECFs have scene log luminances in units of  $\log_{10}$  candela per square meter as input and include the effects of the camera lens and associated flare. Focal plane OECFs do not include these effects because they are scene independent and have focal plane log exposures in units of  $\log_{10}$  lux seconds as input. The camera OECF test charts are designed to simulate the image formation effects produced by a scene with a specific luminance ratio and average distribution of luminances. For scenes, which are significantly different from average, the camera OECF measurements may be quite different. The main advantage of focal plane OECFs over camera OECFs is that they are scene independent. The camera OECF measurement method, on the other hand, allows for a one-step determination of the camera system characteristics for the scene simulated by the test chart being used, and focal plane values to be estimated from the camera OECF values for the midtone and highlight regions of most images if they are covered by the test chart being used.

The standard describes two methods for the focal plane OECF measurement and one for the camera OECF measurement. The first, more accurate, focal plane OECF measurement method involves exposing the electronic still-picture camera sensor directly to specific quantities of uniform illumination with the camera lens removed. The second method is used when the camera does not have a removable lens. This method involves using a uniformly emissive, approximately Lambertian reflective or illuminating target,

which is imaged by the camera lens on the sensor. The remainder of this standard's summary will focus on the camera OECF measurement method, since it is a target-based method.

The camera OECF measurement method requires the camera lens to be on the camera. The chart illumination source should be equivalent to either the daylight or tungsten ISO standard source defined in 7589, *Photography – Illuminants for sensitometry – Specifications for daylight and incandescent tungsten*, which was described on page 18. The chart or target, and the camera lens should be shielded from external illumination sources and reflective surfaces. The shielding materials and the wall behind the chart or target shall be black. The reflective chart or target shall be illuminated at a 45° angle from both sides of the normal. The standard specifies that the ambient temperature and relative humidity shall be  $23^{\circ}\text{C} \pm 2^{\circ}\text{C}$  and  $50\% \pm 20\%$ , respectively, when the test chart is imaged. The white balance shall be set to provide neutral digital output levels for the camera OECF test-chart background and the type of white balance (fixed, variable, automatic) shall be specified. An infrared-blocking filter shall be placed in front of the camera lens if required. Also, the camera lens shall be focused so that the test chart image appears sharp.

The standard camera OECF test chart is shown in Figure 4. The specifications for this chart are described in an annex in the standard.

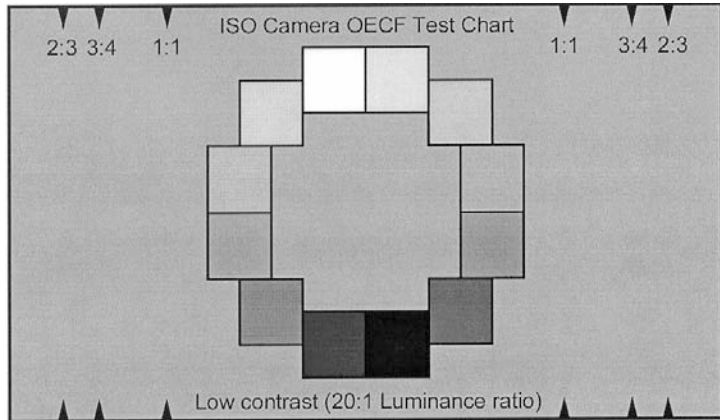


Figure 4. ISO Camera OECF Test Chart.

The chart luminances should be measured using a telescopic photometer placed where the camera would be. When each patch is measured, they should be masked with black in order to prevent flare from affecting the measurements. Alternatively, if a telescopic photometer is not available, the chart luminances may be calculated from the chart densities and illuminance. The chart shall be imaged a minimum of nine times each exposure level, where a trial shall consist of separate exposures for the camera being measured. The mean digital output level of each patch should be determined using a centrally located 64 by 64 pixel area at the same relative position of each image. The final digital output level data are calculated as the mean of the nine mean digital output levels. The results of the OECF measurement shall be presented in tabular and/or graphical form, which are described in more detail in the standard. In addition, all log luminances shall be to base 10.

In an informative annex in the standard, the relevancy of ISO/SDI calculations, described in ISO standard 7589, to the qualification of illumination sources for digital

still cameras is discussed, since this designation was based on the total photographic responses of the three component emulsions of average color films.

*ISO 15739, Photography – Electronic still-picture imaging – Noise measurements*

The noise performance of a digital image sensor may vary significantly with exposure time and operating temperature. The magnitude of the noise, the apparent tone of the area containing the noise, and the spatial frequency of the noise all affect the visibility of the noise to human observers. The noise visibility is different for the luminance channel and the color channels. The amount of noise in an output image depends on the noise present in the stored image data and the contrast amplification or gain applied to the data during image processing of the image. The standard accounts for these factors in the noise measurements and the reporting of them. The standard specifies the methods for measuring and reporting the noise versus signal level and dynamic range of electronic still-picture cameras. It can be used to characterize the noise in both monochromatic and color electronic still-picture cameras.

The noise measurement procedures described in the standard shall be used to determine the total signal-to-noise ratio (S/N), the fixed pattern signal-to-noise ratio, the temporal signal-to-noise ratio, and the dynamic range of the camera. In addition, total noise can be weighted to match a known expression for the human visual response. There are three types of noise measurement procedures described in the standard. One is a uniform field noise measurement method with the camera lens removed, the second is a uniform field noise measurement method with the camera lens attached to the camera,

and the third is a test chart noise measurement method. This third method will be focused on for the remainder of this standard's summary.

The general test conditions for this method are as follows. The noise measurements shall indicate whether a source conforming to the daylight or tungsten illuminant, as they are defined in ISO standard 7589, *Photography – Illuminants for sensitometry – Specifications for daylight and incandescent tungsten*, which was described on page 18, was used. For daylight illumination, the spectral characteristics of the illuminant shall be equivalent to CIE illuminant D55. For tungsten illumination, the spectral characteristics of the illuminant shall be equivalent to the product of the average spectral power distribution of experimentally measured sources having a color temperature of approximately 3050K. The reflective chart or target shall be illuminated at a 45° angle from both sides of the normal. The standard specifies that the ambient temperature and relative humidity shall be  $23^{\circ}\text{C} \pm 2^{\circ}\text{C}$  and  $50\% \pm 20\%$ , respectively, when the test chart is imaged. The camera white balance shall be adjusted so that equal RGB signal levels are achieved for the illumination light source. Also, an infrared-blocking filter shall be used, if required. The photosite integration time should not be longer than 1/30s. During the noise measurements, any compression shall be disabled. Equations are given for determining visually weighted luminance from the individual red, green and blue channel outputs for color cameras using a single exposure process, and for determining the visually weighted standard deviation of the test chart patches for color cameras with luminance and color-difference outputs, which are each used when visually weighted camera noise is calculated.

The standard camera noise test chart is shown in Figure 5. The specifications for this chart are described in an annex in the standard.

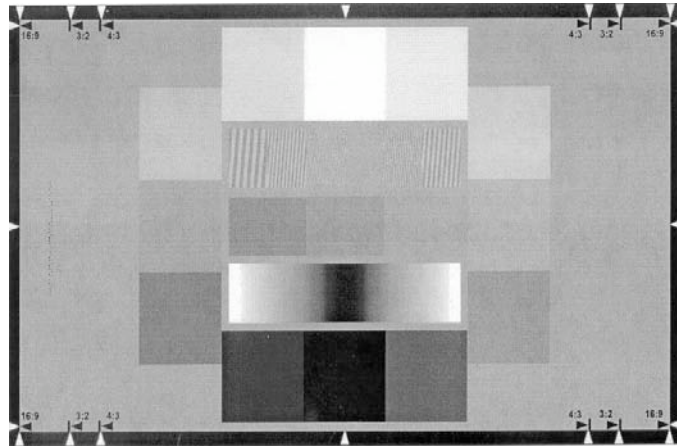


Figure 5. ISO Camera Noise Test Chart.

The major components of the test chart noise measurement procedure is as follows. The camera OECF shall first be measured according to the ISO standard *14524, Photography – Electronic still-picture cameras – Methods for measuring opto-electronic conversion functions (OECFs)*, which is described on page 34. The light source shall be fixed level and shall be adjusted so that the lightest patch of the test chart gives the maximum unclipped level from the camera. A neutral density filter can be used over the camera lens to achieve this result. The camera lens may be shielded from any stray illumination. Non-uniformity in the test chart density patches shall be less than 1/10<sup>th</sup> of the expected camera noise level. The test chart shall be correctly focused by the camera. The whole apparatus shall be securely mounted to reduce movement between exposures less than \_ of a pixel.

A minimum of eight images shall be captured of the test chart. An Adobe Photoshop® plug-in is available that will perform the following determinations and calculations, along with visual noise measurements. The mean digital code value and rms noise level shall be determined from a centrally located area of not less than 64 by 64 for each patch in each image. The first derivative of the OECF is calculated in order to produce the incremental gain function, which is defined in the standard as the change in digital code value divided by the change in luminance or exposure as a function of light level. It is used in each of the equations, which are used to determine the total, fixed pattern, and temporal S/N ratios, and the ISO dynamic range. The three S/N ratio equations use the data from the central three patches of the chart shown in Figure 5. The ISO digital still camera dynamic range is the ratio of the maximum unclipped luminance level to the minimum luminance level that can be reproduced with a temporal S/N ratio of at least 1. The camera dynamic range is obtained by measuring the temporal S/N ratio using the darkest patch in the chart shown in Figure 5. More details about these calculations can be found in the standard. In addition, an informative annex in the standard explains how to determine edge noise using the square wave part of the chart in Figure 5. This edge noise is termed the ISO standard camera high frequency S/N ratio.

*ISO 17321-1, Graphic Technology and photography – Colour characterization of digital still cameras (DSCs) – Part 1: Stimuli, metrology, and test procedures*

The spectral responses of the color analysis channels of digital still cameras do not, in general, match those of a typical human observer. Nor do the responses of different digital still cameras ordinarily match each other. In characterizing these

cameras, it is therefore necessary to take account of their spectral sensitivities, illumination, and encoding color space. Part 1 of this unpublished standard, which is summarized here, will define stimuli (spectral illumination or a color target), metrology and photographic test procedures for acquiring digital still camera characterization data. This characterization data will be expressed as raw (sensor-referred) data. Some operations, such as color pixel reconstruction, flare removal, and white balancing, may be performed without disqualifying the data as being raw. Two alternative methods are described in the standard for obtaining this raw digital still camera data. A spectral method will use narrow band spectral illumination as stimuli for measuring the color performance of a digital camera. A target method will involve the use of a physical spectrally and colorimetrically calibrated color test target under specific lighting conditions to measure the color performance of the camera.

The two methods contained in the standard for obtaining raw digital still camera characterization data will be described next. If little is known about the scene spectral content then the spectral method is preferred. However, in cases where scene spectral correlation statistics are well understood (e.g. the hardcopy colorants and the image capture illumination are pre-determined), then the target-based method is preferred.

Spectral sensitivity based characterization measurements shall be obtained by using a light source, with an output radiation where the power is a smooth function of wavelength (e.g. quartz-halogen), and a monochromator, with a spectral sampling interval that shall not be greater than 10nm and should not be greater than 5nm, to evenly illuminate a diffuse transmissive or reflective surface with selected wavelengths. The camera shall have the following settings. Fixed exposure settings shall be selected to

provide peak output levels between 50% and 90% of saturation. Any automatic gain or adaptive tone reproduction shall be disabled, compression shall be minimized, white balancing shall be fixed, the flash should be disabled, and all user settings shall be recorded.

The diffuse surface shall be lit by the monochromator, so that it fills the field of view of the digital camera. Capture images of the illuminated surface at wavelengths ranging from 360nm to at least 830nm and preferably to 1100nm in 10nm or smaller increments. The images shall be captured with the digital still camera lens and any filters used for general picture taking. Integrated relative radiance measurements, as a function of wavelength, of the illuminated surface shall be obtained and recorded for each selected wavelength using a radiance or irradiance meter. Apply an inverse OECF, which can be obtained using ISO standard *14524, Photography – Electronic still picture cameras – Methods for measuring the opto-electronic conversion functions (OECFs)*, summarized on page 34, to linearize the raw digital camera responses at each wavelength. Then average a 64 x 64 pixel block of values at the center of each image to determine the linearized digital camera response at each wavelength. Finally, calculate the relative spectral sensitivities at each wavelength for each color analysis channel by dividing the linearized digital camera response by the relative surface radiance. Normalize the spectral sensitivities so the sum of the green channel sensitivities is unity and report this resulting data in tabular form.

The target based characterization method consists of imaging a reflective or transmissive color target of known spectral and colorimetric characteristics, under specified illumination. The spectral data for each patch of the color test target shall be

from at least 380nm to 730nm and should be from 360nm to 830nm, at least every 10nm. An informative annex in the standard describes some of the characteristics that the test target should have. The standard gives the 24 patch ColorChecker and the 237 patch ColorChecker DC Digital Camera Reference Chart as examples of test targets that may be used. The spectral power distribution for illuminating the test target shall be D<sub>55</sub>. The illuminance at the target plane should be between 2000 lux and 4000 lux and have a maximum variation of 1% over the area being imaged. An additional informative annex in the standard outlines a recommended laboratory set-up for photographing a color reflection test target. At least two illumination sources shall be used to illuminate the target at 45° relative to the normal of the surface of the test target.

The target should fill the field of view of the camera and be in sharp focus. The flash shall be turned off, any automatic gain control shall be disabled, compression shall be minimized, white balancing should be fixed, and all user settings shall be recorded. At least three images of the color target shall be recorded. The mean and standard deviation of the digital still camera digital code values shall be obtained for each channel corresponding to the central area of each patch. This data shall be recorded for subsequent processing, which is described in *Part 2: Methods for determining transforms from raw DSC to scene-referred image data*, along with measured patch data, the spectral power distribution of the illumination, the OECF used for analysis, and other information about the target and camera used.

In order to guarantee the colorimetric reproduction, a set of camera sensitivity curves must be a linear transformation of color matching functions. An informative annex in the standard describes a digital still camera / sensitivity metamerism index

(DSC/SMI) designed to give a measure for such potential color error. The indices consist of two elements: average and special DSC/SMIs. Average DSC/SMI will give a measure of camera metamerism for ordinary reflective objects and special DSC/SMI is an optional measure by defining arbitrary objects depending on applications. Procedures for measuring both DSC/SMIs with both camera characterization methods, described above, are given in this annex.

*ISO 17321-2, Graphic Technology and photography – Colour characterization of digital still cameras (DSCs) – Part 2: Methods for determining transforms from raw DSC to scene-referred image data*

The spectral responses of the color analysis channels of digital still cameras do not, in general, match those of a typical human observer. Nor do the responses of different digital still cameras ordinarily match each other. In characterizing these cameras, it is therefore necessary to take account of their spectral sensitivities, illumination, and encoding color space. Part 2 of this unpublished standard, which is discussed here, specifies methods for the determination of such characterization transforms from raw digital still camera image data to scene-referred image data based on the minimization of errors in a scene analysis color space based on CIE colorimetry. The digital still camera characterization data obtained in *Part 1: Stimuli, metrology, and test procedures* can serve as the raw image data used in this part of the standard.

Three alternative methods are described for obtaining characterization transforms. The first method takes advantage of the pre-defined colorant and illumination characteristics encountered when scanning hardcopy originals to produce transforms

specifically for that capture condition. The second method takes advantage of some set of statistically expected assumptions about the spectral characteristics of the scene or original (e.g. artwork captured in a studio with known uniform illumination) being captured to produce characterization transforms that are more reliable where these assumptions hold true. Method three makes no assumptions about scene spectral correlation statistics, and is the most robust to highly variable natural scene capture under different illumination sources. For the first two methods, the digital still camera data can consist of captured test target patch values or spectral characterization data. Method three requires spectral data for the determination of characterization transforms.

With each method, the characterization transformation determination procedure shall be as follows. First, determine the class of scene analysis to select the appropriate characterization transformation determination method. Second, obtain the raw digital still camera characterization data. Third, determine the inverse camera OECF, from the OECF measured according to ISO standard 14524, *Photography – Electronic still picture cameras – Methods for measuring the opto-electronic conversion functions (OECFs)*, summarized on page 34, and use it to linearize the raw digital camera characterization data. Next, select the scene analysis error minimization color space, and patch or wavelength error weights (if any). Then, determine the aim patch or spectral values in the scene analysis error minimization color space. Finally, determine the color characterization transformation matrix, that when applied to the linearized raw data to transform it to the scene analysis color space, produces the smallest weighted mean error in the scene analysis error minimization color space.

Only the second method will be described here in more detail, since it relates the closest to this research thesis. This method assumes that all colors analyzed will have relatively smooth spectra consistent with surface reflectance colorants. Either the spectral-based or target-based methods in *Part 1* can be used to obtain the raw characterization data. If spectral characterization data are used, the signals that target samples would create should be calculated from the spectral characterization data. The adopted white should be a perfectly reflecting diffuser illuminated identically to the test chart. The recommended scene analysis error minimization color space is CIELAB. An informative annex in the standard gives considerations for scene analysis error minimization color space selection. The samples should be equally weighted, unless the matrix is not constrained to be white point preserving, in which case, the neutral samples should be given higher weights, or experience indicates that certain colors should be given higher weights, either because they are analyzed with larger errors, or are accuracy-critical. The row sums of the matrix should be constrained to enforce white point preservation. The matrix should be normalized so that the middle row sum is unity for reporting. The characterization transformation reported shall consist of the inverse OECF for each channel, the normalized matrix, the adopted white, the sample weights used (if any), and a description of the scene analysis error minimization color space according to ISO standard 22028-1, *Photography and graphic technology – Extended colour encodings for digital image storage, manipulation and interchange – Part 1: Architecture and requirements*, summarized on page 48. The weighted mean error magnitude in the scene analysis estimates, as expressed in the scene analysis error minimization color space, may additionally be reported as the scene analysis error index.

*ISO 22028-1, Photography and graphic technology – Extended colour encodings for digital image storage, manipulation and interchange – Part 1: Architecture and requirements*

A fundamental choice for any imaging system architecture is how to represent images numerically, in what color space and with what digital encoding. It is necessary to unambiguously describe the meaning of the color values used to encode digital images. The color encoding definitions need to not only include a specification of the relationship between the digital code values and corresponding physical color values, but they also need to clearly specify any other information needed to unambiguously interpret the color values. This unpublished standard specifies a set of requirements to be met by color encodings defined for various digital-imaging applications involving digital image storage, manipulation, and/or interchange. It also describes a reference image-state-based digital imaging architecture that is flexible enough to support a wide variety of applications and workflows and can be used to classify extended color encodings into a number of different image states.

One important aspect of a digital imaging architecture is how the digital image data are encoded as it progresses through the system workflow from image capture/creation through image processing/storage/interchange, and finally to output on one or more output devices. The standard defines scene-referred color encodings and picture-referred color encodings, which can be subdivided into original-referred and output-referred color encodings. Scene-referred color encodings are representations of the estimated color-space coordinates of the elements of an original scene. Picture-referred color encodings are representations of the color-space coordinates of a hardcopy

or softcopy image. Original-referred color encodings are representations of color-space coordinates of a two-dimensional hardcopy or softcopy input image. Output-referred color encodings are representative of the color-space coordinates of image data that are appropriate for a specified real or virtual output device and viewing conditions. Also defined in the standard are color rendering transforms, which are used to transform a scene-referred image to an output-referred image, color re-rendering transforms, which are used to transform an original-referred image to an output-referred image, and also film rendering and unrendering transforms.

Color encodings can be specified at two levels. A color space encoding includes the specification of a digital encoding method. A color image encoding further includes any additional information necessary to properly interpret the image color values, such as the image state, the image viewing environment and the reference imaging medium.

Information needed to define a color space is given in the standard for three types of color spaces: colorimetric (e.g. CIE color spaces, additive RGB color spaces, luma-chroma color spaces derived from additive RGB color spaces), color appearance (e.g. CIECAM97s) and device-dependent (e.g. input and output device-dependent color spaces).

Defining a color space encoding requires the identification of a color space as well as a digital encoding method. Both a forward and inverse encoding transform shall be specified. Digital encoding methods will typically be integer digital encoding methods, although floating-point digital encoding methods will be useful in certain applications. The definitions of each of these digital encoding methods are given in the standard.

Information needed to define a color image encoding includes the identification of a color space encoding, together with the specification of the image state (scene-, original-, or output-referred), a reference image viewing environment in which the image is intended to be viewed (including the image surround, assumed adapted white point, luminance of adapting field, and viewing flare), and the set of valid color values in the color space encoding. Color image encodings intended for an output-referred image state shall also define the characteristics of a reference imaging medium.

An informative annex in the standard gives examples of a number of different workflows commonly encountered in digital photography and graphic technology. They include generic workflows for digital photography, digital cameras producing CRT-ready images, copy stand photography, scanning hardcopy, hardcopy scanners producing CRT-ready images, scanning color negatives, and video imaging systems. A second informative annex in the standard lists some characteristics of some existing color encodings (e.g. sRGB, sYCC, ROMM RGB, RIMM RGB) for comparison. In a third informative annex in the standard, a set of guidelines for making the appropriate selection of color encodings for image storage, manipulation and interchange in digital photography and graphic technology applications are specified. The selection criteria include: the image state associated with the color image encoding, the extent of its color gamut, its luminance dynamic range, the ability of a color encoding to represent image values brighter than a “perfect white”, the quantization error associated with the discrete nature of the digital color values, the quantization efficiency, the visual uniformity of the color encoding, the complexity of conversions to other important color encodings, its

compressibility, its compatibility with existing industry practice, and hue shifts induced by nonlinear tone scale manipulations.

## 2.2 IEC

The IEC is an international standards body made up of a network of national standards institutes from 62 countries that prepares and publishes standards for electrical, electronic, and related technologies.

*IEC 61966-2-1, Multimedia systems and equipment – Colour measurement and management – Part 2-1: Colour management – Default RGB colour space – sRGB*

The standard color space, sRGB, is a simple and robust device-independent color definition. It is suited for CRT and flat panel displays, television, scanners, digital cameras, and printing systems. The three factors of this RGB space are the colorimetric RGB definition, the simple exponent value of 2.2, and well-defined viewing conditions. It serves the needs of personal computer and World Wide Web-based color imaging systems, and is based on the average performance of personal computer displays. There are two parts to the methodology described in the standard; the encoding transformations and the reference conditions. The encoding transformations provide all of the necessary information to encode an image for optimum display in the reference conditions.

The reference image display system is a computer controlled CRT display with a luminance level of  $80\text{cd}/\text{m}^2$ , a white point of  $D_{65}$  ( $x=0.3127$ ,  $y=0.3290$ ), a model offset (R, G and B) of 0.0 and an input/output characteristic (R, G and B) of 2.2. The CIE chromaticities of the red, green and blue reference display primaries are listed in the

standard. The reference viewing conditions are derived from ISO standard 3664, *Viewing conditions for graphic technology and photography*. Specifically, the reference ambient illuminance level shall be 64lx, the reference background and proximal field shall have a luminance level of 16 cd/m<sup>2</sup> and an average chromaticity of illuminant D<sub>65</sub>, the reference surround shall have a luminance level of 4.1cd/m<sup>2</sup> and an average chromaticity of illuminant D<sub>50</sub>, the reference ambient white point shall be illuminant D<sub>50</sub>, and the reference veiling glare shall be 0.2cd/m<sup>2</sup>. The reference observer shall be the CIE 1931 2° standard observer.

The encoding transformations between CIE 1931 XYZ tristimulus values and 8-bit RGB values provide unambiguous methods for representing optimum image colorimetry when viewed on the reference display in the reference viewing conditions by the reference observer, and as measured on the faceplate of the display, which assumes the absence of any significant veiling glare. The transformation from sRGB values to CIE XYZ values and the reverse transformation are outlined in the standard. The matrices given in this standard for these linear transformations are shown in Equation 1 and Equation 2, respectively.

$$\begin{bmatrix} X \\ Y \\ Z \end{bmatrix} = \begin{bmatrix} 0.4124 & 0.3576 & 0.1805 \\ 0.2126 & 0.7152 & 0.0722 \\ 0.0193 & 0.1193 & 0.9505 \end{bmatrix} \begin{bmatrix} R_{sRGB} \\ G_{sRGB} \\ B_{sRGB} \end{bmatrix} \quad (1)$$

$$\begin{bmatrix} R_{sRGB} \\ G_{sRGB} \\ B_{sRGB} \end{bmatrix} = \begin{bmatrix} 3.2406 & -1.5372 & -0.4986 \\ -0.9689 & 1.8758 & 0.0415 \\ 0.0557 & -0.2040 & 1.0570 \end{bmatrix} \begin{bmatrix} X \\ Y \\ Z \end{bmatrix} \quad (2)$$

One of the informative annexes in the standard describes usage guidelines for the sRGB color space when it is used with or without ICC profiles in color management applications. It also describes several different scenarios to consider when dealing with

palletized images and displays. In two other informative annexes in the standard, recommendations are given for situations where the viewing conditions are different than the reference viewing conditions. Amendment 1 of the standard consists of three additional annexes. The first annex standardizes a default transformation between sRGB and a standard luma-chroma-chroma color space, sYCC. The same reference conditions are shared by both color spaces. The second annex provides equations necessary for extended gamut encoding for sRGB, called bg-sRGB, and its YCC transformation, called bg-sYCC. The transformations between these color spaces and sRGB, YCC and CIE 1931 XYZ are given. The third and final annex gives equations for describing the relationship between sRGB and L\*a\*b\* coordinates.

*IEC 61966-8, Multimedia systems and equipment – Colour measurement and management – Part 8: Multimedia colour scanners*

This standard provides a way of obtaining colorimetric characterization data of color scanners, which is necessary for color management in open multimedia systems. The mulitmedia color scanner characterization of the standard focuses on the characterization of spectral transfer functions of the three channels as multiband sensitivities and achromatic tone characteristics. Further objective performance assessment can be performed using methods, which are also described in the standard. The standard assumes that the originals, which will be scanned, are reflective. Even though the standard is geared toward scanner characterization, most of the methods described, which are different from the methods described in *Part 9: Digital cameras*, summarized on page 57, can be used to characterize digital cameras as well. These

particular methods will be the focus of this summation. Figures 6 a and b show two test targets used in the standard.

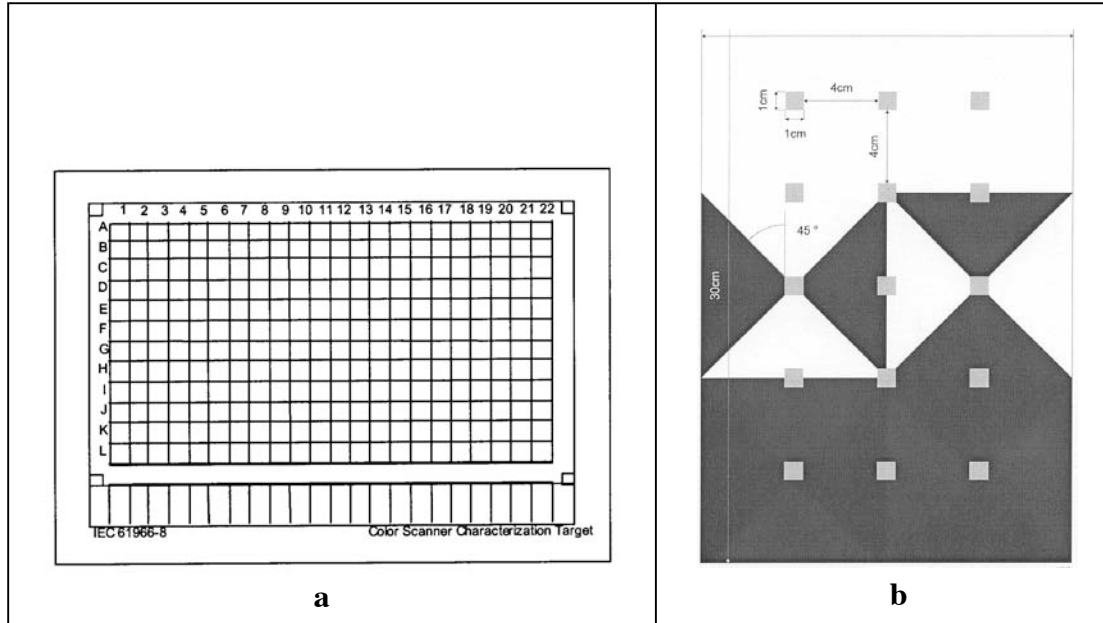


Figure 6 a, b. a) Color and grayscale target, b) Target for measurement of spatial cross-talk.

The spectrophotometer, with a minimum wavelength range of 400nm to 700nm, an interval of 10nm, and a geometry of either 45/0 or 0/45, shall be used for the measurements. A one-shot spectroradiometer, with a minimum wavelength range and interval that is the same as for the spectrophotometer, shall be used to measure the spectral distribution of the light source. Figure 6a shows the reflective target used for some of the measurements made in the standard, where the top part of the target consists of color patches and the bottom part consists of gray patches.

The spectroradiometer shall be used to measure the spectral power distribution of the light source and the data shall be reported in tabular and graphical forms. The tone characteristics shall be measured as follows. First, the spectral reflectance of each gray patch of the target shall be measured using the spectrophotometer. Then, the target shall be captured 10 times and the red, green and blue data shall be determined by averaging the picture elements in the center of each gray patch for each image and then the average values of the 10 images shall be averaged. The measured and averaged data shall be normalized and recorded. A 4<sup>th</sup> order polynomial characterization is performed on these data and the results are reported in graphical form as light flux vs. output data. The equations for calculating the inverse tone characteristics, which represent the polynomial transformation from normalized output data to captured light flux of the red, green, and blue channels, are also given in the standard.

The spectral responsivity characteristics of the device are measured as follows. First, the spectral reflectances of each color patch of the target shall be measured. Next, the target shall be captured 10 times and the red, green and blue data shall be determined by averaging the picture elements in the center of each color patch for each image and then the average values of the 10 images shall be averaged. Then, the normalized light flux values shall be calculated. The multiband spectral responsivity characteristics for the red, green, and blue channels shall be estimated using the spectral reflectances of the color patches, the spectral power distribution of the light source, and the averaged and normalized red, green, and blue channel output data. The algorithm for performing this estimation is described in an annex in the standard. The spectral responsivity data shall be reported both in tabular and graphical form. The overall responsivity characteristics

shall also be reported taking into account the spectral power distribution of the light source. Examples for the application of the spectral characteristics are given in an informative annex in the standard, specifically for the calculation of the ICC profiles and the calculation of an optimized conversion for the sRGB color space.

A method for measuring spatial non-uniformity is also described in the standard. A gray sheet of paper with reflectance between 60% and 80% shall be used for the measurements as the target. After this target is captured so that it fills the image, the mean and mean square deviation values shall be determined from 25 equally spaced image areas. Alternatively, the tristimulus values and color differences in either the CIE 1976 UCS or CIELAB space shall be calculated. These results shall be reported as indices of non-uniformity, along with the reflectance of the uniform gray target. A method for characterizing the instability of output data upon turning on the multimedia color scanner is also described in the standard.

Large area spatial cross-talk is the dependency of the output digital data of a color patch on the reflectance of surrounding areas. It can be measured using the target shown in Figure 6b. The target shall be printed on a sheet of non-fluorescent paper and the 15 square test patches shall be uniform gray with reflectance between 20% and 40%. The white areas of the target are the surface reflectances of the paper and the black areas are printed at the maximum density of the printing system. The target shall be captured three times in one direction and three times after being rotated 180°. The mean values of each gray patch of all six images shall be recorded. The mean data values of all 15 patches shall be determined for each color channel and recorded, along with the relative difference between the maximum and minimum values and the relative root mean

standard deviations resulting from all of the patches, both calculated as percentage points for each color channel.

*IEC 61966-9, Multimedia systems and equipment – Colour measurement and management – Part 9: Digital cameras*

This standard defines test charts, measurement conditions and methods of measurement for assessing the color reproduction of digital cameras used to capture color still and moving images for use in multimedia applications. Figures 7 a, b, and c show both an equipment arrangement and test charts used in the standard.

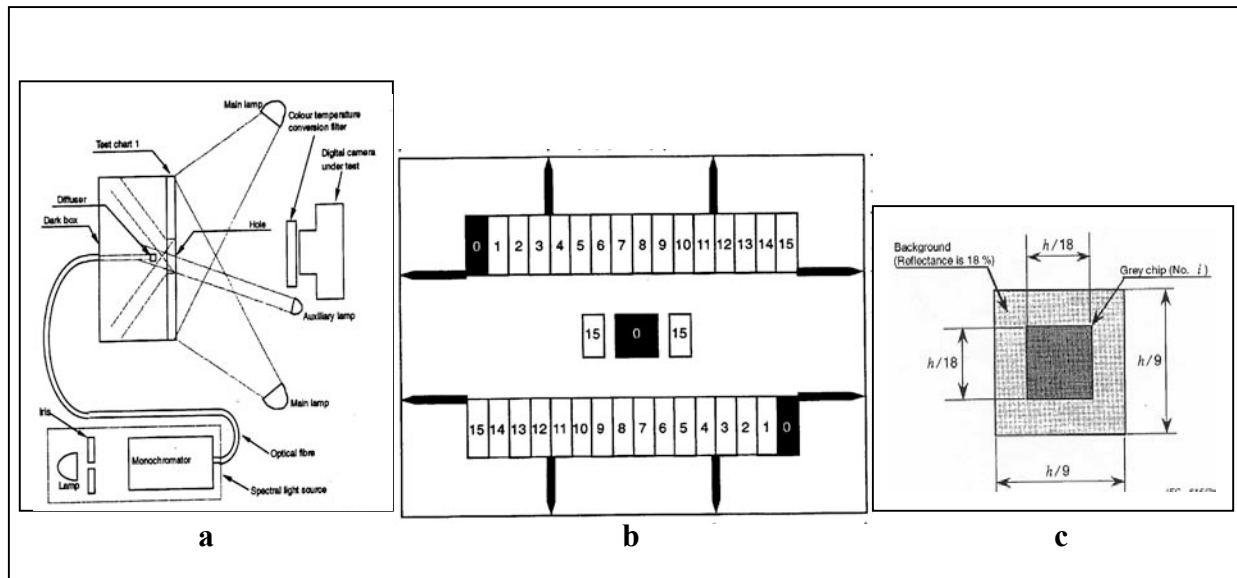


Figure 7 a, b, c. a) Equipment arrangement for measurements, b) Test chart, c) Test chart with replaceable chip.

All measurements specified in the standard shall be carried out in a dark room.  
Figure 7a shows the configuration of the equipment used for measuring the tone and

spectral responsivity characteristics of the digital camera and the spectral distribution of the built-in electronic flash. The conditions of this configuration are as follows. The test charts that are used in this configuration are shown in Figures 7 b and c, where patches marked 1 through 15 are gray patches, with reflectances that are defined in the standard, and patches marked 0 are holes. The illumination of the test charts shall be performed by two or four main lamps, which shall be  $45^\circ$  relative to the surface of the test chart, and one auxiliary lamp, which illuminates the diffuser in Figure 7a. These lamps shall be halogen lamps. The main lamps shall not be directly illuminating the diffuser. The correlated color temperature of the lamps shall be  $3100K \pm 100K$ . The non-uniformity of illumination shall be less than 5%. The average illumination on the test chart shall be  $2000\text{ lx} \pm 100\text{ lx}$ . The camera shall be placed normal to the test chart. The test chart shall fill the frame of the camera when captured. The spectral light source in Figure 7a consists of a halogen lamp, an iris, a monochromator and an optical fiber with a diffuser. Specifications of these parts are listed in the standard, for example, the wavelength range and spectral bandwidth of the monochromator shall be 380nm to 780nm and 5nm, respectively. A color temperature conversion filter used to achieve a color temperature of  $5500K \pm 300K$  shall be used over the camera lens, where needed in the standard. The reflectance of the inside of the dark box shall be less than 2%.

The radiance meter used for the measurements of the output from the spectral light source is specified in the standard. Its wavelength range should be from 380nm to 780nm. A spectroradiometer can also be used for this measurement and should be used for measuring a built-in electronic flash. Its specifications are also listed in the standard. It shall have a wavelength range of 380nm to 780nm and a bandpass of 5nm or less. A

luminance meter shall be used for measuring in the standard. Its specifications are also listed in the standard. Alternatively, a colorimeter with luminance output in Y can also be used for the luminance measurement.

For the measurement of the tone characteristics, the equipment shall be as arranged in Figure 7a. The optical fiber shall be removed, the auxiliary lamp shall be switched off, and the hole at rear side of the dark box shall be covered with a lid painted black like the inside of the box. Two separate measurements shall be made, one with each color temperature (5500K and 3100K). The test chart shown in Figure 7c shall be inserted into the hole at the center of the test chart shown in Figure 7b sequentially with gray chips  $i = 0$  to 15, where  $i = 0$  is a hole. The luminance of each gray chip shall be measured and captured with the digital camera. The mean red, green and blue digital value data shall be recorded for each gray chip image. The mean values of the upper gray steps shall also be noted for each image. The recorded data shall be compensated to eliminate any autonomous exposure control or errors of a mechanical shutter of the digital camera. The measured and calculated data shall be presented in both tabular and graphical form, along with the effective correlated color temperature of the illumination.

The measurement of the spectral responsivity characteristics of the digital camera are performed as follows. First, the intensity of the auxiliary lamp, with the iris shut, shall be adjusted so that the digital image data corresponding to the diffuser are around 20% of a full data range of the digital camera. Next, with the auxiliary lamp still on, the iris shall be adjusted once so that the maximum data in the red, green and blue channels are between 70% and 80% inclusive of the full scale. Two separate measurements shall be made, one with each color temperature (5500K and 3100K). Next, the radiance on the

diffuser from the spectral light source shall be measured using the radiance meter with the auxiliary lamp switched off. Then, with the auxiliary lamp switched on and the iris shut, the digital image data corresponding to the diffuser shall be recorded, pixel-by-pixel, for each color channel. Next, the iris is opened and the test chart is captured by the digital camera, with the diffuser lit at each of the 81 wavelengths from 380nm to 780nm in 5nm intervals. The digital image data for each image shall be recorded pixel-by-pixel for each color channel. Also, the mean values of the upper gray steps shall also be noted for each image for each color channel. Finally, the auxiliary lamp shall be switched off and the test chart shown in Figure 7c with gray chip 8 shall be inserted into the front hole in the center of the test chart shown in Figure 7b. The spectral distribution characteristics shall be measured using the spectroradiometer with the diffuser lit at each of the 81 wavelengths from 380nm to 780nm in 5nm intervals. The pixel-by-pixel data shall be compensated to eliminate any autonomous exposure control or errors of a mechanical shutter of the digital camera, linearized using the tone characterization data, and averaged over the center portion of the image corresponding to the monochromatic radiation. The radiance of the spectral light source is then taken into account. This data shall be reported in electronic and graphical forms, together with the effective correlated color temperature.

The method for measuring the spectral distribution of the built-in electronic flash that is described in the standard will not be discussed here. The spatial non-uniformity of the digital image data shall be measured by photographing an evenly illuminated uniform white chart. The white chart shall be illuminated by two lamps that are 45° relative to the surface of the chart. The color temperature conversion filter shall be placed over the

camera lens in order to achieve an effective correlated color temperature of 5500K. .

After this target is captured so that it fills the image, the mean digital image values shall be determined from 25 equally spaced image areas for each color channel. The R, G, and B data shall be converted to the tristimulus values X, Y, and Z in accordance with *Part 2-1: Colour management – Default RGB colour space – sRGB*, summarized on page 51.

Color differences in either the CIE 1976 UCS or CIELAB space shall be calculated as indices of non-uniformity and shall be reported as a table.

In an informative annex in the standard, an example is given for the use of the reported results for color management. In another informative annex, recommendations are given for the automatic extraction of data from the test chart image.

### **2.3 ANSI**

ANSI is a private, non-profit non-governmental organization that administers and coordinates standards developed in the United States. It is supported by both private and public organizations. ANSI is the official United States representative to both the ISO and IEC.

#### *ANSI IT8.7/2, Graphic technology – Color reflection target for input scanner calibration*

This standard defines an input reflection test target that will allow any color-input scanner to be calibrated with any film dye set used to create the target. Although this test target is intended for use with scanners, it can also be photographed with digital cameras, which is why its description in the standard is pertinent to this research. In the design of the test target, which is printed on photographic paper, the colors of the target patches

were chosen most effectively by uniform spacing of hue, lightness, and chroma in the CIELAB color space based on the D<sub>50</sub> illuminant and the CIE 2° standard observer.

Table III lists CIELAB hue angles, lightness values, and chroma values specified for this test target.

Table III. CIELAB hue angles, lightness values and chroma values specified for the ANSI IT8.7/2 test target.

Row	L* and C* <sub>ab</sub> Values vs. Hue Angle															
	Hue Angle	L1	C1	C2	C3	C4	L2	C1	C2	C3	C4	L3	C1	C2	C3	C4
A	16	20	12	25	37	*	40	15	30	44	*	70	7	14	21	*
B	41	20	12	24	35	*	40	20	36	54	*	70	8	16	24	*
C	67	25	11	21	32	*	55	22	44	66	*	75	10	20	30	*
D	92	25	10	19	29	*	60	20	40	60	*	80	10	21	31	*
E	119	25	11	21	32	*	45	16	32	48	*	70	9	18	27	*
F	161	15	9	19	28	*	35	14	28	42	*	70	6	12	18	*
G	190	20	10	20	30	*	40	13	25	38	*	70	6	13	19	*
H	229	20	9	18	27	*	40	12	24	36	*	70	7	13	20	*
I	274	25	12	24	35	*	45	9	19	28	*	70	5	10	15	*
J	299	15	15	29	44	*	40	11	22	33	*	70	6	11	17	*
K	325	25	16	33	49	*	45	14	28	42	*	70	8	16	24	*
L	350	20	13	26	38	*	40	16	32	48	*	70	8	15	22	*
Column		1	2	3	4		5	6	7	8		9	10	11	12	

The chroma values marked with a \* in Table III are specific to the product used to create the target and equal to the maximum C\*<sub>ab</sub> available at the hue angle and L\* value specified. They are to be defined by the manufacturer of the product used to make the test target.

The color gamut of the test target is common to most of the commonly used color photographic paper dye sets. The Kodak Q-60 target, which uses 12 uniformly spaced hue angles in CIELAB sampled at three chroma values at each of three lightness levels,

was adopted as this target with the addition of a fourth product-specific maximum chroma value at each hue angle/lightness combination. Also included in the target were scales in each of the individual dyes, dye pairs, and a dye neutral, the product minimum and maximum densities, and a “vendor-optional” area where the target manufacturer could add unique elements beyond those defined in the standard. Manufacturing tolerances specified in the form of  $\Delta E$  units are also defined for the test target in the standard. All of the non-image areas of the target shall be approximately neutral with a lightness  $L^*$  of approximately 50.

The physical layout of the test target is described in detail in the standard. Figure 8 shows the layout of the IT8 target.

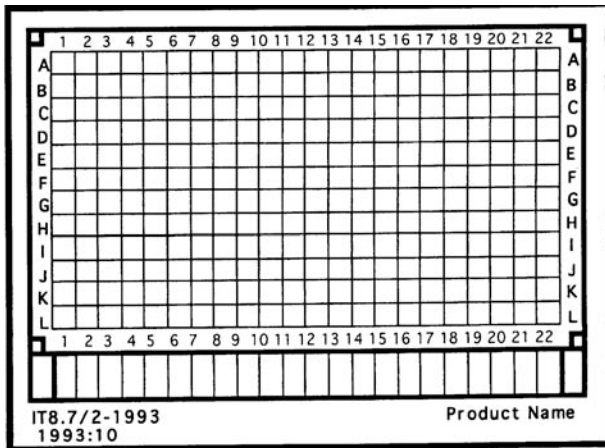


Figure 8. Layout of color reflection input calibration target.

The standard also specifies that calibrated test targets shall be measured using a reflection spectrophotometer with a measurement geometry of 0/45 or 45/0. During measurement, the sample shall be backed with a black material with a density of at least 1.5.

Tristimulus values shall be calculated based upon a 2° standard observer and the D<sub>50</sub> illuminant, with no greater than a 10nm data interval and a bandpass equal to the measurement interval. The mean and standard deviation values shall be reported as X, Y, Z tristimulus values to two decimal places. The mean values shall also be provided as CIELAB and standard deviation as CIE ΔE\*<sub>ab</sub>. The file format shall be an ASCII format keyword value file. The required keyword fields, values, and data format identifiers are listed in the standard. Also, the standard states that each test target manufacturer shall provide the monitoring procedure to be used for each target type.

In addition, an informative annex in the standard describes how to use this target for the application of calibrating a color scanner. There are two distinct ways in which a scanner may be operated. The calibration procedure for each is different. When the scanner is a “color digitizer,” its objective is to capture the color information of the original image being scanned for subsequent processing elsewhere. Therefore, the output data must have some unique relationship to the tristimulus values of the original. In the other case, when the scanner is a “gamut mapped color digitizer,” it is operated in a device dependent manner, so the output data must have some unique relationship to the tristimulus values of the reproduction. The calibrated input target will provide colors with known XYZ tristimulus values as an input to the color scanner. The primary objective of the target is to enable the user to calibrate his system using whatever calibration facility exists. For a colorimetric calibration, data obtained by scanning the target may be used to derive a transformation which maps the data back to the tristimulus values provided with the calibrated target or some transformation of them. The derivation of the transformation is application dependent. Helpful guidelines are listed in

the annex of the standard. For a closed system calibration without a two-stage transformation using colorimetric data, the target is scanned and output on a specific device (e.g. monitor or printer). Visual assessment under controlled viewing conditions, possibly supplemented by color or density measurement, is often used to determine the quality of the match.

## 2.4 CIE

The CIE is an international standards body, which is recognized as such by the ISO. It is a technical, scientific, and cultural non-profit organization, which comprises of 38 member bodies. It is devoted to the cooperation and exchange of information among member countries on matters relating to lighting. The publications summarized below are referred to as technical committee reports, not as standards, so their purpose is to advise or recommend, but not mandate.

### CIE 15.2, Colorimetry

This report provides a consistent and comprehensive account of the basic colorimetric recommendations of the CIE. The first recommendation given in this publication is the illuminants to be used for general colorimetry. They include illuminants A, B, C, D<sub>50</sub>, D<sub>55</sub>, D<sub>65</sub>, and D<sub>75</sub>. Their relative spectral power distributions are given in this report at 5nm intervals. A formula for calculating the relative spectral power distribution of daylight illuminants with correlated color temperatures from 4000K to 25,000K is also given. When fluorescent samples are involved, a D illuminant should always be used over illuminant C, because of its insufficient ultraviolet content. CIE

sources for colorimetry are also listed for illuminants A, B, and C, which are artificial sources recommended when the illuminants are to be realized in a laboratory environment. There is no artificial source recommended to realize the D illuminants.

The publication recommends using pressed barium sulphate as a perfect reflecting diffuser, or standard of reflectance factor, because its reflectance is approximately equal to unity. For specifying reflecting samples, the following illuminating and viewing conditions, or geometries, are recommended: 45/0 (45°/normal), 0/45, d/0 (diffuse/normal), and 0/d. For transmitting samples, 0/0, 0/d, and d/d geometries are recommended.

The CIE 1931 standard colorimetric observer, or 2° observer, and the CIE 1964 supplementary standard colorimetric observer, or 10° observer, color-matching functions are given in this report from 360nm to 830nm in 1nm intervals. The formulas for calculating tristimulus values for both reflecting and transmitting objects, and self-luminous objects are also given, along with formulas for deriving chromaticity coordinates from tristimulus values.

This publication recommends the CIE 1976 Uniform Chromaticity Scale (UCS) diagram, the CIE 1976 L\*u\*v\* (CIELUV) color space, and the CIE 1976 L\*a\*b\* (CIELAB) color space as uniform color spaces. The formulas for calculating the coordinates for each uniform color space are listed, along with the Euclidean distance color difference equations for CIELUV and CIELAB.

In the final section of the report are recommendations concerning miscellaneous colorimetric practices and formulae. They include recommendations for defining dominant wavelength, complementary wavelength, colorimetric purity, excitation purity

and forms of representing relationships between color stimuli, evaluating whiteness, and calculating special metamerism index: change in illuminant and correlated color temperature. A third edition is near completion at the time of writing this summary.

*CIE 51, A method for assessing the quality of daylight simulators for colorimetry*

This report provides a method for evaluating the suitability of a test source as a simulator of CIE Standard Illuminant D<sub>55</sub>, D<sub>65</sub>, or D<sub>75</sub>. For each of these illuminants and the 10° standard observer, spectral radiance factor data are supplied for five pairs of non-fluorescent samples that are each metamerically matches. The colorimetric differences of the five pairs are computed for the test illuminant. The visible range metamerism index is the average of these differences and is used as a measure of the quality of the test illuminant as a simulator for non-fluorescent samples for the visible wavelength range. For fluorescent samples, the ultraviolet range metamerism index, which is the average of the colorimetric differences computed with the test illuminant for three other metamerically sample pairs, each consisting of a fluorescent and a non-fluorescent sample, is used. The fluorescent sample in each metamer pair is specified by values of spectral radiance factor, relative spectral distribution or radiance emitted by fluorescence, and spectral external radiant efficiency in the report.

The procedure for evaluating the suitability of a test source as a simulator of CIE Standard Illuminant D<sub>55</sub>, D<sub>65</sub>, or D<sub>75</sub> is as follows. First, the spectral power distribution of the test source is determined by spectroradiometry. The radiometric quantity measured should be the spectral irradiance at the sample surface. The data must be presented in the form of the spectral concentration of irradiance of 5nm intervals and over

5nm bands from 300nm to 700nm. Sources with significant spectral irradiance at the sample surface for wavelengths less than 300nm are not suitable daylight simulators. Next, the spectral power distribution of the test source is normalized so that it is independent of the absolute level of illumination. Then, as a preliminary test, the chromaticity coordinates of the test source are evaluated to see if they fall within a circle of radius 0.015 from the centered chromaticity coordinates of the standard daylight illuminant concerned, in the CIE 1976 Uniform Chromaticity Scale diagram,  $u'$ <sub>10</sub>,  $v'$ <sub>10</sub>.

For the visible range metamerism index, first, the tristimulus values are calculated for the five metamerous pairs using the normalized spectral power distribution of the test source and the 10° standard observer from 400nm to 700nm in 5nm intervals. Then, the color differences between the five sets of tristimulus values are calculated using either the CIE 1976 L\*u\*v\* or L\*a\*b\* formula and, finally, the visible range metamerism index is calculated as the average of the five color differences ( $\Delta E^*$ <sub>ab</sub> or  $\Delta E^*$ <sub>uv</sub>).

The ultraviolet range metamerism index is determined by first calculating the spectral total radiance factor for the fluorescent sample part of each of the three metamerous pairs using an equation given in the report. The calculation of the tristimulus values, color differences and ultraviolet metamerism index is the same as above for the visible range metamerism index.

The metamerism indices are interpreted by categorizing the test source from A to E, depending on the values of the metamerism indices and the color space used. The category for the visible range metamerism index is presented first and the ultraviolet range metamerism index second in the category rating. The correlation of these category ratings with the requirements for various practical applications must be determined by

experience. For many applications, though, daylight simulators of category BC are found to be useful. The appendix in the report gives the assessment of a number of daylight simulators, using the procedure described here.

## 2.5 NISO

NISO is a non-profit association accredited by ANSI, which identifies, develops, maintains, and publishes technical standards to manage information in the digital environment. NISO standards cover the areas of information-related needs, including retrieval, re-purposing, storage, metadata, and preservation.

### *NISO Data Dictionary – Technical metadata for digital still images*

Technical metadata are perceived as an essential component of any digitization initiative for short-term and long-term management purposes. Work to date on image metadata has focused on defining descriptive elements for discovery and identification. Little attention has been paid to defining the types of information that describe the capture process and technical characteristics of the digital images. Technical metadata must be recorded accurately and consistently to ensure that the image files remain useable well into the future. It is necessary to support two fundamental goals: to document history and to ensure that image data will be rendered accurately on output. This unpublished standard presents a comprehensive list of technical metadata elements required to manage digital image collections. The metadata descriptions in the standard are structured to accommodate practices associated with digital copy photography, such

as the use of technical targets, as well as techniques related to direct digital photography of original scenes.

The design goals of the standard are that the metadata are interchangeable (applicable to many applications and assured to be constant over time), extensible and scalable (allows future needs for metadata to be fulfilled with limited disruption of current solutions), image file format independent (can be supported by many current and future file formats and compression mechanisms), consistent (usable in a variety of application domains and user situations), and network-ready (provides seamless integration with a broad variety of systems and services). This dictionary assumes that metadata mappings are needed to automate the collection of technical metadata. The design model assumes that NISO-compliant metadata will be stored outside the image.

The standard references two documents, which provide supplemental information. The first is *TIFF, Revision 6.0*. The TIFF (Tagged Image File Format) format is highly flexible and platform-independent, is supported by numerous image processing applications and is publicly available. The structure of the header includes a rich set of technical information important for long-term image retention. The second reference is *DIG35 Specification: Metadata for digital images, version 1.1, working draft*, provided by the Digital Imaging Group. This document contains a comprehensive description of a standard set of metadata for digital images, which is not limited to technical metadata, but also includes, for example, a recommended implementation model and intellectual property rights metadata.

The basic image parameter metadata fields, which are fundamental to the reconstruction of the digital file as a viewable image on displays, described in this

dictionary, are as follows. The format information includes: the MIME type, byte order, compression scheme, compression level, color space, ICC profile information, and information about whether the image is stored using either strips or tiles (collectively termed as segments). The file information includes a unique image identifier, file size, type of error detection used (checksum), image orientation, the orientation in which the image should be presented to a conventional monitor, and the designation of the device, application, medium and/or viewing environment to render the image data.

The image creation, or descriptive, metadata, which document irreversible attributes of the analog-to-digital conversion process that may be used for future quality assessment of the image data, will be listed next. The descriptions of the image creation metadata in this dictionary include: the medium of the analog source material, a unique source identifier, the image producer, the host computer, the operating system and version, the classification of the device used to create the image, the scanning system information, the digital camera capture information, which includes the digital camera manufacturer, model, and camera capture settings (f-number, exposure time, brightness, exposure bias, subject distance, metering mode, scene illuminant and its color temperature, focal length of lens, flash information, lighting conditions, exposure index, focus used, and print aspect ratio selected by the user when the picture was taken), type of image sensor, date and time image was created, and methodology and rationale to digitize an object or collection.

The image performance assessment metadata, described next, serve as metrics to assess the accuracy of output and of preservation techniques, particularly migration. The spatial metrics metadata described in the standard include: sampling frequency, image

width and length (in pixels), and the width and height of scanned object. The energetics metadata include: the number of bits per color component, the number of color components per pixel, the colormap (lookup table) information for palette-color images, the gray response curve for grayscale images, and the white point and primary chromaticities. Targets can be used to benchmark spatial and energetic information about the item of interest at the time of capture. Targets can be either external or internal to a digital image. Internal targets are included in the image of the object and external targets are captured in a separate session, which are tied to the image through metadata. The target metadata fields included in the standard are: the identification of the targets as either internal or external, the target manufacturer or organization, name, and version number or media, the path where the image of the target is located, the path of the file that contains the image performance data relative to the target, and the path of the file that contains the ICC color profile or other image management profiles.

Change history metadata documents processes, such as editing or transforming, applied to image data over the life cycle of the image. The following metadata descriptions contain a summary of image processing operations that may be used for future quality assessment of the image data. These metadata descriptions include: the date and time the image was processed, the information about the source image data, the producer of the processed image, the processing software and version, and the processing actions. The last metadata descriptions in this dictionary are the documentation of the previous versions of the technical metadata if image transformation creates a new generation of the image.

### ***3. Testing Procedure and Targets***

The testing procedure and targets that are described in this section were developed for the application of characterizing the image quality produced by digital cameras and digital imaging workflows, used in cultural heritage institutions to create archival quality digital master images of paintings. Some of the targets and procedures were obtained from standards, summarized in the reviews above. They include system spatial uniformity, tone reproduction, color reproduction accuracy (spectral sensitivity and target-based), image noise, dynamic range, spatial cross-talk, and spatial frequency response. The remaining procedures and targets, including color reproduction accuracy (metamerism), color noise, color channel registration, and depth of field were developed subsequent to a literature review of papers relating to both digital camera testing and digital imaging as it is used in cultural heritage institutions. All of the image analysis was performed in The MathWorks MATLAB® programming language. CIE illuminant D<sub>50</sub> was used as the reference illuminant in this testing procedure because it is the standard illuminant used by the graphics and printing community and, therefore, used by most museums in their digital imaging practices.

The testing procedure and targets were first used to characterize both a Nikon D1 and a Sinar Sinarback 54H camera in the Munsell Color Science Laboratory (MCSL). Modifications were then applied to the procedures and targets contained in the testing procedure in order to make it simpler and more applicable. Case study 0 (CS0) was performed in June 2004 using the modified testing procedure. It was applied to a Sinar Sinarback 54H camera within MCSL and is presented as an example.

### **3.1 Case Study Zero: Camera Description and Set-up**

A Sinar Sinarback 54H (SN: 26151754) 3-channel (RGB) area-array-CCD digital camera with a Sinar 4x5 camera body was characterized in the Munsell Color Science Laboratory. It has a maximum native resolution of 4,080p x 5,450p. The lens used during the characterization was a 100mm f/4 Sinaron digital HR lens (SN: 11639548). The filter used between the CCD and the lens was a Schott BG39 3mm thick IR filter. A Balzers Unaxis IR cut-off filter was also placed in front of the lens (Berns, 2004). The front bellows were tilted slightly downward in order to prevent inter-reflections between the Unaxis IR cut-off filter and the lens.

At the beginning of the imaging session, an image area of 26" x 22" was marked out where all of the targets would be placed in the scene. At the top of the marked area was placed a piece of Halon® (pressed polytetrafluoroethylene, or PTFE, powder) and an imaging description label. The Halon, which is almost equivalent to a perfect reflecting diffuser (Weidner, 1981), was the brightest and most neutral object placed in the scene. The scene was lit with two Broncolor HMI F 1200 lights (Model: 42.102.01-16), which each had reflectors and a VWFL lens. These lights simulate daylight illumination. Table IV shows the correlated color temperature (CCT), chromaticity coordinates, and luminance of this illumination. Figure 9 shows the relative spectral power distribution of the HMI lights. These data were obtained by measuring the Halon with a calibrated Photo Research Spectrascan PR650 spectroradiometer.

Table IV. CS0 Broncolor HMI F 1200 taking illuminant characteristics.

<b>Correlated Color Temperature</b>	5026K
<b>Chromaticity x (2° Observer)</b>	0.3440
<b>Chromaticity y (2° Observer)</b>	0.3475
<b>Luminance (2° Observer)</b>	2231cd/m <sup>2</sup>

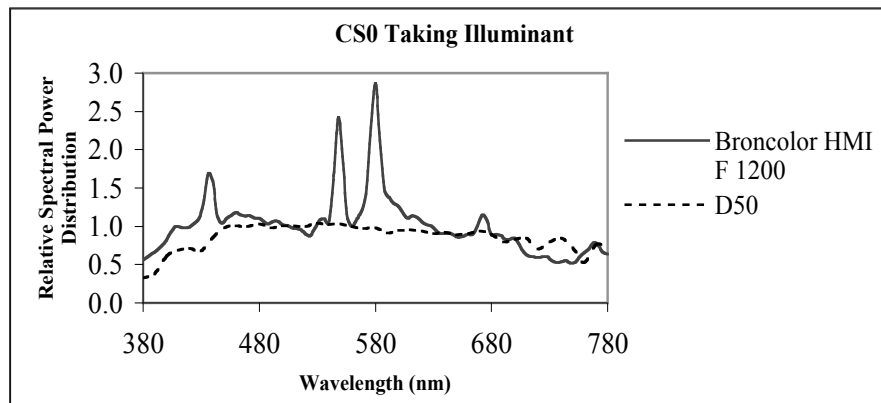


Figure 9. Relative spectral power distribution of the Broncolor HMI F 1200 lights that were used in the CS0 set-up. CIE illuminant D<sub>50</sub> is included for comparison.

Figure 10 shows how the camera and lights were placed in relation to the scene during the imaging procedure. The labeled distances are approximate.

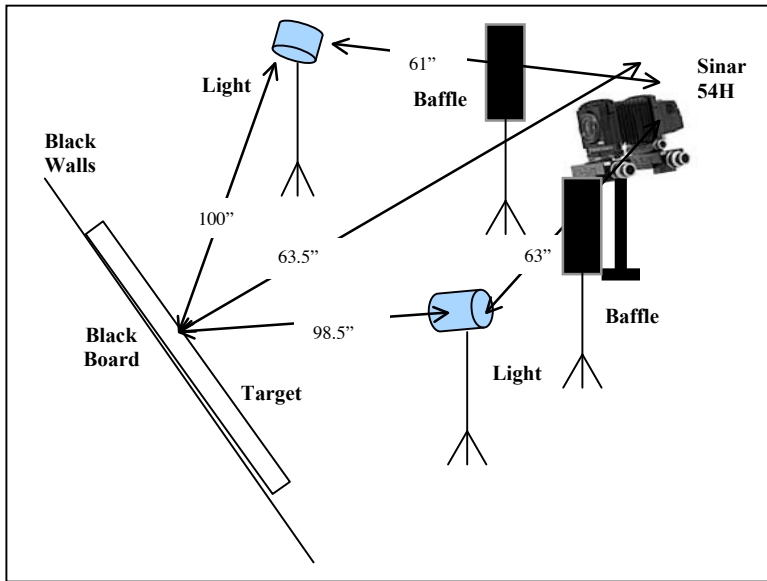


Figure 10. Schematic of CS0 imaging set-up.

According to the ISO 14524 standard,

“with these test methods, the target or chart, and camera lens, shall be shielded from external illumination sources and reflective surfaces, including the walls, ceiling, and floor of the test room, using black shielding materials. The wall behind the target or chart shall be black, and the only illumination sources present shall be those used to illuminate the chart. For reflective targets or charts, the illumination sources shall be positioned so that the angular distribution of influx radiance is at its maximum at  $45^\circ$  to the target or chart normal, and is negligible at angles less than  $40^\circ$  or more than  $50^\circ$  to the normal at any point on the target or chart.” (ISO 14524, 1999).

During the testing procedure imaging, the camera and lighting positions remained the same and the targets were replaced. There were two exceptions to this. First, when the depth of field target (see section 3.10) was imaged, the lights were moved in order to decrease the amount of shadows on the target. Figure 11 shows the new placement of the lights. Second, when the monochromator instrument (see section 3.4.1) was imaged

during the spectral sensitivity characterization part of the testing procedure, the lights were removed and the camera was repositioned. Figure 12 shows this set-up.

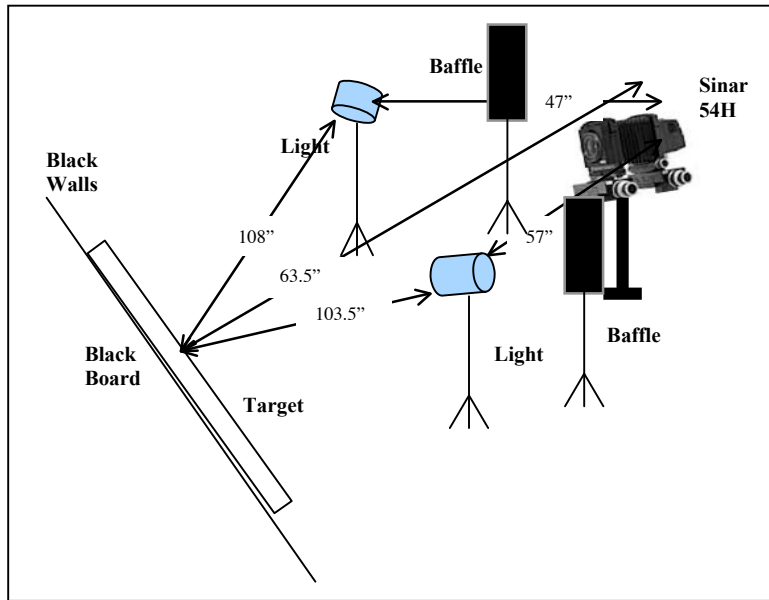


Figure 11. Schematic of the CS0 set-up for the depth of field target imaging.

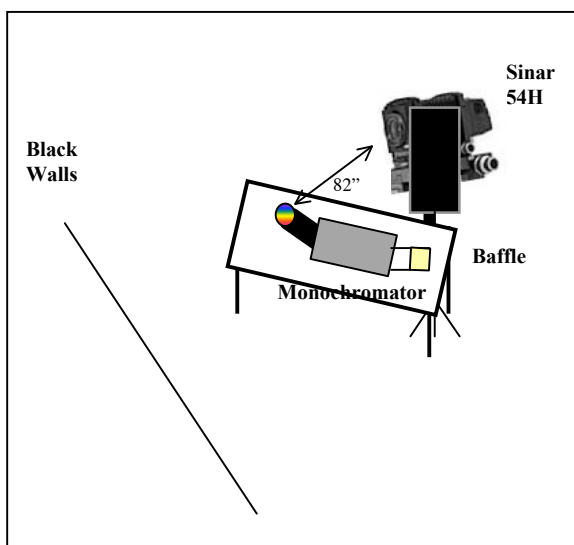


Figure 12. Schematic of the CS0 set-up for the monochromator instrument imaging.

The capture software used was Sinar CaptureShop 4.1. The images were first scanned in preview mode to see if the image area was what it should be, to see if the scan was in correct focus, and to check the exposure level. The nominal exposure times and aperture settings were determined on a target-to-target basis. The only restriction to the nominal exposure settings was that the digital count value of the Halon had to be unclipped in order to assure that none of the target image data were clipped. The ISO speed (see the ISO 12232 standard) was set to 25 for the target imaging, but when the monochromator instrument (see section 3.4.1) was imaged, the ISO speed was set to 50. The integration time of the camera was controlled remotely. The aperture, exposure time, and manual focus, which was determined using the magnified focus tool in the image capture software, were controlled at the camera.

There was no light metering performed before the imaging process because any non-uniformity in the illumination was later corrected mathematically, when necessary, when the target images were analyzed. Dark correction was performed automatically for every image by the capture software. No corrections, such as in the form of gray balancing, tone curve application, color management, compression, or sharpening, were applied in the capture software to the images. This was done in order to assure that the image data that were saved were as raw as possible. The only images that were cropped were the ones taken of the monochromator instrument. The image quality type was set in the capture software to four-shot for the target imaging and one-shot for the monochromator instrument imaging. The images were exported and saved as 16-bit RGB tiffs. The monitor used was a Samsung SyncMaster 210T, but no visual corrections were made to the images.

### 3.2 System Spatial Uniformity

System spatial non-uniformity of an image acquisition system can be caused by many things, such as uneven illumination of the scene, flare, and/or lens fall-off. It was analyzed in this testing procedure similarly to the method described in the IEC 61966-8 and 61966-9 standards. The target consisted of two gray cards placed side-by-side, and was used to evaluate system spatial uniformity. It is shown in Figure 13. These gray cards were made using Gray 6.5 Color-aid paper, which is paper coated uniformly with paint. The reason why two gray cards, which were each the same size as the other targets used in this testing procedure, were used was so that they could be easily transported to each museum case study.



Figure 13. Target consisting of two gray cards side-by-side used to evaluate system spatial uniformity and to perform flat-fielding.

When this target is imaged, it should be in sharp focus. In all of the case study imaging procedures, it was imaged at the same exposure level as the color reproduction accuracy targets. In CS0, the exposure time was 1/15s. the integration time was 1/2s.,

and the aperture was f/11. This target should be imaged twice. The second time that it is imaged, each of the gray cards should be rotated 180°. The two images were averaged together to ensure that any texture in the gray cards would not have an influence on the image data that it was used to flat-field. Only one of the images is needed for the system spatial uniformity evaluation.

This target was used for two purposes. It was used to evaluate system spatial uniformity in this testing procedure and for flat-fielding in CS0 to mathematically perform system spatial uniformity corrections. The analysis of the gray card target image in the evaluation of system spatial uniformity is as follows. First, the RGB images of the gray card target are converted to Lab images. For CS0, since there were no profiles embedded in the images, the gray card target images were converted from RGB to CIELAB in MATLAB (this conversion is described in detail in section 3.4.2). For the profiled images in CS1 through CS4, the RGB image of the gray card target is opened in Adobe Photoshop® (the profile that is embedded with the image is used when the image is opened) and converted from an RGB image to an Lab image. The Lab image is saved and its data are used in the system spatial uniformity evaluation. Using MATLAB, average pixel data from 36 (6 rows by 3 columns from each gray card) evenly spaced patches are obtained. These Lab image data are converted from the ICC version of the CIELAB standard (referred to as ICC Lab later in this thesis) to CIELAB data. Then, the CIELAB image data are converted to XYZ tristimulus image data using the CIE 2° observer and CIE illuminant D<sub>50</sub> with Equations 3 through 5 (for Y/Y<sub>n</sub> > 0.008856).

$$X = X_n \left( \frac{L^* + 16}{116} + \frac{a^*}{500} \right)^3 \quad (3)$$

$$Y = Y_n \left( \frac{L^* + 16}{116} \right)^3 \quad (4)$$

$$Z = Z_n \left( \frac{L^* + 16}{116} - \frac{b^*}{200} \right)^3 \quad (5),$$

where  $X_n$ ,  $Y_n$  and  $Z_n$  are the tristimulus values of the reference white ( $D_{50}$  in this case).

Unfortunately, the reflectances of the two gray cards used in this testing procedure had significantly different spectral reflectances, so their differences had to be compensated for in the system spatial uniformity evaluation procedure. First, their XYZ tristimulus values were calculated using the CIE 2° observer and CIE illuminant  $D_{50}$  with Equations 6 through 9.

$$X = k \sum_{\lambda} S_{\lambda} R_{\lambda} \bar{x}_{\lambda} \Delta\lambda \quad (6)$$

$$Y = k \sum_{\lambda} S_{\lambda} R_{\lambda} \bar{y}_{\lambda} \Delta\lambda \quad (7)$$

$$Z = k \sum_{\lambda} S_{\lambda} R_{\lambda} \bar{z}_{\lambda} \Delta\lambda \quad (8)$$

$$k = \frac{100}{\sum_{\lambda} S_{\lambda} \bar{y}_{\lambda} \Delta\lambda} \quad (9),$$

where  $S_{\lambda}$  is an illuminant,  $R_{\lambda}$  is the object's spectral reflectance factor,  $\bar{x}_{\lambda}$ ,  $\bar{y}_{\lambda}$ , and  $\bar{z}_{\lambda}$  are the CIE 2° observer color-matching functions,  $\Sigma_{\lambda}$  represents summation across wavelength,  $k$  is a normalizing constant, and  $\Delta\lambda$  is the measurement wavelength interval. Then, the image XYZ data (calculated using Equations 3 through 5) were divided by the XYZ tristimulus values for the gray card (calculated using Equations 6 through 9) from which each patch's average pixel data came from, and then rescaled by the mean Y tristimulus value of the two gray cards (calculated using Equations 6 through 9). If the

gray cards had had the same spectral reflectances, this step would not have been necessary.

The [corrected] image Y tristimulus value (luminance) data for each patch are then used to calculate a percent difference from the mean image Y tristimulus value of all 36 patches. Equation 10 was used for this calculation.

$$\%Diff = \left( \frac{(Y_p - Y_{mean})}{Y_{mean}} \right) * 100 \quad (10),$$

where  $Y_p$  is the patch Y tristimulus data and  $Y_{mean}$  is the mean Y tristimulus value of all 36 patches. These data, listed in Tables 7-I through 7-IV for CS1 through CS4 (a table for the CS0 data were not included because the data were negligible) in Appendix 7.1, can be visualized using a surface plot. Figure 14 shows this surface plot for CS0.

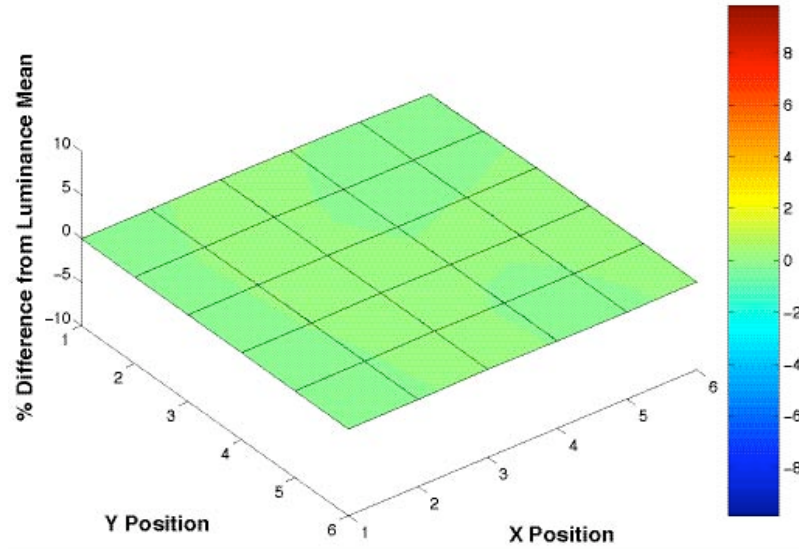


Figure 14. CS0 system spatial uniformity surface plot of % difference from luminance (Y) mean of gray card target.

The system spatial uniformity surface plot in Figure 14 shows that the gray card target image was almost perfectly uniform. This uniformity was achieved by mathematically doing a flat-fielding correction to the gray card target image in MATLAB (see section 3.4.2 for details on the flat-field correction).

The next part of the system spatial uniformity analysis is the comparison of the CIELAB data of each gray card patch to the mean CIELAB data of all 36 of the gray card patches. First, the [corrected] XYZ image tristimulus value data are converted back to CIELAB values using Equations 11 through 14.

$$L^* = 116\left(\frac{Y}{Y_n}\right)^{1/3} - 16 \quad (11)$$

$$a^* = 500\left[\left(\frac{X}{X_n}\right)^{1/3} - \left(\frac{Y}{Y_n}\right)^{1/3}\right] \quad (12)$$

$$b^* = 200\left[\left(\frac{Y}{Y_n}\right)^{1/3} - \left(\frac{Z}{Z_n}\right)^{1/3}\right] \quad (13)$$

$$C^*_{ab} = (a^{*2} + b^{*2})^{1/2} \quad (14)$$

Then,  $\Delta L^*$ ,  $\Delta a^*$ ,  $\Delta b^*$  and  $\Delta C^*_{ab}$  are calculated (patch – mean). Finally, both  $\Delta E^*_{ab}$  and CIEDE2000 ( $\Delta E_{00}$ ) color differences are calculated. The equation used to calculate  $\Delta E^*_{ab}$ , the most basic color difference equation, is shown in Equation 15.

$$\Delta E^*_{ab} = [(\Delta L^*)^2 + (\Delta a^*)^2 + (\Delta b^*)^2]^{1/2} \quad (15)$$

The equation used to calculate  $\Delta E_{00}$  is more complicated, but more precise, because it is optimized for color difference data that were observed by human observers. Its description and derivation are described in Luo (2001). These data are listed in Tables 7-

I through 7-IV for CS1 through CS4 (a table for the CS0 data was not included because the data were negligible) in the Appendix 7.1. The maximum  $\Delta E_{00}$  between the patches and the mean of all the patches, which is a mono-numeric metric that summarizes the case study's system spatial uniformity results, is listed in summary Table XIV for CS0 in section 3.11 and summary Table LXVIII for CS1 through CS4 in section 4.7.2. Figure 15 is a flowchart summarizing the system spatial uniformity analysis described in this section.

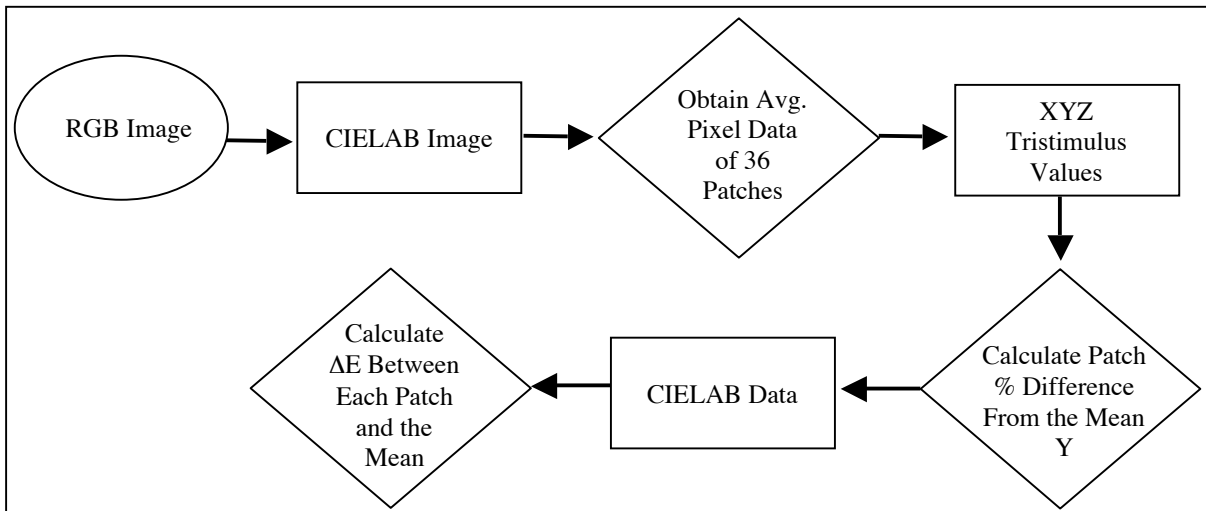


Figure 15. Flowchart of the system spatial uniformity analysis.

### 3.3 Tone Reproduction

The way that a digital camera reproduces tones in an image can be described using an opto-electronic conversion function, or OECF. The ISO has developed a standard (ISO 14524) that explains how to determine a digital camera's OECF. In ISO 14524, OECF is defined as the “relationship between log of input levels and corresponding digital output levels for an opto-electronic digital image capture system”

(ISO 14524, 1999). In this testing procedure, the input levels are in the form of luminance values. Because the OECF data, in the form of digital counts vs. normalized luminance units (0-1), are used in the analysis of other parts of this testing procedure, it was not necessary to report the luminance in log units, which is what is used in the ISO 14524 standard. A test chart, called the ISO OECF Test Chart, is described and used in the ISO 14524 standard to determine the OECF. This chart, which is shown in Figure 16, is also used in this testing procedure to determine the OECF. This chart was purchased at Sinepatterns located in Rochester, NY. It was printed on glossy photographic paper.

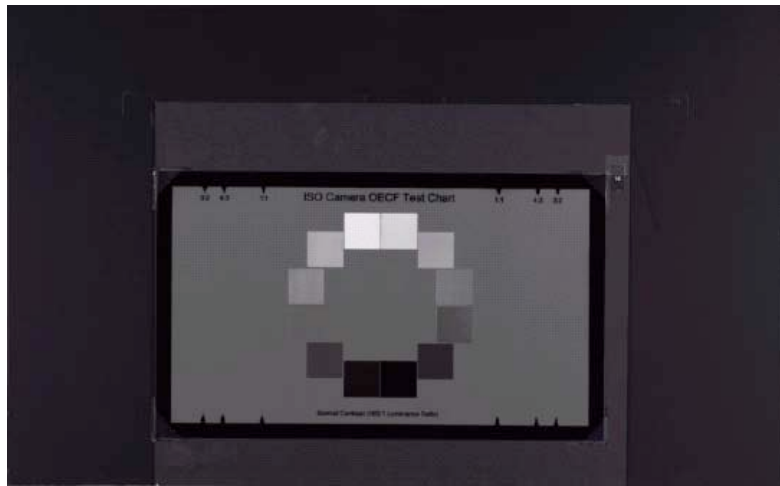


Figure 16. ISO OECF Chart target used to evaluate tone reproduction.

When this target is imaged, it should be in sharp focus. In this testing procedure, this target is imaged once at each of four different exposure levels (ISO 14524 recommends imaging the target nine times at each exposure level). The first image is taken at an exposure level so that the white patch of the target has an average digital count value that is maximum unclipped. The second exposure level is overexposed with

respect to the correctly exposed image, and the third and fourth images are each underexposed, with respect to the correctly exposed image, at different exposure levels. The OECF target is imaged at these four different exposure levels so that image data over the full range of possible digital count values, whether the image is 8-bit (0-255) or 16-bit (0-65535), is obtained. In other words, in the overexposed and underexposed images, some of the data should be clipped. Also, while the OECF target is still in the scene, its luminance should be measured with an instrument that is in the same position as the camera. In CS0, a PR650 spectroradiometer was used to measure the luminance of the 12 patches and the Halon, which was placed in the scene centered above the OECF target.

The analysis of the images and measured luminance data is as follows. First, the average red channel, green channel, and blue channel digital count values of each of the 12 patches and the Halon are obtained from each image. These values are then normalized (0 - 1) by dividing them by the maximum possible digital count value (255 for 8-bit or 65535 for 16-bit images). Next, the measured luminances that correspond to the overexposed and underexposed images are rescaled so that they correspond to the same measured luminances as the correctly exposed image normalized digital counts (DCs). This is accomplished using Equation 16 to calculate a luminance correction factor (LCF), which is multiplied by the measured luminance values.

$$LCF = \frac{t}{f - stop^2} * \frac{t_c}{f - stop_c^2} \quad (16),$$

where  $t$  is the exposure time of the image,  $f\text{-stop}$  is the f-stop of the image, and  $c$  stands for the correctly exposed image. Three one-dimensional OECF look-up tables (LUTs) are built from these data, which have normalized digital counts as input and luminance as

output. Then the DCs that have the same corresponding adjusted luminance values are averaged together. Next, clipped DC values, which are those above 0.95 normalized DCs and below 0, are discarded. Then, the effective maximum normalized DC value, which is  $\leq 0.95$  for each channel is determined. If the effective maximum DC is  $< 0.95$ , then DC values between the effective maximum value and 0.95 are set equal to the maximum luminance value that corresponds to the effective maximum DC . Finally, the points are linearly interpolated and extrapolated from 0 to 1 DCs and smoothed using first a smoothing kernel that is 0.1 DCs wide and a then a moving average (with endpoints replicated first) to form the final OECF LUT. The OECFs of the red, green and blue channels for CS0 are shown in Figure 17. In other parts of this testing procedure, the OECFs are used to linearize RGB digital count data. In order to use them later, the luminance data on the y-axis are also normalized from zero to unity by dividing the luminance by the maximum luminance value. A gamma curve can be fit to these LUT data for each channel using least squares. The gamma equation used to fit the LUT data is shown in Equation 17. The endpoints of the gamma fit were constrained to zero and one.

$$l = a * d^\gamma \quad (17),$$

where  $l$  is normalized luminance,  $d$  is normalized digital counts,  $a$  is a scaling constant (set equal to 1), and  $\gamma$  is gamma.

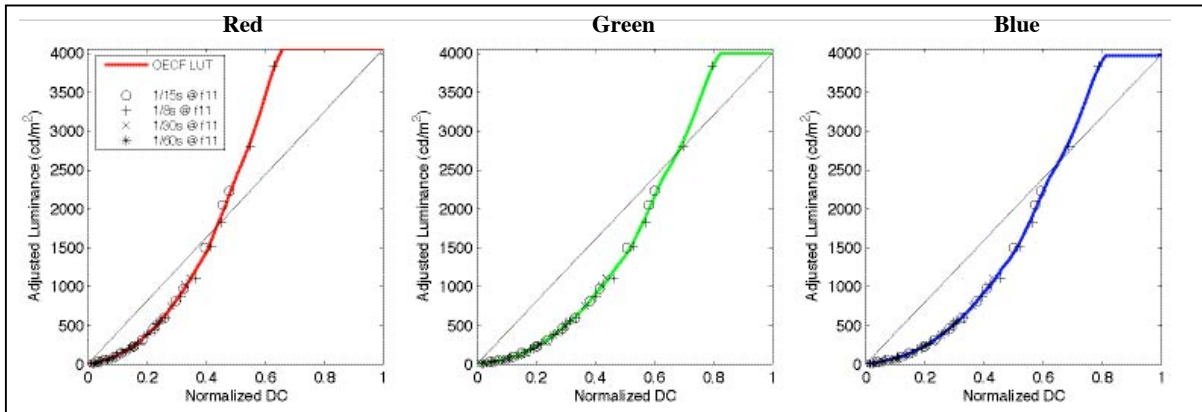


Figure 17. CS0 OECF curves.

The legend in Figure 17 shows the exposure times and aperture settings for the OECF images taken in CS0, with the nominal exposure at the top. These curves are flat on the top because the overexposed image did not include digital count values on that part of the curve ( $DCs >$  the effective maximum DC). In other words, only digital count values on the curved part of the OECFs were obtained from the image data. These data were sufficient when the OECFs were used to linearize data in other parts of the testing procedure, because none of the digital counts in those images were larger than the effective maximum normalized DC value. There was no gamma curve fit to these data because it did not include all of the normalized DC data from zero to unity. The mean gamma between the three color channels, which is a mono-numeric metric that summarizes the case study's OECF results, is listed in summary Table LXVIII for CS1 through CS4 in section 4.7.2. Tables 7-V through 7-IX in the Appendix 7.2 list the mean DCs for each exposure and the measured luminances for CS0 through CS4. Figure 18 is a flowchart summarizing the tone reproduction analysis described in this section.

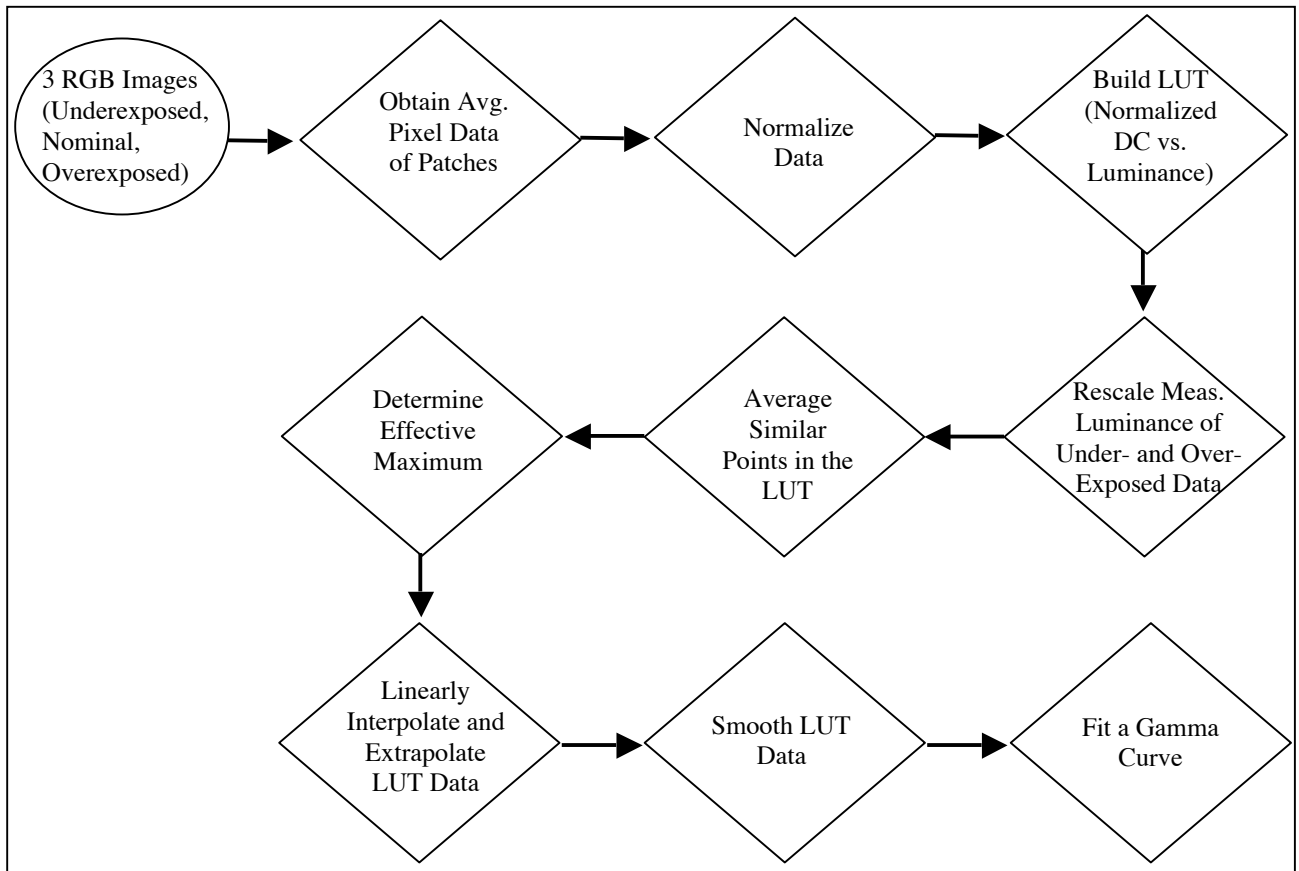


Figure 18. Flowchart of the tone reproduction analysis performed on each channel.

### 3.4 Color Reproduction Accuracy

In this testing procedure, color reproduction accuracy is tested using two different methods. One is a spectral sensitivity-based method and the other is a target-based method. The metamerism analysis is added as a tool to help with the visualization of the color reproduction inaccuracies of a digital imaging system.

### 3.4.1 Spectral Sensitivity

The spectral sensitivity of a digital imaging system is its fundamental ability to reproduce color. Most digital camera spectral sensitivities are not linear transformations of an average human visual system's spectral sensitivities. This is the fundamental limiting reason why color errors occur in digital image acquisition. Although camera manufacturers are aware of these inherent color inaccuracies, they still exist because of limitations in the production of the cameras and the trade-off between the improvements of color and the improvements of other image quality and cost parameters. Both the ISO 17321-1 standard and the IEC 61966-9 standard describe how the spectral sensitivity of a digital camera is measured.

In the spectral sensitivity evaluation part of this testing procedure, monochromatic light output from a monochromator instrument shown in Figure 19 was imaged.

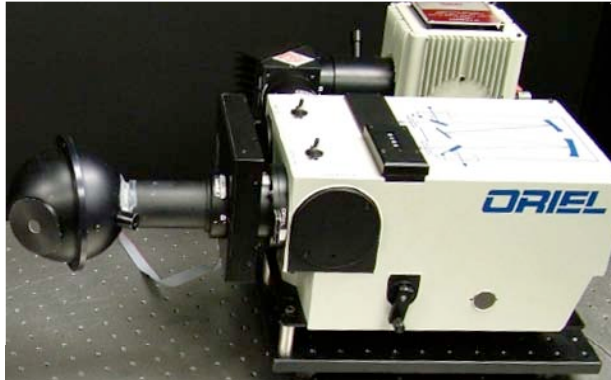


Figure 19. Monochromator instrument used to evaluate spectral sensitivity.

A schematic showing how this monochromator works is shown in Figure 20.

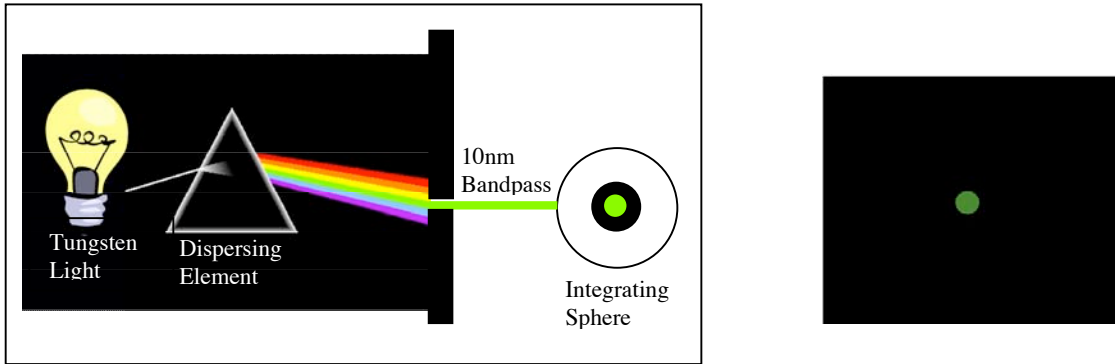


Figure 20. Schematic of how a monochromator works (left) and the resulting image taken with the camera (right).

Basically, tungsten light, after being passed through a series of lenses and reflected off of several mirrors, is spectrally dispersed with an adjustable diffraction grating, causing it to form a rainbow of colors. A series of slits allow only a 10nm spectral bandpass of light to pass into an integrating sphere. Before the approximately monochromatic light enters the integrating sphere, it is passed through a series of filters so that the radiance of the range of bandpasses from 380nm to 730nm is approximately equal. Thus, the full bandpass range can be imaged using only one camera exposure setting. The integrating sphere causes the output light to be diffuse. The voltage of the power supply of the monochromator used in the imaging procedure was held constant at 12V. The current and wattage varied by an insignificant amount at any given time that the monochromator was imaged in the case studies.

In the imaging procedure, the camera was focused on the opening of the monochromator's integrating sphere. The light was hitting only a small central area of the camera's sensor. It would have been more desirable to fill the entire image area with the monochromator light or image the monochromatic light at different locations on the sensor, but this was not possible given the size of the integrating sphere and the amount

of time that it took to image the monochromator in the imaging procedure. Because the light output of the monochromator was exceedingly low, when it was imaged, the aperture of the lens was opened up all of the way. The aperture setting in CS0 was f/4. The exposure time was determined so that when the monochromator's bandpass peak wavelength was set to approximately 450nm, a digital count value of at least 50% of the maximum value was obtained. In CS0, the ISO speed setting was increased from 25 to 50 in order to increase the sensitivity. The exposure time was determined to be 1s. and the integration time was also set to 1s. After the exposure settings were determined, the monochromator instrument was imaged 36 times from bandpass peaks of approximately 360nm to 730nm in 10nm increments. After the images were taken, the radiance of the monochromator output for the same bandpass peaks were measured with a PR650 spectroradiometer.

The image and radiance data are analyzed as follows. First, the RGB digital count values of the spot of light are averaged for each image. Then, these data are linearized by applying the inverse OECF curve. In CS0, the OECF curves shown in Figure 17 were used. In the museum case studies, the OECF curves, which were determined from the OECF target image that was imaged at the same non-color-managed settings as the monochromator, were used to linearize the monochromator image DC data. These linearized data for CS0 is shown in the plot on the left of Figure 21. Next, the actual peak radiance wavelengths are determined as the wavelength corresponding the maximum radiance from each measured spectral radiance curve. The summed spectral radiances are plotted against wavelength in the plot on the right in Figure 21.

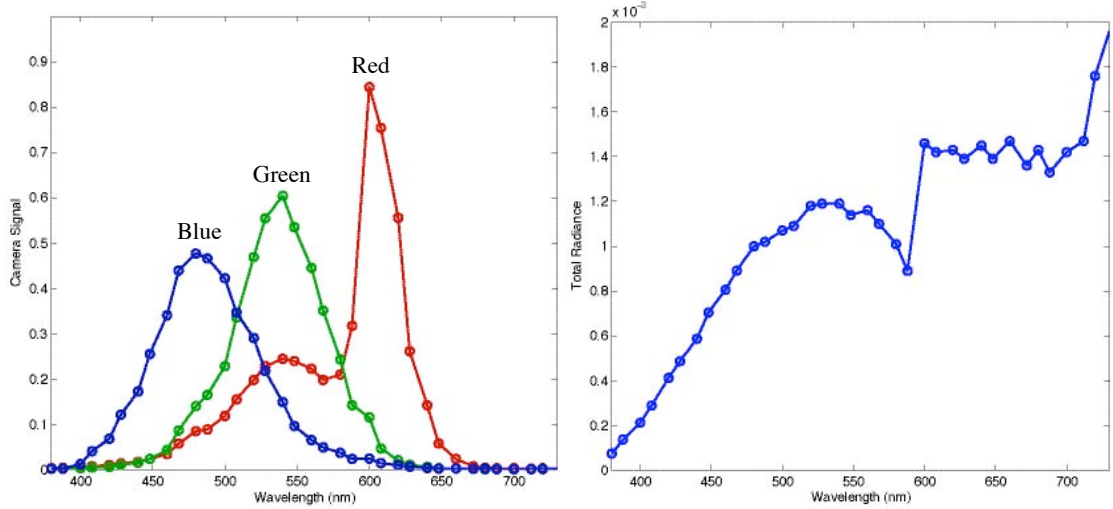


Figure 21. CS0 wavelength vs. RGB linearized average camera digital count values from monochromator images (left) and wavelength vs. the sum of the measured spectral radiances in  $\text{W}/\text{sr}^*\text{m}^2$  (right).

The linearized digital count values are then divided by the radiance to obtain relative spectral sensitivities. The maximum relative spectral sensitivity values are normalized so that the maximum relative sensitivity is unity. The relative spectral sensitivity results for CS0 are shown in the left plot of Figure 22. These relative spectral sensitivities are those of the camera (the affect of the lens' spectral transmittance on spectral sensitivity is assumed to be negligible) combined with the IR filters.

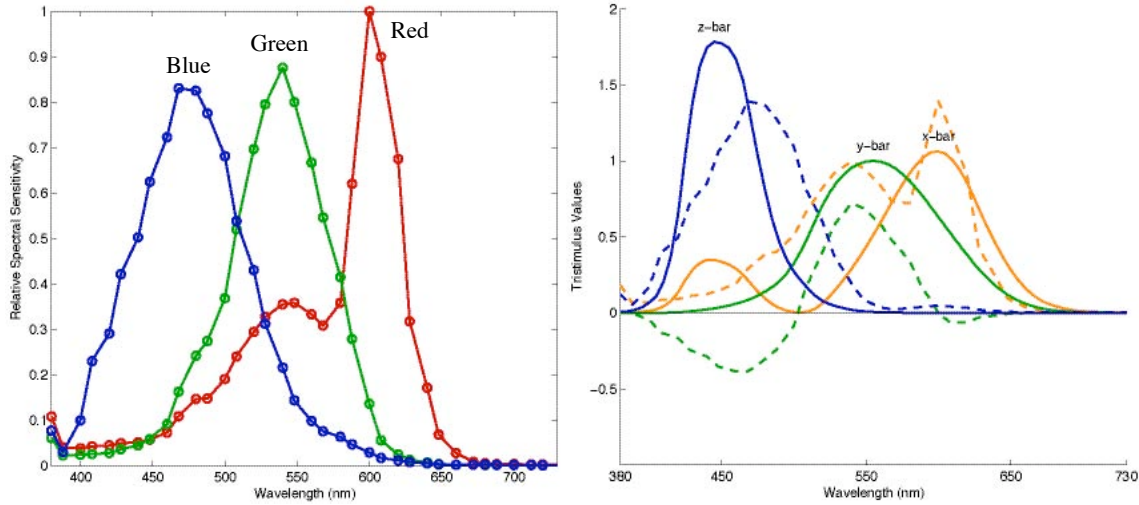


Figure 22. CS0 relative spectral sensitivities (left) and relative spectral sensitivities (dotted line) rotated to fit the CIE 2° observer (right).

The plot on the right of Figure 22 shows the relative spectral sensitivity curves rotated to fit the CIE 2° observer color-matching functions. Equations 18 and 19 are used to perform the prediction of the CIE 2° observer color-matching functions,  $cmf_{est}$  using a linear transformation.

$$cmf_{est} = SS * cmf^T * SS^+ \quad (18)$$

$$SS^+ = (SS^T * SS)^{-1} * SS^T \quad (19),$$

where  $SS$  is the matrix of the relative spectral sensitivity data,  $cmf$  is the CIE 2° observer color-matching functions, and  $SS^+$  is the pseudoinverse of  $SS$ .

The lack of fit of the relative spectral sensitivities to the CIE 2° observer color-matching functions can be described by the shifts in peak sensitivity wavelengths, different sensitivity levels at the peaks, negative lobes, and more overlap between the channels. The goodness of fit of the relative spectral sensitivities to the CIE 2° observer color-matching functions, given a specific taking illuminant and viewing illuminant, can

be evaluated using a quality metric,  $\mu$ -factor (Vora, 1993). Equations 20 through 22 are used to determine  $\mu$ -factor.

$$\mu\text{-factor} = \frac{\text{Trace}(S^T * A * (A^T * A)^{-1} * A^T * S * (S^T * S)^{-1})}{3} \quad (20)$$

$$S = \text{diag}(\text{illum}_{,t} * SS) \quad (21)$$

$$A = \text{diag}(\text{illum}_{,v} * cmf) \quad (22),$$

where  $SS$  is the relative spectral sensitivities,  $\text{illum}_{,t}$  is the taking illuminant,  $\text{illum}_{,v}$  is the viewing illuminant, and  $cmf$  is the CIE 2° observer color-matching functions (Quan, 2002). The  $\mu$ -factor quality metric can range in values from zero to one, where a value of one means that the spectral sensitivities are a perfect match to the color-matching functions, or a linear combination of them, and a value of zero means that they do not match. In other words, if a set of spectral sensitivity curves provide a  $\mu$ -factor of one, the camera is colorimetric, which means that it “sees” color in the same way as the standard observer. A  $\mu$ -factor value of at least 0.90 is desirable for a digital camera used to image cultural heritage. The  $\mu$ -factor results for CS0 are shown in Table V. In the first row, both the effects of the taking illuminant and the camera’s spectral sensitivities on  $\mu$ -factor are taken into account. In the second row, only the effect of the camera’s spectral sensitivities are taken into account. In the third row, only the effect of the taking illuminant is taken into account. In the fourth row, neither the taking illuminant nor the spectral sensitivities are taken into account in the  $\mu$ -factor determinations.

Table V. CS0  $\mu$ -factor results.

<u>Detector</u>	<u>Color Matching Functions</u>	<u>Taking Illuminant (Measured CCT)</u>	<u>Viewing Illuminant</u>	<u><math>\mu</math>-Factor</u>
Camera CIE 2° Observer	CIE 2° Observer	HMI (5026K)	$D_{50}$	0.84
		$D_{50}$		0.85
		HMI (5026K)		0.91
		$D_{50}$		1.00

The  $\mu$ -factor results in CS0 show that the digital imaging system as a whole, produced a  $\mu$ -factor of 0.84, which is slightly less than the desired  $\mu$ -factor. There is only a slight improvement in the  $\mu$ -factor when the taking illuminant is not taken into account. The effect of just the taking illuminant further increases the  $\mu$ -factor. The  $\mu$ -factor in the first row, which is a mono-numeric metric that summarizes the case study's spectral sensitivity results, is listed in summary Table XIV for CS0 in section 3.11 and in summary Table LXVIII for CS1 through CS4 in section 4.7.2.

The plot in Figure 23 shows how  $\mu$ -factor correlates with average  $\Delta E^*_{94}$ , which is a color difference metric that is more precise than  $\Delta E^*_{ab}$ , but less precise than  $\Delta E_{00}$ . This plot shows that  $\mu$ -factor is roughly linearly related to average  $\Delta E^*_{94}$  if  $\mu \geq 0.95$ . However, color imaging devices with poor  $\mu$ -factor may still generate satisfactory color reproduction (Quan, 2002).

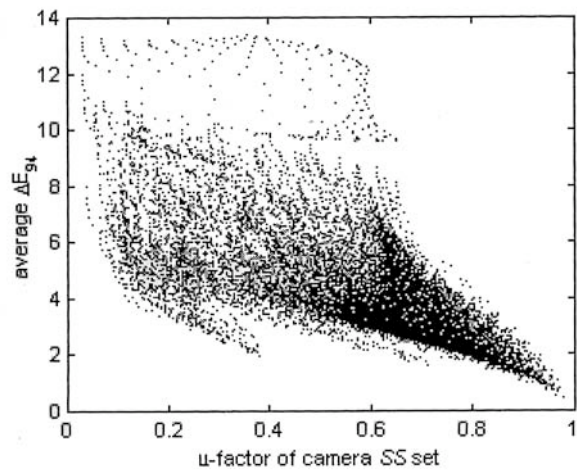


Figure 23. Relationship between  $\mu$ -factor and average color difference ( $\Delta E^*_{94}$ ) between reference and estimation of an ensemble of reflectance spectra (Quan, 2002).

Figure 24 is a flowchart summarizing the tone reproduction analysis described in this section.

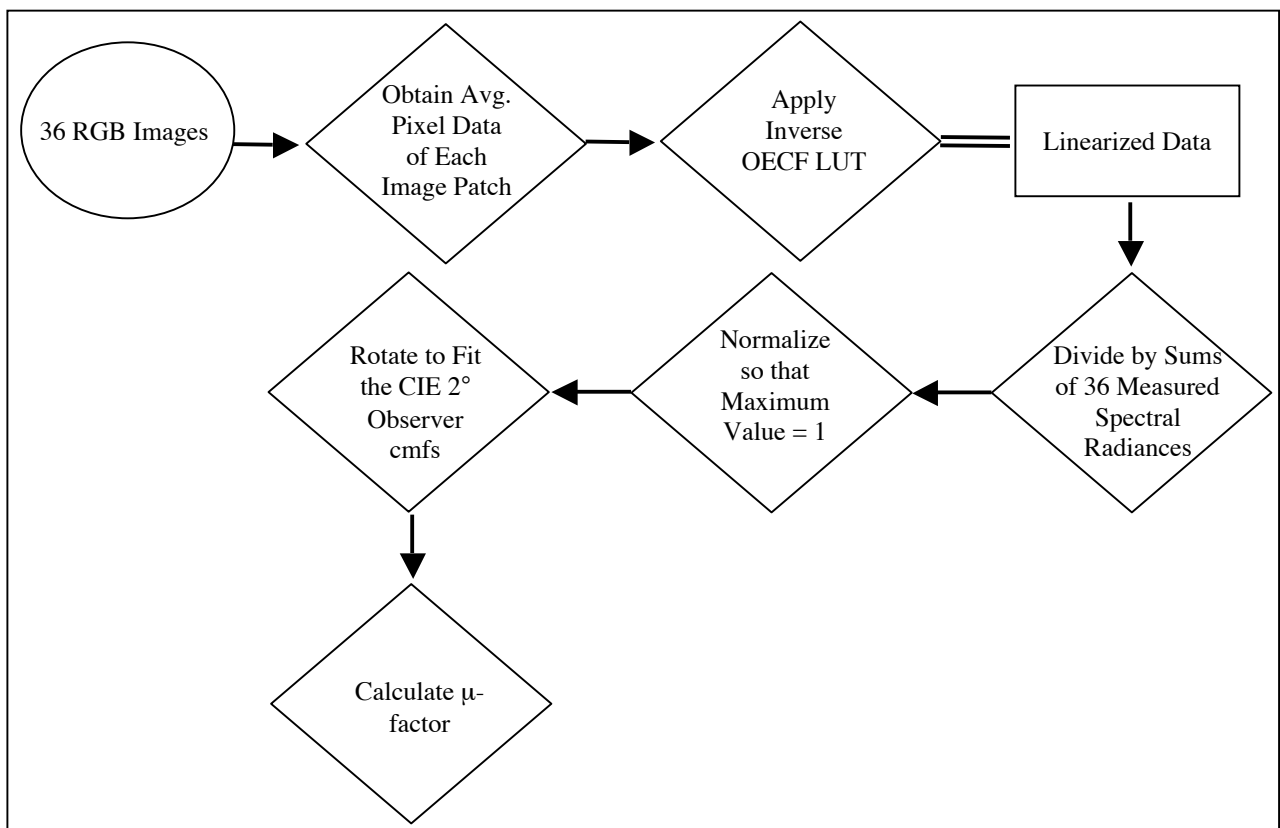


Figure 24. Flowchart of the spectral sensitivity analysis.

### 3.4.2 Target-based Color Reproduction Accuracy

The target-based method of characterizing a digital camera's color reproduction accuracy is more practical for a typical camera user to perform than the camera's spectral sensitivity analysis. The ISO 17321-1 standard describes how the target-based method can be used to evaluate a digital camera's color reproduction capabilities. It is recommended that a color target used to characterize the color reproduction accuracy of a digital camera be made of the same materials as those that are being imaged with the camera. In the case of this research, the target colors should be in the form of painted

samples. It is further recommended that these target color paint samples be created with the same pigments as those used in the paintings, if possible.

In this testing procedure, three targets consisting of eight color target charts were used to characterize the color reproduction accuracy of the digital cameras. These color reproduction accuracy charts were made up of different materials and pigments. Some included painted samples and some did not. This large number of targets was used in this testing procedure for two reasons. The first reason was to enable an analysis of the way that a digital camera reproduces the color of different materials. Second, during the literature review, it was found that there were different types of charts being used at the cultural heritage institutions, so most of these targets were included. Practically, only one target, which includes colors and pigments that are representative of the objects being imaged by the digital camera, is necessary to use for a target-based color reproduction accuracy evaluation.

Figures 25, 26, and 27 show the three targets that include eight color reproduction accuracy charts. The target shown in Figure 25 consists of four of the color reproduction accuracy charts. The GretagMacbeth ColorChecker® (CC) is a commercial chart with 24 painted color and grayscale patches. The Esser TE221 Test Chart (consisting of Esser and Esser Grayscale), which is described in IEC 61966-8 as a flatbed scanner calibration chart, has 264 patches made up of 12 different printing inks. The Blue Pigments chart has seven patches consisting of pure cobalt blue pigment and cobalt blue pigment mixed with both white and black pigment. This chart was included in this part of the testing procedure because cobalt blue reflects a significant amount of light in the longer wavelength part of the visible spectrum and, therefore, is harder to reproduce

with digital cameras, especially those that are very sensitive to longer wavelengths. See Figure 46 in section 4.1 for a percent reflectance curve of cobalt blue pigment. None of the commercial targets include this pigment, so this chart was produced in MCSL. The Pigment chart, also produced in MCSL, was made up of the 11 Gamblin Artist's Oil Colors that were in the paintings, which were used in the four museum case studies, CS1 to CS4, to evaluate the colorimetric accuracy of their digital imaging workflows (see section 4.1). All 11 pigments in this chart, except the Titanium White, were painted using both pure pigment and mixed with the Titanium White, yielding 21 patches. The Davidson and Hemmendinger (D&H) Color Rule was used in the metamerism (see section 3.4.3) part of the color reproduction accuracy evaluation.

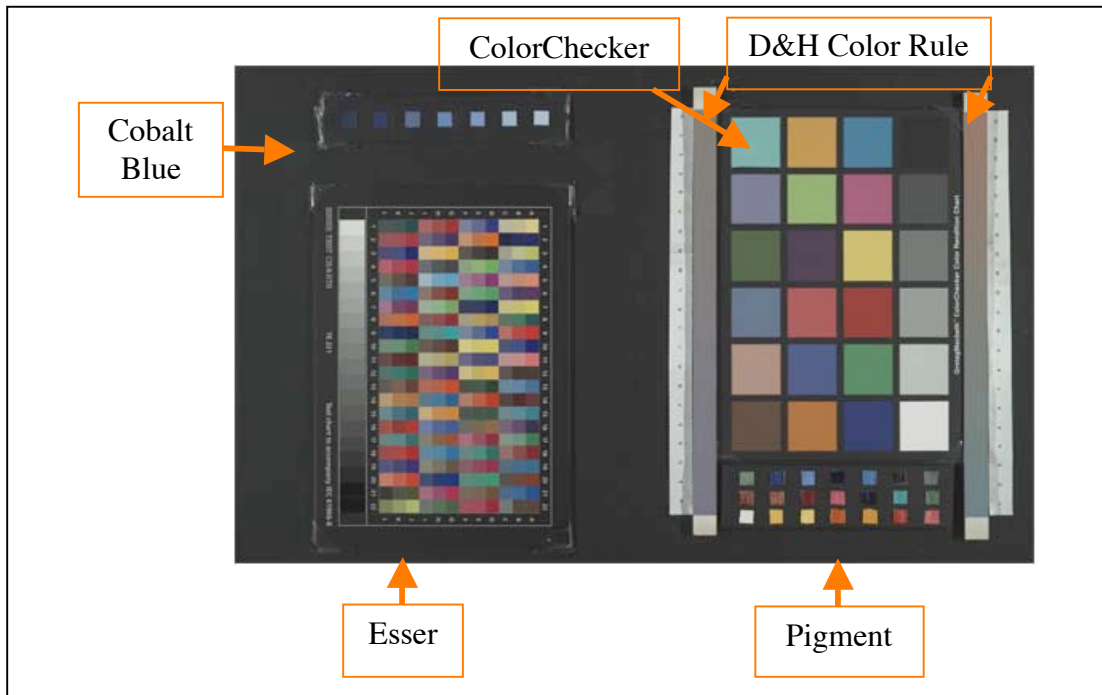


Figure 25. Target consisting of Cobalt Blue Pigments, Esser, Macbeth ColorChecker, D&H Color Rule, and Pigment charts, which were used to evaluate color reproduction accuracy (target-based or metamerism). Pigment chart was not available for CS0. The Macbeth ColorChecker chart was also used to evaluate color noise.

The target shown in Figure 26 consists of three more of the color reproduction accuracy charts. The GretagMacbeth ColorChecker DC® (CCDC) is a commercial chart with 240 painted color and grayscale patches. The patches of the Kodak Q-13 chart (consisting of 18 Kodak Color Separation and 20 Kodak Grayscale patches) were made using automobile paint applied to a coated paper substrate (Myers, 2002). The IT8.7/2 chart consists of 264 color and 24 grayscale patches. This chart was designed for the purpose of calibrating flatbed scanners. The one used in this testing procedure was printed on glossy Fuji photographic paper. Kodak also makes an IT8.7/2 standard chart called the Q-60 chart.

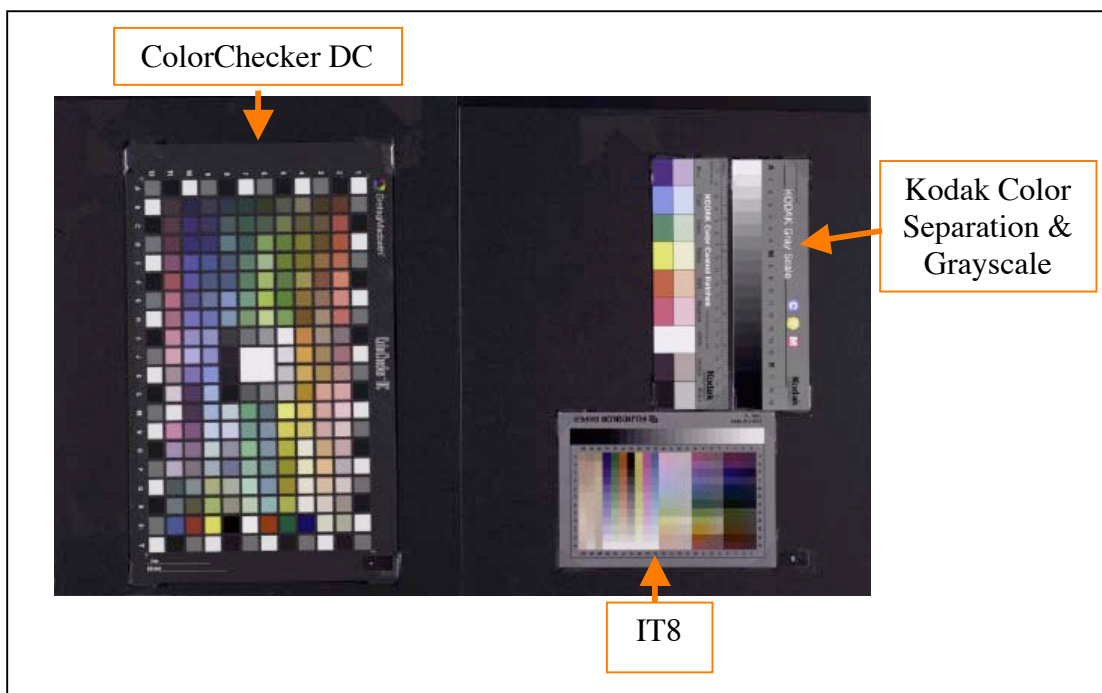


Figure 26. Target consisting of Macbeth ColorChecker DC, Kodak Color Separation & Grayscale, and IT8 charts, which were used to evaluate target-based color reproduction accuracy.

The target shown in Figure 27 consists of the eighth color reproduction accuracy chart. This chart is made up of 13 glossy ceramic tiles called BCRA tiles (British Ceramic Research Association), which are standards used for the calibration of spectrophotometers.



Figure 27. BCRA target used to evaluate target-based color reproduction accuracy.

The spectral reflectances of all of the color reproduction accuracy charts described above were measured with a GretagMacbeth ColorEye XTH hand-held integrating sphere spectrophotometer from 360nm to 750nm in 10nm intervals after calibration of the instrument. Three measurements were averaged using the small area of view, which has a 5mm circular diameter illumination area and a 2mm circular diameter measurement area. This area of view was chosen because it was needed to measure the small patches of the IT8 target and it was kept consistent for all of the targets. The specular component was excluded for these measurements.

In the imaging procedure, each of the three targets should be imaged once in sharp focus. They should all be imaged at the same exposure, which causes the brightest patch to have a digital count value that is maximum unclipped. In CS0, these targets were imaged at an exposure time of 1/15s. an integration time of 1/2s. and an aperture of f/11.

The color targets were evaluated using two different methods in CS1, CS2, CS3, and CS4. The first method involves comparing the profiled CIELAB images directly to measured spectral reflectance and the second method involves comparing the RGB images, which were first flat-fielded and then converted to CIELAB images using a simple optimized transformation (profile) performed in MATLAB, to measured spectral reflectance. In CS0, only the second method was used, because there were no profiles embedded in the images. The two color target evaluation methods are described in detail next.

In the first evaluation method, for the profiled images in CS1 through CS4, the RGB image of each of the three targets is first opened in Adobe Photoshop® (the profile that is embedded with the image is used when the image is opened) and converted from an RGB image to an Lab image. The Lab image is saved and its data are used in this evaluation method. In MATLAB, first the average values of each of the color patches are obtained from each image. Then this Lab image data are converted from ICC Lab data to CIELAB data. Using Equations 6 to 9, the XYZ tristimulus values of the measured spectral reflectance data of each patch are calculated using the CIE 2° observer and CIE illuminant D<sub>50</sub>. Then Equations 11 to 13 are used to calculate the CIELAB data of the measured data. The white point used for this calculation was illuminant D<sub>50</sub>. For CS1 to

CS4, the CIELAB image data was compared to the measured CIELAB data using both  $\Delta E^*_{ab}$ , shown in Equation 15, and  $\Delta E_{00}$ . Next, in order to decrease the effect of the lightness errors in the color difference calculation caused by the exposure level of the image, it was necessary to also compare the image CIELAB data to the measured data after correcting for this lightness difference. The lightness correction was made by first calculating XYZ tristimulus values from the CIELAB image data using Equations 3 to 5 using illuminant D<sub>50</sub> as the white point. This was repeated for the Halon, which was included in the images, CIELAB image data. Then the Y tristimulus image values were divided by the Y tristimulus Halon values. CIELAB values were then calculated from these new XYZ tristimulus image values. This normalized each image so that the Halon was equal to an L\* value of 100. Finally, the lightness corrected CIELAB image data was compared to the measured CIELAB data (the CIELAB values of the Halon, using its measured data, the CIE 2° observer and CIE illuminant D<sub>50</sub>, were L\* = 99.17, a\* = 0.09, and b\* = -0.01) using both  $\Delta E^*_{ab}$ , shown in Equation 15 and  $\Delta E_{00}$ . The first evaluation method is outlined in the flowchart in Figure 28.

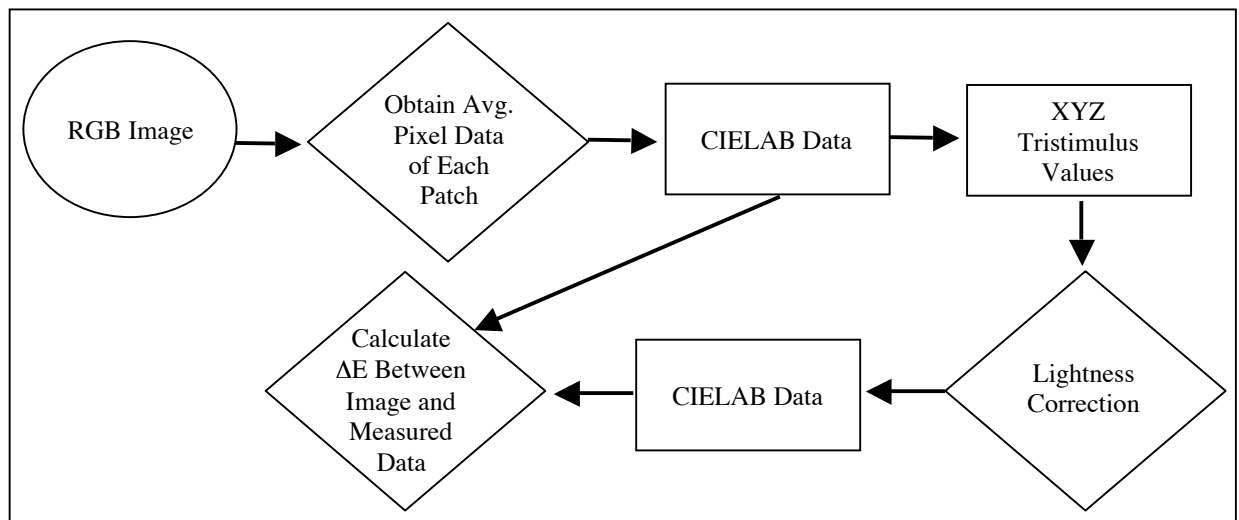


Figure 28. Flowchart of the target-based color reproduction accuracy first evaluation method.

In the second evaluation method, the RGB image digital count value data was used. First, using these image data, the inverse OECF look-up table was applied to each channel to photometrically convert the digital count values into normalized linear values. In order to convert the linear image data from RGB to XYZ, a flat-field correction must first be performed and a transformation must be created. Because a flat-field correction is also applied during the creation of the transform, details about how it is applied will be described in the explanation of how the transform is created, next.

A simple 3x3 matrix transformation is created to convert linearized digital counts into XYZ tristimulus values in order to determine whether an improvement (a smaller color difference) of this conversion could be achieved over what the profiles used by the digital cameras/image-capture software were achieving. The CCDC chart was chosen as the characterization chart for the creation of this transform in all cases where this transform was used in this testing procedure. First, the average RGB values of each of

the color patches of the CCDC chart image are obtained. Then these values are linearized using the inverse OECF. Next, they are flat-fielded. A flat-field correction is performed using the average of the two gray card target images taken in the imaging procedure. Equation 23 is used for the flat-field calculation for each color channel.

$$DC_{ff} = \left( \frac{DC_{image}}{DC_{gray}} \right) * \overline{DC}_{gray} \quad (23),$$

where  $DC_{image}$  is the linearized digital counts of the patch data in the image,  $DC_{gray}$  is the linearized digital counts of the gray card data that are located in the same place as the patch data, and  $\overline{DC}_{gray}$  is the mean linearized digital counts of all of the gray image data patches. Using Equations 6 to 9, the XYZ tristimulus values of the measured spectral reflectance data of each patch of the characterization chart, the CCDC chart, are calculated using the CIE 2° observer and CIE illuminant D<sub>50</sub>. The transformation is initially created using Equation 24 in order to minimize the root mean square of the error between the image data and the measured data.

$$T_{3x3} = XYZ_{meas} * RGB_{image}^+ \quad (24),$$

where  $XYZ_{meas}$  is the matrix of tristimulus values of the measured patches of the characterization chart and  $RGB_{image}^+$  is the pseudoinverse of the matrix of flat-field corrected linearized characterization chart image RGB data (see Equation 19 for the pseudo-inverse equation). Then this transform is further optimized iteratively by minimizing the mean ΔE<sub>00</sub> between the measured data XYZ tristimulus values and the image data XYZ tristimulus values that are estimated using Equation 25.

$$XYZ_{est} = T_{3x3} * RGB_{image} \quad (25)$$

In the second evaluation method, Equation 23 is used to flat-field the linearized image RGB data for the patches of each chart. In this case,  $DC_{gray}$  is the linearized (using inverse OECF) digital counts of the gray card data that are located in the same place as the chart image patch data, and  $\bar{DC}_{gray}$  is the mean linearized (using inverse OECF) digital counts of all of the gray image data patches that were located in the same place as the characterization chart image patch data used to build the transform. This is done to ensure that the data for each color reproduction accuracy chart image is scaled by the same amount. Then Equation 25 is used to convert these linearized flat-fielded data to XYZ tristimulus values. Because the reflectances of the two gray cards used in this testing procedure had significantly different spectral reflectances, if the gray card that was placed in the same position as the chart being evaluated was different than the one placed in the same place as the characterization chart during the imaging procedure, then a compensation was made. This was performed by multiplying the XYZ tristimulus values of the gray card (calculated using Equations 6 to 9 with the CIE 2° observer and CIE illuminant D<sub>50</sub>), which was placed in the same position as the chart being evaluated in the imaging procedure, by the XYZ tristimulus values of the linearized flat-fielded data of the image chart being evaluated. Next, using Equations 6 to 9, the XYZ tristimulus values of the measured spectral reflectance data of each patch are calculated using the CIE 2° observer and CIE illuminant D<sub>50</sub>. Then Equations 11 to 13 are used to calculate the CIELAB data of both the measured data and the image data XYZ tristimulus values. The white point used for this calculation was illuminant D<sub>50</sub>. Finally, the CIELAB image

data are compared to the measured CIELAB data using both  $\Delta E^*_{ab}$ , shown in Equation 15 and  $\Delta E_{00}$ . The second evaluation method is outlined in the flowchart in Figure 29.

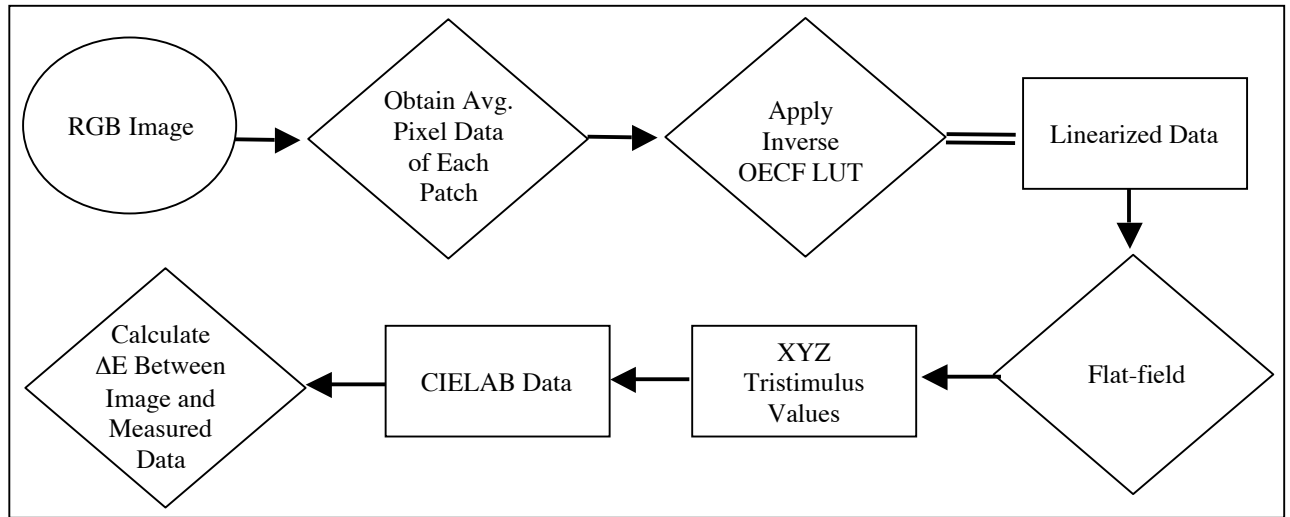


Figure 29. Flowchart of the target-based color reproduction accuracy second evaluation method.

In CS1 to CS4, the first evaluation method was used to evaluate all eleven of the color reproduction accuracy charts and the second evaluation method was used to evaluate both the CCDC, which are dependent data because it was used to build the transform, and the CC, which are independent (verification) data. In CS0, because there were no profiles embedded in the images, only the second evaluation method was used to evaluate ten of the eleven color reproduction accuracy charts. The Pigment chart shown in Figure 25 was not used in CS0. The results of CS0 are shown below.

In Figure 25, the CIELAB error vector plots are shown between the measured patch data and the image patch data of the Macbeth ColorChecker determined using the second evaluation method.

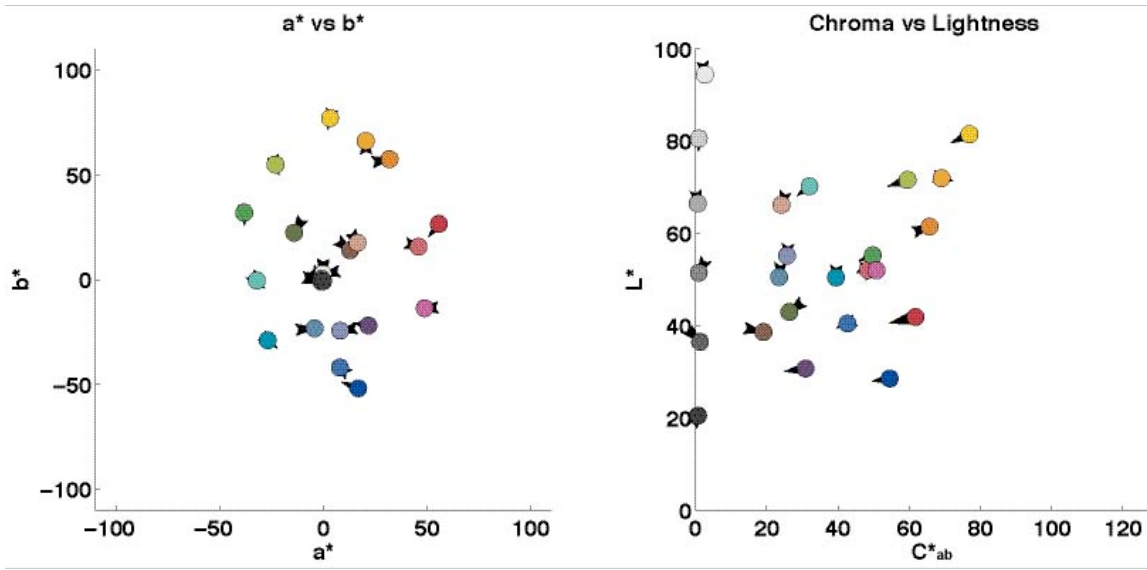


Figure 30. CS0 CIELAB  $a^*$  vs.  $b^*$  (left) and  $C^*_{ab}$  vs.  $L^*$  (right) error vector plots of the Macbeth ColorChecker between the measured patch data (dot) and the image patch data (point of vector arrow) determined using the second evaluation method with the CCDC as the characterization chart used to build the 3x3 transform.

In this type of plot, the longer the error vectors, the greater the error. Some general trends that can be found in this type of plot are as follows. In the  $a^*$  vs.  $b^*$  plot on the left, if the vector arrows are systematically pointing in toward the origin at the center of the plot, then the image data are less chromatic (more neutral) than the measured data and vice versa if the arrows are pointing away from the origin. Arrows in other directions denote a hue change. Errors in lightness are not considered in this plot, but they are in the  $C^*_{ab}$  vs.  $L^*$  plot on the right (see Equation 14 for the calculation of  $C^*_{ab}$ ). General trends that can be found in this type of plot are as follows. If the vector arrows are systematically pointing upward, then the image data are lighter than the measured data and vice versa if the arrow is pointing downward. If the vector arrows are systematically pointing to the right, then the image data are more chromatic than the measured data (equivalent to if the arrows in the  $a^*$  vs.  $b^*$  plot are pointing directly outward from the

origin), and vice versa if the arrow is pointing to the left. In CS0, the plots in Figure 30 show that the errors are very small and there are no general trends in the data.

Figure 31 is a histogram of the  $\Delta E_{00}$  error distributions of the Macbeth ColorChecker for CS0, which was evaluated, again, using the second evaluation method.

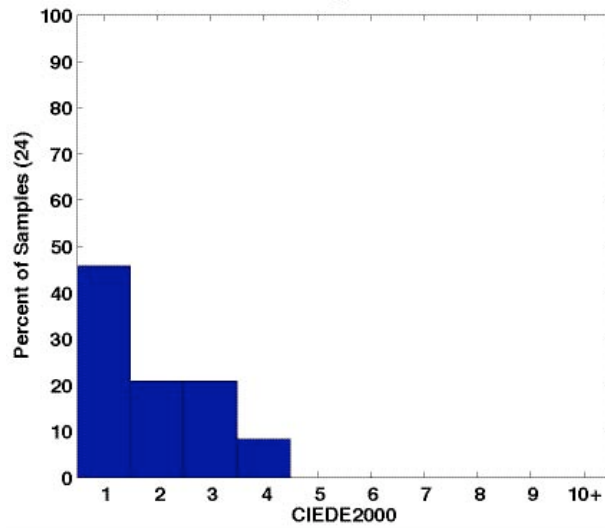


Figure 31. CS0 histogram of the  $\Delta E_{00}$  error distributions of the Macbeth ColorChecker between the measured patch data and the image patch data determined using the second evaluation method with the CCDC as the characterization chart used to build the 3x3 transform.

This graph shows that, since most of the error bars are on the left side, the errors are relatively low. In Table VI, the mean, standard deviation and the 90<sup>th</sup> percentile (at least 90% of the errors take this value or less and at least 10% of the errors take this value or more) data are given for the  $\Delta E^*_{ab}$  and  $\Delta E_{00}$  data between the measured patch data and the image patch data for each color reproduction accuracy chart in CS0.

Table VI. CS0 mean, standard deviation, and 90<sup>th</sup> percentile of the  $\Delta E^*_{ab}$  and  $\Delta E_{00}$  data between the measured patch data and the image patch data for each color reproduction accuracy chart determined using the second evaluation method with the CCDC as the characterization chart used to build the 3x3 transform.

<u>Color Reproduction Accuracy Chart</u>	<u><math>\Delta E^*_{ab}</math></u>			<u><math>\Delta E_{00}</math></u>		
	<u>Mean</u>	<u>Std. Dev.</u>	<u>90<sup>th</sup> Perc.</u>	<u>Mean</u>	<u>Std. Dev.</u>	<u>90<sup>th</sup> Perc.</u>
ColorChecker DC	3.15	2.79	6.79	1.92	1.25	3.68
ColorChecker	3.93	2.32	7.77	2.31	1.02	3.72
Esser	3.96	2.53	7.28	2.45	1.53	4.03
Esser Grayscale	1.63	0.77	2.98	1.87	0.92	3.54
BCRA	4.65	3.54	9.89	2.58	1.49	4.81
Blue Pigments	4.50	1.02	5.47	3.27	0.74	4.00
Kodak Color Separation	3.75	2.10	6.55	2.50	1.28	4.18
Kodak Grayscale	1.86	0.74	2.98	1.79	0.74	2.89
IT8	3.80	1.88	6.23	2.52	1.27	4.14
IT8 Grayscale	3.22	1.12	5.00	3.43	1.56	5.86
Mean	3.45	1.88	6.09	2.46	1.18	4.09

What can be seen from this table is that, for the most part, there is an improvement in the color difference between  $\Delta E^*_{ab}$  and  $\Delta E_{00}$ . This is because  $\Delta E_{00}$  is a color difference metric that more accurately computes color differences that relate to what human observers see. With either color difference metric,  $\Delta E^*_{ab}$  or  $\Delta E_{00}$ , the lower the number the better. Stokes, Uroz, and Song have performed studies evaluating the color difference

of complex images (Stokes, 1991, Uroz, 2001, Song, 2000). The results of their studies roughly showed that a  $\Delta E^*_{ab}$  value of approximately 2.00 is perceptible when the color error is not caused by systematic errors (vector directions) in hue, lightness, and chroma, which can be seen in the CIELAB error vector plots in Figure 30. A  $\Delta E^*_{ab}$  value of approximately 4.00-6.00 is acceptable. The mean  $\Delta E^*_{ab}$  color difference of the color target images that is desirable for high quality digital imaging is 2.00 without any systematic errors. The overall color reproduction accuracy of CS0 is good, but not desirable, and there are minimal systematic errors.

In CS0, looking at the  $\Delta E_{00}$  data, the color reproduction accuracy of the Esser Grayscale chart was the most accurate. The IT8 Grayscale chart was reproduced the least accurately, followed by the Blue Pigments and BCRA charts. It is preferred, since this testing procedure is geared toward imaging paintings, that the Macbeth ColorChecker DC, the Macbeth ColorChecker the Blue Pigments, and the Pigment Target charts are reproduced the most accurately. In this case, the CCDC and CC charts were reproduced intermediary in accuracy compared to the other charts. The Blue Pigments chart was not reproduced very accurately in comparison to the other charts. The 90<sup>th</sup> percentile of the mean  $\Delta E_{00}$  of all of the color reproduction accuracy charts, which is a mono-numeric metric that summarizes the case study's color reproduction accuracy results, is listed in summary Table XIV for CS0 in section 3.11 and in summary Table LXVIII for CS1 through CS4 (the normalized CIELAB image data, where the Halon L\* = 100, which were determined in the first target-based color reproduction accuracy method, was used) in section 4.7.2.

### **3.4.3 Metamerism**

Metamerism occurs when spectrally different stimuli match to a given observer under a given light source (Berns, 2000). There are two types of metamerism. The first is observer metamerism, where two spectrally different stimuli viewed under the same light source match to one observer, but don't match to another observer. The second type, illuminant metamerism, occurs when two spectrally different stimuli viewed under one light source by a single observer match, but when the light source is changed, they don't appear to match. In this testing procedure, a metameric pair is found through the use of a tool called the Davidson & Hemmendinger (D&H) Color Rule, and only observer metamerism is evaluated. It is included in the target shown in Figure 25. Figure 32 also shows what the D&H Color Rule looks like. It consists of two strips of colors, one labeled alphabetically and one labeled numerically. When placed behind a mask (see Figure 32) with only one color of each strip showing at a time, these two color strips can be slid back and forth by an observer under a light source until the best match is made. In each case study, including CS0, this best match was made by the photographer under the taking illuminant (in CS3, it was made under the fluorescent viewing illuminant, because Xenon strobes were used as the taking illuminant).



Figure 32. Image of Davidson & Hemmendinger (D&H) Color Rule.

The 42 colors of the D&H Color Rule were measured with the GretagMacbeth ColorEye XTH spectrophotometer in the same way as the color reproduction accuracy charts. Figure 33 shows the plots of those spectral reflectance measurements.

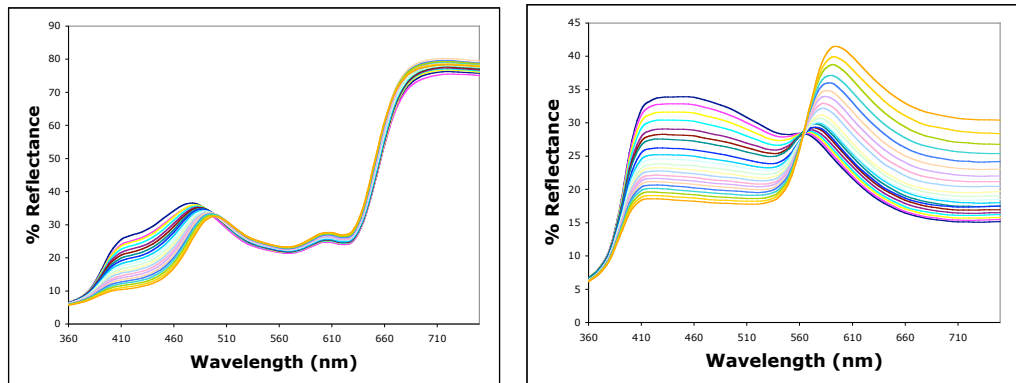


Figure 33. Percent reflectance of the Davidson & Hemmendinger Color Rule letter patches (left) and number patches (right).

In this testing procedure, there are three possible observers, or detectors: the camera, the standard CIE  $2^\circ$  observer, and the photographer. In CS0 they all made a match under the same illuminant. In CS1 through CS4, the best possible camera match

was determined using the Lab images obtained by opening the RGB image in Adobe Photoshop® (the profile that is embedded with the image is used when the image is opened) and converting it from an RGB image to an Lab image. In MATLAB, first the average values of each of the 42 color patches are obtained from the Lab image. Then this Lab image data are converted from ICC Lab data to CIELAB data. In CS0, the CIELAB image was obtained using the second evaluation method described in section 3.4.2. The CIELAB values between the alphabetic and numeric strips are then compared by calculating  $\Delta E_{00}$ . The alphabetic patch and the numeric patch that have the lowest color difference between them is deemed the camera match. Prior to calculating the color differences, the CIELAB image patch data for the D&H Color Rule is first flat-fielded and then corrected for lightness so that the average  $L^*$  of the Halon is equal to 100. Because this comparison is relative within the image, the flat-fielding was necessary, especially since the two color strips were not placed next to each other in the image. The lightness correction was performed in order to make the metamerич matches comparable across the case studies.

In order to perform flat-fielding, first the two gray card target images are converted from RGB images to Lab images in Adobe Photoshop® and then the average patch data (between the two images) corresponding to the same areas as the patches of the D&H Color Rule are obtained and converted from ICC Lab to CIELAB in MATLAB in the same way as the D&H Color Rule. Next, both the D&H Color Rule and corresponding gray card CIELAB patch data are converted to XYZ tristimulus values using Equations 3 to 5 with illuminant  $D_{50}$  used as the white point. Then Equation 26 is used to flat-field the XYZ tristimulus data.

$$XYZ_{ff} = \left( \frac{XYZ_{image}}{Y_{gray}} \right) * \bar{Y}_{gray} \quad (26)$$

The lightness correction is performed in the same way as in section 3.4.2 above. First, the Halon, which was included in the images, CIELAB image data are obtained and converted to XYZ tristimulus values. Then the Y tristimulus image D&H Color Rule values are divided by the Y tristimulus Halon values. Finally, the flat-fielded lightness-corrected D&H Color Rule image data are converted back to CIELAB using Equations 11 to 13 with illuminant D<sub>50</sub> used as the white point. Figure 34 is a flowchart summarizing the camera metameristic match determination procedure.

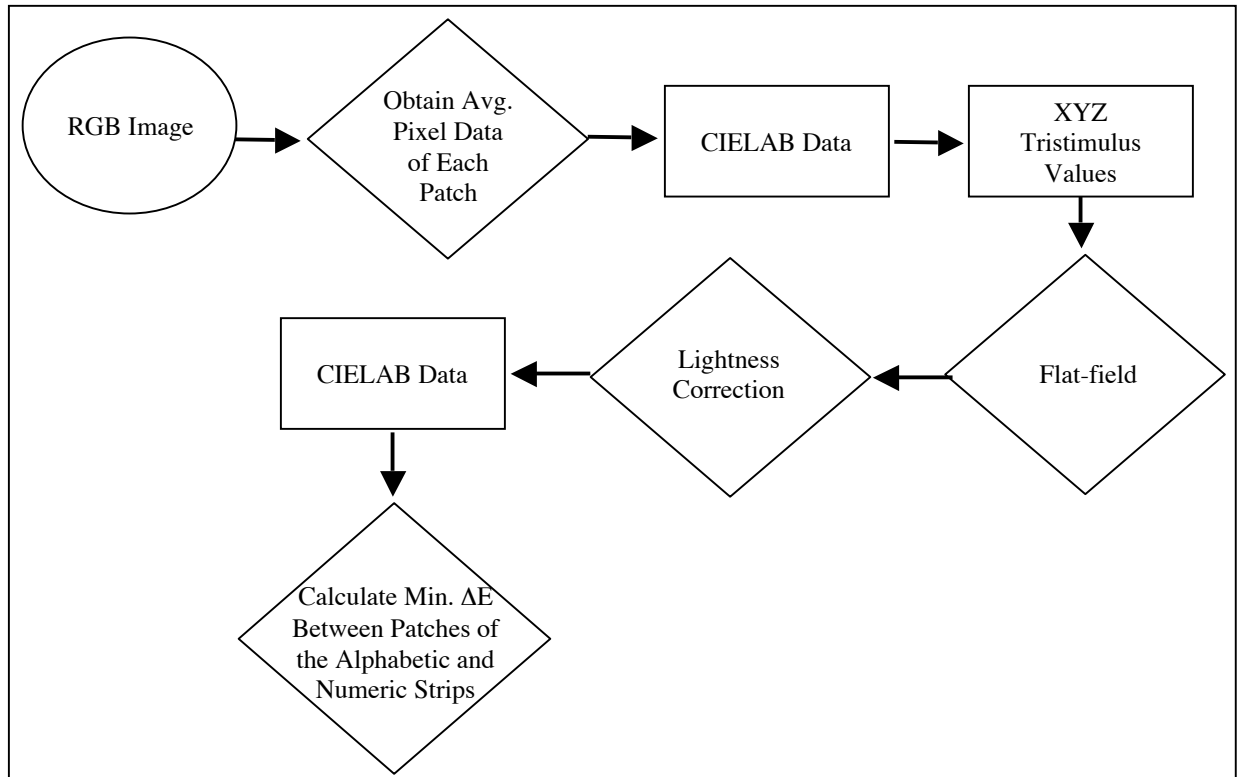


Figure 34. Flowchart of the procedure used to determine the camera metameristic match.

Figure 35 shows a pseudo-image of the camera match for CS0. This image was created by converting the CIELAB flat-fielded lightness-corrected image data back to XYZ tristimulus values, which were then converted to sRGB values. See standard IEC 61966-2-1 (1999) and IEC 61966-2-1 Amendment 1 (2003) for the details about this calculation.

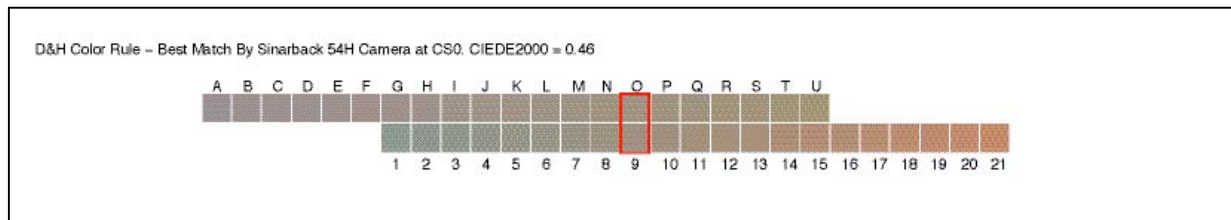


Figure 35. CS0 D&H Color Rule camera metameric match (O-9).

The match made by the standard CIE  $2^\circ$  observer under the taking illuminant (white point) is calculated by first determining the XYZ tristimulus values from the measured spectral reflectances using Equations 6 to 9 and then converting them to CIELAB values using Equations 11 to 13 and finally determining the lowest  $\Delta E_{00}$  match between the alphabetic and numeric strips. Figure 36 shows a plot of the spectral reflectance curves of the CIE  $2^\circ$  observer match made under the HMI taking illuminant in CS0.

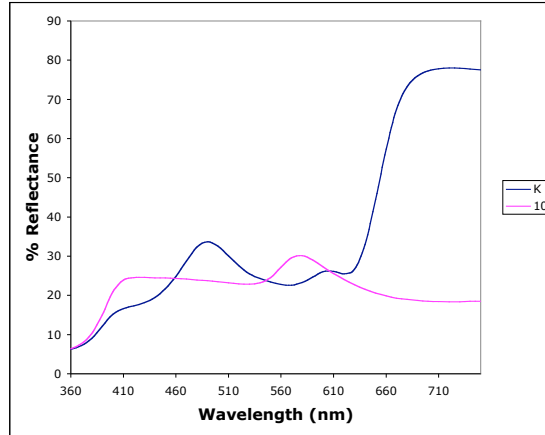


Figure 36. CS0 percent reflectance curves of the CIE 2° observer D&H Color Rule metameristic match (K-10).

Table VII shows the D&H Color Rule metameristic match data of CS0. The indices of the alphabetic and numeric matches are listed which had the lowest  $\Delta E_{00}$  match for the camera and the CIE 2° observer as described above. The photographer's best match is also listed. The HMI taking illuminant was the illuminant for all three matches in CS0. Also listed in the table are the  $\Delta E^*_{ab}$  and  $\Delta E_{00}$  values for both the camera and CIE 2° observer as detectors of the three metameristic matches under the taking illuminant.

Table VII. CS0 D&H Color Rule metameristic matches and the  $\Delta E^*_{ab}$  or  $\Delta E_{00}$  color differences of each metameristic match as “seen” by the camera and CIE 2° observer under the HMI taking illuminant.

<u><b>Detector</b></u>	<u><b>Metameristic Match</b></u>	<u><b>Camera</b></u>	<u><b>CIE 2° Observer</b></u>	<u><b>Camera</b></u>	<u><b>CIE 2° Observer</b></u>
		<u><math>\Delta E^*_{ab}</math></u>	<u><math>\Delta E_{00}</math></u>	<u><math>\Delta E_{00}</math></u>	<u><math>\Delta E_{00}</math></u>
<b>Camera</b>	O-9	0.40	6.64	0.46	5.51
<b>CIE 2° Observer</b>	K-10	4.25	0.85	4.03	0.79
<b>Photographer</b>	G-7	5.97	4.19	6.39	5.13

What can be seen from Table VII is that none of the three detectors had the same match under the same illuminant, which means that the camera is not “seeing” the same colors of the D&H Color Rule as that of the photographer or the CIE 2° observer. The difference in the match between the CIE 2° observer and the photographer could be caused by the photographer having slightly different spectral sensitivities (color-matching functions), since the CIE 2° observer is only an average human observer response. The color differences of the CIE 2° observer and photographer’s metamerically matches as “seen” by the camera are large, which reiterates the fact that their spectral sensitivities differ.

The same is true for the CIE 2° observer as the detector of the camera match in CS0.

### 3.5 Noise

Noise is defined in the ISO 15739 standard as “unwanted variations in the response of an imaging system” (ISO 15739, 2003). It is formed when incoming light is converted from photons to an electrical signal. Sometimes the sensor has electrical activity, which will generate noise. Gain, which is applied to an image before it is outputted for the purpose of increasing the signal, can simultaneously increase the amount of image noise.

It is recommended that a dark correction be performed on every image taken with a digital camera system in order to reduce both the total and fixed pattern noise in the final image. In some camera systems, like the Sinarback 54H (used in CS0 and CS3), this is performed automatically by the image capture software. When the dark correction is not done automatically, this correction can be achieved by subtracting an average of at least 3 dark images. These images should be taken at the same exposure and focus

settings as the image from which it will be subtracted. The dark images can be simply obtained by imaging a lens cap, which is placed on the lens. Dark corrections were not applied to any of the images in the testing procedure, unless they were performed automatically by the image capture software, in order to reduce the number of images obtained in the imaging procedure.

### **3.5.1 Image Noise**

Every time an image is captured, the placement of some of the noise in the image will vary and some will remain fixed. The amount of noise present in an image can vary significantly with the camera's exposure time and ISO speed setting and with changes in the temperature in which the camera is operated. In this testing procedure, four types of image noise are determined. They are total noise, fixed pattern noise, temporal noise, and black temporal noise. The average noise is determined for all four types of image noise and the signal to noise ratio (S/N) is determined for the first three types. In this analysis, it is assumed that the fixed pattern and temporal noise components are not correlated and that the variance of the total noise is equal to the sum of the variances of the fixed pattern and temporal noise.

The ISO has developed a standard (ISO 15739) that explains how to correctly determine a digital camera's image noise. A test chart, called the ISO Noise Test Chart, is described and used in the ISO 15739 standard to determine the amount of noise in an image. This chart, which is shown in Figure 37, is also used in this testing procedure to determine the image noise. This chart was printed on semi-glossy paper with an Epson

inkjet printer from a template, which allowed for the calibration of the gray patches so that they had the same density values that are listed in the ISO 15739 standard.

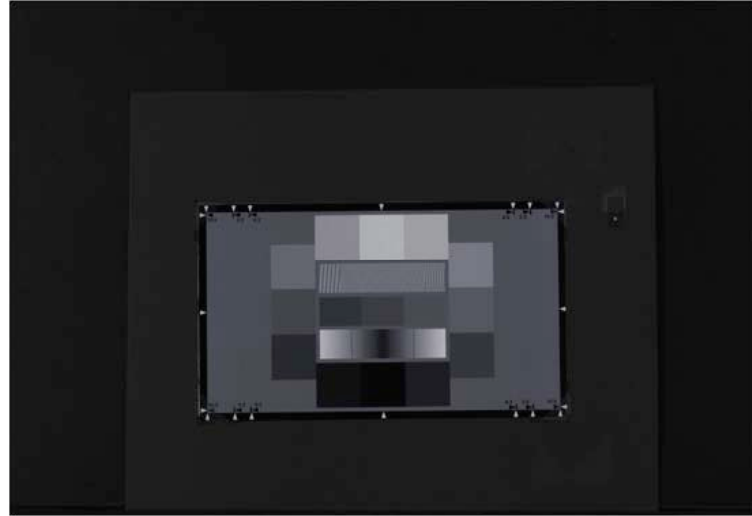


Figure 37. ISO Noise Chart target used to evaluate image noise and dynamic range.

This target should be imaged eight times in the same position and at the same exposure settings. When this target is imaged, it should be in sharp focus and the exposure level should be set so that the white part of the target has digital count values that are maximally unclipped. In CS0, the exposure settings that met this criterion were an exposure time of 1/5s. and a lens aperture of f/11. The integration time was 1/2s. The ISO speed setting was 25.

The noise analysis performed in this testing procedure follows the same analysis procedure described in the ISO 15739 standard. Five out of the fifteen gray patches of the noise target are used in this analysis. They include the center three patches (#13a, b, and c from left to right in ISO 15739), the black patch (#1) and the second darkest patch (#2). The center three patches of the target are used to evaluate the total noise, fixed

pattern noise and temporal noise. The other two patches are used to evaluate the black temporal noise, which is ultimately used to determine the ISO digital still camera dynamic range (see section 3.6). The RGB pixel data are first obtained from each of the five patches of each of the eight images.

The analysis of the total, fixed pattern and temporal noise is as follows. First, the mean across all eight images for each channel is calculated for each of the center three patches (#13a, b, and c). The mean RGB data ( $\overline{DC}$ ) of each of these three patches and the measured reflectance values (R) of each patch are then used to calculate the incremental gain (IG). The ISO 15739 standard recommends using the first derivative of the OECF function, determined in ISO 14524 standard, as the incremental gain, but instead, Equation 27 is used as described in ISO 15739, because the OECF function determined in this testing procedure is not determined in the exact same way as described in the ISO 14524 standard. The incremental gain equation, Equation 27, is repeated for each channel.

$$IG = 0.5 * \left( \frac{\overline{DC}_{13b} - \overline{DC}_{13a}}{R_{13b} - R_{13a}} + \frac{\overline{DC}_{13c} - \overline{DC}_{13b}}{R_{13c} - R_{13b}} \right) \quad (27)$$

The center patch (#13b) is used for the calculations of the total, fixed pattern and temporal average noise and signal to noise ratios.

Total noise is defined in ISO 15739 as “all the unwanted variations captured by a single exposure” (ISO 15739, 2003). Equation 28 is used to calculate the average total noise for each channel.

$$Avg.noise_{total} = \sqrt{\frac{1}{n} \sum_{j=1}^n \sigma_{total,j}^2} \quad (28),$$

where  $n$  is the number of images (eight for CS0) and  $\sigma_{total,j}^2$  is the variance of the pixel digital count values of patch #13b for each of the eight images (ISO 15739, 2003). Equation 29 is used to calculate the total noise signal-to-noise ratio (SNR) for each channel.

$$SNR_{total} = \frac{R_{13b} * IG}{Avg.noise_{total}} \quad (29)$$

Fixed pattern noise is defined in ISO 15739 as “unwanted variations, which are consistent for every exposure” (ISO 15739, 2003). Equations 30 and 31 are used to calculate the average fixed pattern noise for each channel.

$$Avg.noise_{fp} = \sqrt{\sigma_{avg}^2 - \frac{1}{n-1}\sigma_{diff}^2} \quad (30),$$

$$\sigma_{diff}^2 = \frac{1}{n} \sum_{j=1}^n \sigma_{diff,j}^2 \quad (31),$$

where  $\sigma_{avg}^2$  is the variance of the pixel digital count values of patch #13b for the mean of the eight images and  $\sigma_{diff,j}^2$  is the variance of the pixel digital count values of patch #13b for the differences of the average mean of the eight images and each of the individual eight images (ISO 15739, 2003). Equation 29 is used to calculate the fixed pattern signal-to-noise ratio for each channel, but  $Avg.noise_{fp}$  is substituted for  $Avg.noise_{total}$ .

Temporal noise is defined in ISO 15739 as “random noise due to sensor dark current, photon shot noise, analog processing and quantization, which varies from one image to the next” (ISO 15739, 2003). Equations 31 and 32 are used to calculate the average temporal noise.

$$Avg.noise_{temp} = \sqrt{\frac{n}{n-1}\sigma_{diff}^2} \quad (32)$$

Equation 29 is used to calculate the temporal signal-to-noise ratio for each channel, but

$Avg.noise_{temp}$  is substituted for  $Avg.noise_{total}$ .

Black temporal average noise ( $Avg.noise_{blk,temp}$ ) is calculated in order to determine the ISO digital still camera dynamic range (luminance ratio). In this calculation, the darkest patch, patch #1, is used. Equations 31 and 32 are used, but  $\sigma_{diff,j}^2$  is the variance of the pixel digital count values of patch #1 for the differences of the average mean of the eight images and each of the individual eight images.

These calculations were performed in MATLAB, but there is also an Adobe Photoshop® plug-in (ISO 15739, 2003) that performs these calculations along with the dynamic range calculation using eight images and their RGB OECF functions. Table VIII shows the image noise results of CS0 for each channel and the mean of all three channels. In CS0, a dark correction was performed automatically by the image capture software for every image taken.

Table VIII. CS0 image total, fixed pattern and temporal noise results.

	<u>Red Channel</u>	<u>Green Channel</u>	<u>Blue Channel</u>	<u>Mean of RGB Channels</u>
<b>Total Average Noise (DC)</b>	372.68	331.59	352.11	352.13
<b>Total Signal to Noise Ratio</b>	27.92	39.08	37.13	34.71
<b>Fixed Pattern Average Noise (DC)</b>	348.84	317.04	339.67	335.18
<b>Fixed Pattern Signal to Noise Ratio</b>	29.83	40.88	38.49	36.40
<b>Temporal Average Noise (DC)</b>	131.15	97.15	92.76	107.02
<b>Temporal Signal to Noise Ratio</b>	79.34	133.40	140.96	117.90
<b>Black Temporal Average Noise (DC)</b>	229.92	157.59	157.44	181.65

It is desirable to have low average noise and a high signal to noise ratio. When digitizing archival materials, for an 8-bit image, it is desirable that the total average noise does not exceed 1.0 digital count for original objects with a maximum density of 2.0 and 0.7 digital counts for original objects with a maximum density that is greater than 2.0 (Puglia, et al., 2004). For a 16-bit image, which is what was used in CS0, these limits correspond to 257 and 180 digital counts, respectively. The noise target imaged in this part of the testing procedure had a maximum density of 2.0. For CS0, the total average noise exceeds the desirable amount of noise limit of 257 digital counts in all three channels. Table VIII shows that the red channel had the most amount of total noise of the three channels and the green channel had the least amount of total noise in CS0. The amount of temporal noise is significantly less than the fixed pattern noise. The mean total signal to noise ratio of the red, green and blue channels, listed in Table VIII, which is a mono-numeric metric that summarizes the case study's image noise results, is listed in

summary Table XIV for CS0 in section 3.11 and in summary Table LXVIII for CS1 through CS4 in section 4.7.2.

### 3.5.2 Color Noise

Color noise is defined as image noise that is color dependent. It is seen as pixel variations in an image of a uniform patch of color. In this testing procedure, the color noise of the Macbeth ColorChecker was determined for selected patches using two metrics, the percent standard deviation and the mean color difference from the mean (MCDM) (Berns, 2000).

The percent standard deviation is determined using the RGB image data of the CC target. The percent standard deviation of normalized RGB digital counts for each channel of a color patch were found by first calculating the mean of the digital count values of the patch, normalizing them by dividing by the maximum possible digital count value, and then dividing the standard deviation by the mean and multiplying by 100.

The MCDM is determined using the CIELAB image, which is created by converting the RGB image to ICC Lab in Adobe Photoshop® and then converting that image to CIELAB in MATLAB. First, the mean of the pixel CIELAB image data of each color patch is determined. Next, the color difference of the each pixel of the patch from the mean is determined using both  $\Delta E^*_{ab}$  (see Equation 15) and  $\Delta E_{00}$ . Then, the MCDM is calculated from the color differences of all of the pixels.

Table IX shows the color noise results for CS0.

Table IX. CS0 color noise results of selected patches of the Macbeth ColorChecker.

<b>ColorChecker Patch</b>	<b>Mean Normalized DC</b>			<b>% Standard Deviation (Norm. DC)</b>			<b>MCDM</b>	
	<b>R</b>	<b>G</b>	<b>B</b>	<b>R</b>	<b>G</b>	<b>B</b>	<b><math>\Delta E^*_{ab}</math></b>	<b><math>\Delta E_{00}</math></b>
<b>Red (15)</b>	0.17	0.20	0.17	1.54	1.20	1.53	1.11	0.83
<b>Green (14)</b>	0.32	0.37	0.34	0.71	0.53	0.59	0.79	0.53
<b>Blue (13)</b>	0.22	0.30	0.36	1.16	0.59	0.44	1.08	0.93
<b>Cyan (18)</b>	0.17	0.24	0.19	1.60	0.82	1.35	1.34	0.90
<b>Magenta (17)</b>	0.25	0.32	0.39	0.95	0.56	0.40	0.99	0.87
<b>Yellow (16)</b>	0.30	0.43	0.43	0.79	0.39	0.40	1.09	0.57
<b>White (19)</b>	0.31	0.31	0.19	0.66	0.64	1.56	1.03	0.48
<b>Gray (22)</b>	0.18	0.25	0.35	1.70	0.88	0.53	1.26	0.90
<b>Black (24)</b>	0.27	0.23	0.24	0.75	0.84	0.81	0.80	0.41
<b>Mean</b>			1.10	0.72	0.85			
						<b>MMCDM</b>	1.05	0.71

The data in Table IX shows that there were small differences between the amounts of noise of each color patch. The % standard deviation results show that the green channel had the least amount of color noise and the red channel had the most. The color difference results show that the green patch and the black patch had the least amount of color noise and the cyan and gray patches had the most amount of color noise. The mean, mean color difference from the mean (MMCDM), which is the mean color difference of the mean color differences of the color patches listed in Table IX, using  $\Delta E_{00}$  is a mono-numeric metric that summarizes the case study's color noise results, is listed in summary Table XIV for CS0 in section 3.11 and in summary Table LXVIII for CS1 through CS4 in section 4.7.2.

### 3.6 Dynamic Range

The dynamic range, otherwise known as tonal range, of a digital camera system is the capacity of the camera to capture extreme density variations. The broader the

system's dynamic range, the more tones it can reproduce and the smoother the transition between the dark and light tones of the image. Dynamic range can be reduced by flare.

The ISO standard (ISO 15739), which explains how to correctly determine a digital camera's image noise, also describes the procedure for determining the camera's dynamic range. ISO digital still camera dynamic range is defined in ISO 15739 as "the ratio of the maximum unclipped luminance level to the minimum unclipped luminance level that can be reproduced with a temporal SNR of at least one" (ISO 15739, 2003).

The same test chart, called the ISO Noise Test Chart, which is shown in Figure 37, and the same RGB data from the eight images are also used in this testing procedure to determine the dynamic range. Two of the grayscale patches of this target are used in this analysis. They include the black patch (#1) and the second darkest patch (#2).

The analysis of the ISO digital still camera dynamic range is as follows. First, the mean RGB data ( $\overline{DC}$ ) across all eight images, which is calculated for each channel of each of the two patches, and the measured reflectance values (R) of each patch are used to calculate the incremental gain ( $IG_{black}$ ) shown in Equation 33.

$$IG_{black} = 0.5 * \left( \frac{\overline{DC}_1 - \overline{DC}_2}{R_1 - R_2} \right) \quad (33)$$

Then the black temporal noise, which is determined as described in section 3.5.1, is used in Equation 34 to determine the ISO digital still camera dynamic range as a luminance ratio (ISO 15739, 2003).

$$ISOdyn.range_{lum.ratio} = \frac{R_1 * IG_{black} * 100}{Avg.noise_{blk.temp}} \quad (34)$$

The ISO digital still camera dynamic range, calculated as a luminance ratio in Equation 34, can be converted to density units by taking the  $\log_{10}$  of the  $ISOdyn.range_{lum.ratio}$ . This

value can then be compared to the theoretical dynamic range, determined based on the number of bits per channel, which many digital camera manufacturers use to report the dynamic range of the digital camera in their specifications. . Theoretical dynamic range (TDR) is calculated using Equation 35.

$$TDR = \log_{10}(2^n - 1) \quad (35),$$

where  $n$  is the number of bits per channel. Table X shows the dynamic range results of CS0 for each channel and the mean of all three channels.

Table X. CS0 dynamic range results.

	<u>Red Channel</u>	<u>Green Channel</u>	<u>Blue Channel</u>	<u>Mean of RGB Channels</u>
<b>ISO Digital Still Camera Dynamic Range (Luminance Ratio)</b>	1187.38	2100.49	2267.89	1851.92
<b>ISO Digital Still Camera Dynamic Range (Density)</b>	3.07	3.32	3.36	3.27
<b>Theoretical Dynamic Range (Density)</b>	4.81	4.81	4.81	4.81

It is desirable to have a high dynamic range. Even though the ISO 15739 standard reports the dynamic range as a luminance ratio, in traditional photography as well as digital photography, the dynamic range is more commonly expressed in density units, where 0.3 density units is equal to one stop of light ( $\log_{10}2$ ). The measured CS0 dynamic range was less than the theoretical dynamic range in all three channels. The theoretical dynamic range assumes a linear OECF curve (gamma encoding = 1.0) in each color channel. The ISO 15739 dynamic range calculation basically extrapolates the slope between the black patch (#1) values and the second darkest patch (#2) values of the ISO

Noise Test Chart to determine the dynamic range luminance ratio. This slope is dependent on the gamma encoding of the image. The difference in the OECF curves between the CS0 dynamic range and the theoretical dynamic range and the accuracy of the extrapolation of the slope between patch #1 and patch #2 in the dynamic range calculation contribute to the difference between the CS0 dynamic range and the theoretical dynamic range. Because of affect of these factors on the difference between the dynamic range calculated using the ISO 15739 dynamic range equations and the theoretical dynamic range, it is possible for the case studys' dynamic ranges to be larger or smaller than the theoretical dynamic range. The theoretical dynamic range can be used as a dynamic range reference point.

In CS0, the blue channel had the most amount of dynamic range of the three channels and the red channel had the least. The mean ISO DSC dynamic range (density) across the red, green and blue channels, listed in Table X, which is a mono-numeric metric that summarizes the case study's dynamic range results, is listed in summary Table XIV for CS0 in section 3.11 and in summary Table LXVIII for CS1 through CS4 in section 4.7.2.

### **3.7 Spatial Cross-talk**

Spatial cross-talk, otherwise known as image flare, is the dependency of the output digital data of a color patch on the reflectance of surrounding areas (IEC 61966-8, 2001). In other words, it occurs when an object in a scene, which is surrounded by an area brighter than itself, is reproduced at a digital count value that is higher than what it would be if the object were surrounded by an area that is darker than it.

The target used to evaluate spatial cross-talk contains the IEC Large Area Spatial Cross-talk Chart, which was printed on semi-glossy paper with an Epson inkjet printer. This target is shown in Figure 38. When this target is imaged, it should be in sharp focus and the exposure level should be set so that the white part of the target has digital count values that are maximum unclipped. In CS0, the exposure settings that met this criterion were an exposure time of 1/15s. and a lens aperture of f/11. The integration time was 1/2s. This target was imaged once in the center of the scene and a second time with the chart rotated 180° so that the gray squares were in the same position of the image as before but surrounded by white instead of black or vice versa.



Figure 38. IEC Large Area Spatial Cross-talk Chart target used to evaluate spatial cross-talk oriented at 0° (left) and at 180° (right).

The 15 equally spaced gray squares in this target are used to evaluate spatial cross-talk in this testing procedure. Using the RGB image data, first the mean of each of the 15 gray patches of each of the two images are determined. Next, they are linearized by applying the inverse OECF look-up table to each channel to photometrically convert the digital count values into normalized linear values. These linearized means are listed in Tables 7-X through 7-XIV in Appendix 7.3 for CS0 through CS4. For each channel,

two metrics are calculated. First, the maximum of the percent relative differences, which are calculated using Equation 36, is determined.

$$\% Rel.Diff. = \frac{|\bar{p}_{0^\circ} - \bar{p}_{180^\circ}|}{\bar{p}_{all}} * 100 \quad (36),$$

where  $\bar{p}_{0^\circ}$  is the mean linearized value of a gray patch in the image oriented at  $0^\circ$ ,  $\bar{p}_{180^\circ}$  is the mean linearized value of the gray patch in the same place in the image oriented at  $180^\circ$ , and  $\bar{p}_{all}$  is the mean linearized value of all 30 gray patch means. The second metric is the percent relative standard deviation, which is calculated using Equation 37.

$$\% Rel.Std.Dev. = \frac{std.dev.[|\bar{p}_{0^\circ} - \bar{p}_{180^\circ}|]^{\frac{1}{2}}}{\bar{p}_{all}} * 100 \quad (37)$$

Table XI shows, for each channel, the mean linearized value of all 30 gray patch means, the percent relative maximum difference, and the percent relative standard deviation values for CS0.

Table XI. CS0 summary of spatial cross-talk results.

	<u>Red Channel</u>	<u>Green Channel</u>	<u>Blue Channel</u>	<u>Mean of RGB Channels</u>
<b>Mean Linearized DC</b>	0.16	0.16	0.19	0.17
<b>Relative Maximum Difference (%)</b>	4.78	5.20	6.95	5.64
<b>Relative Standard Deviation (%)</b>	1.53	1.55	2.54	1.88

The data in Table 7-X for CS0 in Appendix 7.3 shows that the mean digital count value of a gray patch that is surrounded by white in one image is always higher than the value of the patch in the same position surrounded by black in the other image. This shows that spatial cross-talk is having an effect on the image. Table XI shows that the

spatial cross-talk affected the blue channel the most and the red channel the least in CS0.

The mean of all three RGB channels' relative maximum difference values, which is a mono-numeric metric that summarizes the case study's spatial cross-talk results, is listed in summary Table XIV for CS0 in section 3.11 and in summary Table LXVIII for CS1 through CS4 in section 4.7.2. It is desirable for the relative maximum difference values to be as close to zero as possible.

### **3.8 Spatial Frequency Response (SFR)**

According to the standard ISO 12233, resolution is defined as a "measure of the ability of a camera system, or a component of a camera system, to depict picture detail" and the spatial frequency response, or SFR, which is defined as the "measured amplitude response of an imaging system as a function of relative input spatial frequency," is used to measure resolution (ISO 12233, 2000). Although the term modulation transfer function, or MTF, is sometimes used interchangeably with SFR, they are different. The MTF measurement takes into account the input edge modulation, whereas the SFR does not (Burns, 2000). In this procedure, the SFR is evaluated. There are many aspects of a digital imaging system that can have an effect on the SFR. They include lens aperture, field position, optics, detector motion, sampling, and image processing (Williams, 2001).

The black and white target, which was used to analyze the SFR, is shown in Figure 39. The chart contained in the target is the ISO Resolution Chart. It contains many elements and patterns, but the elements that were used in this procedure were the slanted black bars and squares. They are slanted 5° and form what are commonly known as knife-edges. This chart was purchased at Sinepatterns located in Rochester, NY. It

was printed on matte photographic paper. The standard, ISO 12233, describes this chart's specifications.

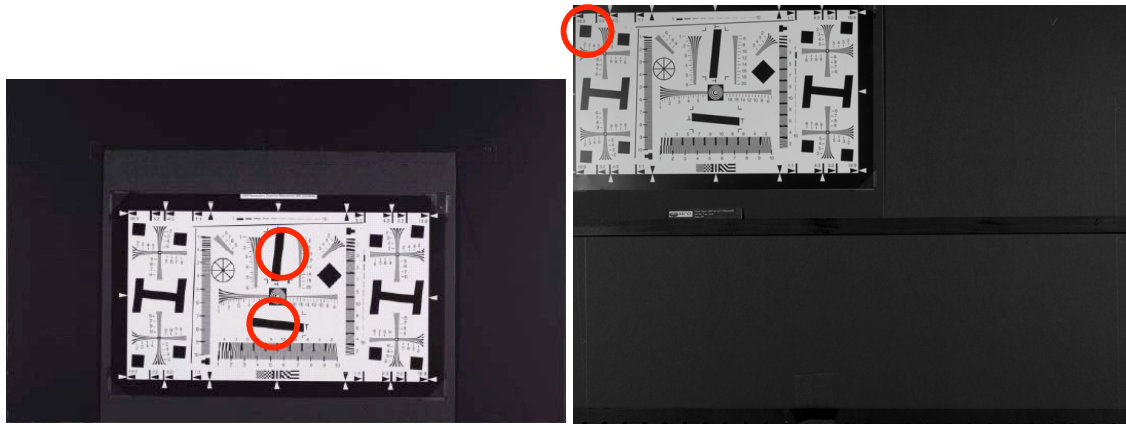


Figure 39. ISO Resolution Chart target used to evaluate spatial frequency response (SFR) and color channel registration centered (left) and in the upper left corner (right). The knife-edges used in the analysis are circled in red.

When this target is imaged, the camera should be focused so that the zone plate in the center of the chart exhibits the maximum aliasing possible. The camera lens aperture and the exposure time should be adjusted to provide a near maximum signal level from the white test target areas. The settings shall not result in signal clipping in either the white or black areas of the test chart, or regions of edge transitions (ISO 12233, 2000). In CS0, the exposure settings that met this criterion were an exposure time of 1/6s. and a lens aperture of f/11. The integration time was 1/2s. This target was imaged once in the center of the scene and once in the upper left corner. It was imaged both on-axis and off-axis to test the effect of field position on the SFR of the digital imaging system. Although the lens is usually thought of as the source of off-axis effects, the color filter array lenslets can also dramatically suppress SFR responses (Williams, 2001).

A MATLAB program that implements the ISO SFR measurement procedure, called sfrmat2, which was developed by Burns, was used to evaluate the knife-edges circled in red in Figure 39. Figure 40 is a flowchart of the implementation of this program.

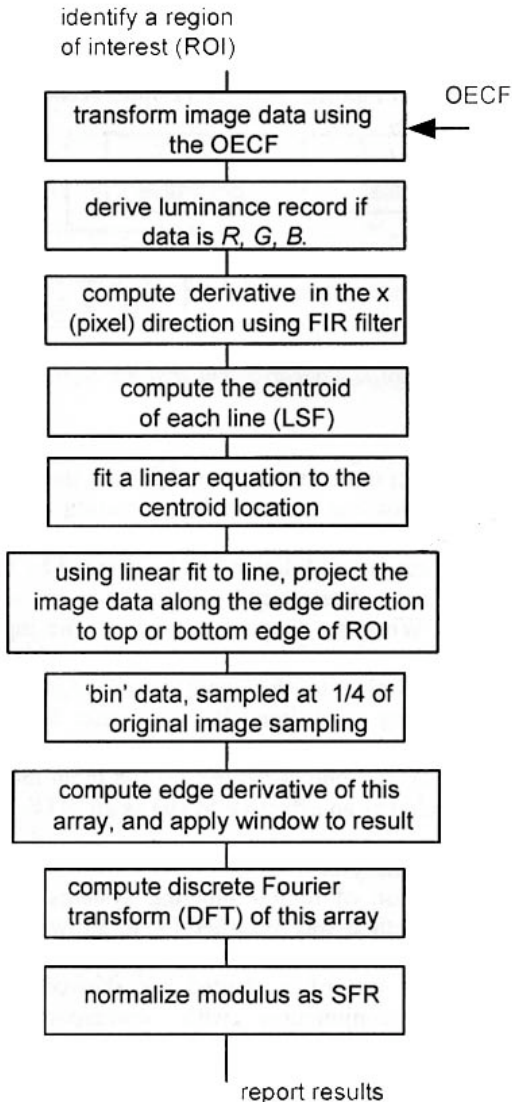


Figure 40. Flowchart of the ISO 12233 spatial frequency response evaluation method used in sfrmat2. (Burns, 2000).

The sfrmat2 program has been evaluated and found to provide a robust SFR measurement, largely insensitive to edge angle and region of interest selection (Burns, 2000). The SFR results of this program for CS0 are shown in Figure 41.

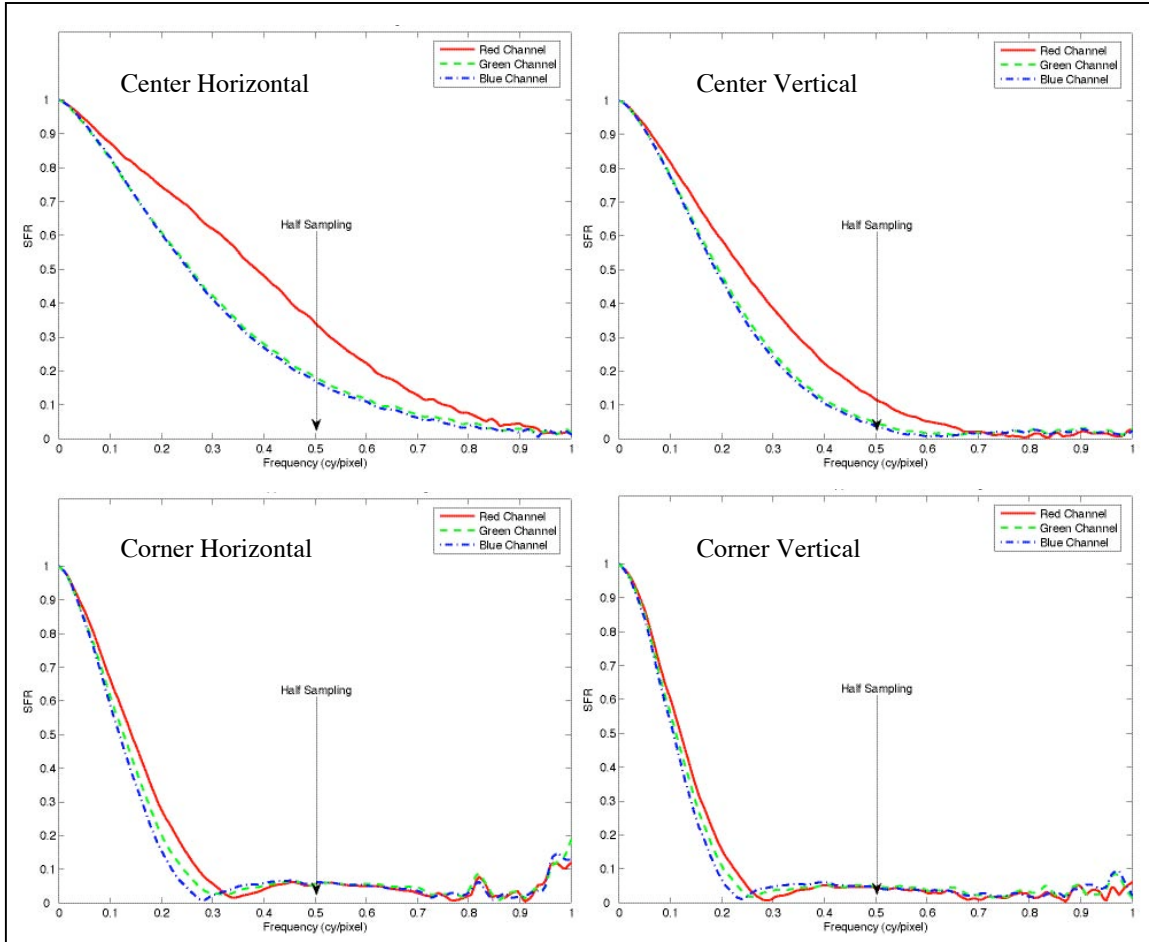


Figure 41. CS0 SFR of center horizontal edge (top left), center vertical edge (top right), upper left corner horizontal edge (bottom left), and upper left corner vertical edge (bottom right).

The SFR curves, shown in Figure 41, are normalized so that at a spatial frequency of 0 has an SFR value of 1. If SFR values are greater than 1, then sharpening has been applied to the image during image processing. There was no sharpening applied in CS0. The higher the SFR values in the plot over the range of spatial frequencies, the better the

preservation of detail at those frequencies. Differences in the SFR curves between the channels were caused by color channel misregistration in the image (see section 3.9 for more details) or a difference in the image processing which was performed on each channel. Half sampling is at a frequency of 0.5cycles/pixel. This is the Nyquist frequency, which is where aliasing starts to occur. Aliasing is defined in ISO 12233 as “output image artifacts that occur in a sampled imaging system for input images having significant energy at frequencies higher than the Nyquist frequency of the system” (ISO 12233, 2000). This explains why the SFR is noisier above 0.5cycles/pixel.

It is easier to compare the SFR data between the horizontal and vertical edges and between the centered and corner edges by summarizing the plot with one number, the area under the SFR curve from frequencies of 0.0 to 0.5cycles/pixel. These areas were normalized so that if the SFR were equal to one from frequencies of 0.0 to 0.5cycles/pixel, then the area would be also be equal to one. Table XII includes these areas for CS0.

Table XII. CS0 SFR area results.

<u><b>Edge</b></u>	<u><b>Area Under SFR Curve From Frequencies of 0.0 to 0.5cy/pixel</b></u>			
	<u><b>Red Channel</b></u>	<u><b>Green Channel</b></u>	<u><b>Blue Channel</b></u>	<u><b>Mean of RGB Channels</b></u>
<b>Center Horizontal</b>	0.679	0.546	0.541	0.589
<b>Center Vertical</b>	0.516	0.432	0.423	0.457
<b>Corner Horizontal</b>	0.315	0.288	0.273	0.292
<b>Corner Vertical</b>	0.271	0.257	0.247	0.258
<b>Mean</b>				0.399

It is evident, from the data shown in Table XII and Figure 41, that the SFR in the horizontal direction was better than the SFR in the vertical direction. Secondly, the SFR in the center (on-axis) was better than the SFR in the corner (off-axis) of the uncropped image area. Thirdly, the red channel SFR was higher than the green channel, which was slightly higher than the blue channel. The mean area of the mean of the RGB channels across the four edges, which is in Table XII, is a mono-numeric metric that summarizes the case study's SFR, which is listed in section 3.11 in summary Table XIV for CS0 and in summary Table LXVIII in section 4.7.2 to compare the spatial frequency response across the four museum case studies.

### **3.9 Color Channel Registration**

Whether or not a digital camera is an area array CCD camera or a tri-linear scanning camera, there is usually some amount of color channel misregistration, or translation error present. In scanning cameras, the amount of misregistration is usually greater than that of area array CCD cameras. In scanning cameras, the misregistration is most prominent in the direction that the linear array is scanning because of misalignment of the final image, which can be caused by the design of the scanning components or image processing. Misregistration in images from both scanning and area array CCD cameras can be caused by chromatic aberration of the lens or color filter array lenslets. Chromatic aberration is caused when different wavelengths of light are bent at different angles and focus at different points behind the lens due to the index of refraction of a lens. A digital image that has misregistration between the color channels can cause an

image that is displayed on a monitor or printed to exhibit a loss of sharpness or color distortion artifacts, particularly at the edges of objects in the scene (Burns, 1999).

The target shown in Figure 39, which was used to evaluate SFR, was also used to determine the misregistration of the camera's color channels in the image. The same knife-edges, which are circled in red in Figure 39 were evaluated. Burns' sfrmat2 MATLAB program was used as a tool for the analysis of color channel registration. The flowchart shown in Figure 42 shows the process of how the amount of misregistration shift was determined. It is the same as the first five boxes in Figure 34.

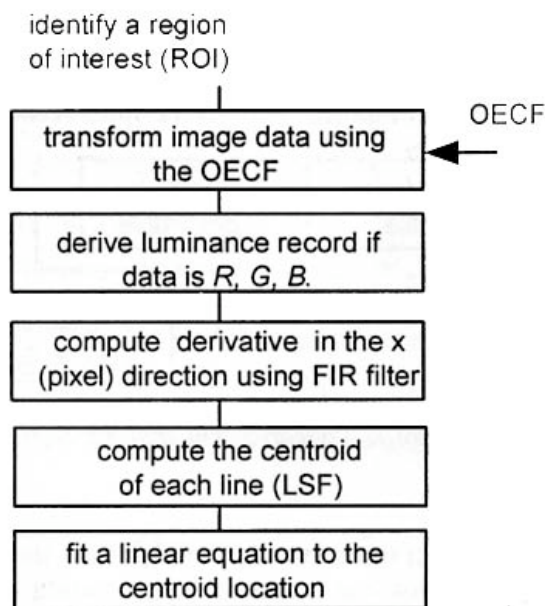


Figure 42. Flowchart of the color channel misregistration error evaluation method used in sfrmat2. (Burns, 2000).

The steps shown in the flowchart to determine the amount of misregistration error are repeated for each channel separately. The output of this procedure is a linear equation for

each color channel, which is used to determine the edge location for each color channel within the region of interest. This linear equation is shown in Equation 38.

$$x = a + b(y - 1) \quad (38),$$

where  $x$  is the x-direction (pixel) location,  $y$  is the y-direction line number, and  $a$  (the location of the edge on the first line of the region of interest) and  $b$  are constants (Burns, 1999). Table XIII shows the results of the color channel registration for CS0. The red and blue channel misregistration shifts are determined relative to the green channel. The camera used in CS0 has an area array CCD. Color channel misregistration errors of less than 0.5 pixels are desirable, but errors less than one pixel are sufficient.

Table XIII. CS0 color channel registration results.

<u>Edge</u>	<u>Misregistration Shift (pixels)</u>		
	<u>Red Channel</u>	<u>Green Channel</u>	<u>Blue Channel</u>
<b>Center Horizontal</b>	0.179	0.000	0.063
<b>Center Vertical</b>	0.028	0.000	0.022
<b>Corner Horizontal</b>	0.132	0.000	0.022
<b>Corner Vertical</b>	0.164	0.000	0.048
<b>Maximum</b>	0.179	0.000	0.063
<b>Mean</b>	0.126	0.000	0.039
<b>Mean of RGB Channels</b>			0.055
Note: Green channel used as reference			

It is evident, from the data in Table XIII, that the red channel misregistration shift was greater than that of the blue in comparison to the green channel. The maximum amount of misregistration was less than 0.2 pixels. Out of the four edges, the center horizontal edge had the most amount of misregistration shift. On the other hand, the center vertical edge had the least amount of misregistration shift. The mean misregistration shift (in pixels) of the RGB Channels across the four edges, which is in

Table XIII, is a mono-numeric metric that summarizes the case study's color channel misregistration, which is listed in summary Table XIV in section 3.11 for CS0 and in summary Table LXVIII in section 4.7.2 to compare the spatial frequency response across the four museum case studies.

### 3.10 Depth of Field

Depth of field is the range of distance for which the subject is rendered acceptably sharp in an image. It increases as the lens is closed down (f-stop increases). It is greater for short focal lengths than for long ones, and it increases with the subject distance (Wrotniak, 2003). A digital imaging system should have a suitable depth of field when it is used to image paintings because a painting is a three dimensional object that has some depth and a large painting could be warped. The target used in the depth of field analysis part of the testing procedure is shown in Figure 43.

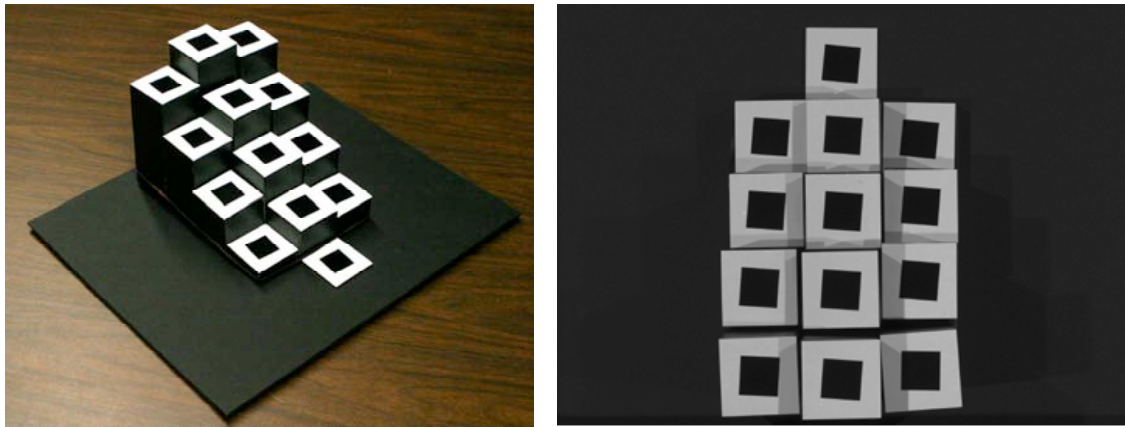


Figure 43. Target used to evaluate depth of field (left) and resulting image taken with the camera (right). Target consists of 13 columns ranging from 0" to 6" in 0.5" increments.

This target was designed and made by the author. It consists of 13 columns that range in height from 0" to 6" in increments of 0.5" off of the board. A knife-edge, which was at an angle equal to the knife-edges in the ISO Resolution Chart (see Figure 39), was placed at the top of each column. The columns in this target were placed next to each other so that when the target is imaged, the columns are in the same approximate spatial area in the scene. When this target is imaged, one time, it should be lit so that the presence of shadows is minimized. At least one vertical and one horizontal edge on every column should be free of shadows in the image. The target should be focused so that the center, 3", column knife-edge is in sharp focus.

This target was analyzed using the sfrmat2 SFR analysis described in section 3.8, but only in the direction (horizontal or vertical) that had the best SFR results from the SFR analysis, since there is no need to compare the horizontal and vertical results again. After the SFR curves and areas were determined (see Appendix 7.4 for these data for CS0 and the four museum case studies), the SFR areas were plotted against the differences in height from the center, 3", column knife-edges, on which the target was supposed to be focused. Figure 44 shows the plot of the depth of field distance vs. area under the SFR curve for the horizontal edge of each color channel. Differences between the red, green and blue color channels were caused by their misregistration shifts (see section 3.9 for more details). When the depth of field target was imaged in CS0, the exposure settings were an exposure time of 1/6s. and a lens aperture of f/11. The integration time was 1/2s. The subject distance was approximately 60.5" from the 3" high column to the camera's sensor. The focal length of the lens was 100mm. The focus was determined manually by

the photographer while she looked at the magnified live preview image in the capture software.

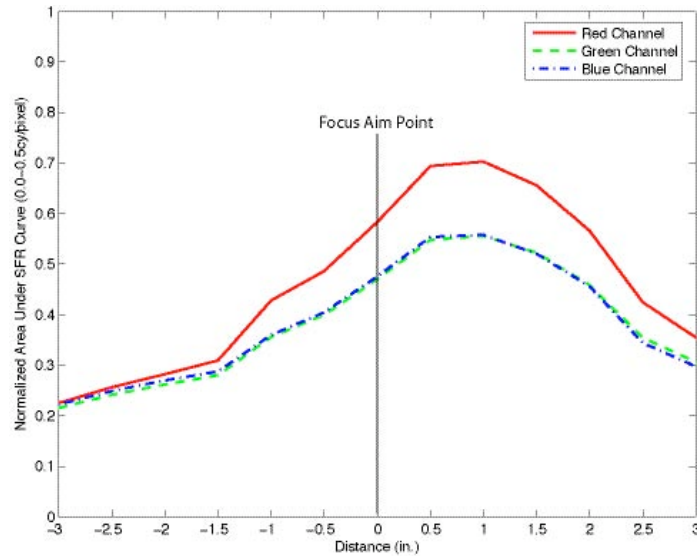


Figure 44. CS0 depth of field distance vs. area under SFR curve of the horizontal edge.

Differences between the red, green and blue color channels in the plot in Figure 44 were caused by their misregistration shifts (see section 3.9). Two pieces of information can be obtained about the depth of field image of CS0 from the plot in Figure 44. One is that the sharpness, and therefore the depth of field, of the image decreased as the camera-to-subject distance changed. The other is that the focusing tool, which was used to focus on the 3" high column during the imaging of the depth of field target, was not accurate. Instead of the focus being at the focus aim point, it was somewhere between 0.5" and 1" closer to the camera. The mean of the mean areas under the SFR curves from frequencies of 0.0 to 0.5cycles/pixel of the RGB channels across the 13 distances, which was normalized by the maximum mean SFR area of the RGB channels

(see Tables 7-XV to 7-XIX in Appendix 7.4), is a mono-numeric metric that summarizes each case study's depth of field, which is listed in summary Table XIV in section 3.11 for CS0 and in summary Table LXVIII in section 4.7.2 to compare the depth of field across the four museum case studies.

### **3.11 Case Study Zero Summary**

Table XIV summarizes the mono-numeric metrics for the characterization results of each image quality parameter of CS0. There is a similar table, Table LXVIII, in section 4.7.2 with the characterization results of CS1 through CS4. See section 3.1 for the process used to obtain the target images for CS0 and sections 3.2 through 3.10 for explanations of how the target images were analyzed and the data in Table XIV obtained.

Table XIV. Summarization of characterization mono-numeric metrics for CS0 results.

<u>Image Quality Parameter</u>	<u>Mono-numeric Metric Value</u>
<b>System Spatial Uniformity</b>	0.10
Max $\Delta E_{00}$ from Mean of All Patches	
<b>Tone Reproduction</b>	N/A
Mean Gamma of RGB Channels	
<b>Color Reproduction Accuracy – Spectral Sensitivity</b>	
$\mu$ -Factor (Camera – CIE 2° Observer, Taking Illuminant – D <sub>50</sub> )	0.84
<b>Color Reproduction Accuracy – Target-based</b>	
Mean $\Delta E_{00}$ 90 <sup>th</sup> Percentile of All Charts	4.09
<b>Noise – Image</b>	34.71
Mean of RGB Channels Total Signal to Noise Ratio	
<b>Noise – Color</b>	0.71
MMCDM	
<b>Dynamic Range</b>	3.27
Mean of RGB Channels ISO DSC Dynamic Range (Density)	
<b>Spatial Cross-talk</b>	5.64
Mean of RGB Channels of Relative Maximum Difference (%)	
<b>Spatial Frequency Response</b>	
Mean of Mean of RGB Channels Across Four Edges - Area Under SFR Curve From Frequencies of 0.0 to 0.5 cy/pixel	0.399
<b>Color Channel Registration</b>	
Mean of RGB Channels Across Four Edges - Misregistration Shift (pixels)	0.055
<b>Depth of Field</b>	
Mean of Mean of RGB Channels Across 13 Distances Normalized by the Largest RGB Channel Mean – Area Under SFR Curve From Frequencies of 0.0 to 0.5 cy/pixel	0.675

## **4. Case Studies**

There were four museums chosen for the case studies. They were chosen because they were early adopters of the direct-digital-capture of artwork. The four case studies, denoted CS1, CS2, CS3, and CS4, respectively, in the sections that follow, were performed during the months of June and July of 2004. These experimental case studies were performed in order to benchmark the digital camera systems and imaging procedures currently used by the cultural heritage community for the digital documentation and reproduction of paintings. There were two parts to the case studies. The purpose of the first part was to learn about each museum's digital imaging workflows. The purpose of the second part was to characterize their camera systems. The images that were analyzed in the second part were representative of digital masters.

In the first part, the paintings shown in Figure 45 were used. The procedure used to analyze the painting images in this part is described in section 4.1. In the second part, the rest of the testing procedure and targets (see section 3) were used. Differences between the testing procedure described in section 3 and the case study procedures, which were caused by time constraints during the case study imaging, are discussed in section 4.2.

### **4.1 Procedure Used to Analyze the Colorimetric Accuracy of Case Study Digital Imaging Workflows**

In order to analyze the colorimetric accuracy of each case study's digital imaging workflow, two paintings, the "flower" and "fish" (see Figure 45), were imaged by the photographer. The two paintings were placed side-by-side (with the fish painting rotated 90° counterclockwise) in the image area when they were imaged. In each case study, the

photographer was asked to image the pair of paintings as he would a typical painting in his day-to-day imaging. This included everything from the set-up of the camera and lights to the processing of the image for storage as a digital master. In CS1, only a digital master image was stored (see section 4.3.2), in CS2, a camera image, digital master image and visually corrected image were stored (see section 4.4.2), and in CS3 and CS4, both a digital master image and a visually corrected image were stored (see sections 4.5.2 and 4.6.2, respectively). The only restriction that was set on the photographer when imaging the paintings was the exposure settings. They were supposed to be set so that the Halon, placed above the paintings, had digital count values that were maximum unclipped. When the paintings image was visually corrected in the case studies, both paintings were corrected as if they were one painting since they both contained the same pigments.

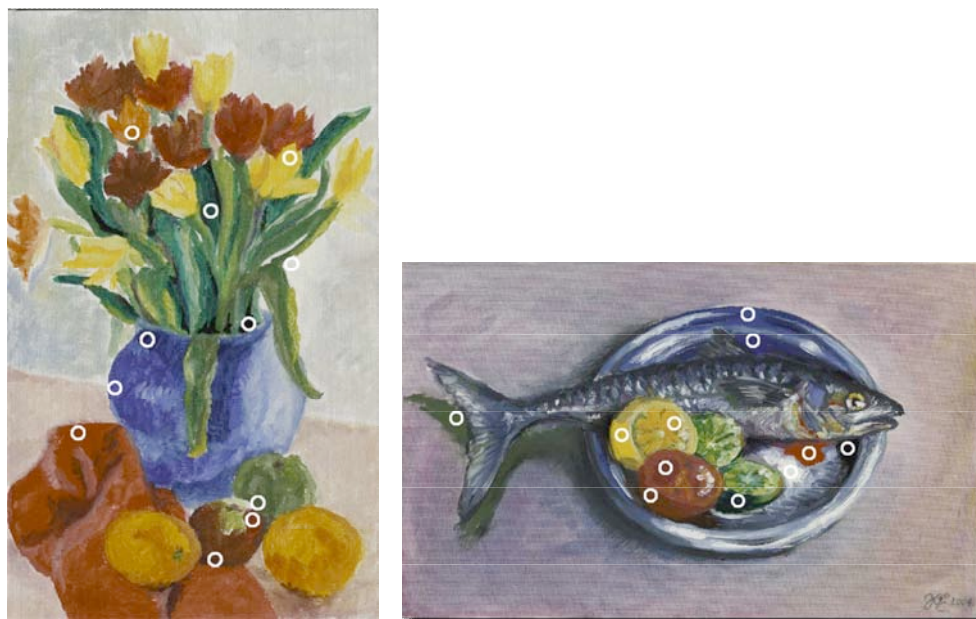


Figure 45. Flower (left) and fish (right) paintings used for the analysis of each museum's digital imaging workflow. Uniform areas of pigment are marked with a white circle.

The two paintings, shown in Figure 45, were each painted with 11 Gamblin Artist's Oil Colors paints. There were uniform patch areas on each painting of each oil paint pigment, which were the same as those used to paint the pigment target used in the target-based color reproduction accuracy analysis procedure of the testing procedure characterization. The spectral reflectances of the 22, total, uniform patch areas of the pigments, marked with a white circle in Figure 45, were measured with a GretagMacbeth ColorEye XTH hand-held integrating sphere spectrophotometer in the same way as the color targets used in the target-based color reproduction accuracy analysis procedure of the testing procedure characterization in section 3.4.2. Figure 46 shows the spectral reflectances of the 11 oil paints used in the two paintings.

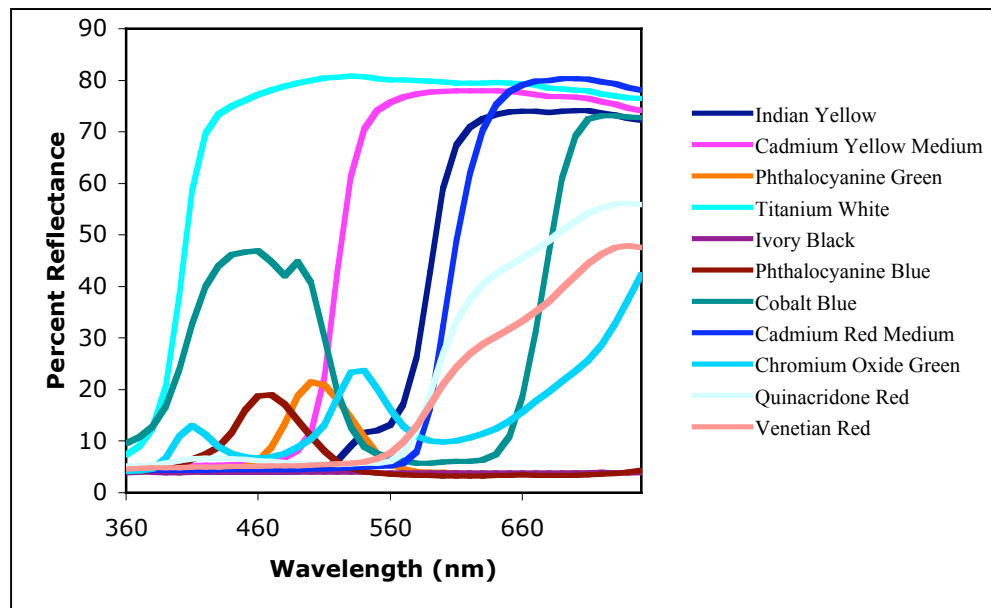


Figure 46. Percent reflectance of 11 Gamblin Artist's Oil Colors used in each painting.

The cobalt blue pigment, one of the 11 pigments used in the paintings, is one of the most difficult pigment colors to reproduce accurately, because it reflects a lot of light in the lower wavelengths (blue) part of the spectrum and also has a tail in the higher wavelengths (red). This is why a cobalt blue pigment target was included in the target-based color reproduction accuracy analysis procedure of the testing procedure characterization.

The 11 uniform areas of pigment of each painting were evaluated in the colorimetric analysis of the digital imaging workflows. During the imaging at each museum, if the paintings image was visually edited, then spectroradiometric measurements were taken of each of the 22 uniform areas of the visually edited image off of the CRT monitor screen using the PR650 spectroradiometer. These measurements

were also analyzed. In addition, a white (255, 255, 255) patch was measured in order to determine the CRT monitor's white point.

Using the profiled digital master in CS1 and both of the profiled digital master and visually corrected images in CS2 through CS4, the RGB images were first opened in Adobe Photoshop® (the profile that was embedded with each of the images was used when the image was opened) and converted from RGB images to an Lab images. The Lab images were saved and their data were used in this analysis. In MATLAB, first the average values of each of the uniform color patches were obtained from each image. Then these Lab image data were converted from ICC Lab data to CIELAB data. Using Equations 6 to 9, the XYZ tristimulus values of the measured spectral reflectance data of each patch were calculated using the CIE 2° observer and CIE illuminant D<sub>50</sub>. Then Equations 11 to 13 were used to calculate the CIELAB data of the measured data. The white point used for this calculation was illuminant D<sub>50</sub>. The CIELAB image data were then compared to the spectrophotometrically measured CIELAB data using ΔE<sub>00</sub>.

Next, in order to decrease the effect of the lightness errors in the color difference calculation caused by the exposure level of the image, it was necessary to also compare the image CIELAB data to the measured data after correcting for this lightness difference. The lightness correction was made by first calculating XYZ tristimulus values from the CIELAB image data using Equations 3 to 5 using illuminant D<sub>50</sub> as the white point. This was repeated for the Halon, which was included in the images, CIELAB image data. Then the Y tristimulus image values were divided by the Y tristimulus Halon values. CIELAB values were then calculated from these new XYZ tristimulus image values. This normalized each image so that the Halon was equal to an

$L^*$  value of 100. The lightness corrected CIELAB image data were compared to the spectrophotometrically measured CIELAB data using  $\Delta E_{00}$ .

Then, the XYZ tristimulus values of the 22 paintings uniform areas and the white patch were determined by multiplying the array of their measured spectral radiance values by the array of color-matching functions of the 2° standard observer. Then, using Equations 11 to 13, the XYZ tristimulus values of the 22 paintings uniform areas were converted to CIELAB data with the XYZ tristimulus values of the white patch as the CRT monitor white point. These CIELAB values were compared to the spectrophotometrically measured CIELAB data using  $\Delta E_{00}$ .

In the Results and Discussion sections of CS1 (section 4.3.3), CS2 (section 4.4.3), CS3 (section 4.5.3), and CS4 (section 4.6.3), three  $\Delta E_{00}$  comparison results are discussed. They include the comparison of the lightness corrected digital master image, the lightness corrected visually corrected image (except CS1), and the spectroradiometric CRT measurements (except CS1) of the 22 uniform areas of the paintings to the spectrophotometrically measured data. Also, CIELAB error vector plots ( $a^*$  vs.  $b^*$  and  $C^*_{ab}$  vs.  $L^*$ ) are included (see Equation 14 for the calculation of  $C^*_{ab}$ ), which show these three comparisons.

#### **4.2 Differences Between the CS0 Testing Procedure and the Museum Case Study Procedures**

Due to the time constraints on the performance of the case studies at the museums, the testing procedure was slightly modified from the recommended procedures used in CS0, which are described in section 3. There were three major changes. The first change was that there were only three exposure levels (one at nominal exposure, one

underexposed and one overexposed) used when the OECF target was imaged instead of four exposure levels. The second change was that there were only five images taken of the noise target instead of eight. Thirdly, instead of determining and using the optimal exposure time for the imaging of each target, the nominal exposure time that was determined by the photographer for the paintings image, which caused the digital counts of the Halon to be maximum unclipped, was used throughout the imaging procedure (except for the spectral sensitivity part) at each museum. Although the basic imaging procedure was consistent for all four of the museum case studies, they were each still unique because the photographer had the freedom to follow his normal imaging procedure and set-up the camera and lights as he would normally when imaging paintings of a similar size to the targets that were imaged.

### **4.3 Case Study One**

Case study one, CS1, was performed on June 21, 2004.

#### **4.3.1 Case Study One: Digital Imaging System Description**

The camera used at the museum's photography studio was a Leica S1 Pro (SN: 2286090) digital camera, which is a 3-channel (RGB) tri-linear-array-CCD scanning camera that scans from top to bottom across the image plane. The maximum native resolution of the camera is 5140p x 5140p. The lens used was a 100mm f/2.8 Leica APO-Macro-ELMARIT-R1 lens (SN: 3762982). The filter used between the lens and CCD was a Leica daylight balancing/IR cut-off filter. This camera is typically used to image paintings (varnished and unvarnished) and other flat works, such as textiles and

books, for the purpose of protecting vulnerable originals from use and to include the digital images in a collection management system. Reproductions are created in the forms of prints and Internet images. Five people in the photography department at the museum can operate this camera. The photographer did not receive background training for this camera system, but he did receive training on the procedure that he follows.

There were four Lowel Scandles lights with reflectors used to light the scene. These lights simulated daylight illumination. In his day-to-day imaging, the photographer changes the positions of the lights for every object imaged. Table XV shows the CCT, chromaticity coordinates, and luminance of this illumination. Figure 47 shows the relative spectral power distribution of the Lowel Scandles lights. These data were obtained by measuring the Halon, which was placed in the scene, with a calibrated PR650 spectroradiometer.

Table XV. Lowel Scandles taking illuminant characteristics.

<b>Correlated Color Temperature</b>	4834K
<b>Chromaticity x (CIE 2° Observer)</b>	0.3513
<b>Chromaticity y (CIE 2° Observer)</b>	0.3676
<b>Luminance (CIE 2° Observer)</b>	393.3cd/m <sup>2</sup>

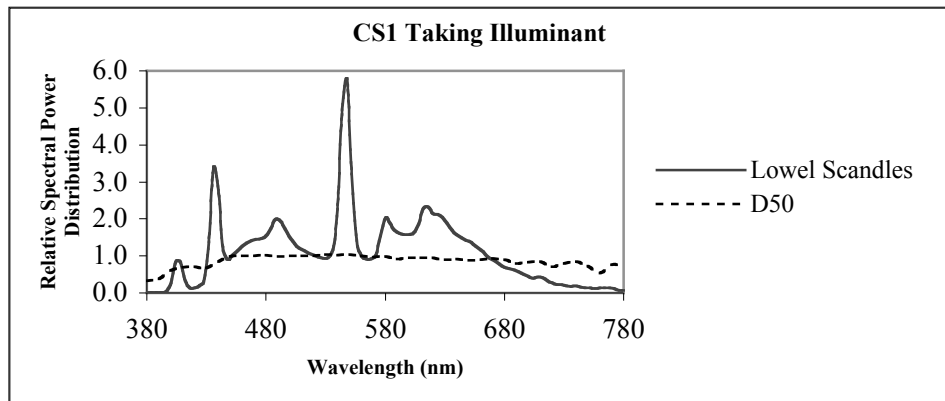


Figure 41. Relative spectral power distribution of the Lowel Scandles lights that were used in the CS1 set-up. CIE illuminant D<sub>50</sub> is included for comparison.

The capture software used was Silver Fast Leica S1 ver. 5.5.2. The monitor used was an Apple LCD monitor, on which no visual corrections were made to the images. The monitor was set so that it had a color depth of millions of colors, a resolution of 1024dpi x 760dpi and a 5500K white point.

#### 4.3.2 Case Study One: Imaging Procedure

At the start of the case study, a piece of black foam core board, which was used as the background during the imaging, was placed on the easel and taped there. Then the 26" x 22" image area was marked out and the Halon was centrally taped at the top, along with a case-study-imaging description label. Inside the marked-out area were also placed the two paintings (flower and fish). The photographer was asked to set up the camera, lights, and easel in the same way that he would if he were imaging paintings in his usual everyday imaging at the museum. He was asked to light the entire marked out area. He used the tiles on the floor to make sure that the lights were equidistant from the easel and camera and to center the camera with respect to the easel. Because the easel was tilted

slightly backward, the photographer positioned the camera so that it was tilted slightly forward facing down on the easel and used a level to make sure that it was parallel to the easel. The set-up was concluded after the photographer used a light meter to take incident light measurements over the entire image area to ensure uniform illumination. Figure 48 shows how the camera and lights were placed in relation to the easel during the imaging procedure. The labeled distances are approximate.

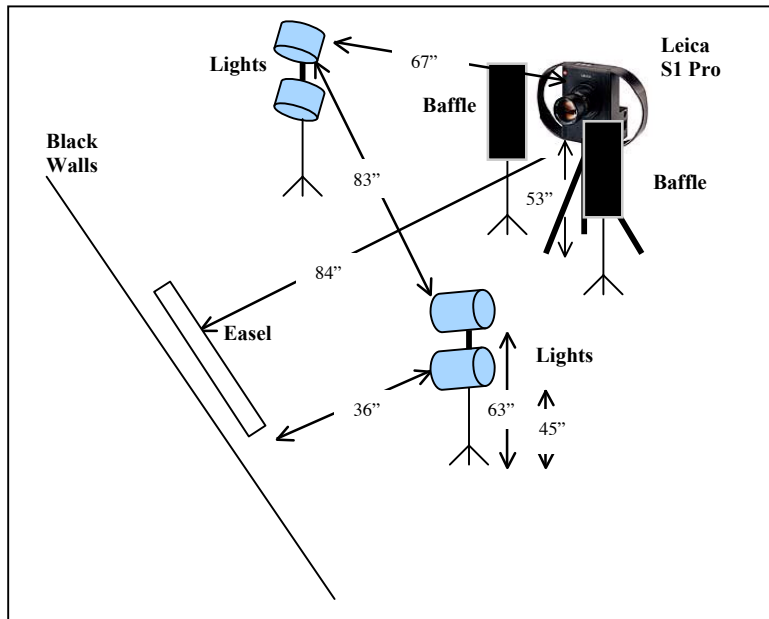


Figure 48. Schematic of CS1-imaging set-up.

After the camera, lights, and easel were set up, the photographer placed the Kodak Color Separation and Gray Scale targets in between the paintings, which he later used as a gray balance reference guide. Next, he focused the camera on the two paintings manually by looking through the viewfinder. He set the lens aperture to f/8 at the camera. Then the image was scanned in preview mode. The correct scanning exposure

time was determined remotely, using the Silver Fast Leica S1 image capture software's lightness control, by setting the white of the Kodak Color Separation to approximately 240dc in the range of 0dc – 255dc. The photographer was asked to make sure that the Halon was not clipped. The image was scanned in preview mode again to make sure that the exposure time was correct and that the Halon was not clipped. The exposure time of 0.1160119s. and aperture of f/8 became the nominal exposure settings of the case-study-imaging session. There was no ISO speed setting available with the Leica S1 Pro camera. The scanning image area was cropped on all four sides of the image in order to decrease the scanning time. Figure 49 shows approximately where the painting image was cropped.

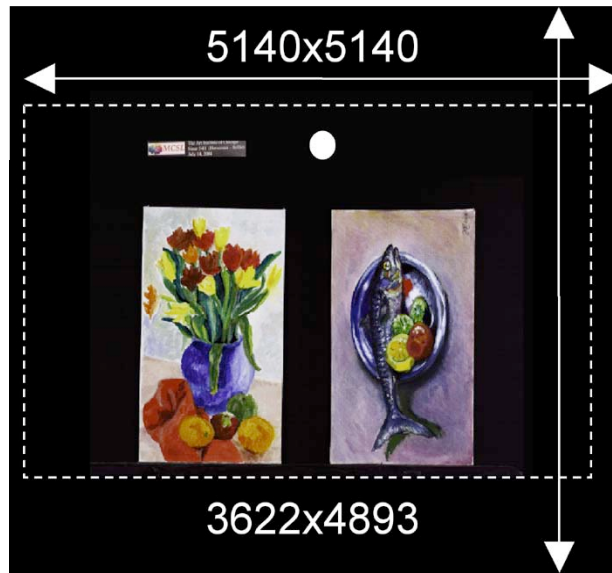


Figure 49. CS1 native resolution and cropped painting image area in pixels.

The image of the paintings was then scanned and automatically exported into Adobe Photoshop®. This image was saved in the IBM PC byte order as a 16-bit RGB tiff

file. The photographer was then asked to do any corrections to the paintings image that he would normally do before storing the image as the digital master file. In response to this, he looked at the image at 100% on his monitor and saved it without applying any further visual (tone, color, or sharpening) corrections. Figure 50 is a flowchart showing what processing and color management was applied to this tiff file before it was saved as the digital master.

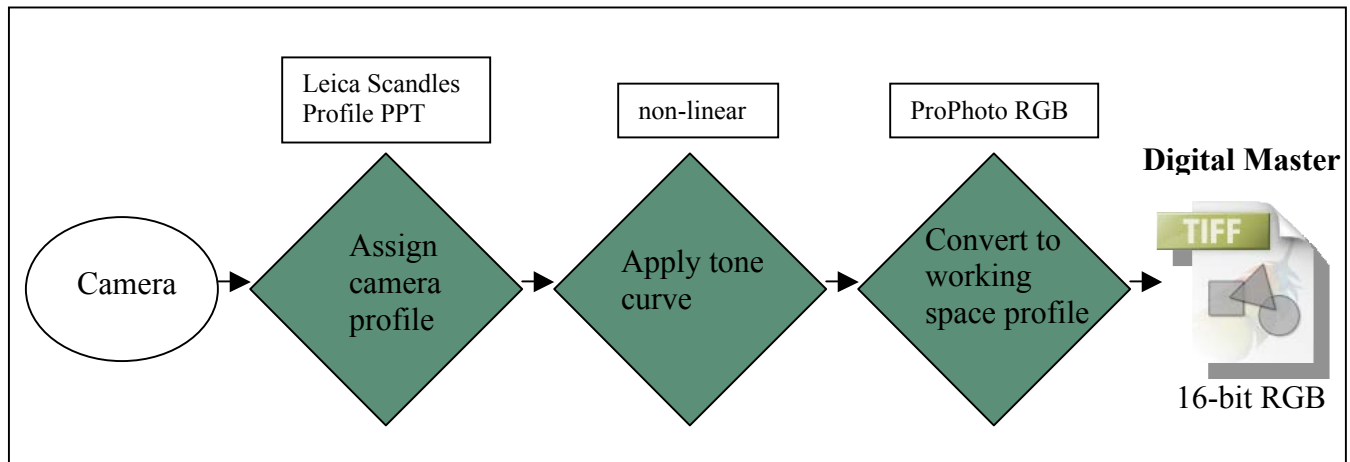


Figure 50. Flowchart of CS1 digital imaging workflow. A green background in the diamond means that the action was performed in the capture software.

A screen shot of the tone curve that was applied in the Silver Fast Leica S1 capture software is shown in Figure 51.

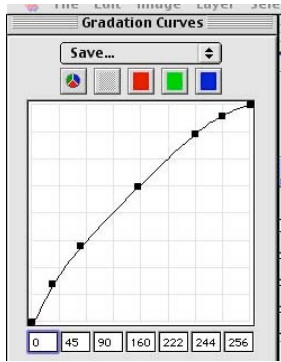


Figure 51. Screen shot of the tone curve applied by the CS1 capture software.

The digital master file had an effective resolution of 184ppi and the file size was 101 MB. This concluded the first part of the case study.

In the second part of the case study, the camera and lights set-up remained the same. Unless otherwise specified, the images taken in the second part were saved as digital master files with the same digital workflow as shown in Figure 50. The paintings were replaced by each of the three color-reproduction-accuracy targets (see Figures 25, 26, and 27) one at a time, which were each imaged once at the nominal exposure settings. The photographer refocused the camera before each image was taken. The cropped area remained the same as it was for the paintings image. The system spatial-uniformity-gray-card target, shown in Figure 13, was imaged next, after the photographer refocused. It was imaged at the nominal exposure settings and in the same cropped area as before. It was imaged twice. For the second image, the two gray cards were each rotated 180°. In the same way, after refocusing, the spatial cross-talk target, shown in Figure 38, was imaged next, twice. In the second image, the spatial cross-talk target was rotated 180°. The next target that was imaged after refocusing by the photographer was the spatial-

frequency-response target, which is shown on the left side of Figure 39. This target was also imaged at the nominal exposure settings and in the same cropped image area.

The OECF target, shown in Figure 16, was the next target to be imaged. There was no need for the photographer to refocus before imaging this target because it was at the same distance from the camera as the previous target, the SFR target. The cropped image area was the same as before. This target was imaged three times. It was imaged once at the nominal exposure settings, a second time overexposed, by setting the aperture to f/5.6 and keeping the exposure time the same, and a third time underexposed, by, again, keeping the exposure time the same and setting the aperture to f/16. After the OECF target was imaged, the camera position was marked and the PR650 spectroradiometer, which was set up on a tripod, was put in its place and aimed at the OECF target. It was then moved closer to the target in order to fit the area to be measured by the spectroradiometer inside each of the twelve patches on the OECF chart. All twelve of the patches were measured from the darkest patch to the lightest patch. The Halon was also measured. While each patch was being measured by the spectroradiometer, the rest of the target was masked by placing a piece of opaque black cardboard over it. After all of the measurements were taken with the spectroradiometer, the camera was put back in the same position that it was before it was moved.

Next, the SFR target was imaged a second time, but this time the target was placed in the upper left corner of the same cropped image area that had been used previously (see Figure 52 below). The photographer did not refocus the camera before imaging this target. This target was imaged at the nominal exposure settings.

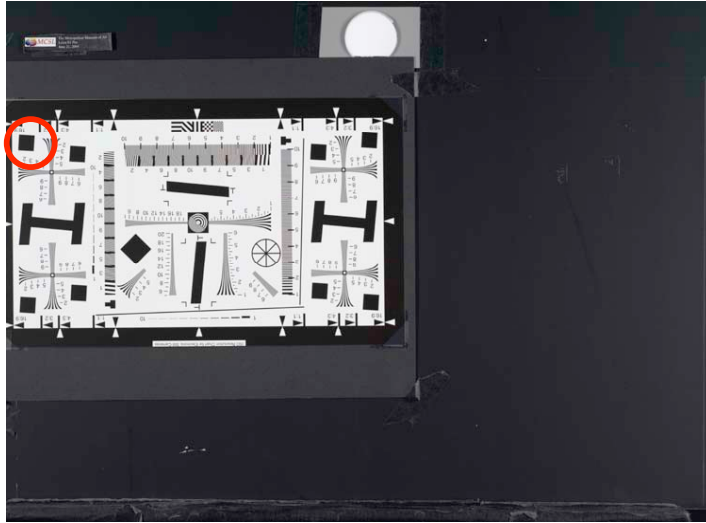


Figure 52. Placement of the SFR target in the CS1 cropped image area. The knife-edges used in the analysis are circled in red.

For the next target, the noise target, which is shown in Figure 37, the cropped image area was changed by cropping the scanned image area so that it only included the noise chart, not the Halon and museum description. This was done in order to further reduce the camera's scanning time. Again, there was no need for the photographer to refocus the camera before imaging this target, because it was at the same distance from the camera as the previous target. It was imaged at the nominal exposure settings five times.

The depth of field target was set up on the easel next. Because there were unwanted shadows on this target, the lights had to be moved closer to each other so that they illuminated this target more from the front. The lights were the only things that were changed from the set-up shown in Figure 48 above. The schematic of this new set-up is shown in Figure 53, on the right. The image on the left in Figure 53 is a digital photograph of this set-up.

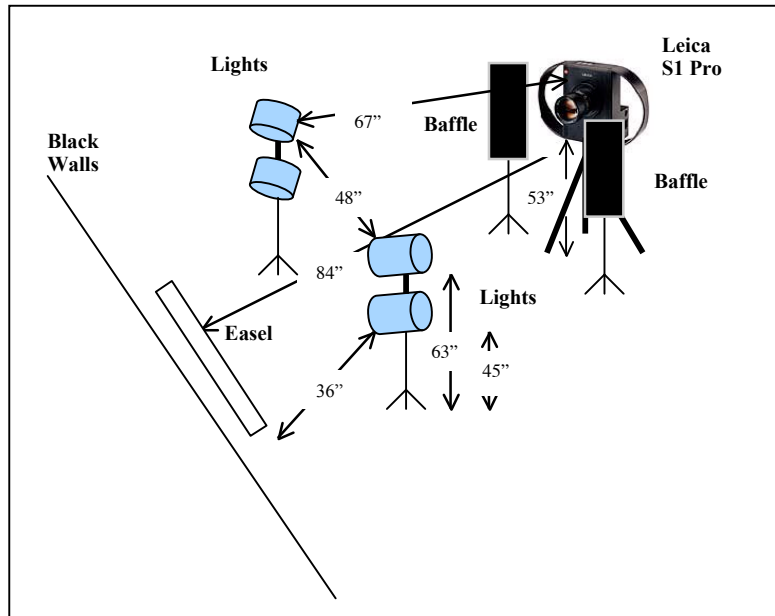


Figure 53. Image (left) and schematic (right) of the CS1 set-up for the depth of field target imaging.

The scanned image area of this target was cropped so that only the depth of field chart was inside the cropped image area. This cropping was done; again, to reduce the amount of time it took to scan the image. The photographer focused on the edge of the center square, the 3" high square. The exposure time was changed in order to compensate for the repositioning of the lights. It was determined, again using the Silver Fast Leica S1 software's lightness control by changing the exposure in the prescan so that the white of the depth of field chart was maximum unclipped. The resulting exposure time was 0.055s and the aperture remained at f/8.

The monochromator instrument was the final thing to be imaged. The set-up for the monochromator imaging is shown in Figure 54.

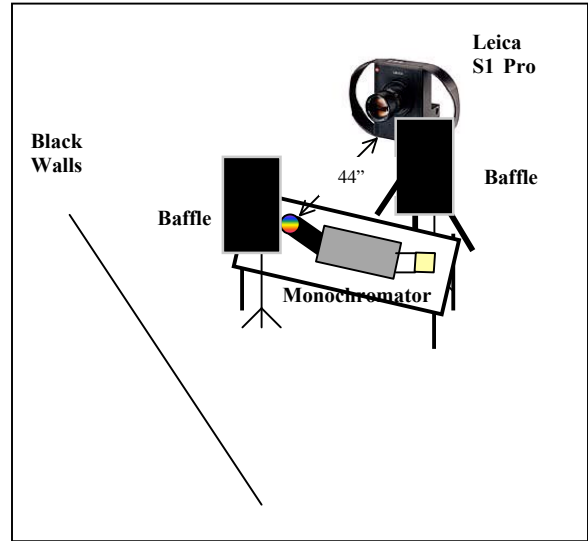
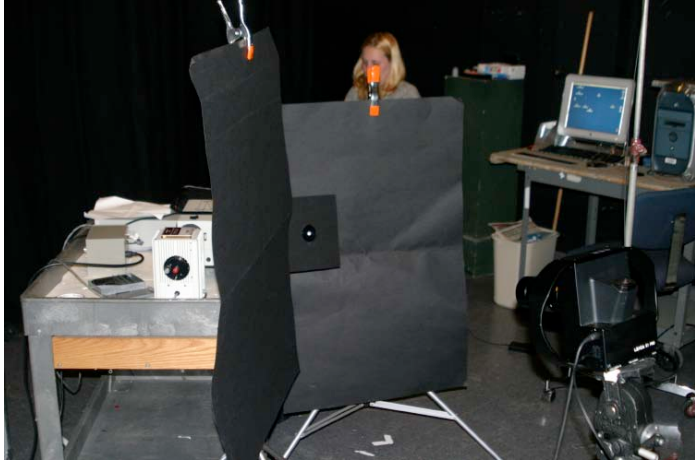


Figure 54. Image (left) and schematic (right) of the CS1 set-up for the monochromator instrument imaging.

There were no lights on when the monochromator was imaged. The photographer focused the camera so that the opening of the monochromator sphere was in focus. The aperture was opened all the way up to f/2.8 in order to maximize the amount of light being imaged by the camera. The optimal exposure time was determined to be 0.116s. Because the image was scanned from top to bottom, in order to reduce the scanning time, the camera was aimed at the spot of light coming out of the monochromator, so that it was centered at the top of the scan. The cropped area was adjusted so that it was slightly larger than the spot of light. Prior to the monochromator instrument imaging, the color management was turned off so that no profiles (camera and working space) were assigned to the images. In other words, the workflow shown in Figure 50 was not used in this case, except for the automatic tone curve application that the capture software made to each image, which was overlooked and not turned off, but should have been. This was done in order to obtain images that were as raw as possible. Thirty-six images were

taken as the monochromator bandpass peak settings ranged from 380nm to 730nm in 10nm increments. These images were saved as 16-bit RGB tiffs. Following the imaging, the PR650 spectroradiometer was used to measure the monochromator at the same bandpass peak settings that were imaged. This concluded the imaging procedure of case study one. Before the case study was ended, the photographer was asked to make his best possible visual match with the Davidson & Hemmendinger Color Rule under the Lowel Scandles lights.

Subsequent to the CS1 imaging session, the photographer was asked to image a Macbeth ColorChecker DC target that was correctly exposed, underexposed, and overexposed, and a gray card that was correctly exposed. These images, like the images taken of the monochromator instrument, had no profiles assigned to them, but the capture software applied the tone curve. The ColorChecker DC images were taken at apertures of f/8, f/16, and f/5.6 with a constant exposure time, which was not recorded. The gray card was imaged at an aperture of f/8 with the same exposure time. The camera, lights, and easel set-up was similar to that shown in Figure 48, but in this case, only one light was used on each side, not two.

#### **4.3.3 Case Study One: Results and Discussion**

##### *Colorimetric Accuracy of Digital Imaging Workflow*

Figure 55 shows the CIELAB error vector plots between the spectrophotometrically measured fish painting data and the lightness corrected digital master fish painting image CIELAB data. Table XVI shows the mean  $\Delta E_{00}$  of the fish

and flower paintings between the spectrophotometrically measured data and the lightness corrected digital master paintings image CIELAB data.

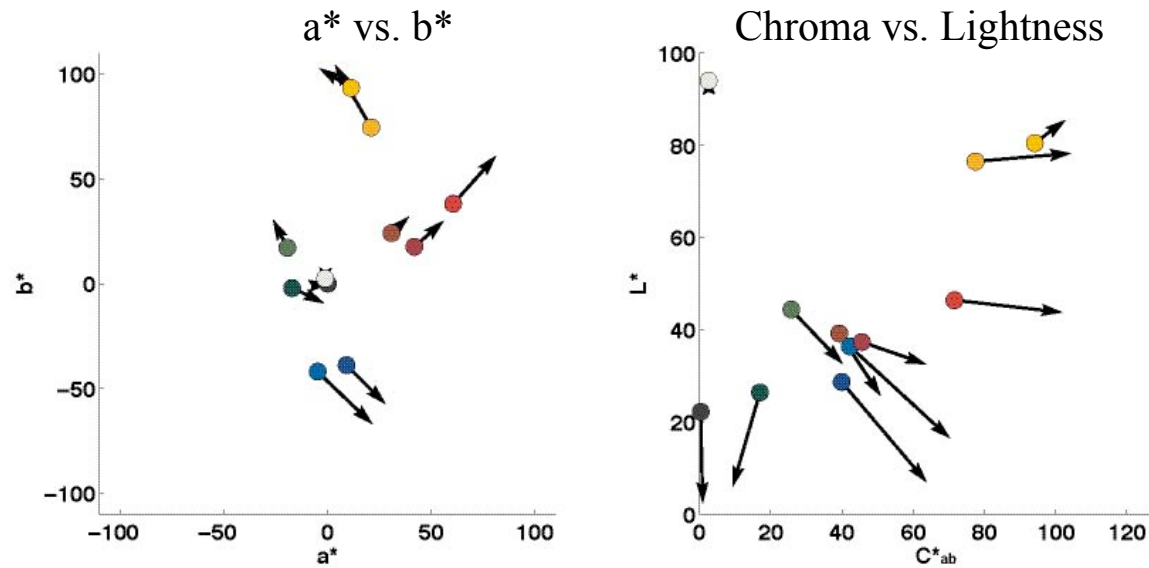


Figure 55. CS1 CIELAB  $a^*$  vs.  $b^*$  (left) and  $C^*_{ab}$  vs.  $L^*$  (right) error vector plots of the fish painting uniform patch areas between the measured patch data (dot) and the digital master image patch data (point of vector arrow).

Table XVI. CS1 mean  $\Delta E_{00}$  of fish and flower paintings' 22 total uniform patch areas between the measured spectral reflectance and the CIELAB data of the digital master image.

	<u>Lab Image Data</u>	<u>Lab Image Normalized to Halon <math>L^* = 100</math></u>
	<u><math>\Delta E_{00}</math></u>	
Digital Master Image	12.26	12.22

The  $\Delta E_{00}$  values shown in Table XVI are large. There is a small amount of improvement in the  $\Delta E_{00}$  value after the lightness correction. The causes of the color difference error can be seen in Figure 55. In general, the digital master image is more

chromatic and darker than the measured spectral reflectance data. There is some hue error, especially in the blue pigments.

### System Spatial Uniformity

The results of the system spatial uniformity for CS1 are shown in Figure 56. A table of supplemental data, Table 7-I, is in Appendix 7.1.

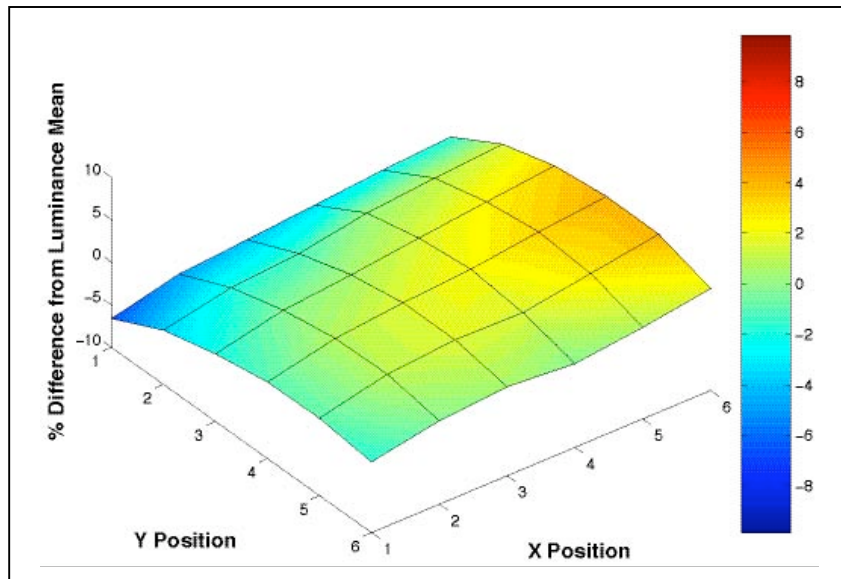


Figure 56. CS1 system spatial uniformity surface plot of % difference from luminance (Y) mean of gray card target.

In CS1, the photographer used a light meter during the set-up of the lights. The system spatial uniformity surface plot in Figure 56 shows that there was slightly more light on the right side of the gray card target image and slightly less light on the left and upper edges in comparison to the middle of the image.

### Tone Reproduction

The results of the tone reproduction for CS1 are shown in Figure 57. A table of supplemental data, Table 7-VI, is in Appendix 7.2.

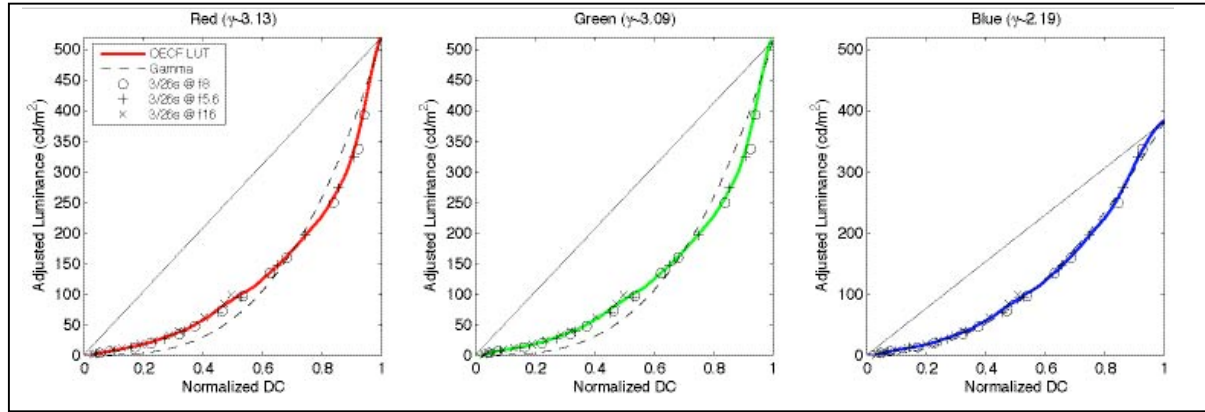


Figure 57. CS1 OECF curves.

The OECF curves for each channel have a different gamma encoding. The working space profile, ProPhoto RGB, which the CS1 images get converted to when opened, has a gamma encoding of 1.8 for all three channels. This means that the images will get interpreted with a gamma encoding that is different than the gamma encoding of the image.

### Color Reproduction Accuracy

#### *Spectral Sensitivity*

In the CS1 imaging procedure, the OECF target was not imaged with the same settings as the monochromator images. Instead, the photographer later imaged a Macbeth ColorChecker DC target that was correctly exposed, underexposed, and overexposed, and a gray card that was correctly exposed with the same settings used as the monochromator

images taken during the CS1 imaging session. Relative luminances were determined based on the measured reflectance of the central ColorChecker DC grayscale chart patches. In order to obtain the relative luminance data, the Y tristimulus value was first calculated for each of the 16 grayscale patches using their spectral reflectances, the CIE 2° observer and the spectral power distribution of the taking illuminant (Lowel Scandles) (see Equation 7 for this calculation). Equation 39 was used to calculate the relative luminances,  $l$ , for each patch of the ColorChecker DC grayscale.

$$l = (Y/Y_{\max}) * 100 \quad (39)$$

This calculation was performed based on the assumption that the illumination of the CCDC grayscale was uniform. The plot in Figure 56 of the system spatial uniformity of CS1 shows that this was an accurate assumption since the camera and lights were set up the same, so the gray card image was not used. The resulting OECF curves were similar to the OECF curves in Figure 57 in the range of digital count values that were used in the monochromator images, so the OECF data shown in Figure 57 was used, instead, to linearize the monochromator RGB image data.

The relative spectral sensitivity results for CS1 are shown in the left plot of Figure 58 and the relative spectral sensitivity curves rotated to fit the CIE 2° observer color-matching functions are shown in the right plot. These relative spectral sensitivities are those of the camera combined with the Leica daylight balancing/IR cut-off filter.

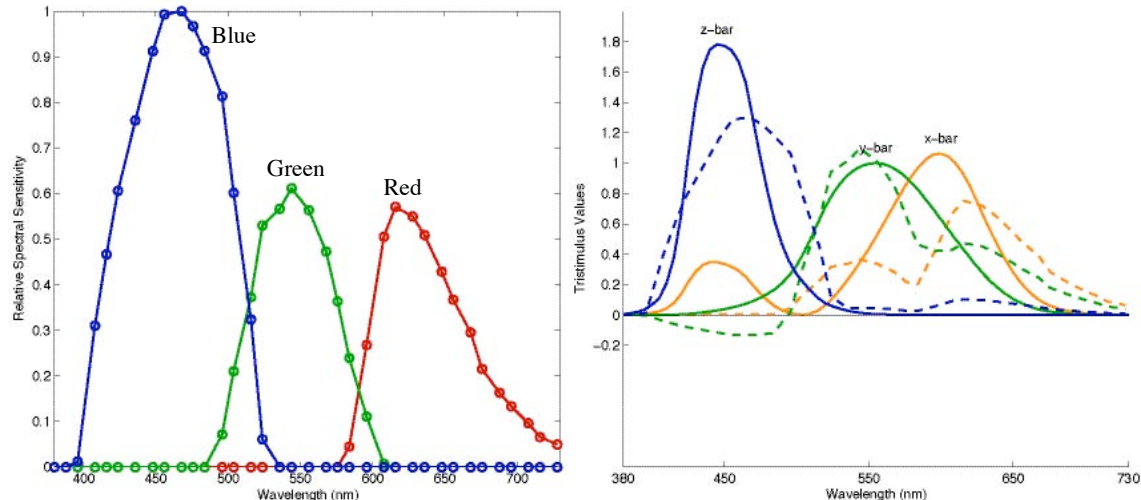


Figure 58. CS1 relative spectral sensitivities (left) and relative spectral sensitivities (dotted line) rotated to fit the CIE 2° observer (right).

The plots in Figure 58 show that even though an IR cut-off filter was used in the camera, there was a significant amount of long-wavelength visible radiation being imaged by the camera. The high amount of sensitivity of the camera to the longer wavelength part of the spectrum causes a color, such as the cobalt blue pigment, with a significant amount of reflectance in this part of the spectrum to be imaged more red (purple) in color. The lack of fit of the relative spectral sensitivities to the CIE 2° observer color-matching functions (shown in the plot on the right of Figure 58) can be explained by the shifts in peak sensitivities, a stronger (green channel) or weaker (red and blue channels) peak sensitivity, a negative lobe in the green channel, and less overlap between the channels.

The  $\mu$ -factor results for CS1 are shown in Table XVII.

Table XVII. CS1  $\mu$ -factor results.

<u>Detector</u>	<u>Color Matching Functions</u>	<u>Taking Illuminant (Measured CCT)</u>	<u>Viewing Illuminant</u>	<u><math>\mu</math>-Factor</u>
Camera CIE 2° Observer	CIE 2° Observer	Scandles (4834K)	$D_{50}$	0.68
		$D_{50}$		0.79
		Scandles (4834K)		0.82
		$D_{50}$		1.00

The  $\mu$ -factor results in CS1 show that the digital imaging system as a whole, produced a  $\mu$ -factor of 0.68, which is significantly less than the desired  $\mu$ -factor of 0.90. There is an improvement in the  $\mu$ -factor when the taking illuminant is not taken into account.

#### *Target-based Color Reproduction Accuracy*

In Figure 59, the CIELAB error vector plots are shown between the measured patch data and the image patch data of the Macbeth ColorChecker for CS1 using the Lab image data, which was normalized so that the Halon L\* equaled 100.

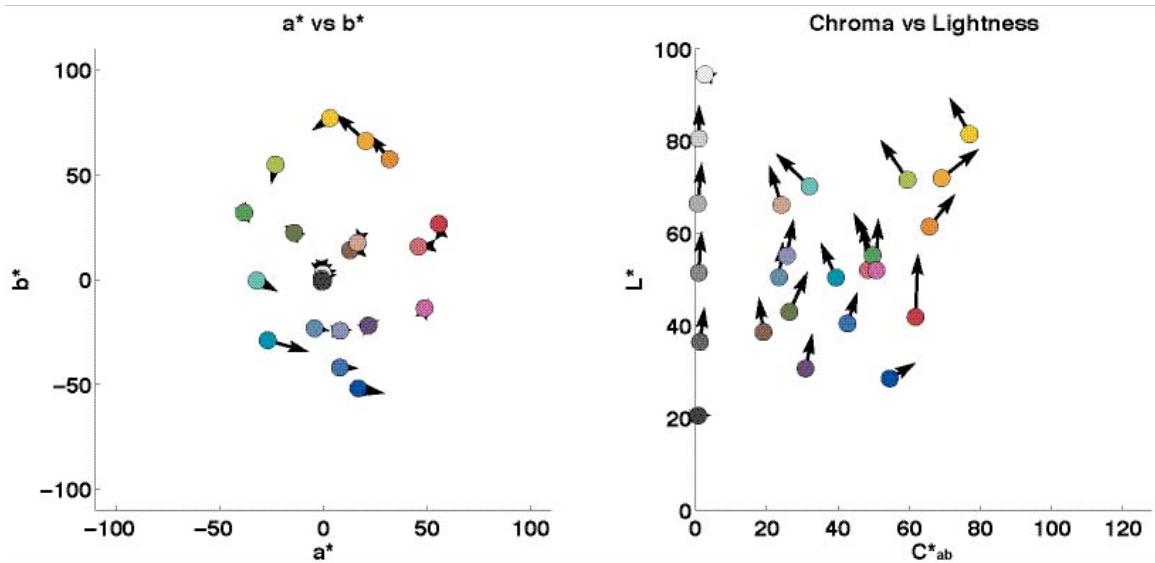


Figure 59. CS1 CIELAB  $a^*$  vs.  $b^*$  (left) and  $C^*_{ab}$  vs.  $L^*$  (right) error vector plots of the Macbeth ColorChecker between the measured patch data (dot) and the lightness corrected Lab image patch data (point of vector arrow).

In CS1, the  $a^*$  vs.  $b^*$  plot in Figure 59 shows that the more chromatic colors had a larger error than the neutral colors and these errors were mostly in hue. The errors in the  $C^*_{ab}$  vs.  $L^*$  plot were larger. Generally, the image data are systematically lighter than the measured data.

Figure 60 is a histogram of the  $\Delta E_{00}$  error distributions of the Macbeth ColorChecker for CS1, which was evaluated, again, using the lightness corrected Lab image data.

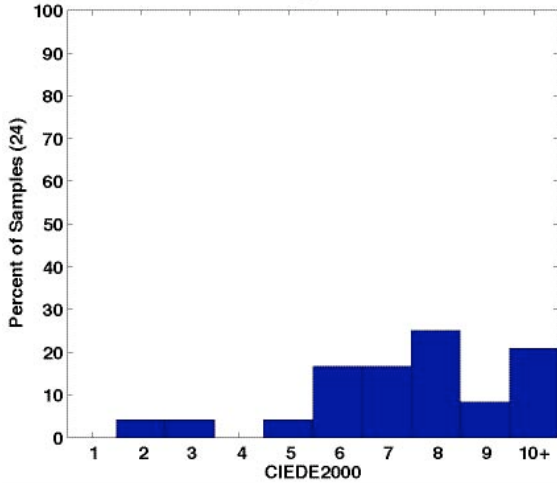


Figure 60. CS1 histogram of the  $\Delta E_{00}$  error distributions of the Macbeth ColorChecker between the measured patch data and the lightness corrected Lab image patch data.

This graph shows that, since most of the error bars are on the right side, the color difference errors were relatively high.

In Table XVIII, the mean, standard deviation and the 90<sup>th</sup> percentile data are given for the  $\Delta E^*_{ab}$  and  $\Delta E_{00}$  data between the measured patch data and the image patch data for each color reproduction accuracy chart in CS1.

Table XVIII. CS1 mean, standard deviation, and 90<sup>th</sup> percentile of the  $\Delta E^*_{ab}$  and  $\Delta E_{00}$  data between the measured patch data and the image patch data for each color reproduction accuracy chart.

<u>Color Reproduction Accuracy Chart</u>	Lab Image Data						Lab Image Normalized to Halon L* = 100					
	<u><math>\Delta E^*_{ab}</math></u>			<u><math>\Delta E_{00}</math></u>			<u><math>\Delta E^*_{ab}</math></u>			<u><math>\Delta E_{00}</math></u>		
	<u>Mean</u>	<u>Std. Dev.</u>	<u>90<sup>th</sup> Perc.</u>	<u>Mean</u>	<u>Std. Dev.</u>	<u>90<sup>th</sup> Perc.</u>	<u>Mean</u>	<u>Std. Dev.</u>	<u>90<sup>th</sup> Perc.</u>	<u>Mean</u>	<u>Std. Dev.</u>	<u>90<sup>th</sup> Perc.</u>
ColorChecker DC	9.48	5.71	17.92	6.68	2.70	10.45	11.11	5.55	18.51	7.98	2.70	11.85
ColorChecker	11.15	4.50	17.77	8.27	2.60	11.84	13.05	4.51	19.98	9.77	2.78	12.92
Esser	11.92	8.41	22.36	7.04	3.13	11.22	13.41	8.40	21.91	8.19	2.82	11.70
Esser Grayscale	5.67	4.17	10.86	4.50	2.45	7.59	7.37	3.64	10.22	5.73	2.06	7.43
BCRA	12.54	8.06	20.73	8.47	3.81	12.96	14.29	8.19	22.31	9.85	3.91	14.78
Blue Pigments	15.46	3.67	19.69	10.73	3.02	14.18	16.79	3.49	20.93	11.25	3.30	14.78
Pigment Target	22.38	22.99	47.39	14.35	12.42	25.82	23.31	22.50	47.37	15.21	11.88	26.01
Kodak Color Separation	12.70	6.13	20.94	7.68	2.75	11.78	14.03	5.66	21.68	8.63	2.70	12.48
Kodak Grayscale	7.74	5.04	16.82	6.06	3.06	11.27	8.88	4.44	16.46	6.96	2.69	11.06
IT8	8.54	4.78	14.68	5.48	1.88	8.35	10.38	4.53	16.08	6.83	1.71	9.11
IT8 Grayscale	7.08	2.01	10.65	5.57	1.26	7.15	8.54	1.41	10.44	6.63	1.04	8.07
Mean	11.33	6.86	19.98	7.71	3.55	12.06	12.83	6.57	20.54	8.82	3.42	12.74

What can be seen from this table is that the lightness corrected image data had higher  $\Delta E^*_{ab}$  and  $\Delta E_{00}$  values in comparison to the measured data than the non-lightness corrected image data. Also, when comparing the lightness corrected  $\Delta E_{00}$  values, the

color reproduction accuracy of the Esser Grayscale chart was the most accurate followed by the IT8 Grayscale chart. The Pigment Target chart was reproduced the least accurately, followed by the Blue Pigments and the BCRA charts. It is preferred, since this testing procedure is geared toward imaging paintings, that the Macbeth ColorChecker DC, the Macbeth ColorChecker, the Blue Pigments, and the Pigment Target charts are reproduced the most accurately. In this case, the CCDC and CC charts were reproduced intermediary in accuracy and the Blue Pigments chart and the Pigment Target chart were reproduced the least accurately compared to the other charts. The mean  $\Delta E^*_{ab}$  values of all of the color charts were poor compared to the desired value of 2.00.

Table XIX. CS1 mean, standard deviation, and 90<sup>th</sup> percentile of the  $\Delta E^*_{ab}$  and  $\Delta E_{00}$  data between the measured patch data and the image patch data for the Macbeth ColorChecker and ColorChecker DC charts using both the lightness corrected Lab image patch data and the RGB image patch data (CCDC characterization chart data used to build a linearized RGB to XYZ 3x3 transform) to determine the CIELAB data.

<u><b>Color Reproduction Accuracy Chart</b></u>	<u><b><math>\Delta E^*_{ab}</math></b></u>			<u><b><math>\Delta E_{00}</math></b></u>		
	<u><b>Mean</b></u>	<u><b>Std. Dev.</b></u>	<u><b>90<sup>th</sup> Perc.</b></u>	<u><b>Mean</b></u>	<u><b>Std. Dev.</b></u>	<u><b>90<sup>th</sup> Perc.</b></u>
<b>ColorChecker DC (Lab/Profile)</b>	11.11	5.55	18.51	7.98	2.70	11.85
<b>ColorChecker DC (RGB/CCDC)</b>	4.73	4.34	8.68	2.97	2.03	6.32
<b>ColorChecker (Lab/Profile)</b>	13.05	4.51	19.98	9.77	2.78	12.92
<b>ColorChecker (RGB/CCDC)</b>	5.32	3.59	10.12	2.85	1.56	5.12

Table XIX compares the color differences between the image CIELAB data determined using an embedded profile in Adobe Photoshop® (the first evaluation method described in Section 3.4.2), which are listed in Table XVIII above, and determined using an OECF linearization combined with a 3x3 RGB to XYZ transform created and optimized with

the CCDC data (the second evaluation method described in Section 3.4.2). The data in this table show that the simple 3x3 transformation performed significantly better for both charts. This means that there can be an improvement in the embedded profile used at the museum.

### *Metamerism*

Table XX shows the D&H Color Rule metameristic match data of CS1. The Lowel Scandles taking illuminant was the illuminant for all three matches in this case study.

Table XX. CS1 D&H Color Rule metameristic matches and the  $\Delta E^*_{ab}$  or  $\Delta E_{00}$  color differences of each metameristic match as “seen” by the camera and CIE 2° observer under the Lowel Scandles taking illuminant.

<u>Detector</u>	<u>Metameristic Match</u>	<u>Camera</u>	<u>CIE 2° Observer</u>	<u>Camera</u>	<u>CIE 2° Observer</u>
		$\Delta E^*_{ab}$		$\Delta E_{00}$	
<b>Camera</b>	U-18	1.03	13.91	0.83	15.70
<b>CIE 2° Observer</b>	K-10	11.92	0.85	14.10	0.86
<b>Photographer</b>	H-9	13.86	3.52	15.73	3.77

What can be seen from Table XX is that none of the three detectors had the same match under the same illuminant, which means that the camera is not “seeing” the same colors of the D&H Color Rule as that of the photographer or the CIE 2° observer. The difference in the match between the CIE 2° observer and the photographer could be caused by the photographer having slightly different spectral sensitivities (color-matching functions), since the CIE 2° observer is only an average human observer response. The color differences of the CIE 2° observer and photographer’s metameristic matches as “seen”

by the camera are very large, which reiterates the fact that their spectral sensitivities differ. The same is true for the CIE 2° observer as the detector of the camera match in CS1.

### Noise

#### *Image Noise*

Table XXI shows the image noise results of CS1 for each channel and the mean of all three channels.

Table XXI. CS1 image total, fixed pattern and temporal noise results.

	<u>Red Channel</u>	<u>Green Channel</u>	<u>Blue Channel</u>	<u>Mean of RGB Channels</u>
<b>Total Average Noise (DC)</b>	329.28	334.98	458.25	374.17
<b>Total Signal to Noise Ratio</b>	40.09	38.48	28.97	35.85
<b>Fixed Pattern Average Noise (DC)</b>	175.06	199.65	310.58	228.43
<b>Fixed Pattern Signal to Noise Ratio</b>	75.41	64.56	42.74	60.90
<b>Temporal Average Noise (DC)</b>	278.89	268.99	336.95	294.94
<b>Temporal Signal to Noise Ratio</b>	47.34	47.91	39.39	44.88
<b>Black Temporal Average Noise (DC)</b>	327.20	302.39	450.16	359.92

For CS1, the total average noise exceeds the desirable amount of noise limit of 257 digital counts in all three channels. Table XXI shows that the blue channel had significantly more total noise than the other two channels and the red channel had the

least amount of total noise in CS1. The amount of temporal noise is greater than the fixed pattern noise.

### *Color Noise*

Table XXII shows the color noise results for CS1.

Table XXII. CS1 color noise results of selected patches of the Macbeth ColorChecker.

<u>ColorChecker Patch</u>	<u>Mean Normalized DC</u>			<u>% Standard Deviation (Norm. DC)</u>			<u>MCDM</u>	
	<u>R</u>	<u>G</u>	<u>B</u>	<u>R</u>	<u>G</u>	<u>B</u>	<u><math>\Delta E^*_{ab}</math></u>	<u><math>\Delta E_{00}</math></u>
<b>Red (15)</b>	0.39	0.34	0.28	1.16	1.39	3.06	1.96	1.66
<b>Green (14)</b>	0.73	0.64	0.57	0.45	0.54	0.90	0.99	0.77
<b>Blue (13)</b>	0.48	0.48	0.64	0.77	0.82	0.75	1.15	0.75
<b>Cyan (18)</b>	0.36	0.43	0.27	1.25	0.94	3.18	1.96	1.01
<b>Magenta (17)</b>	0.57	0.52	0.70	0.62	0.75	0.69	1.05	0.63
<b>Yellow (16)</b>	0.62	0.73	0.74	0.52	0.48	0.70	0.99	0.67
<b>White (19)</b>	0.68	0.56	0.20	0.53	0.57	11.79	4.32	1.40
<b>Gray (22)</b>	0.40	0.35	0.63	1.04	1.31	0.77	1.38	0.71
<b>Black (24)</b>	0.68	0.45	0.43	0.51	0.80	1.26	1.19	0.64
<b>Mean</b>				0.76	0.84	2.57		
							<b>MMCDM</b>	1.67
								0.92

The data in Table XXII show that, for the most part, there were small differences between the amounts of noise of each color patch. The % standard deviation results show that the red channel had the least amount of color noise and the blue channel had the most. The  $\Delta E_{00}$  color difference results show that the magenta patch, the black patch and the yellow patch had the least amount of color noise and the red and white patches had the most amount of color noise.

### Dynamic Range

Table XXIII shows the dynamic range results of CS1 for each channel and the mean of all three channels.

Table XXIII. CS1 dynamic range results.

	<u>Red Channel</u>	<u>Green Channel</u>	<u>Blue Channel</u>	<u>Mean of RGB Channels</u>
<b>ISO Digital Still Camera Dynamic Range (Luminance Ratio)</b>	700.74	749.54	721.26	723.85
<b>ISO Digital Still Camera Dynamic Range (Density)</b>	2.85	2.87	2.86	2.86
<b>Theoretical Dynamic Range (Density)</b>	4.81	4.81	4.81	4.81

In CS1, the measured dynamic range was significantly less than the theoretical dynamic range in all three channels. The green channel had the most amount of dynamic range of the three channels and the red channel had the least.

### Spatial Cross-talk

Table XXIV shows, for each channel, the mean linearized value of all 30 gray patch means, the percent relative maximum difference, and the percent relative standard deviation values for CS1.

Table XXIV. CS1 summary of spatial cross-talk results.

	<u>Red Channel</u>	<u>Green Channel</u>	<u>Blue Channel</u>	<u>Mean of RGB Channels</u>
<b>Mean Linearized DC</b>	0.19	0.19	0.31	0.23
<b>Relative Maximum Difference (%)</b>	4.49	3.98	9.02	5.83
<b>Relative Standard Deviation (%)</b>	1.59	1.37	2.92	1.96

The data in Table 7-XI for CS1 in Appendix 7.3 show that the mean digital count value of a gray patch that is surrounded by white in one image is, for the most part, higher than the value of the patch in the same position surrounded by black in the other image. This is always true for the blue channel. This shows that spatial cross-talk is having an effect on the image. Table XXIV shows that the spatial cross-talk affected the blue channel the most and the green channel the least in CS1.

#### Spatial Frequency Response (SFR)

The results of the SFR for CS1 are shown in Figure 61 and Table XXV.

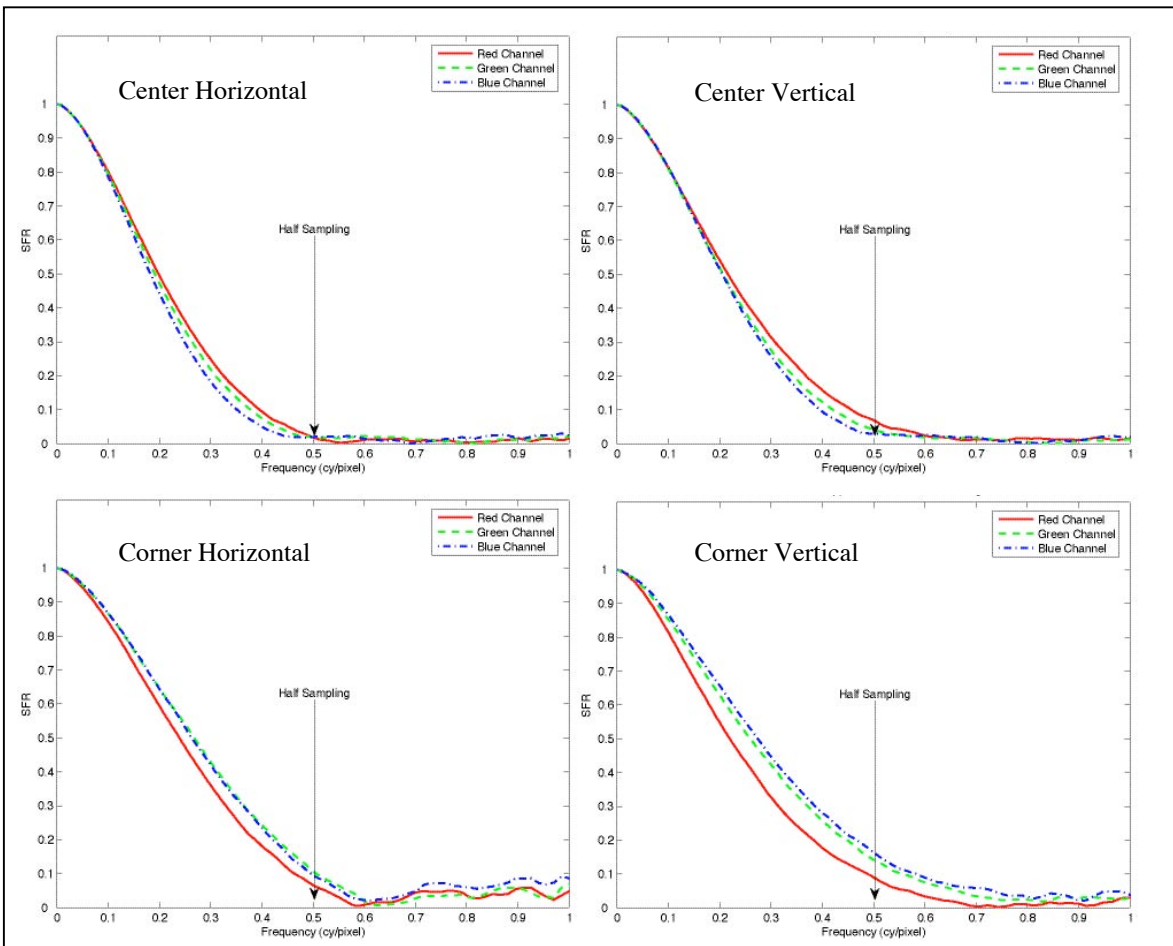


Figure 61. CS1 SFR of center horizontal edge (top left), center vertical edge (top right), upper left corner horizontal edge (bottom left), and upper left corner vertical edge (bottom right).

Table XXV. CS1 SFR area results.

Edge	Area Under SFR Curve From Frequencies of 0.0 to 0.5cy/pixel			
	Red Channel	Green Channel	Blue Channel	Mean of RGB Channels
Center Horizontal	0.431	0.415	0.395	0.414
Center Vertical	0.474	0.452	0.441	0.455
Corner Horizontal	0.504	0.550	0.545	0.533
Corner Vertical	0.485	0.548	0.569	0.534
	Mean			0.484

It is evident, from the data shown in Table XXV and Figure 61, that the SFR in the vertical direction was, generally, better than the SFR in the horizontal direction, more so in the center of the image area than the corner. Since this camera is a scanning camera that scans vertically (from top to bottom), this implies that the SFR caused by the linear array itself was better than the SFR caused by the linear array's scanning. Secondly, the SFR in the corner (off-axis) was better than the SFR in the center (on-axis) of the cropped image area. Thirdly, the red channel SFR was higher than the green channel, which was slightly higher than the blue channel in the center of the image area, but the red channel's SFR was worse than the blue and green channels in the corner of the image area.

#### Color Channel Registration

Table XXVI shows the results of the color channel registration for CS1.

Table XXVI. CS1 color channel registration results.

<u>Edge</u>	<u>Misregistration Shift (pixels)</u>		
	<u>Red Channel</u>	<u>Green Channel</u>	<u>Blue Channel</u>
<b>Center Horizontal</b>	0.066	0.000	0.527
<b>Center Vertical</b>	0.005	0.000	0.083
<b>Corner Horizontal</b>	0.129	0.000	0.373
<b>Corner Vertical</b>	0.071	0.000	0.305
<b>Maximum</b>	0.129	0.000	0.527
<b>Mean</b>	0.067	0.000	0.322
<b>Mean of RGB Channels</b>			0.130

\*Green channel used as reference

It is evident, from the data in Table XXVI, that the blue channel misregistration shift was much greater than that of the red in comparison to the green channel. The maximum amount of misregistration was approximately half of a pixel, which was on the

blue channel's center horizontal edge. Out of the four edges, the center vertical edge had the least amount of misregistration shift. The misregistration error on the horizontal knife-edge was greater than that of the vertical edge in both the center and corner of the cropped image area. Since this camera is a scanning camera that scans vertically (from top to bottom), this implies that the misregistration error caused by the linear array itself was less than that caused by the linear array's scanning.

### Depth of Field

Figure 62 shows the plot of the depth of field distance vs. area under the SFR curve for the vertical edge of each color channel for CS1.

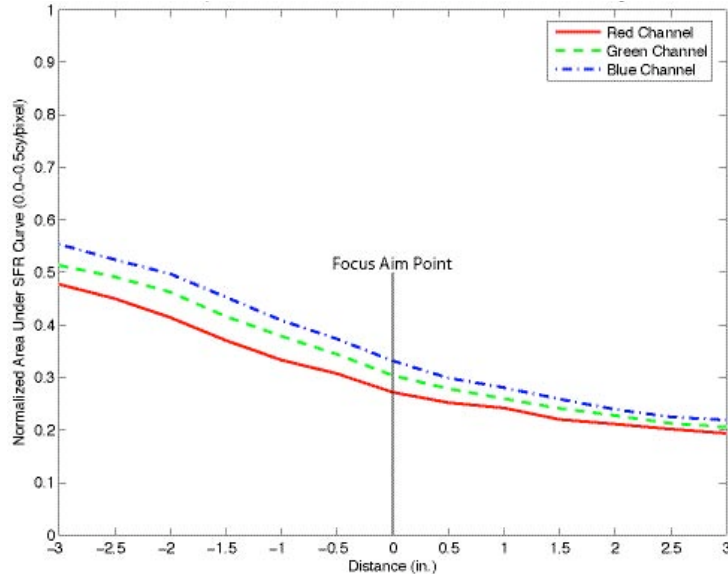


Figure 62. CS1 depth of field area under SFR curve vs. distance of the vertical edge.

Differences between the red, green and blue color channels in the plot in Figure 62 were caused by their misregistration shifts (see the Color Channel Registration part of this section). Two pieces of information can be obtained about the depth of field image of CS1 from this plot. One is that the sharpness, and therefore the depth of field, of the image decreased as the camera-to-subject distance changed. The other is that the focusing method (looking through the ground glass), which was used to focus on the 3" high column during the imaging of the depth of field target, was not accurate. Instead of the focus being at the focus aim point, it was at least 3" farther away from the camera.

#### **4.4 Case Study Two**

Case study two, CS2, was performed on July 8-9, 2004.

##### **4.4.1 Case Study Two: Digital Imaging System Description**

The camera used at the museum's studio, which was located in an art collection storage space, was a Phase One PowerPhase FX (SN: EG000472) digital camera, which is a 3-channel (RGB) tri-linear-array-CCD scanning back camera that scans from left to right across the image plane. The maximum native resolution of the camera is 10,500p x 12,600p. The scanning back was on a TTI 4x5 view camera body. The lens used was a 150mm Schneider enlarging lens. The filter used behind the lens was a Phase One tungsten balancing/IR cut-off filter. The camera was set up on a copy stand and the distance of the lights from the table was adjustable. This camera is typically used to image paintings (varnished and unvarnished) and other flat works, such as photographs, prints and drawings, for the purpose of protecting vulnerable originals from use, to

document conservation treatment, and to include the digital images in a collection management system. Reproductions are created in the forms of prints and Internet images. Three people in the photography department at the museum can operate this camera. Two photographers did the imaging, one on the first day and the other on the second day. The photographers did receive background training for this camera system.

There were two TTI Reflective Lighting tungsten lights, which each had 4 OSRAM 250W Quartz Halogen photo optic bulbs with diffusers in front of them, used to light the scene. In his day-to-day imaging, the photographer does not usually change the positions of the lights when a new object is imaged unless the object being imaged changes drastically in size. When the light positions are changed, the uniformity of it is checked with a light meter. Table XXVII shows the CCT, chromaticity coordinates, and luminance of this illumination. Figure 63 shows the relative spectral power distribution of the TTI tungsten lights. These data were obtained by measuring the Halon, which was placed in the scene, with a calibrated PR650 spectroradiometer.

Table XXVII. TTI tungsten taking illuminant characteristics

<b>Correlated Color Temperature</b>	2980K
<b>Chromaticity x (2° Observer)</b>	0.4419
<b>Chromaticity y (2° Observer)</b>	0.4119
<b>Luminance (2° Observer)</b>	1274cd/m <sup>2</sup>

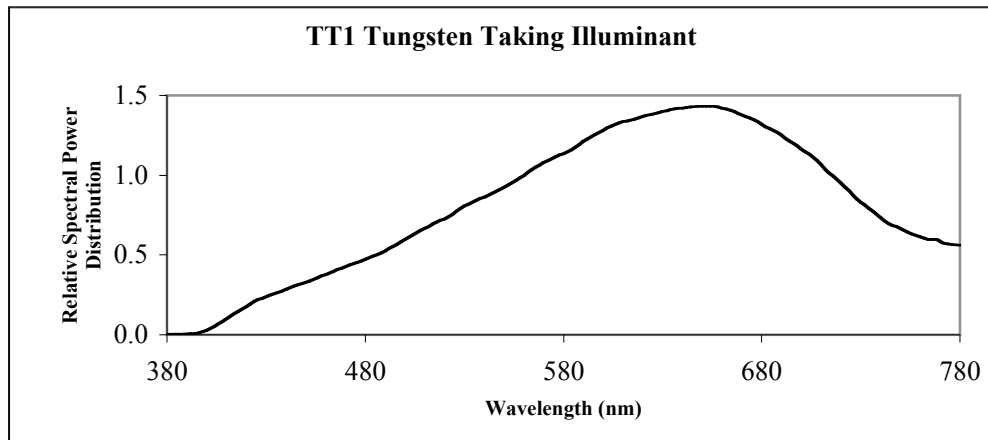


Figure 63. Relative spectral power distribution of the TTI tungsten lights that were used in the CS2 set-up.

The capture software used was Image Capture 3.5.2 for Phase One FX. The monitors used were a Barco monitor, on which the visual corrections were made, and an Apple LCD display, which was not used to make visual corrections. The Barco monitor was set so that it had a color depth of millions of colors, a resolution of 1152dpi x 870dpi at 80Hz, a gamma of 2.2 and a 5500K white point.

#### 4.4.2 Case Study Two: Imaging Procedure

At the start of the case study on day one, a piece of black board, which was used as the background during the imaging, was placed on the copy stand table and taped there. The monochromator instrument was first to be imaged. The set-up for the monochromator imaging is shown in Figure 64. The labeled distances are approximate.

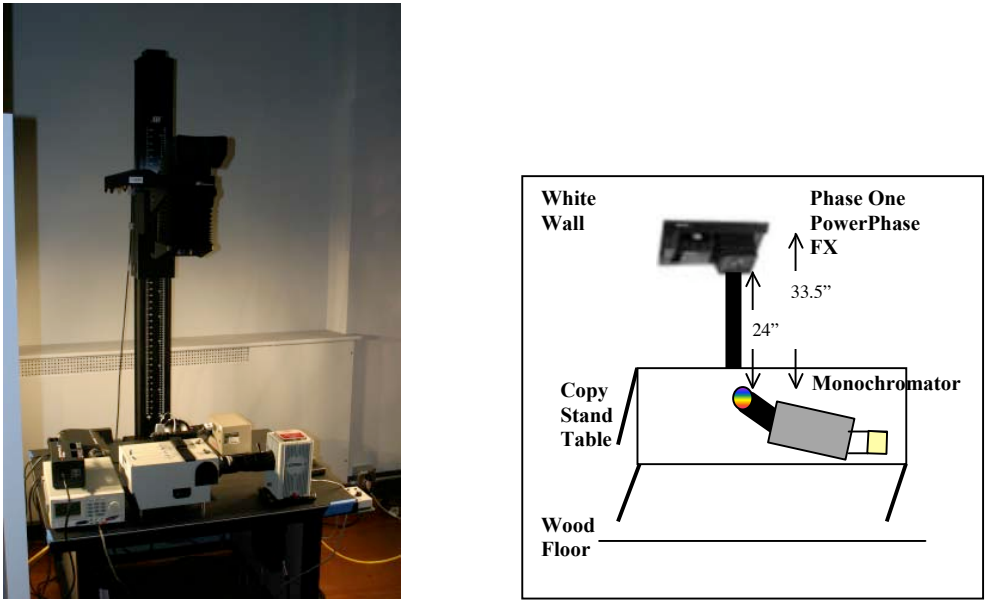


Figure 64. Image (left) and schematic (right) of the CS2 set-up for the monochromator imaging.

There were no lights on when the monochromator was imaged. The photographer focused the camera so that the opening of the monochromator sphere was in focus. The aperture was opened all the way up to f/4 in order to maximize the amount of light being imaged by the camera. The optimal exposure time was determined to be 1/10s. The ISO speed was set to 200 and remained at that setting throughout the entire case study imaging procedure. In order to reduce the scanning time, the scanned image area was cropped so that it was slightly larger than the spot of light coming out of the monochromator. Prior to the monochromator instrument imaging, the color management was turned off so that no profiles (camera and working space) were assigned to the images. Also, any automatic corrections that the software would make to the images were turned off. This was done in order to obtain images that were as raw as possible. Thirty-six images were taken as the monochromator bandpass peak settings ranged from

380nm to 730nm in 10nm increments. These images were saved as 16-bit RGB tiffs.

Following the imaging, the PR650 was used to measure the monochromator at the same bandpass peak settings that were imaged. It was found, during these measurements, that the monochromator bandpass had shifted down approximately 20nm during shipping. In other words, when the bandpass peak should have been at 380nm, it was actually at about 360nm. Because of this shift, the PR650 spectroradiometer was not sensitive enough to measure the 360nm and 370nm bandpass peaks. In the spectral sensitivity analysis, these bandpass peaks were omitted and only the bandpass peak range of 380nm to 710nm was analyzed.

Next, the monochromator was removed and the paintings were next to be imaged. Before the paintings were set-up on the copy stand table, the 26" by 22" image area was marked out and the Halon was centrally taped at the top, along with the case study-imaging description label. The two paintings (flower and fish) were then placed inside the marked-out area. The photographer was asked to set up the camera and lights in the same way that he would if he were imaging paintings in his usual everyday imaging at the museum. He was asked to light the entire marked out area. The photographer decided to leave the lights in the same position that they were from his previous imaging and he didn't think that it was necessary to check the illumination uniformity with a light meter. Figure 65 shows how the copy stand was set up for the imaging of the paintings.

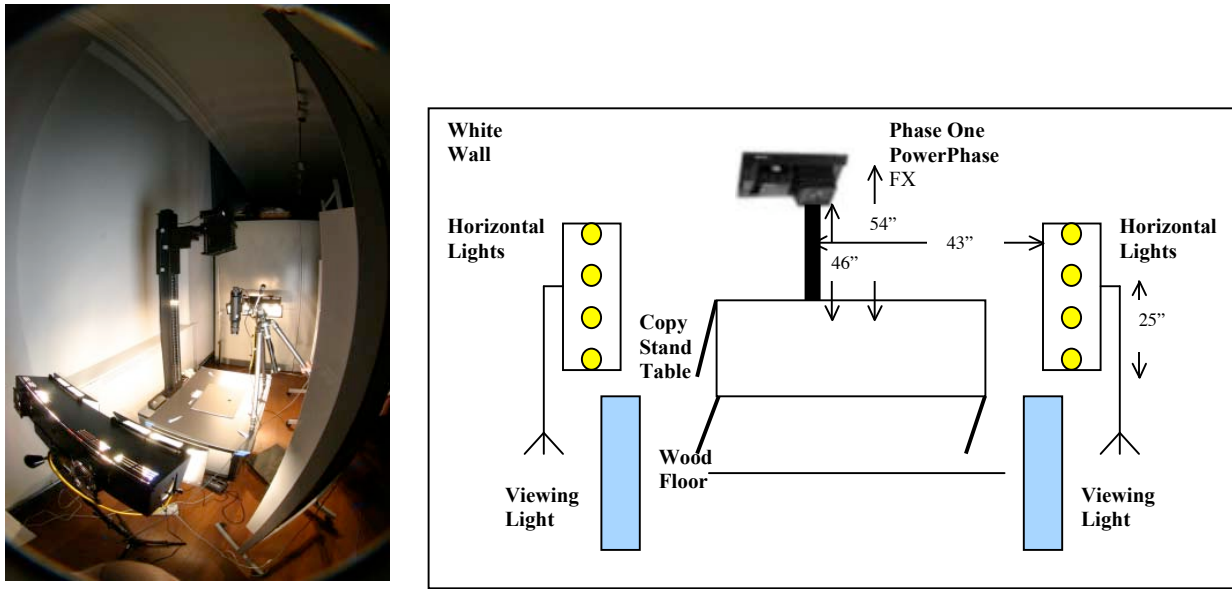


Figure 65. Image (left) and schematic (right) of CS2-imaging set-up. The OECF target was being measured by the PR650 spectroradiometer when this image was taken.

After the copy stand was set up, the photographer placed a QpCard 101 in the scene with the paintings, which he later used as a gray balance reference guide. Next, he focused the camera on the two paintings manually, using a frequency-based focusing tool in the image capture software. He set the lens aperture, which was continuous, to f/11 at the camera. Then the image was scanned in preview mode. The photographer was asked to make sure that the Halon was not clipped in the scanned image. The photographer determined the exposure time in the image capture software so that the digital count value of the Halon was maximum unclipped. The exposure time of 1/20s. and aperture of f/11 became the nominal exposure settings of the case-study-imaging session. The ISO speed setting remained at 200. The scanned image of the paintings was not cropped. The scan method in the image capture software was set to “high resolution,” which scanned the image so that only half of the pixels were present in the final image. Therefore, the

image area was half of the native resolution. After the paintings image was scanned, it was exported from the capture software and saved in the Macintosh byte order as a 16-bit RGB tiff file. This image is denoted as the “camera” image in Figure 66.

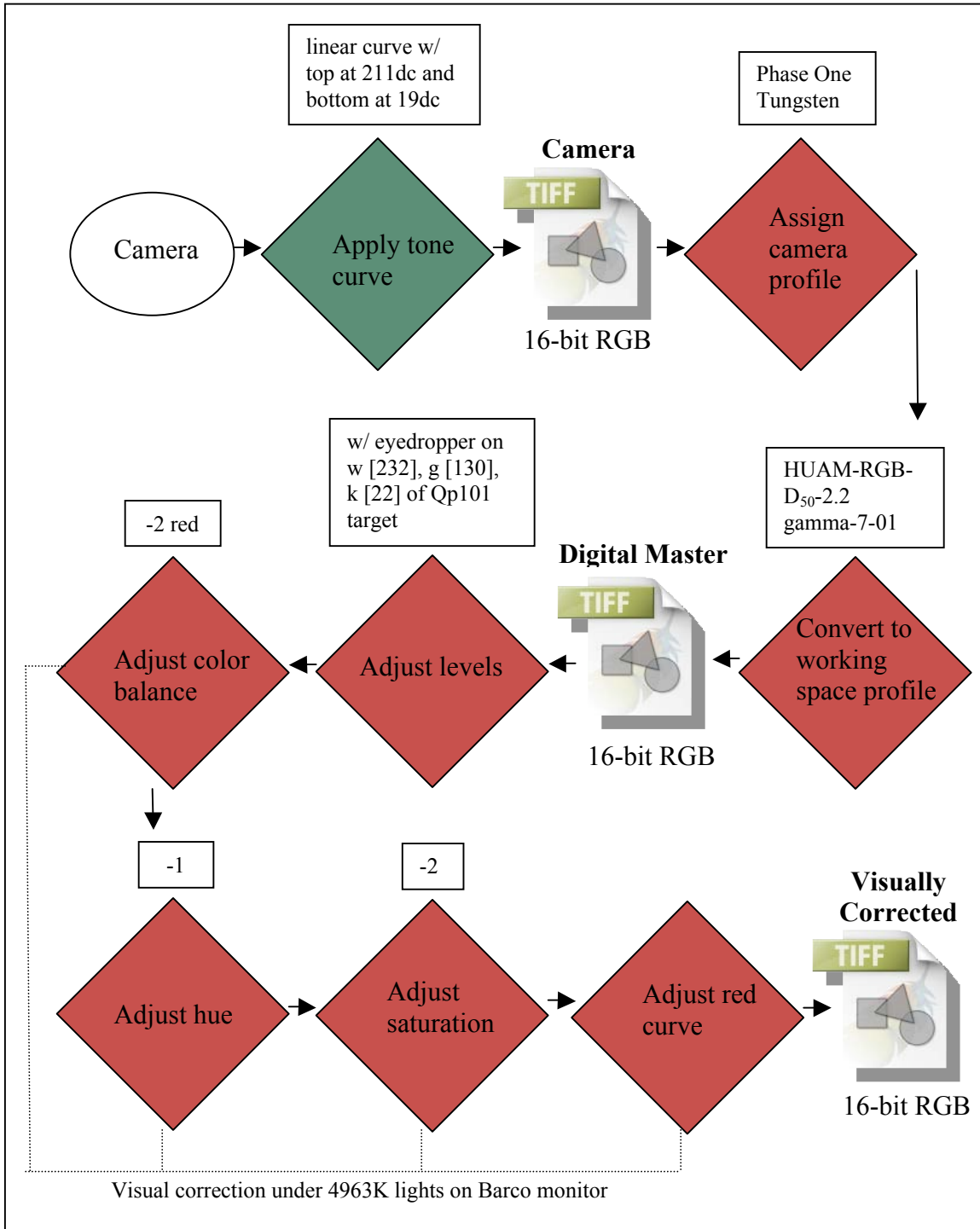


Figure 66. Flowchart of CS2 digital imaging workflow. A green background in the diamond means that the action was performed in the capture software. A red background in the diamond means that the action was performed in Adobe Photoshop®.

The image capture software had automatically applied a tone curve before the “camera” image was exported. A screen shot of the linear tone curve that was applied in the Phase One Image Capture software is shown in Figure 67.

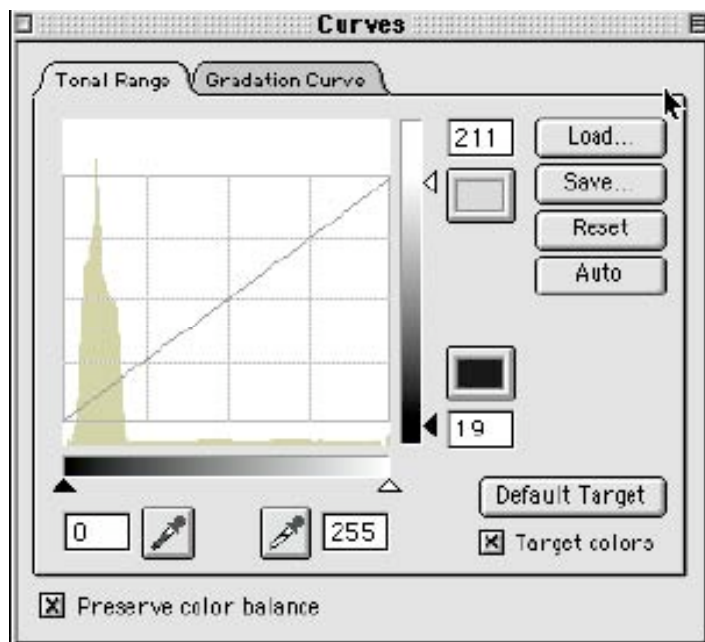


Figure 67. Screen shot of the tone curve applied by the CS2 capture software.

The photographer was then asked to do any corrections to the paintings image that he would normally do before storing the image as the digital master file. In response to this, the photographer opened the “camera” image in Adobe Photoshop®, assigned a camera profile to the image and converted it to a working space. This image was saved as the digital master 16-bit RGB tiff image file (see Figure 66). The digital master file had an effective resolution of 229ppi and the file size was 189MB. Because the photographer usually also creates a visually corrected image, he was asked to visually correct the paintings digital master image and save it. Figure 66 shows what processing

the photographer did to the visually corrected image before it was saved as a 16-bit RGB tiff image file. It took the photographer approximately 15 minutes to do the visual corrections. When this image was visually corrected, both paintings were corrected as if they were one painting since they both contained the same pigments. During the visual correction, the photographer turned off the TTI tungsten lights and viewed the paintings under two “D<sub>50</sub>” fluorescent lights. The image in Figure 68 shows the photographer making his visual corrections. Table XXVIII shows the CCT, chromaticity coordinates, and luminance of the viewing illumination. Figure 69 shows the relative spectral power distribution of the fluorescent viewing illumination. These data were obtained by measuring the Halon, that was in the scene, with a calibrated PR650 spectroradiometer.



Figure 68. Image of CS2 photographer making visual corrections to the paintings image.

Table XXVIII. 4963K fluorescent viewing illuminant characteristics.

<b>Correlated Color Temperature</b>	4963K
<b>Chromaticity x (2° Observer)</b>	0.2540
<b>Chromaticity y (2° Observer)</b>	0.3538
<b>Luminance (2° Observer)</b>	401.7cd/m <sup>2</sup>

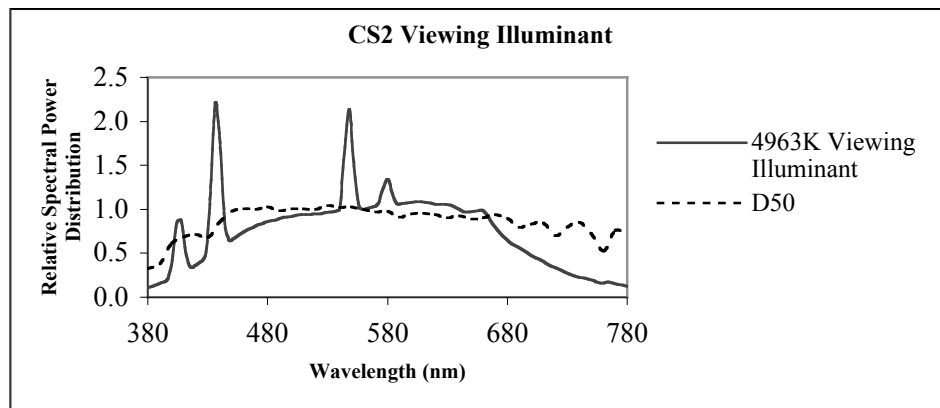


Figure 69. Relative spectral power distribution of the CS2 viewing illumination. CIE illuminant D<sub>50</sub> is included for comparison.

In the next part of the case study, the copy stand set-up remained the same. Unless otherwise specified, the images taken in the remainder of the case study were saved as both “camera” and digital master images with the same digital workflow as shown in Figure 66. The paintings were replaced by each of the three color-reproduction-accuracy targets (see Figures 25, 26, and 27) one at a time, which were each imaged once at the nominal exposure settings. The photographer refocused the camera before each image was taken. The scanned image area remained uncropped for these images. The system-spatial-uniformity-gray-card target, shown in Figure 13, was imaged next, after the photographer refocused. It was imaged at the nominal exposure settings and in the same, uncropped area as before. It was imaged twice. For the second image,

the two gray cards were each rotated 180°. In the same way, after refocusing, the spatial cross-talk target, shown in Figure 38, was imaged next, twice. In the second image, the spatial cross-talk target was rotated 180°.

The next target that was imaged by the photographer was the noise target, which is shown in Figure 37. It was not necessary to refocus the camera before imaging this target because it was the same distance from the camera as the previous target. The image scanning area was cropped down so that the scanning time was decreased. It was imaged at the nominal exposure settings five times. The spatial-frequency-response target, shown in the left image in Figure 39, was the next target to be imaged. Again, there was no need for the photographer to refocus the camera before this target was imaged. This target was scanned, uncropped, at the nominal exposure settings. The SFR target was then imaged a second time at the nominal exposure settings, but this time the target was placed in the upper left corner of the uncropped image area (see Figure 70 below). The photographer did not refocus the camera before imaging the SFR target again.

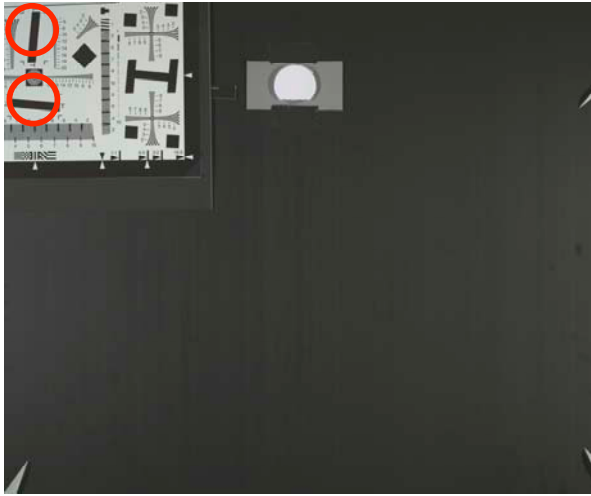


Figure 70. Placement of the SFR target in the CS2 uncropped image area. The knife-edges used in the analysis are circled in red.

This concluded the imaging on the first day of the case study. Before the case study was ended for the day, the photographer was asked to make his best possible visual match with the Davidson & Hemmendinger Color Rule under the TTI tungsten lights.

On the second day of CS2, a different photographer did the imaging. The first target that she imaged was the OECF target, shown in Figure 16. The photographer made sure that the target was in sharp focus and the scanned image area remained uncropped. This target was imaged three times. It was imaged once at the nominal exposure settings, a second time overexposed, by setting exposure time to 1/10s. and keeping the aperture the same, and a third time underexposed, by, again, keeping the aperture the same and setting the exposure time to 1/60s. The OECF target was then imaged three more times at the same exposure settings as before. This time, like the monochromator instrument imaging, the color management was turned off so that no profiles (camera and working space) were assigned to the images. Also, any automatic corrections that the software would make to the images were turned off. These three images were saved as 16-bit

RGB tiffs. After the OECF target was imaged, it was measured with the PR650 spectroradiometer, which was set up on a tripod at an angle to the OECF target that was approximately the same as the camera. All twelve of the patches were measured from the darkest patch to the lightest patch. The Halon was also measured. While each patch was being measured by the spectroradiometer, the rest of the target was masked by placing a piece of opaque black cardboard over it. After all of the measurements were taken with the spectroradiometer, it was removed.

Before the depth of field target was imaged next, the settings were returned to the same settings as the first set of OECF images, which is the same as the “camera” and digital master file, shown in Figure 66. Because there were unwanted shadows on the depth of field target, the lights had to be moved closer to each other so that they illuminated this target more from above. The lights were the only things that were changed from the set-up shown in Figure 65 above. The schematic of the new set-up is shown in Figure 71.

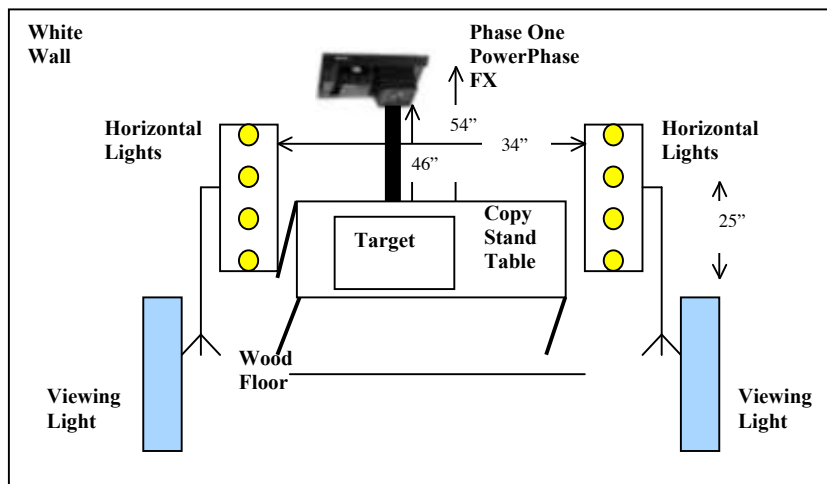


Figure 71. Schematic of the CS2 set-up for the depth of field target imaging.

The photographer focused on the edge of the center square, the 3" high square. The exposure time was changed in order to compensate for the repositioning of the lights. The new exposure time was 1/40s. and the aperture remained the same. This concluded the imaging procedure of case study two. After the imaging procedure was finished, measurements were made off of the monitor with the PR650 spectroradiometer. First, the visually corrected paintings image was opened in Adobe Photoshop® with the embedded HUAM-RGB profile used and the eleven uniform patches of pigment of each painting were zoomed in on and measured. Then the digital master image with the ColorChecker target in it was opened with the embedded HUAM-RGB profile used and each of the 24 patches were measured. Next, the ColorChecker digital master image was cropped down and, using the paint bucket tool, was filled with red (255, 0, 0), green (0, 255, 0), blue (0, 0, 255), white (255, 255, 255), black (0, 0, 0), and grays with equal digital values of 24, 48, 90, 180, and 224, consecutively. Each of these colors were measured with the PR650 spectroradiometer. Finally, the Halon was placed on the monitor and the ambient room light that was hitting the monitor was measured. Before the case study was ended, the photographer was asked to make her best possible visual match with the Davidson & Hemmendinger Color Rule under the TTI tungsten lights.

#### **4.4.3 Case Study Two: Results and Discussion**

##### Colorimetric Accuracy of Digital Imaging Workflow

Figure 72 shows the CIELAB error vector plots between the spectrophotometrically measured fish painting data and the lightness corrected digital master fish painting image CIELAB data, between the lightness corrected digital master

fish painting image CIELAB data and the lightness corrected visually corrected fish painting image CIELAB data, and between the spectrophotometrically measured fish painting data and the CIELAB data obtained from the CRT spectral radiance measurements of the non-lightness corrected visually corrected image. Table XXIX shows the mean  $\Delta E_{00}$  of the fish and flower paintings between the spectrophotometrically measured data and the lightness corrected digital master paintings image CIELAB data, the lightness corrected visually corrected paintings image CIELAB data and the CRT spectral radiance measurement CIELAB data.

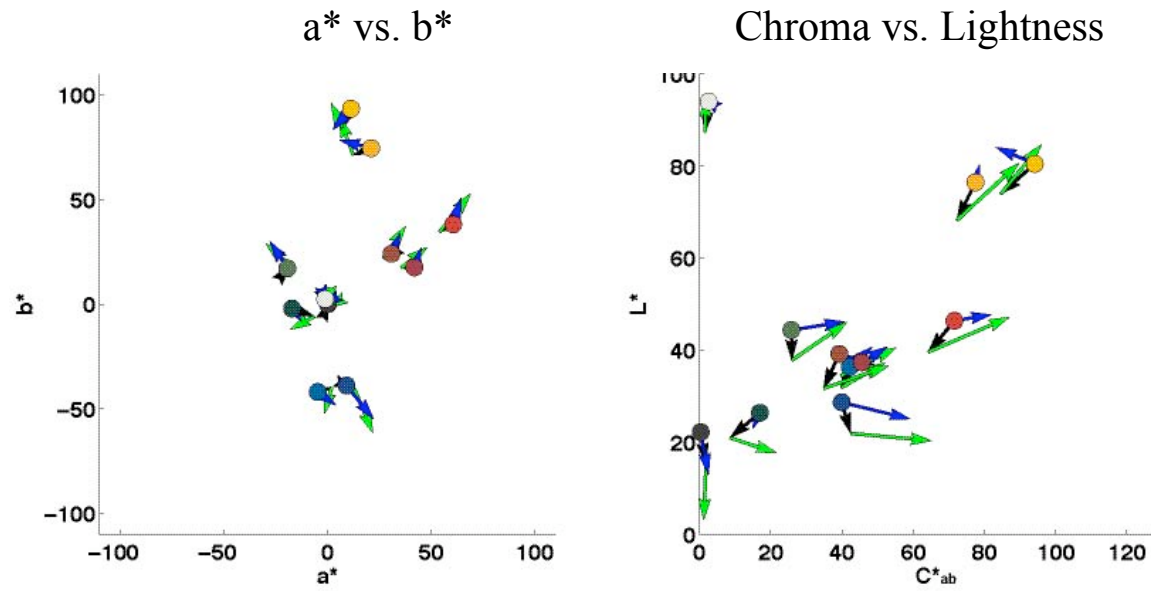


Figure 72. CS2 CIELAB  $a^*$  vs.  $b^*$  (left) and  $C^*_{ab}$  vs.  $L^*$  (right) error vector plots of the fish painting uniform patch areas between the measured patch data (dot) and the 1. Digital master image patch data (point of black vector arrow), 2. Visually corrected image patch data (point of green vector arrow), and 3. Spectroradiometric measurements of the CRT monitor of the non-lightness corrected visually corrected image patch data (point of blue vector arrow).

Table XXIX. CS2 mean  $\Delta E_{00}$  of fish and flower paintings' 22 total uniform patch areas between the measured spectral reflectance and the CIELAB data of the digital master image, visually corrected image, and the CRT spectroradiometric measurements of the visually corrected image.

	<u>Lab Image Data</u>	<u>Lab Image Normalized to Halon L* = 100</u>
	<u><math>\Delta E_{00}</math></u>	
<b>Digital Master Image</b>	6.87	4.01
<b>Visually Corrected Image</b>	6.94	7.58
<b>CRT Measurements</b>	5.75	N/A

Since the purpose of visual editing the digital master image is to improve its color accuracy (make it appear more like the original), it would be expected that the  $\Delta E_{00}$  of the visually corrected image would be less than the digital master image. It would also be expected that the green error vectors would be the same length as, but in the exact opposite direction than the black vectors in Figure 72, that is, aiming back to the spectrophotometrically-measured values depicted by the colored dots. The results show that the  $\Delta E_{00}$  of the visually corrected image is larger than that of the digital master image. The green vectors should point to the measured values (colored dots) in Figure 72, but, for the most part, they do not. Also, it would be expected, if the monitor was calibrated accurately, that the CRT measurements' blue error vectors would point to the same place as the visually corrected image green vectors, which means that the photographer would see the same colors on the monitor that are in the visually corrected image file. This is not always the case, as can be seen in Figure 72. Even though there were inaccuracies of the monitor calibration, the  $\Delta E_{00}$  of the CRT measurements were smaller than those of the digital master, which shows that the photographer did improve the color of the image on the monitor, but those improvements did not get stored in the visually edited image file itself, which will be viewed later on a different monitor.

The  $\Delta E_{00}$  values shown in Table XXIX are not very large. There is a small amount of improvement in the  $\Delta E_{00}$  value after the lightness correction for the digital master image, but the color difference gets larger after the lightness correction of the visually corrected image. The causes of the color difference error can be seen in Figure 72. Overall, the error vectors are short (the amounts of error are small). In general, the digital master image is slightly less chromatic and darker than the measured spectral reflectance data, and the visually corrected image is more chromatic than the measured spectral reflectance data and the digital master image.

### System Spatial Uniformity

The results of the system spatial uniformity for CS2 are shown in Figure 73. A table of supplemental data, Table 7-II, is in Appendix 7.1. The camera image of the gray card target was used for this analysis.

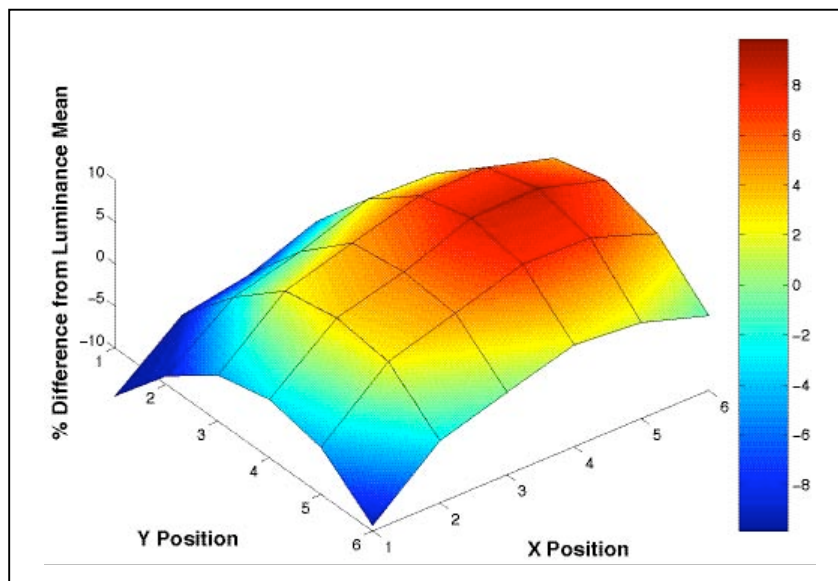


Figure 73. CS2 system spatial uniformity surface plot of % difference from luminance (Y) mean of gray card target.

In CS2, the photographer did not use a light meter during the set-up of the copy stand lights. The system spatial uniformity surface plot in Figure 73 shows that there was a hot spot on the right side of the gray card target image and much less light on the left and upper edges in comparison to the middle of the image.

### Tone Reproduction

The results of the tone reproduction for CS2 are shown in Figure 74. A table of supplemental data, Table 7-VII, is in Appendix 7.2. The digital master images of the OECF target were used for this analysis.

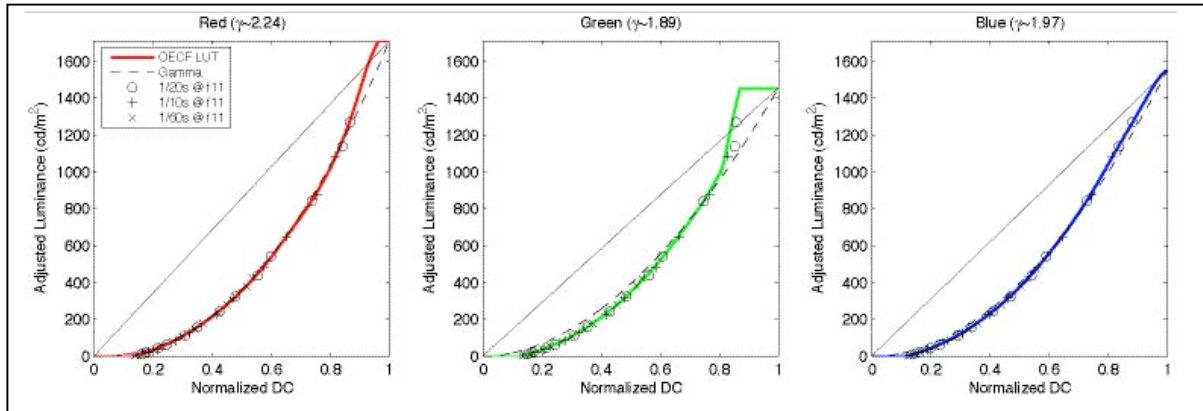


Figure 74. CS2 OECF curves.

The OECF curves for each channel have a different gamma encoding. The photographer clipped the green channel at a digital count value that was less than the maximum during the imaging. The working space profile, HUAM-RGB-D<sub>50</sub>-2.2 gamma-7-01, which the CS2 images get converted to when opened, has a gamma encoding of 2.2 for all three channels. This means that the images will get interpreted with a gamma

encoding that is different than the gamma encoding of the image, except for the red channel.

### Color Reproduction Accuracy

#### *Spectral Sensitivity*

The relative spectral sensitivity results for CS2 are shown in the left plot of Figure 75 and the relative spectral sensitivity curves rotated to fit the CIE 2° observer color-matching functions are shown in the right plot. These relative spectral sensitivities are those of the camera combined with the Phase One tungsten balancing/IR cut-off filter.

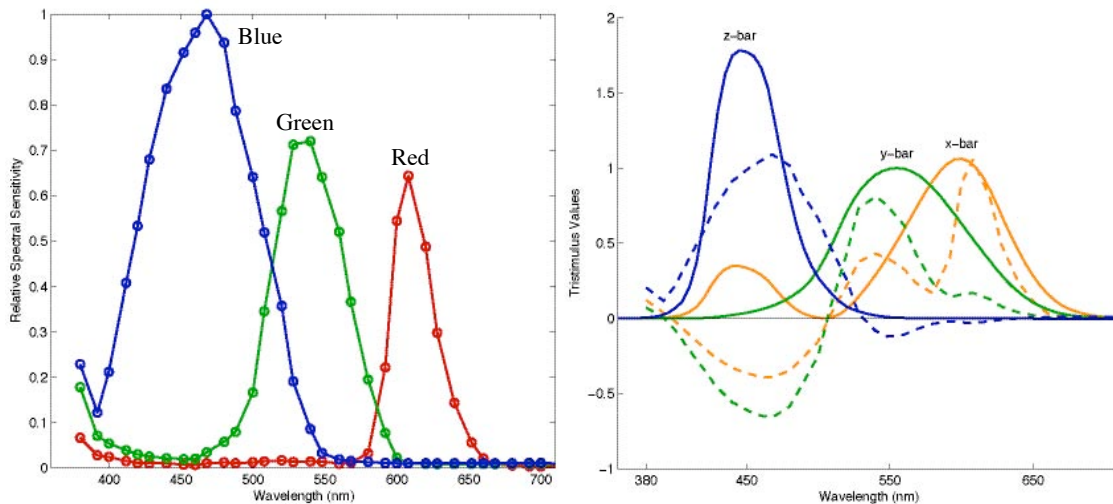


Figure 75. CS2 relative spectral sensitivities (left) and relative spectral sensitivities (dotted line) rotated to fit the CIE 2° observer (right).

From the plots in Figure 75, one can infer that there was a significant amount of UV radiation being imaged by the camera since the spectral sensitivities increase at 380 and 390 nm. The lack of fit of the relative spectral sensitivities to the CIE 2° observer color-matching functions (shown in the plot on the right of Figure 75) can be explained by the

shifts in peak sensitivities, a weaker (green and blue channels) peak sensitivity, and a negative lobe in each of the channels.

The  $\mu$ -factor results for CS2 are shown in Table XXX.

Table XXX. CS2  $\mu$ -factor results.

<u>Detector</u>	<u>Color Matching Functions</u>	<u>Taking Illuminant (Measured CCT)</u>	<u>Viewing Illuminant</u>	<u><math>\mu</math>-Factor</u>
Camera	CIE 2° Observer	TTI tungsten (2980K)	$D_{50}$	0.79
		$D_{50}$		0.82
		TTI tungsten (2980K)		0.98
		$D_{50}$		1.00

The  $\mu$ -factor results in CS2 show that the digital imaging system as a whole, produced a  $\mu$ -factor of 0.79, which is less than the desired  $\mu$ -factor of 0.90. There is a slight improvement in the  $\mu$ -factor when the taking illuminant is not considered. The effect of just the taking illuminant further greatly increases the  $\mu$ -factor.

#### *Target-based Color Reproduction Accuracy*

In Figure 76, the CIELAB error vector plots are shown between the measured patch data and the image patch data of the Macbeth ColorChecker for CS2 using the Lab image data, which was normalized so that the Halon L\* equaled 100. The camera images of the color targets were used for this analysis.

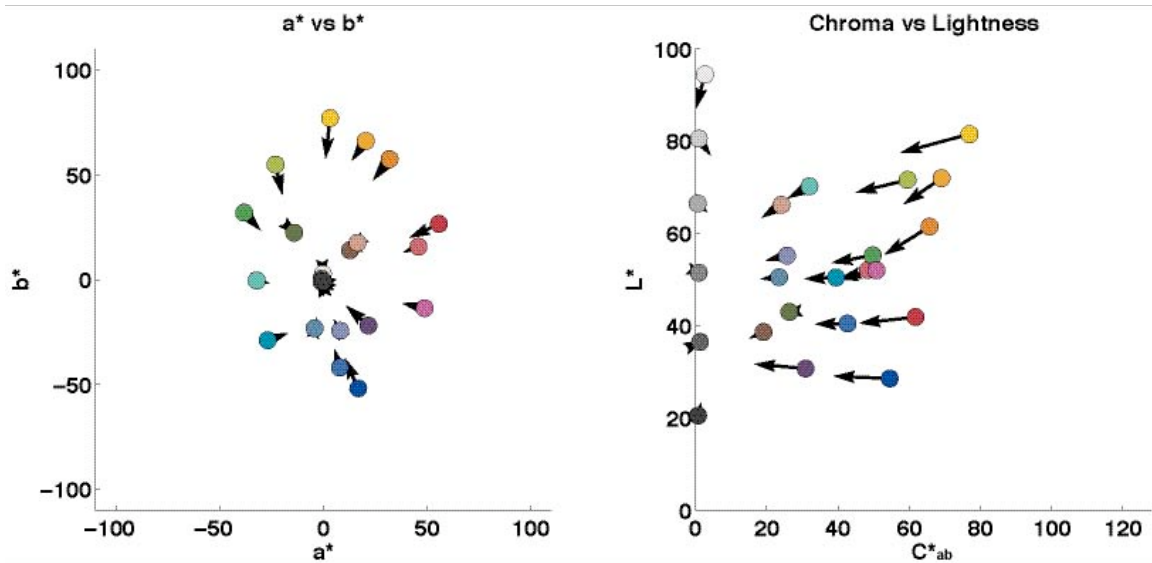


Figure 76. CS2 CIELAB  $a^*$  vs.  $b^*$  (left) and  $C^*_{ab}$  vs.  $L^*$  (right) error vector plots of the Macbeth ColorChecker between the measured patch data (dot) and the lightness corrected Lab image patch data (point of vector arrow).

In CS2, the  $a^*$  vs.  $b^*$  plot in Figure 76 shows that the more chromatic colors had a larger error than the neutral colors. Both plots show that, in general, the errors were caused by the image data being systematically less chromatic than the measured data.

Figure 77 is a histogram of the  $\Delta E_{00}$  error distributions of the Macbeth ColorChecker for CS2, which was evaluated, again, using the lightness corrected Lab image data.

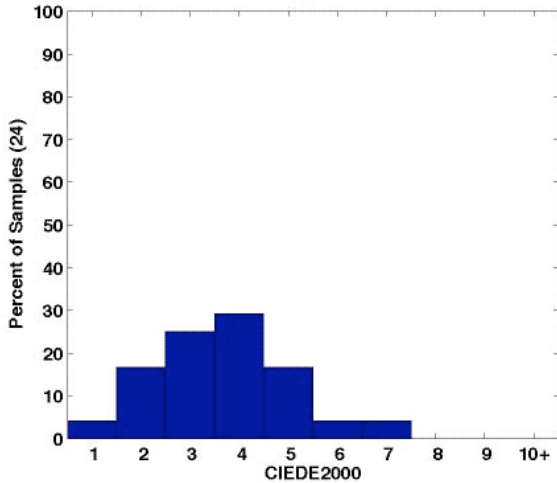


Figure 77. CS2 histogram of the  $\Delta E_{00}$  error distributions of the Macbeth ColorChecker between the measured patch data and the lightness corrected Lab image patch data.

This graph shows that, since most of the error bars are on the left side, the color difference errors were relatively low in comparison to the other case studies.

In Table XXXI, the mean, standard deviation and the 90<sup>th</sup> percentile data are given for the  $\Delta E^*_{ab}$  and  $\Delta E_{00}$  data between the measured patch data and the image patch data for each color reproduction accuracy chart in CS2.

Table XXXI. CS2 mean, standard deviation, and 90<sup>th</sup> percentile of the  $\Delta E^*_{ab}$  and  $\Delta E_{00}$  data between the measured patch data and the image patch data for each color reproduction accuracy chart.

<u>Color Reproduction Accuracy Chart</u>	Lab Image Data						Lab Image Normalized to Halon L* = 100					
	<u><math>\Delta E^*_{ab}</math></u>			<u><math>\Delta E_{00}</math></u>			<u><math>\Delta E^*_{ab}</math></u>			<u><math>\Delta E_{00}</math></u>		
	<u>Mean</u>	<u>Std. Dev.</u>	<u>90<sup>th</sup> Perc.</u>	<u>Mean</u>	<u>Std. Dev.</u>	<u>90<sup>th</sup> Perc.</u>	<u>Mean</u>	<u>Std. Dev.</u>	<u>90<sup>th</sup> Perc.</u>	<u>Mean</u>	<u>Std. Dev.</u>	<u>90<sup>th</sup> Perc.</u>
ColorChecker DC	8.22	4.87	13.37	4.99	1.58	6.82	7.52	3.54	10.93	5.26	1.38	7.04
ColorChecker	8.96	4.97	15.70	4.15	1.37	5.83	8.87	2.45	12.80	6.07	1.25	7.69
Esser	10.81	4.45	16.30	6.79	2.76	8.74	5.60	3.61	10.62	3.13	2.37	4.71
Esser Grayscale	7.00	1.08	8.03	6.09	0.82	6.79	4.08	1.32	5.92	3.93	0.96	5.24
BCRA	10.70	7.24	21.23	4.98	2.31	7.01	10.62	4.88	17.17	6.58	2.14	9.09
Blue Pigments	6.16	0.46	6.79	3.97	0.46	4.64	5.56	0.38	5.98	4.22	0.54	5.03
Pigment Target	12.40	6.07	21.49	6.53	2.17	8.59	8.25	3.87	12.71	4.59	1.92	7.18
Kodak Color Separation	9.71	4.37	16.98	6.15	1.79	9.10	6.04	3.58	12.19	4.03	2.35	7.97
Kodak Grayscale	5.73	0.93	7.18	4.88	0.84	6.01	3.60	1.08	5.31	3.52	1.08	5.21
IT8	10.24	3.50	14.68	6.57	1.11	7.96	6.06	3.60	10.84	3.59	1.78	6.32
IT8 Grayscale	6.23	2.22	9.34	5.57	1.77	8.40	5.77	3.06	10.37	5.11	2.32	8.52
Mean	8.74	3.65	13.74	5.52	1.54	7.26	6.54	2.85	10.44	4.55	1.64	6.73

What can be seen from this table is that the lightness corrected image data had lower  $\Delta E^*_{ab}$  and  $\Delta E_{00}$  values in comparison to the measured data than the non-lightness corrected image data. Also, when comparing the lightness corrected  $\Delta E_{00}$  values, the color reproduction accuracy of the Esser chart was the most accurate followed by the

Kodak Grayscale chart. The BCRA chart was reproduced the least accurately, followed by the ColorChecker and the ColorChecker DC charts. It is preferred, since this testing procedure is geared toward imaging paintings, that the Macbeth ColorChecker DC, the Macbeth ColorChecker the Blue Pigments and the Pigment Target charts are reproduced the most accurately. In this case, the CCDC and CC charts were reproduced very inaccurately and the Blue Pigments and the Pigment Target charts were reproduced intermediary in accuracy compared to the other charts. The mean  $\Delta E^*_{ab}$  values of all of the color charts were inadequate compared to the desired value of 2.00.

Table XXXII. CS2 mean, standard deviation, and 90<sup>th</sup> percentile of the  $\Delta E^*_{ab}$  and  $\Delta E_{00}$  data between the measured patch data and the image patch data for the Macbeth ColorChecker and ColorChecker DC charts using both the lightness corrected Lab image patch data and the RGB image patch data (CCDC characterization chart data used to build a linearized RGB to XYZ 3x3 transform) to determine the CIELAB data.

<b><u>Color Reproduction Accuracy</u></b> <b><u>Chart (Image Data/Transformation)</u></b>	<b><u><math>\Delta E^*_{ab}</math></u></b>			<b><u><math>\Delta E_{00}</math></u></b>		
	<b><u>Mean</u></b>	<b><u>Std. Dev.</u></b>	<b><u>90<sup>th</sup> Perc.</u></b>	<b><u>Mean</u></b>	<b><u>Std. Dev.</u></b>	<b><u>90<sup>th</sup> Perc.</u></b>
<b>ColorChecker DC (Lab/Profile)</b>	7.52	3.54	10.93	5.26	1.38	7.04
<b>ColorChecker DC (RGB/CCDC)</b>	5.26	3.74	9.66	3.41	1.90	6.02
<b>ColorChecker (Lab/Profile)</b>	8.87	2.45	12.80	6.07	1.25	7.69
<b>ColorChecker (RGB/CCDC)</b>	6.65	3.48	11.71	4.75	2.58	9.31

Table XXXII compares the color differences between the image CIELAB data determined using an embedded profile in Adobe Photoshop® (the first evaluation method described in Section 3.4.2), which are listed in Table XXXI above, and determined using an OECF linearization combined with a 3x3 RGB to XYZ transform created and optimized with the CCDC data (the second evaluation method described in Section 3.4.2). The data in this table show that the simple 3x3 transformation performed better

for both charts. This means that there can be an improvement in the embedded profile used at this museum.

### *Metamerism*

Table XXXIII shows the D&H Color Rule metameristic match data of CS2. The TTI tungsten taking illuminant was the illuminant for all three matches in this case study. The camera image of the D&H Color Rule was used for this analysis.

Table XXXIII. CS2 D&H Color Rule metameristic matches and the  $\Delta E^*_{ab}$  or  $\Delta E_{00}$  color differences of each metameristic match as “seen” by the camera and CIE 2° observer under the TTI tungsten taking illuminant.

<u>Detector</u>	<u>Metameric Match</u>	<u>Camera</u>	<u>CIE 2° Observer</u>	<u>Camera</u>	<u>CIE 2° Observer</u>
		$\Delta E^*_{ab}$	$\Delta E_{00}$		
<b>Camera</b>	U-13	0.76	7.33	0.63	4.96
<b>CIE 2° Observer</b>	Q-14	5.33	0.52	4.24	0.61
<b>Photographer</b>	O-12	5.48	3.79	5.52	4.52

What can be seen from Table XXXIII is that none of the three detectors had the same match under the same illuminant, which means that the camera is not “seeing” the same colors of the D&H Color Rule as that of the photographer or the CIE 2° observer. The difference in the match between the CIE 2° observer and the photographer could be caused by the photographer having slightly different spectral sensitivities (color-matching functions), since the CIE 2° observer is only an average human observer response. The color differences of the CIE 2° observer and photographer’s metameristic matches as “seen”

by the camera are large, which reiterates the fact that their spectral sensitivities differ.

The same is true for the CIE 2° observer as the detector of the camera match in CS1.

### Noise

#### *Image Noise*

Table XXXIV shows the image noise results of CS2 for each channel and the mean of all three channels. The digital master images of the noise target were used for this analysis.

Table XXXIV. CS2 image total, fixed pattern and temporal noise results.

	<u>Red Channel</u>	<u>Green Channel</u>	<u>Blue Channel</u>	<u>Mean of RGB Channels</u>
<b>Total Average Noise (DC)</b>	697.97	616.57	844.14	719.56
<b>Total Signal to Noise Ratio</b>	13.93	16.04	12.51	14.16
<b>Fixed Pattern Average Noise (DC)</b>	617.03	580.05	763.16	653.41
<b>Fixed Pattern Signal to Noise Ratio</b>	15.75	17.05	13.83	15.54
<b>Temporal Average Noise (DC)</b>	326.26	209.06	360.78	298.70
<b>Temporal Signal to Noise Ratio</b>	29.79	47.32	29.26	35.46
<b>Black Temporal Average Noise (DC)</b>	390.36	178.18	323.77	297.44

For CS2, the total average noise greatly exceeds the desirable amount of noise limit of 257 digital counts in all three channels. Table XXXIV shows that the blue channel had significantly more total noise than the other two channels and the green channel had the least amount of total noise in CS2. The amount of temporal noise is significantly less than the fixed pattern noise.

### *Color Noise*

Table XXXV shows the color noise results for CS2. The camera image of the Macbeth ColorChecker chart was used for this analysis.

Table XXXV. CS2 color noise results of selected patches of the Macbeth ColorChecker.

<u>ColorChecker Patch</u>	<u>Mean Normalized DC</u>			<u>% Standard Deviation (Norm. DC)</u>			<u>MCDM</u>	
	<u>R</u>	<u>G</u>	<u>B</u>	<u>R</u>	<u>G</u>	<u>B</u>	$\Delta E^*_{ab}$	$\Delta E_{00}$
<b>Red (15)</b>	0.33	0.26	0.22	2.18	1.58	1.97	1.48	1.30
<b>Green (14)</b>	0.63	0.51	0.45	1.20	0.92	1.04	1.30	1.05
<b>Blue (13)</b>	0.35	0.41	0.49	2.10	1.09	0.92	1.47	1.24
<b>Cyan (18)</b>	0.29	0.35	0.25	2.73	1.33	1.96	1.60	1.05
<b>Magenta (17)</b>	0.43	0.43	0.53	1.76	1.03	0.89	1.43	1.19
<b>Yellow (16)</b>	0.44	0.64	0.61	1.74	0.75	0.79	1.36	0.81
<b>White (19)</b>	0.63	0.39	0.22	1.18	1.25	2.42	1.42	0.77
<b>Gray (22)</b>	0.26	0.31	0.47	2.91	1.56	1.01	1.62	0.91
<b>Black (24)</b>	0.62	0.30	0.31	1.17	1.42	1.44	1.38	0.78
				<b>Mean</b>	1.89	1.21	1.38	
							<b>MMCDM</b>	1.45
								1.01

The data in Table XXXV show that there were small differences between the amounts of noise of each color patch. The % standard deviation results show that the green channel had the least amount of color noise and the red channel had the most. The  $\Delta E_{00}$  color difference results show that the black patch and the yellow patch had the least amount of color noise and the red and blue patches had the most amount of color noise.

### Dynamic Range

Table XXXVI shows the dynamic range results of CS2 for each channel and the mean of all three channels. The digital master images of the noise target were used for this analysis.

Table XXXVI. CS2 dynamic range results.

	<u>Red</u> <u>Channel</u>	<u>Green</u> <u>Channel</u>	<u>Blue</u> <u>Channel</u>	<u>Mean of RGB</u> <u>Channels</u>
<b>ISO Digital Still Camera Dynamic Range (Luminance Ratio)</b>	395.03	930.94	595.49	640.49
<b>ISO Digital Still Camera Dynamic Range (Density)</b>	2.60	2.97	2.77	2.81
<b>Theoretical Dynamic Range (Density)</b>	4.81	4.81	4.81	4.81

In CS2, the measured dynamic range was significantly less than the theoretical dynamic range in all three channels. The green channel had significantly more dynamic range than the other two channels and the red channel had the least amount of dynamic range.

#### Spatial Cross-talk

Table XXXVII shows, for each channel, the mean linearized value of all 30 gray patch means, the percent relative maximum difference, and the percent relative standard deviation values for CS2. The digital master images of the spatial cross-talk target were used for this analysis.

Table XXXVII. CS2 summary of spatial cross-talk results.

	<u>Red</u> <u>Channel</u>	<u>Green</u> <u>Channel</u>	<u>Blue</u> <u>Channel</u>	<u>Mean of RGB</u> <u>Channels</u>
<b>Mean Linearized DC</b>	0.23	0.35	0.32	0.30
<b>Relative Maximum Difference (%)</b>	5.63	5.40	8.54	6.52
<b>Relative Standard Deviation (%)</b>	1.98	2.00	3.27	2.42

The data in Table 7-XII for CS2 in Appendix 7.3 show that the mean digital count value of a gray patch that is surrounded by white in one image is always higher than the value

of the patch in the same position surrounded by black in the other image. This shows that spatial cross-talk is having an effect on the image. Table XXXVII shows that the spatial cross-talk affected the blue channel the most in CS2.

#### *Spatial Frequency Response (SFR)*

The results of the SFR for CS2 are shown in Figure 78 and Table XXXVIII. The digital master images of the resolution target were used for this analysis.

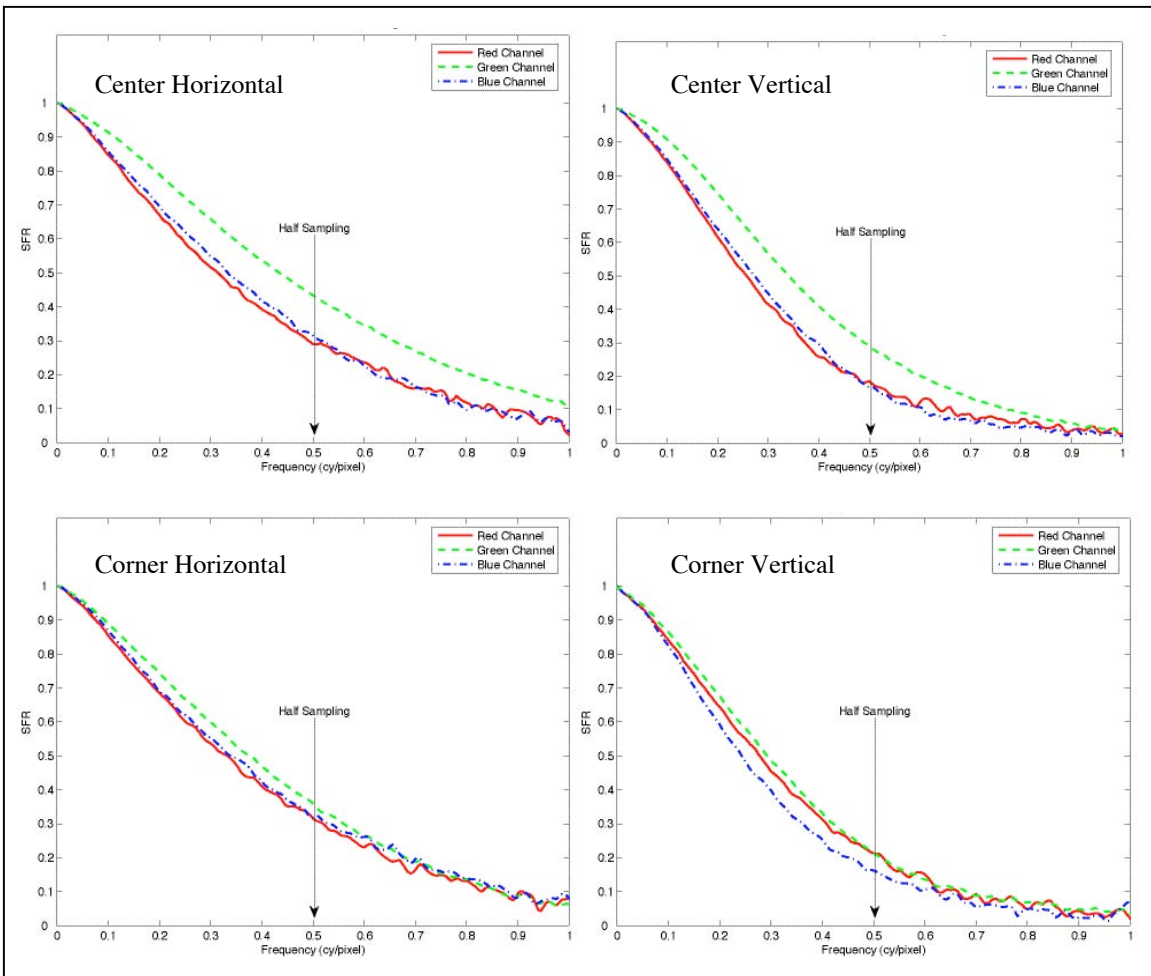


Figure 78. CS2 SFR of center horizontal edge (top left), center vertical edge (top right), upper left corner horizontal edge (bottom left), and upper left corner vertical edge (bottom right).

Table XXXVIII. CS2 SFR area results.

<u>Edge</u>	Area Under SFR Curve From Frequencies of 0.0 to 0.5cy/pixel			
	<u>Red Channel</u>	<u>Green Channel</u>	<u>Blue Channel</u>	<u>Mean of RGB Channels</u>
Center Horizontal	0.617	0.724	0.637	0.659
Center Vertical	0.546	0.657	0.563	0.589
Corner Horizontal	0.630	0.677	0.642	0.650
Corner Vertical	0.572	0.593	0.528	0.565
	<b>Mean</b>			0.616

It is evident, from the data shown in Table XXXVIII and Figure 78, that the SFR in the horizontal direction was better than the SFR in the vertical direction. Since this camera is a scanning camera that scans horizontally (from left to right), this implies that the SFR caused by the linear array itself was better than the SFR caused by the linear array's scanning. Secondly, the SFR in the center (on-axis) was about equal, generally, to the SFR in the corner (off-axis) of the uncropped image area. It varies, depending on the channel. Thirdly, the green channel SFR was higher than both the red and blue channels in the center and corner of the image area.

### Color Channel Registration

Table XXXIX shows the results of the color channel registration for CS2. The digital master images of the resolution target were used for this analysis.

Table XXXIX. CS2 color channel registration results.

<u>Edge</u>	<u>Misregistration Shift (pixels)</u>		
	<u>Red Channel</u>	<u>Green Channel</u>	<u>Blue Channel</u>
<b>Center Horizontal</b>	0.266	0.000	0.267
<b>Center Vertical</b>	0.332	0.000	0.304
<b>Corner Horizontal</b>	0.098	0.000	0.111
<b>Corner Vertical</b>	0.007	0.000	0.252
<b>Maximum</b>	0.332	0.000	0.304
<b>Mean</b>	0.176	0.000	0.234
<b>Mean of RGB Channels</b>			0.136
Note: Green channel used as reference			

It is evident, from the data in Table XXXIX, that, generally, the amount of misregistration shift was about the same for the red and blue channels in comparison to the green channel. The maximum amount of misregistration was less than 0.4 pixels. Out of the four edges, the center vertical edge had the most amount of misregistration

shift. The misregistration error on the vertical knife-edge was, generally, greater than that of the horizontal edge in both the center and corner of the uncropped image area. Since this camera is a scanning camera that scans horizontally (from left to right), this implies that the misregistration error caused by the linear array itself was less than that caused by the linear array's scanning.

### Depth of Field

Figure 79 shows the plot of the depth of field distance vs. area under the SFR curve for the horizontal edge of each color channel for CS2. The camera image of the depth of field target was used for this analysis.

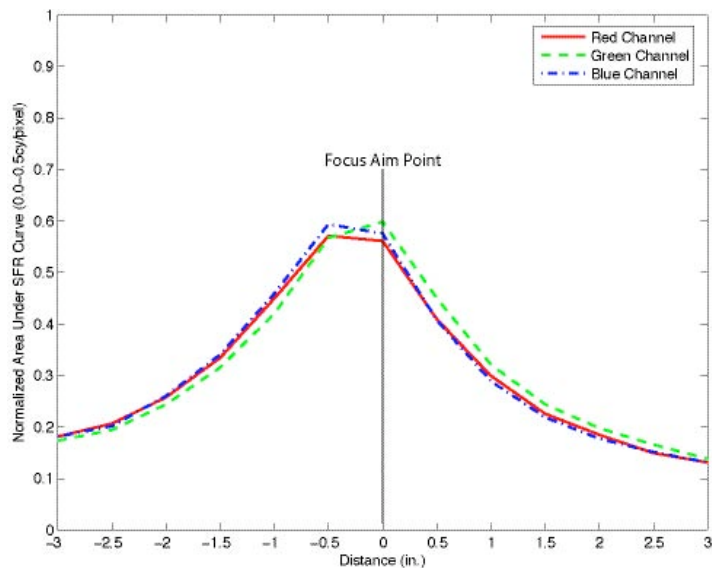


Figure 79. CS2 depth of field area under SFR curve vs. distance of the horizontal edge.

Differences between the red, green and blue color channels in Figure 79 were caused by their misregistration shifts (see the Color Channel Registration part of this section). Two

pieces of information can be obtained about the depth of field image of CS2 from this plot. One is that the sharpness, and therefore the depth of field, of the image decreased as the camera-to-subject distance changed. The other is that the focusing method (using a frequency tool in the image capture software), which was used to focus on the 3" high column during the imaging of the depth of field target, was reasonably accurate. The focus point was only about 0.25" further away from the camera than it should have been.

## **4.5 Case Study Three**

Case study three, CS3, was performed on July 14-15, 2004.

### **4.5.1 Case Study Three: Digital Imaging System Description**

The camera used at the museum's studio was a Sinar Sinarback 54H (SN: 26108654HFO) digital back camera, which is a 3-channel (RGB) area array CCD camera. The maximum native resolution of the camera is 4,080p x 5,440p. The digital back was on a Horseman 4x5 view camera body, which had a Rollie electronic shutter. The lens was a 100mm f/4 Rodenstock Apo Sironar digital HR lens. The filter used between the CCD and the lens was a Sinar IR cut-off filter. This camera is typically used to image paintings (varnished and unvarnished) and other flat works, such as photographs and large works on paper not suitable for imaging on a copy stand, for the purpose of protecting vulnerable originals from use, to document conservation treatment, and to include the digital images in a collection management system. Reproductions are created in the forms of prints and Internet images. One person in the photography department at the museum can operate this camera. The photographer did not receive official background training for this camera system, but was helped by the sales person who sold them the camera.

There were four Speedotron (Model: MW20QC) Xenon strobe lights in a 202VF light unit used to light the scene. These strobe lights had a UV correction filter over the bulb. In his day-to-day imaging, the photographer does not change the positions of the lights unless the object being imaged changes drastically in size. Table XL shows the CCT and chromaticity coordinates of this illumination without the UV correction filter

over the bulb. Figure 80 shows the relative spectral power distribution of the MW20QC strobe lights, also without the UV correction filter over the bulb. These data were obtained from the bulb manufacturer, because it could not be measured with the PR650 spectroradiometer.

Table XL. Speedotron MW20QC Xenon strobe taking illuminant (without UV correction filter) characteristics.

<b>Correlated Color Temperature</b>	6628K
<b>Chromaticity x (2° Observer)</b>	0.3127
<b>Chromaticity y (2° Observer)</b>	0.3145

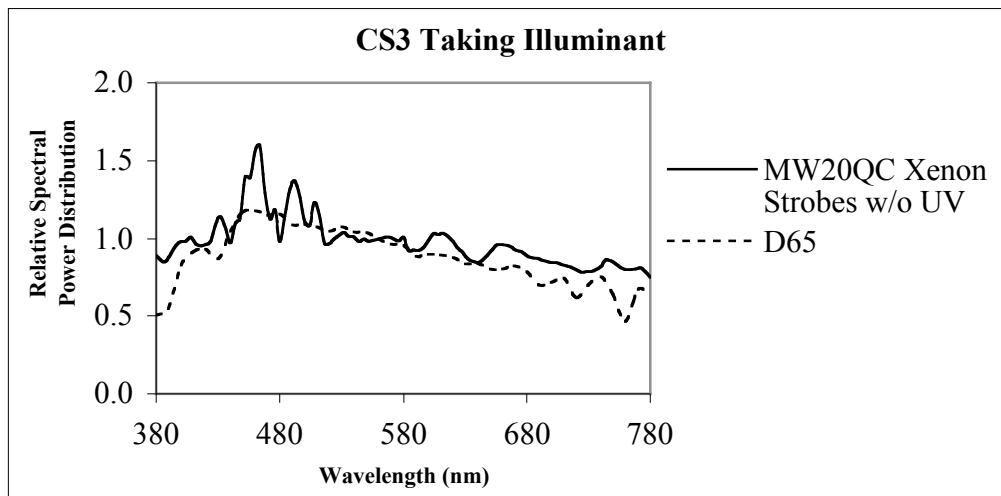


Figure 80. Relative spectral power distribution of the Speedotron strobe lights (without the UV correction filter) used in the CS3 set-up. CIE illuminant D<sub>65</sub> is included for comparison.

The capture software used was Sinar CaptureShop 4.0.15. The monitor used was a Sony Artisan monitor, on which the visual corrections were made. This monitor was

set so that it had a color depth of millions of colors, a resolution of 1152dpi x 870dpi at 75Hz, a gamma of 1.8 and a 5400K white point.

#### **4.5.2 Case Study Three: Imaging Procedure**

At the start of the case study on day one, a piece of black board, which was used as the background during the imaging, was placed on the easel and clamped there. This board was approximately the size of the 26" x 22" marked out area, so it defined the image area. The Halon was centrally taped to the top of the board, along with a case-study-imaging description label. The two paintings (flower and fish) were placed in front of the black board below the Halon and description label. The photographer was asked to set up the camera, lights, and easel in the same way that he would if he were imaging paintings in his usual everyday imaging at the museum. He was asked to light the entire black board. The photographer used the tiles on the floor to make sure that the lights were equidistant from the easel and the camera and to center the camera with respect to the easel. The camera monopod was set up on a track in the middle of the room. The photographer used a level to make sure that it was parallel to the easel. The photographer decided to leave the lights in the same position that they were from his previous imaging. The two lights on the left, when facing the easel, were set to 1 1/3 stops brighter than the two lights on the right, using the power supply box, for the purpose of increasing contrast and sharpness in the images. The illumination uniformity was not checked with a light meter. Figure 81 shows how the camera and lights were placed in relation to the easel during the imaging procedure. The labeled distances are approximate.

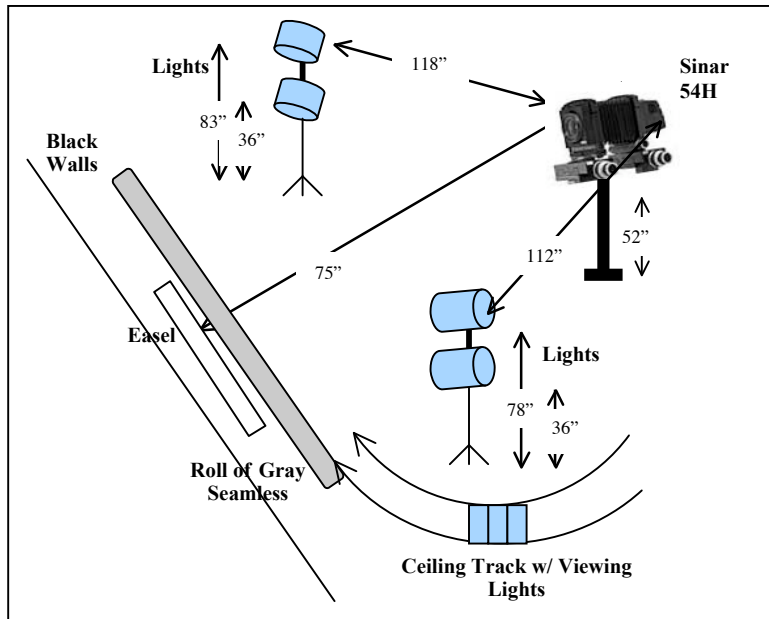


Figure 81. Schematic of the CS3-imaging set-up.

After the camera, lights, and easel were set up, the photographer placed a gray card to the left of the paintings, which he later used for gray balancing, or neutralizing. Next, he created a shading reference, which is controlled using the Sinar CaptureShop software. The photographer pulled a piece of light gray seamless paper down in front of the paintings, which he used to create the shading reference (Sensor+Lens+Scene). This shading reference is used to automatically correct for illumination or spatial non-uniformity when an image is taken with the Sinarback 54H. Next, he focused the camera on the two paintings manually by looking at a magnified area of the live image preview. He set the lens aperture to f/17.8 at the camera. He took a four-shot image of the paintings. He used the n-picker tool in the image capture software to neutralize the image by clicking on the gray card. The photographer was asked to determine the nominal exposure time by making sure that the Halon was not clipped. He determined the

exposure time by reimaging the paintings and reneutralizing the images until the digital count value of the Halon was maximum unclipped. The exposure time (controlled at the camera), which was equivalent to the integration time (controlled in the image capture software) was 1/15s. This exposure time and the f/17.8 aperture became the nominal exposure settings of the case-study-imaging session. The ISO speed was set to 25 and remained there for the rest of the imaging procedure. The paintings image that was exposed at the nominal exposure was then exported and saved in the IBM PC byte order as a 16-bit tiff file. This image was called the digital master. Figure 82 shows what was automatically applied to the digital master in the image capture software before it was saved. The neutralizing, as described above, was done manually by the photographer. Other than assigning a camera profile (created in CaptureShop using a Macbeth ColorChecker DC target), applying the shading reference, unsharp masking, and converting the image to the ProPhoto RGB working space profile, there were a few other settings in the CaptureShop software that also got automatically applied to the digital master image. The saturation was set to 100%, the tone curve was set to linear, the amore SW was set to one, the color alchemist was set to medium, the flash was set to early, the light meter setting was set to underexposed, and the adaptive compensation was on. Dark correction was also performed automatically for every image by the image capture software. The digital master file had an effective resolution of 173ppi and the file size was 129MB.

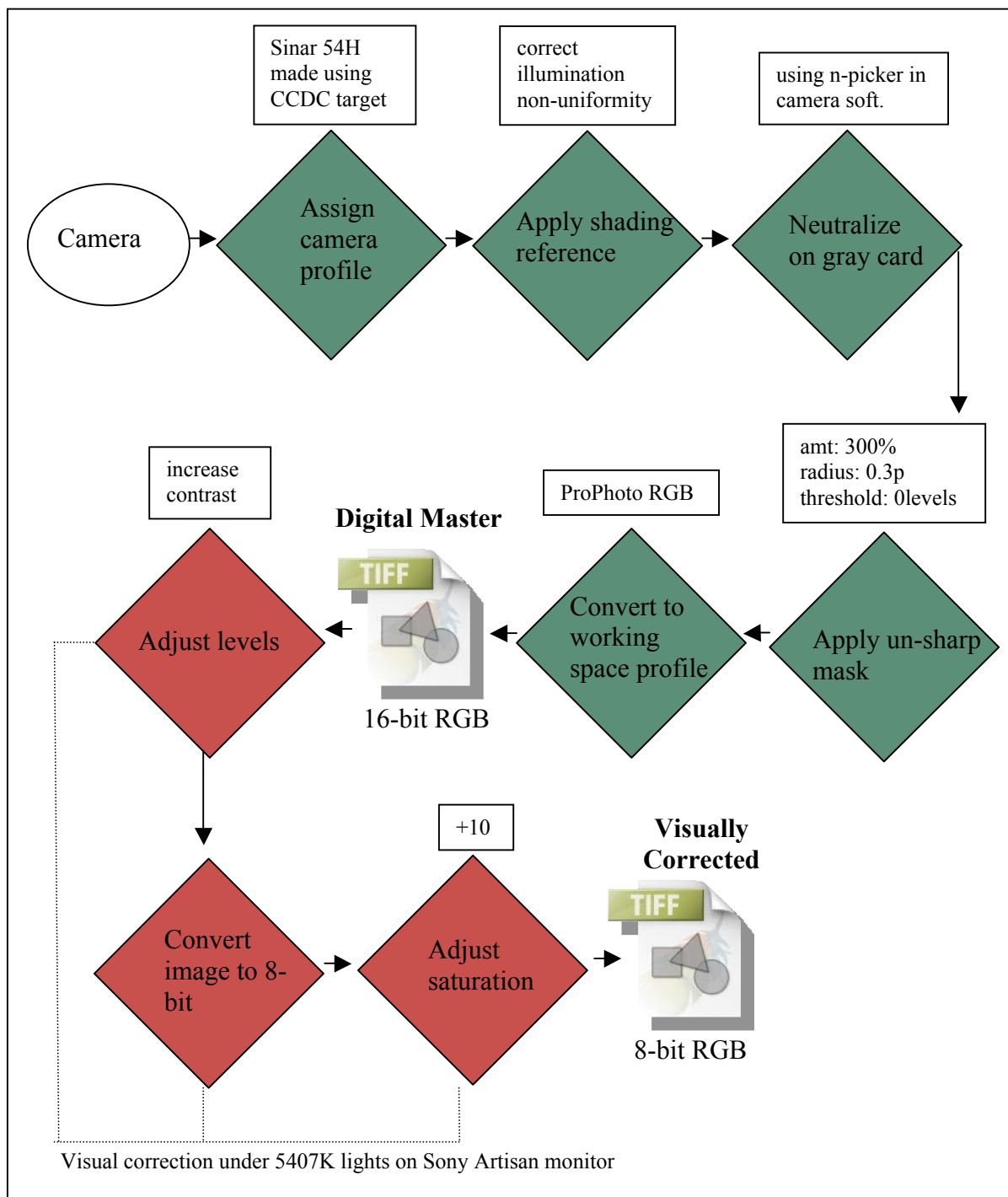


Figure 82. Flowchart of CS3 digital imaging workflow. A green background in the diamond means that the action was performed in the capture software. A red background in the diamond means that the action was performed in Adobe Photoshop®.

Because the photographer usually creates a visually corrected image, he was asked to visually correct the paintings digital master image and save it. Figure 82 shows what processing the photographer did to the visually corrected image before it was saved as an 8-bit tiff image file. Prior to the visual processing, the photographer opened the digital master image in Adobe Photoshop®. The photographer's reasoning behind increasing the contrast and saturation was that, in his opinion, people preferred the digital images when they resembled a chrome transparency in appearance. The image had to be converted to an 8-bit image, because the version of Adobe Photoshop® that he was using would not allow him to adjust the saturation of a 16-bit image. When this image was visually corrected, both paintings were corrected as if they were one painting since they both contained the same pigments. It took the photographer approximately 20 minutes to do the visual corrections. During the visual correction, the photographer turned off the lights and viewed the paintings under a panel of six Macbeth 5400K fluorescent lights. The image in Figure 83 shows how these lights were used to illuminate the paintings. They were set-up on a ceiling track as shown in Figure 83.



Figure 83. Image of viewing lights illuminating the paintings during the CS3 visual corrections.

Table XLI shows the CCT, chromaticity coordinates, and luminance of the viewing illumination. Figure 84 shows the relative spectral power distribution of the fluorescent viewing illumination. These data were obtained by measuring the Halon, that was in the scene, with a calibrated PR650 spectroradiometer.

Table XLI. Macbeth 5407K fluorescent viewing illumination characteristics.

<b>Correlated Color Temperature</b>	5407K
<b>Chromaticity x (2° Observer)</b>	0.3347
<b>Chromaticity y (2° Observer)</b>	0.3526
<b>Luminance (2° Observer)</b>	138.9cd/m <sup>2</sup>

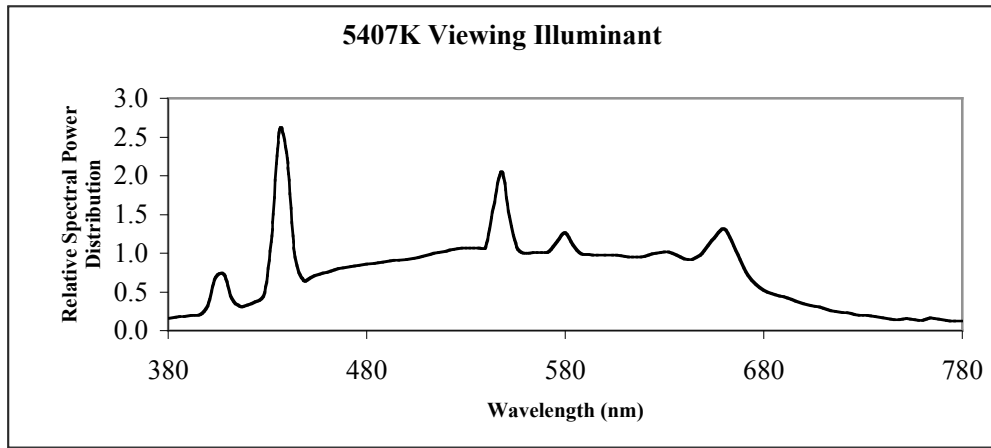


Figure 84. Relative spectral power distribution of the CS3 viewing illumination.

This concluded the first part of the case study.

In the second part of the case study, the camera and lights set-up remained the same. Unless otherwise specified, the images taken in the second part were taken as four-shot images and saved as digital master files with the same digital workflow as shown in Figure 82. Also, the image area remained uncropped throughout the entire imaging process. The paintings were replaced by each of the three color-reproduction-accuracy targets (see Figures 25, 26, and 27) one at a time, which were each imaged once at the nominal exposure settings. The photographer refocused the camera before each image was taken. The system-spatial-uniformity-gray-card target, shown in Figure 13, was imaged next, after the photographer refocused. It was imaged at the nominal exposure settings. It was imaged twice. For the second image, the two gray cards were each rotated 180°. In the same way, after refocusing, the spatial cross-talk target, shown in Figure 38, was imaged next, twice. In the second image, the spatial cross-talk target was rotated 180°.

The next target that was imaged by the photographer was the noise target, which is shown in Figure 37. It was not necessary to refocus the camera before imaging this target because it was the same distance from the camera as the previous target. It was imaged at the nominal exposure settings five times. The spatial-frequency response target, shown in the left image in Figure 39, was the next target to be imaged. Again, there was no need for the photographer to refocus the camera before this target was imaged. The target was imaged at the nominal exposure settings. The SFR target was then imaged a second time at the nominal exposure settings, but this time, the target was placed in the upper left corner of the uncropped image area (see Figure 85 below). The photographer did not refocus the camera before imaging the SFR target again.



Figure 85. Placement of the SFR target in the CS3 uncropped image area. The knife-edges used in the analysis are circled in red.

The OECF target, shown in Figure 16, was the next target to be imaged. There was no need for the photographer to refocus before imaging this target because it was at the same distance from the camera as the previous target, the SFR target. This target was

imaged three times. It was imaged once at the nominal exposure settings, a second time overexposed, by setting the aperture to f/8.3 and keeping the exposure time the same, and a third time underexposed, by, again, keeping the exposure time the same and setting the aperture to f/32.3. The OECF target was then imaged three more times at the same exposure settings as before. This time, prior to the image being taken, the color management was turned off, except for the assignment of the camera profile, because it couldn't be turned off. Also, all of the automatic corrections that the software would make to the images were turned off and the n-picker was not used by the photographer. These would be the same settings used when the monochromator instrument was imaged later in the CS3 imaging procedure. These three images were saved as 16-bit RGB tiffs. Because there were strobe lights used in the imaging procedure, it was not possible to measure the luminances of the OECF chart with the PR650 spectroradiometer. In order to predict the relative luminances, one of the gray cards (see Figure 13) was placed at the same position where the OECF target was. It was imaged four times. The first and second time it was imaged, the color management and capture software settings were the same as the second set of OECF images and the future monochromator instrument images. For the second image, the gray card was rotated 180°. This concluded the imaging on the first day of the case study.

At the beginning of the second day of the case study, the single gray card was imaged a third and fourth time. When it was imaged this time, the settings were returned to the same settings as the first set of OECF images, which is the same as the digital master file, shown in Figure 82. Again, for the fourth image, the gray card was rotated 180°.

The depth of field target was set up on the easel next. Because there were unwanted shadows on this target, the lights had to be moved closer to each other so that they illuminated this target more from the front. The power of the lights were decreased by 2 1/3 stops so that the exposure would remain at the nominal exposure settings. The lights were the only things that were changed from the set-up shown in Figure 81 above. A digital photograph and a schematic of the new set-up are shown in Figure 86.

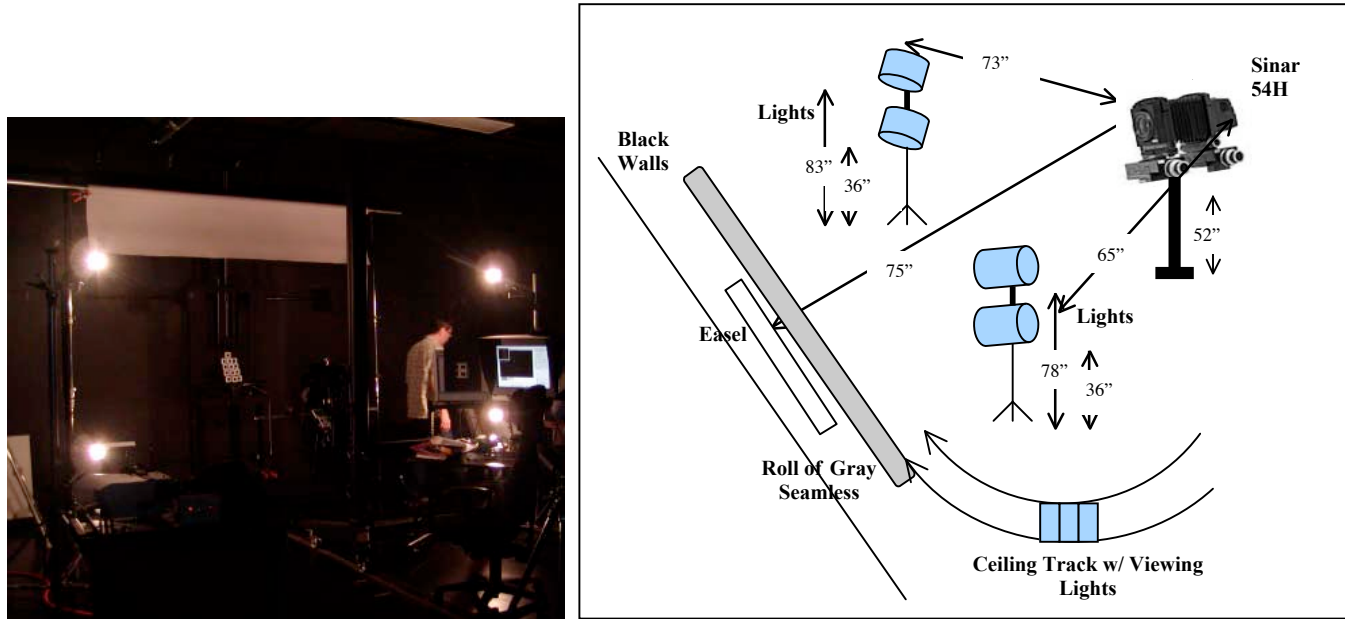


Figure 86. Image (left) and schematic (right) of the CS3 set-up for the depth of field target imaging.

The photographer focused on the edge of the center square, the 3" high square. The only difference between this image and the digital master image shown in Figure 82 was that the photographer was unable to use the n-picker on the gray card, because it was removed.

The monochromator instrument was the final thing to be imaged. The set-up for the monochromator imaging is shown in Figure 87.

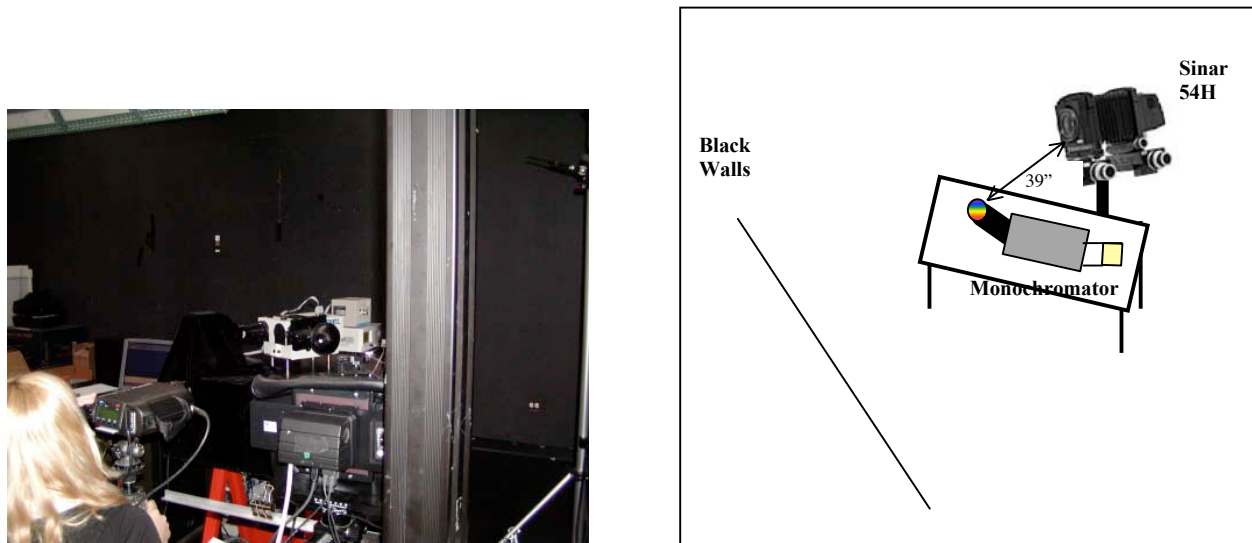


Figure 87. Image (left) and schematic (right) of the CS3 set-up for the monochromator instrument imaging. The PR650 spectroradiometer was being used to measure the monochromator instrument when the photograph on the left was taken.

There were no lights on when the monochromator was imaged. The photographer focused the camera so that the opening of the monochromator sphere was in focus. The aperture was opened up all the way up to f/4 in order to maximize the amount of light being imaged by the camera. The optimal exposure time was determined to be 1/2s. The integration time was set to the same time. Prior to the monochromator imaging, the color management was turned off, except for the assignment of the camera profile, because it couldn't be turned off. Also, all of the automatic corrections that the software would make to the images were turned off and the n-picker was not used by the photographer. In other words, the workflow of the digital master image shown in Figure 82 was not used in this case, except for the assignment of the camera profile. This was done in order to obtain images that were as raw as possible. In order to minimize the image capture time, the monochromator images were taken as one-shot images. Thirty-six images were

taken as the monochromator bandpass peak settings ranged from 380nm to 730nm in 10nm increments. These images were saved as 16-bit RGB tiffs. Following the imaging, the PR650 spectroradiometer was used to measure the monochromator at the same bandpass peak settings that were imaged. This concluded the imaging procedure of case study three.

After the imaging procedure was finished, measurements were made off of the monitor with the PR650 spectroradiometer. First, the visually corrected paintings image was opened in Adobe Photoshop® with the embedded ProPhoto RGB profile used and the eleven uniform patches of pigment of each painting were zoomed in on and measured. Then the digital master image with the ColorChecker target in it was opened with the embedded ProPhoto RGB profile used and each of the 24 patches were measured. Next, the ColorChecker digital master image was cropped down and, using the paint bucket tool, was filled with red (255, 0, 0), green (0, 255, 0), blue (0, 0, 255), white (255, 255, 255), black (0, 0, 0), and grays with equal digital values of 24,48,90,180, and 224, consecutively. Each of these colors were measured with the PR650 spectroradiometer. Finally, the Halon was placed on the monitor and the ambient room light that was hitting the monitor was measured. Before the case study was ended, the photographer was asked to make his best possible visual match with the Davidson & Hemmendinger Color Rule under the 5400K fluorescent viewing lights, since it was not possible for him to do it with the strobe lights.

#### **4.5.3 Case Study Three: Results and Discussion**

##### Colorimetric Accuracy of Digital Imaging Workflow

Figure 88 shows the CIELAB error vector plots between the spectrophotometrically measured fish painting data and the lightness corrected digital master fish painting image CIELAB data, between the lightness corrected digital master fish painting image CIELAB data and the lightness corrected visually corrected fish painting image CIELAB data, and between the spectrophotometrically measured fish painting data and the CIELAB data obtained from the CRT spectral radiance measurements of the non-lightness corrected visually corrected image. Table XLII shows the mean  $\Delta E_{00}$  of the fish and flower paintings between the spectrophotometrically measured data and the lightness corrected digital master paintings image CIELAB data, the lightness corrected visually corrected paintings image CIELAB data and the CRT spectral radiance measurement CIELAB data.

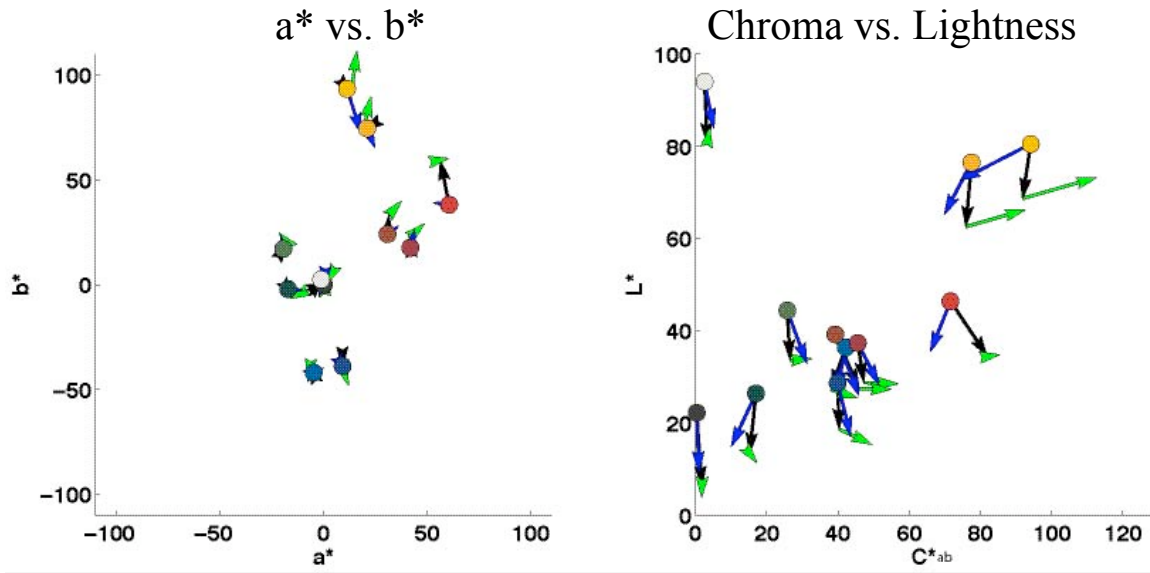


Figure 88. CS3 CIELAB  $a^*$  vs.  $b^*$  (left) and  $C^*_{ab}$  vs.  $L^*$  (right) error vector plots of the fish painting uniform patch areas between the measured patch data (dot) and the 1. Digital master image patch data (point of black vector arrow), 2. Visually corrected image patch data (point of green vector arrow), and 3. Spectroradiometric measurements of the CRT monitor of the non-lightness corrected visually corrected image patch data (point of blue vector arrow).

Table XLII. CS3 mean  $\Delta E_{00}$  of fish and flower paintings' 22 total uniform patch areas between the measured spectral reflectance and the CIELAB data of the digital master image, visually corrected image, and the CRT spectroradiometric measurements of the visually corrected image.

	<u>Lab Image Data</u>	<u>Lab Image Normalized to Halon <math>L^* = 100</math></u>
	<u><math>\Delta E_{00}</math></u>	
<b>Digital Master Image</b>	10.54	6.78
<b>Visually Corrected Image</b>	10.56	8.41
<b>CRT Measurements</b>	9.79	N/A

Since the purpose of visual editing the digital master image is to improve its color accuracy (make it appear more like the original), it would be expected that the  $\Delta E_{00}$  of the visually corrected image would be less than the digital master image. It would also be

expected that the green error vectors would be the same length as, but in the exact opposite direction than the black vectors in Figure 88, that is, aiming back to the spectrophotometrically-measured values depicted by the colored dots. The results show that the  $\Delta E_{00}$  of the visually corrected image is larger than that of the digital master image. The green vectors should point to the measured values (colored dots) in Figure 88, but, for the most part, they do not. Also, it would be expected, if the monitor was calibrated accurately, that the CRT measurements blue error vectors would point to the same place as the visually corrected image green vectors, which means that the photographer would see the same colors on the monitor that are in the visually corrected image file. This is not always the case, as can be seen in Figure 88. Even though there were inaccuracies of the monitor calibration, the  $\Delta E_{00}$  of the CRT measurements were slightly smaller than those of the digital master, which shows that the photographer did improve the color of the image on the monitor, but those improvements did not get stored in the visually edited image file itself, which will be viewed later on a different monitor.

The  $\Delta E_{00}$  values shown in Table XLII are not large. There is an improvement in the  $\Delta E_{00}$  value after the lightness correction for the digital master image and the visually corrected image. The causes of the color difference error can be seen in Figure 88. Overall, the error vectors are short (the amounts of error are small). In general, the digital master image is darker than the measured spectral reflectance data, and the visually corrected image is more chromatic than the digital master image and more chromatic and darker than the measured spectral reflectance data.

### *System Spatial Uniformity*

The results of the system spatial uniformity for CS3 are shown in Figure 89. A table of supplemental data, Table 7-III, is in Appendix 7.1.

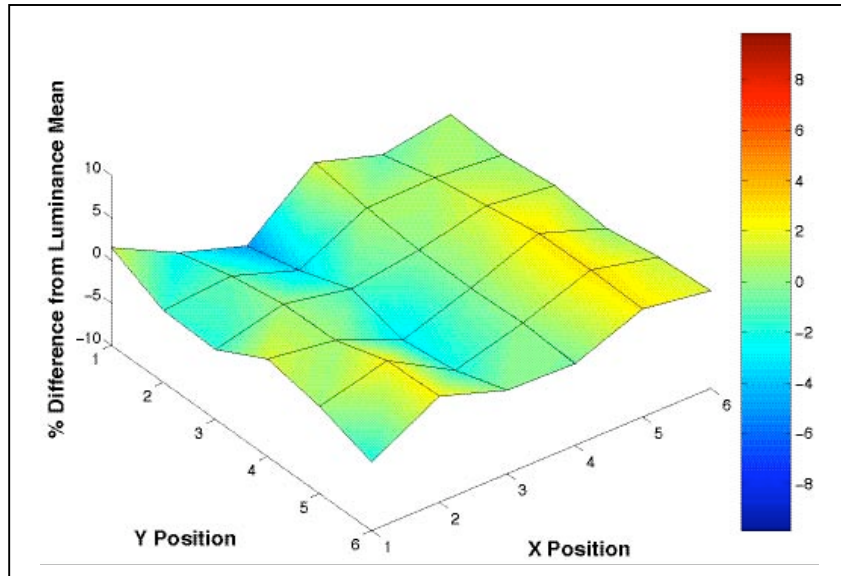


Figure 89. CS3 system spatial uniformity surface plot of % difference from luminance (Y) mean of gray card target.

In CS3, the photographer could not use a light meter during the set-up of the lights because they were Xenon strobes, but he did apply a shading reference in the image capture software to correct for illumination non-uniformity. The system spatial uniformity surface plot in Figure 89 shows that there were slight variations in the uniformity of the gray card target image, but the distribution of the non-uniformities is uneven without any systematic trend.

### Tone Reproduction

The luminance values on the y-axis of the OECF curves that were determined for CS3 were obtained differently than the other case studies (see section 3.3). The luminances of the OECF target patches could not be measured with the PR650 spectroradiometer because strobes were used as the taking illuminant. Because of this, relative luminances were determined based on the measured reflectance of the OECF chart patches and the Halon. In order to obtain the relative luminance data, the Y tristimulus value was first calculated for each of the 12 OECF chart patches and the Halon using their spectral reflectances, the CIE 2° observer and the spectral power distribution of the taking illuminant (Xenon strobes) (see Equation 7 for this calculation). Equation 39 was used to calculate the relative luminances,  $l$ , for each patch of the OECF chart and the Halon. This calculation was performed based on the assumption that the illumination of the OECF patches and Halon was uniform. The plot in Figure 89 of the system spatial uniformity of CS3 shows that this was an accurate assumption, so the gray card image was not used to adjust for illumination non-uniformity. The results of the tone reproduction for CS3 are shown in Figure 90. A table of supplemental data, Table 7-VIII, is in Appendix 7.2.

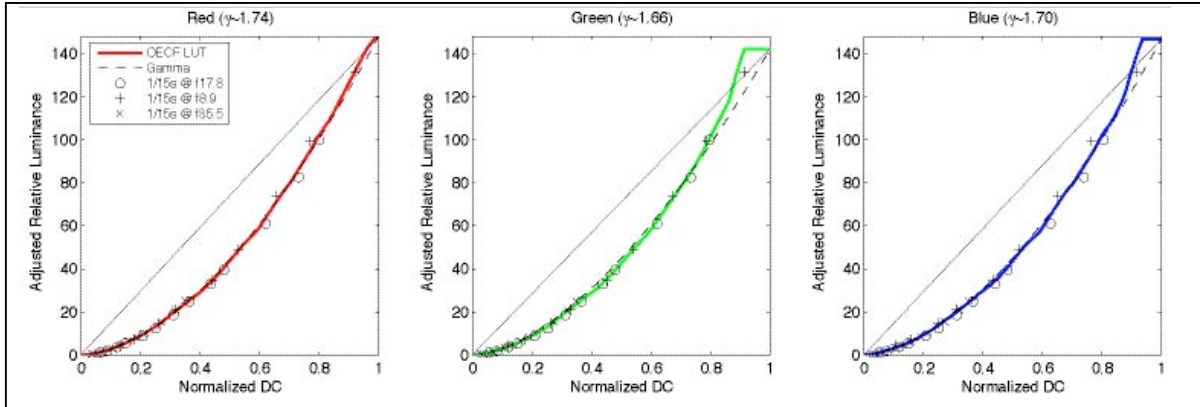


Figure 90. CS3 OECF curves.

The OECF curves for each channel have a different gamma encoding. The photographer clipped the green channel at a digital count value that was less than the maximum during the imaging. For the blue channel OECF measurement, the overexposed image did not include digital count values on the top flat part of the curve, but the data on the other part of the curve were sufficient when the OECFs were used in other parts of the testing procedure. The working space profile, ProPhoto RGB, which the CS3 images get converted to when opened, has a gamma encoding of 1.8 for all three channels. This means that the images will get interpreted with a gamma encoding that is different than the gamma encoding of the image, except for the green channel.

### Color Reproduction Accuracy

#### *Spectral Sensitivity*

The procedure used to determine the OECF curves in order to linearize the monochromator RGB image data were the same as what was described in the tone reproduction section above, except the OECF image used to determine the curves was the one imaged with the same settings as the monochromator images. The resulting OECF

curves were not smoothly curved. Instead of using these curves, since the Sinar CaptureShop .cs files were conveniently saved, they were used to create a tone curve and linearize the spectral sensitivity image data. The raw linear data were extracted from the .cs4 files to obtain the linear OECF curves, and the raw linear data were extracted from the .cs1 files to obtain the monochromator image data. The inverse OECF was then applied to the .cs1 data to obtain linearized RGB image data, which were divided by the measured summed spectral radiances as described in section 3.4.1.

The relative spectral sensitivity results for CS3 are shown in the left plot of Figure 91 and the relative spectral sensitivity curves rotated to fit the CIE 2° observer color-matching functions are shown in the right plot. These relative spectral sensitivities are those of the camera combined with the Sinar IR cut-off filter.

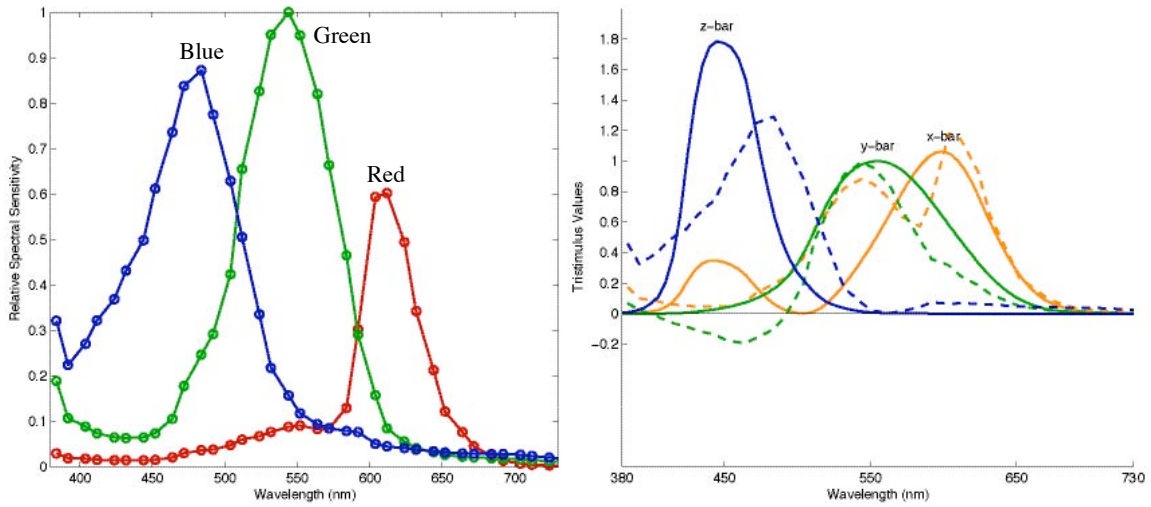


Figure 91. CS3 relative spectral sensitivities (left) and relative spectral sensitivities (dotted line) rotated to fit the CIE 2° observer (right).

The plots in Figure 91 show that there was a significant amount of UV radiation being imaged by the camera. The lack of fit of the relative spectral sensitivities to the CIE 2° observer color-matching functions (shown in the plot on the right of Figure 91) can be explained by the shifts in peak sensitivities, a stronger (red channel) and weaker (blue channel) peak sensitivity, and a negative lobe in the green channel.

The  $\mu$ -factor results for CS3 are shown in Table XLIII.

Table XLIII. CS3  $\mu$ -factor results.

<u>Detector</u>	<u>Color Matching Functions</u>	<u>Taking Illuminant (Measured CCT)</u>	<u>Viewing Illuminant</u>	<u><math>\mu</math>-Factor</u>
Camera	CIE 2° Observer	Xenon strobe (6628K)	$D_{50}$	0.81
		$D_{50}$		0.82
		Xenon strobe (6628K)		0.99
		$D_{50}$		1.00

The  $\mu$ -factor results in CS3 show that the digital imaging system as a whole, produced a  $\mu$ -factor of 0.81, which is less than the desired  $\mu$ -factor of 0.90. There is a slight improvement in the  $\mu$ -factor when the taking illuminant is not taken into account.

#### *Target-based Color Reproduction Accuracy*

In Figure 92, the CIELAB error vector plots are shown between the measured patch data and the image patch data of the Macbeth ColorChecker for CS3 using the Lab image data, which was normalized so that the Halon L\* equaled 100.

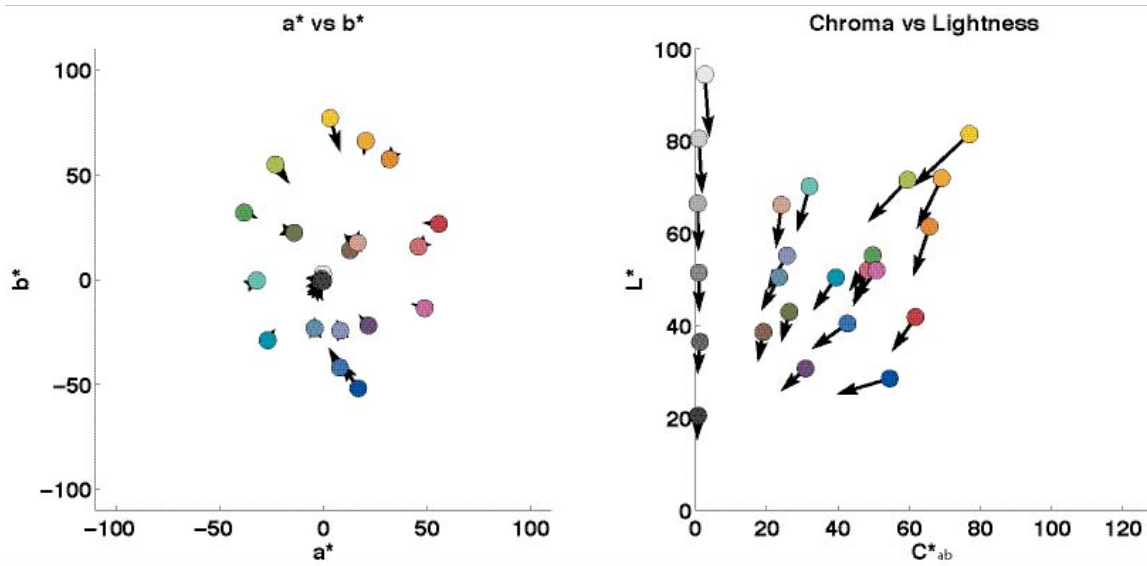


Figure 92. CS3 CIELAB  $a^*$  vs.  $b^*$  (left) and  $C^*_{ab}$  vs.  $L^*$  (right) error vector plots of the Macbeth ColorChecker between the measured patch data (dot) and the lightness corrected Lab image patch data (point of vector arrow).

In CS3, the  $a^*$  vs.  $b^*$  plot in Figure 92 shows that the more chromatic colors had a larger error than the neutral colors. Both plots show that, in general, the errors were caused by the image data being systematically less chromatic than the measured data. The  $C^*_{ab}$  vs.  $L^*$  plot further shows that the image data were also darker than the measured data.

Figure 93 is a histogram of the  $\Delta E_{00}$  error distributions of the Macbeth ColorChecker for CS3, which was evaluated, again, using the lightness corrected Lab image data.

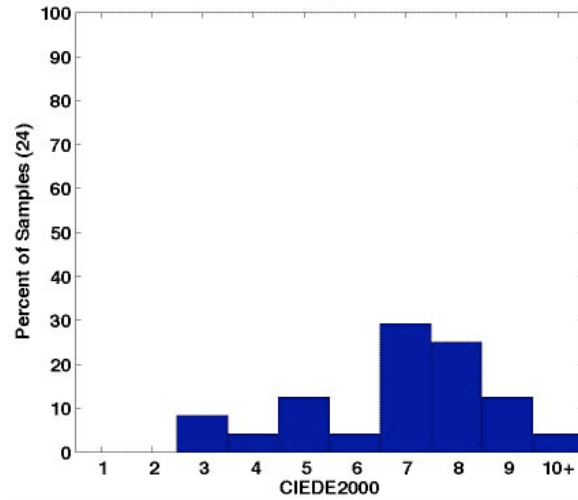


Figure 93. CS3 histogram of the  $\Delta E_{00}$  error distributions of the Macbeth ColorChecker between the measured patch data and the lightness corrected Lab image patch data.

This graph shows that, since most of the error bars are on the right side, the color difference errors were relatively high.

In Table XLIV, the mean, standard deviation and the 90<sup>th</sup> percentile data are given for the  $\Delta E^*_{ab}$  and  $\Delta E_{00}$  data between the measured patch data and the image patch data for each color reproduction accuracy chart in CS3.

Table XLIV. CS3 mean, standard deviation, and 90<sup>th</sup> percentile of the  $\Delta E^*_{ab}$  and  $\Delta E_{00}$  data between the measured patch data and the image patch data for each color reproduction accuracy chart.

<u>Color Reproduction Accuracy Chart</u>	Lab Image Data						Lab Image Normalized to Halon L* = 100					
	<u><math>\Delta E^*_{ab}</math></u>			<u><math>\Delta E_{00}</math></u>			<u><math>\Delta E^*_{ab}</math></u>			<u><math>\Delta E_{00}</math></u>		
	<u>Mean</u>	<u>Std. Dev.</u>	<u>90<sup>th</sup> Perc.</u>	<u>Mean</u>	<u>Std. Dev.</u>	<u>90<sup>th</sup> Perc.</u>	<u>Mean</u>	<u>Std. Dev.</u>	<u>90<sup>th</sup> Perc.</u>	<u>Mean</u>	<u>Std. Dev.</u>	<u>90<sup>th</sup> Perc.</u>
ColorChecker DC	9.75	3.32	13.27	7.21	2.30	9.44	3.12	1.99	4.87	2.11	0.92	3.14
ColorChecker	10.64	3.24	14.69	7.38	1.80	9.17	3.60	2.63	7.51	1.99	0.91	3.10
Esser	13.13	3.61	17.79	9.88	2.76	11.48	6.24	5.15	9.31	3.88	2.72	5.39
Esser Grayscale	11.28	1.82	12.34	9.13	1.54	10.69	4.02	2.73	7.38	3.55	1.61	5.53
BCRA	11.16	4.07	14.73	7.61	1.91	9.73	4.78	3.56	9.74	2.93	1.40	5.08
Blue Pigments	10.47	2.82	13.54	7.29	2.39	9.84	3.16	1.17	4.46	1.37	0.73	2.43
Pigment Target	14.15	4.49	20.20	8.53	2.51	11.90	9.85	6.12	18.08	5.02	2.71	9.47
Kodak Color Separation	14.23	2.50	17.26	10.21	1.30	11.81	6.41	4.19	10.99	4.32	2.13	7.83
Kodak Grayscale	11.76	1.34	13.84	9.13	1.43	11.24	5.41	2.02	8.81	4.30	1.05	6.06
IT8	11.15	2.71	14.11	8.06	1.99	10.00	4.51	2.64	7.20	2.85	1.14	4.11
IT8 Grayscale	8.67	3.21	13.15	6.97	2.69	9.60	2.59	0.85	3.74	2.46	0.76	3.46
Mean	11.49	3.01	14.99	8.31	2.06	10.45	4.88	3.00	8.37	3.16	1.46	5.05

What can be seen from this table is that the lightness corrected image data had lower  $\Delta E^*_{ab}$  and  $\Delta E_{00}$  values in comparison to the measured data than the non-lightness corrected image data. Also, when comparing the lightness corrected  $\Delta E_{00}$  values, the color reproduction accuracy of the Blue Pigment chart was the most accurate, followed

by the ColorChecker chart. The Pigment Target chart was reproduced the least accurately, followed by the Kodak Color Separation and the Kodak Grayscale charts. It is preferred, since this testing procedure is geared toward imaging paintings, that the Macbeth ColorChecker DC, the Macbeth ColorChecker the Blue Pigments and the Pigment Target charts are reproduced the most accurately. In this case, the Pigment Target was reproduced very inaccurately and the CC, CCDC and Blue Pigments charts were reproduced intermediary in accuracy compared to the other charts. The mean  $\Delta E^*_{ab}$  values of all of the color charts were adequate compared to the desired value of 2.00.

Table XLV. CS3 mean, standard deviation, and 90<sup>th</sup> percentile of the  $\Delta E^*_{ab}$  and  $\Delta E_{00}$  data between the measured patch data and the image patch data for the Macbeth ColorChecker and ColorChecker DC charts using both the lightness corrected Lab image patch data and the RGB image patch data (CCDC characterization chart data used to build a linearized RGB to XYZ 3x3 transform) to determine the CIELAB data.

<b><u>Color Reproduction Accuracy</u></b> <b><u>Chart (Image</u></b> <b><u>Data/Transformation)</u></b>	<b><u><math>\Delta E^*_{ab}</math></u></b>			<b><u><math>\Delta E_{00}</math></u></b>		
	<b><u>Mean</u></b>	<b><u>Std.</u></b> <b><u>Dev.</u></b>	<b><u>90<sup>th</sup></u></b> <b><u>Perc.</u></b>	<b><u>Mean</u></b>	<b><u>Std.</u></b> <b><u>Dev.</u></b>	<b><u>90<sup>th</sup></u></b> <b><u>Perc.</u></b>
<b>ColorChecker DC (Lab/Profile)</b>	3.12	1.99	4.87	2.11	0.92	3.14
<b>ColorChecker DC (RGB/CCDC)</b>	2.68	1.93	4.60	1.74	0.88	2.65
<b>ColorChecker (Lab/Profile)</b>	3.60	2.63	7.51	1.99	0.91	3.10
<b>ColorChecker (RGB/CCDC)</b>	5.24	1.77	7.41	3.97	1.02	4.91

Table XLV compares the color differences between the image CIELAB data determined using an embedded profile in Adobe Photoshop® (the first evaluation method described in Section 3.4.2), which are listed in Table XLIV above, and determined using an OECF linearization combined with a 3x3 RGB to XYZ transform created and optimized with the CCDC data (the second evaluation method described in Section 3.4.2). The data in this table show that the simple 3x3 transformation performed better for the CCDC chart and worse for the CC chart. The CCDC chart was used to create the 3x3 transform, so its

color reproduction accuracy would be expected to perform better than the CC chart. This means that there can be an improvement in the embedded profile used at the museum, but the profile that they used already performs satisfactorily.

### *Metamerism*

Table XLVI shows the D&H Color Rule metameristic match data of CS3. The Speedotron MW20QC Xenon strobe taking illuminant was the illuminant for the camera and CIE 2° observer matches in this case study. The photographer made his match under the fluorescent viewing illumination since it was impossible for him to make the match under the strobe lights. For this reason, only the color differences with the CIE 2° observer as the detector could be calculated for the photographer's match under the viewing illuminant.

Table XLVI. CS3 D&H Color Rule metameristic matches and the  $\Delta E^*_{ab}$  or  $\Delta E_{00}$  color differences of each metameristic match as "seen" by the camera and CIE 2° observer under the Speedotron MW20QC Xenon strobe taking illuminant.

<u>Detector</u>	<u>Metameristic Match</u>	<u>Camera</u>	<u>CIE 2° Observer</u>	<u>Camera</u>	<u>CIE 2° Observer</u>
		$\Delta E^*_{ab}$		$\Delta E_{00}$	
<b>Camera</b>	S-15	3.14	7.80	2.89	8.59
<b>CIE 2° Observer</b>	L-12	7.24	0.81	7.76	0.79
<b>Photographer</b>	L-12	N/A	2.52	N/A	3.16

It would be expected that the photographer's metameristic match in Table XLVI would be different from the camera and CIE 2° observer matches because the illuminant is different, but the CIE 2° observer match is the same as the photographer's match. This

doesn't mean that they have similar spectral sensitivities, because of the difference in the illuminant. The camera and CIE 2° observer detectors did not have the same match under the same illuminant, which means that the camera is not "seeing" the same colors of the D&H Color Rule as that of the CIE 2° observer. Since there is a high color difference when the CIE 2° observer is the detector of the camera's match, it would be expected that the photographer's match would also have a high color difference if the illuminant were the same, since the CIE 2° observer is an average human observer response. The color differences of the CIE 2° observer's metamerич matches as "seen" by the camera is large, which reiterates the fact that their spectral sensitivities differ. The same is true for the CIE 2° observer as the detector of the camera match in CS3.

### Noise

#### *Image Noise*

In CS3, a dark correction was performed automatically by the image capture software for every image taken. Table XLVII shows the image noise results of CS3 for each channel and the mean of all three channels.

Table XLVII. CS3 image total, fixed pattern and temporal noise results.

	<u>Red Channel</u>	<u>Green Channel</u>	<u>Blue Channel</u>	<u>Mean of RGB Channels</u>
<b>Total Average Noise (DC)</b>	721.64	593.05	665.93	660.21
<b>Total Signal to Noise Ratio</b>	12.61	15.22	14.51	14.11
<b>Fixed Pattern Average Noise (DC)</b>	602.95	499.61	567.94	556.83
<b>Fixed Pattern Signal to Noise Ratio</b>	15.10	18.07	17.01	16.73
<b>Temporal Average Noise (DC)</b>	396.51	319.52	347.71	354.58
<b>Temporal Signal to Noise Ratio</b>	22.96	28.25	27.78	26.33
<b>Black Temporal Average Noise (DC)</b>	437.64	347.70	364.24	383.19

For CS3, the total average noise greatly exceeds the desirable amount of noise limit of 257 digital counts in all three channels. Even though the noise images were dark corrected in order to reduce the amount of fixed pattern and total noise, the application of the unsharp mask to the digital master image enhanced the amount of noise present (see the SFR Results and Discussion part of this section below for more details). Table XLVII shows that the red channel had more total noise than the other two channels and the green channel had the least amount of total noise in CS3. The amount of temporal noise is significantly less than the fixed pattern noise.

#### *Color Noise*

Table XLVIII shows the color noise results for CS3.

Table XLVIII. CS3 color noise results of selected patches of the Macbeth ColorChecker.

<u>ColorChecker Patch</u>	<u>Mean Normalized DC</u>			<u>% Standard Deviation (Norm. DC)</u>			<u>MCDM</u>	
	<u>R</u>	<u>G</u>	<u>B</u>	<u>R</u>	<u>G</u>	<u>B</u>	<u><math>\Delta E^*_{ab}</math></u>	<u><math>\Delta E_{00}</math></u>
<b>Red (15)</b>	0.27	0.22	0.18	3.15	2.99	3.46	1.12	0.88
<b>Green (14)</b>	0.53	0.44	0.39	2.26	2.14	2.27	1.19	0.93
<b>Blue (13)</b>	0.31	0.34	0.43	3.12	2.42	2.26	1.17	1.02
<b>Cyan (18)</b>	0.24	0.28	0.17	3.58	2.72	3.76	1.19	0.89
<b>Magenta (17)</b>	0.39	0.37	0.48	2.43	2.11	1.91	1.06	0.95
<b>Yellow (16)</b>	0.41	0.54	0.49	3.13	2.17	2.31	1.34	0.95
<b>White (19)</b>	0.50	0.36	0.14	2.70	2.76	5.80	1.40	0.94
<b>Gray (22)</b>	0.25	0.26	0.43	3.35	2.69	2.31	1.16	0.77
<b>Black (24)</b>	0.46	0.28	0.27	2.01	2.18	2.29	1.01	0.69
<b>Mean</b>				2.86	2.46	2.93		
							<b>MMCDM</b>	1.18    0.89

The data in Table XLVIII show that there were small differences between the amounts of noise of each color patch. The % standard deviation results show that the green channel had the least amount of color noise and the blue channel had the most. The  $\Delta E_{00}$  color difference results show that the black patch and the gray patch had the least amount of color noise and the blue, magenta, and yellow patches had the most amount of color noise.

#### Dynamic Range

Table XLIX shows the dynamic range results of CS3 for each channel and the mean of all three channels.

Table XLIX. CS3 dynamic range results.

	<u>Red Channel</u>	<u>Green Channel</u>	<u>Blue Channel</u>	<u>Mean of RGB Channels</u>
<b>ISO Digital Still Camera Dynamic Range (Luminance Ratio)</b>	342.19	474.02	516.29	444.17
<b>ISO Digital Still Camera Dynamic Range (Density)</b>	2.53	2.68	2.71	2.65
<b>Theoretical Dynamic Range (Density)</b>	4.81	4.81	4.81	4.81

In CS3, the measured dynamic range was significantly less than the theoretical dynamic range in all three channels. The blue channel had the most amount of dynamic range of the three channels and the red channel had the least.

#### Spatial Cross-talk

Table L shows, for each channel, the mean linearized value of all 30 gray patch means, the percent relative maximum difference, and the percent relative standard deviation values for CS3.

Table L. CS3 summary of spatial cross-talk results.

	<u>Red Channel</u>	<u>Green Channel</u>	<u>Blue Channel</u>	<u>Mean of RGB Channels</u>
<b>Mean Linearized DC</b>	0.16	0.17	0.20	0.18
<b>Relative Maximum Difference (%)</b>	5.14	4.91	9.23	6.43
<b>Relative Standard Deviation (%)</b>	1.96	1.76	3.05	2.26

The data in Table 7-XIII for CS3 in Appendix 7.3 show that the mean digital count value of a gray patch that is surrounded by white in one image is always higher than the value

of the patch in the same position surrounded by black in the other image. This shows that spatial cross-talk is having an effect on the image. Table L shows that the spatial cross-talk affected the blue channel the most in CS3.

### Spatial Frequency Response (SFR)

The results of the SFR for CS3 are shown in Figure 94 and Table LI.

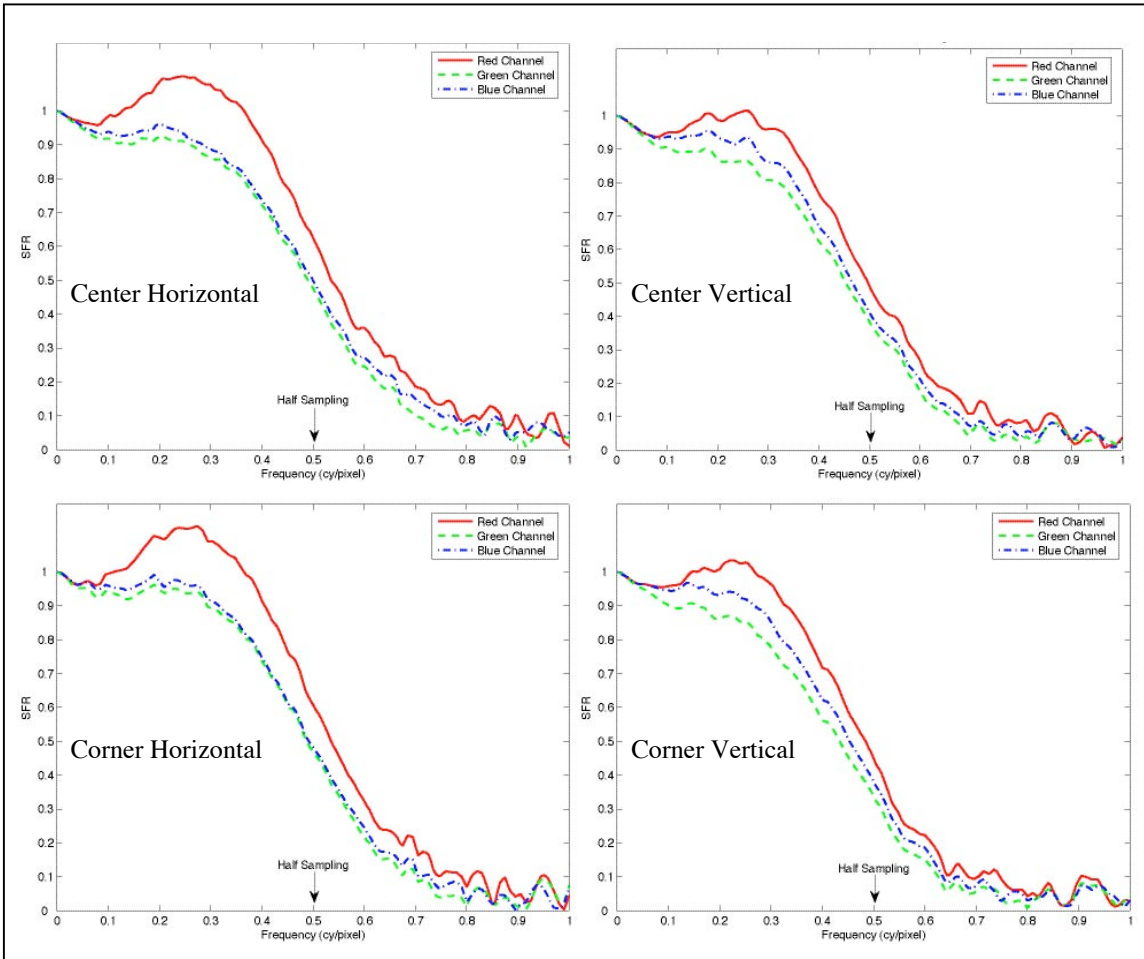


Figure 94. CS3 SFR of center horizontal edge (top left), center vertical edge (top right), upper left corner horizontal edge (bottom left), and upper left corner vertical edge (bottom right).

Table LI. CS3 SFR area results.

<u>Edge</u>	Area Under SFR Curve From Frequencies of 0.0 to 0.5cy/pixel			
	<u>Red Channel</u>	<u>Green Channel</u>	<u>Blue Channel</u>	<u>Mean of RGB Channels</u>
<b>Center Horizontal</b>	0.973	0.834	0.853	0.887
<b>Center Vertical</b>	0.891	0.787	0.830	0.836
<b>Corner Horizontal</b>	0.984	0.854	0.870	0.903
<b>Corner Vertical</b>	0.882	0.763	0.816	0.821
		<b>Mean</b>		0.862

The plots in Figure 94 show how the unsharp masking that was applied by the photographer to the digital master image in this case study effected the SFR results. Although the unsharp masking increased the SFR over the range of spatial frequencies, it also increased the amount of noise at those frequencies. The lack of smoothness of the SFR curves in Figure 94 illustrates the presence of this noise. It is evident, from the data shown in Table LI and Figure 94, that the SFR in the horizontal direction was better than the SFR in the vertical direction. Secondly, the SFR in the corner (off-axis) was better than the SFR in the center (on-axis) of the uncropped image area in the horizontal direction, but the opposite was true in the vertical direction. Thirdly, the red channel SFR was higher than the blue channel, which was slightly higher than the green channel.

#### Color Channel Registration

Table LII shows the color channel results for CS3.

Table LII. CS3 color channel registration results.

<u>Edge</u>	<b>Misregistration Shift (pixels)</b>		
	<b>Red Channel</b>	<b>Green Channel</b>	<b>Blue Channel</b>
<b>Center Horizontal</b>	0.122	0.000	0.003
<b>Center Vertical</b>	0.034	0.000	0.052
<b>Corner Horizontal</b>	0.066	0.000	0.001
<b>Corner Vertical</b>	0.050	0.000	0.090
<b>Maximum</b>	0.122	0.000	0.090
<b>Mean</b>	0.068	0.000	0.036
<b>Mean of RGB Channels</b>			0.035
Note: Green channel used as reference			

The camera used in CS3 has an area array CCD. It is evident, from the data in Table LII, that the red channel and blue channel misregistration shifts were comparable in comparison to the green channel. The maximum amount of misregistration was approximately 0.1 pixels, which was on the red channel's center horizontal edge. The blue channel's corner horizontal edge had the least amount of misregistration shift. The misregistration error on the horizontal knife-edge was comparable to that of the vertical edge in both the center and corner of the uncropped image area.

#### Depth of Field

Figure 95 shows the plot of the depth of field distance vs. area under the SFR curve for the horizontal edge of each color channel for CS3.

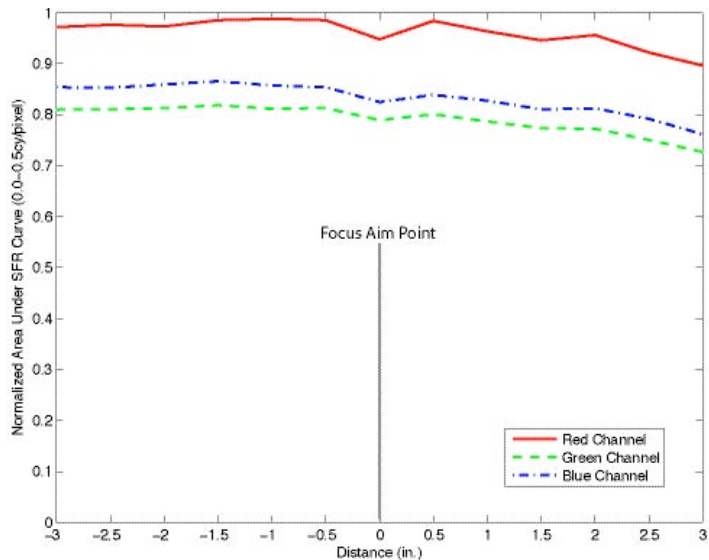


Figure 95. CS3 depth of field area under SFR curve vs. distance of the horizontal edge.

Differences between the red, green and blue color channels in the plot in Figure 95 were caused by their misregistration shifts (see the Color Channel Registration part of this section). The plot also shows that the sharpness of the image did not change very much as the camera-to-subject distance changed, which means that the depth of field was large. The accuracy of the focusing method (looking at a magnified area of the live image preview), which was used to focus on the 3" high column during the imaging of the depth of field target, is hard to determine because the depth of field was so large. The unsharp mask that was applied to the digital master image caused the plot to have a very large area under the SFR curve (see the SFR part of this section).

#### 4.6 Case Study Four

Case study four, CS4, was performed on July 20-21, 2004.

#### **4.6.1 Case Study Four: Digital Imaging System Description**

The camera used at the museum's studio was a Better Light 6000-2 (SN: 1688, Model: 6150) digital camera, which is a 3-channel (RGB) tri-linear-array-CCD scanning camera that scans from right to left across the image plane. The maximum native resolution of the camera is 8,000p x 6,000p. The digital back was on a Sinar 4x5 view camera body. The lens was a 210mm f/5.6 MC Sinaron SE 75°. The filter used between the lens and CCD was a Better Light daylight balancing/IR cut-off filter. This camera is typically used to image paintings (varnished and unvarnished), other flat works, such as large works on paper, and 3D sculptures, for the purpose of protecting vulnerable originals from use and to include the digital images in a collection management system. Reproductions are created in the form of prints. Three people in the photography department at the museum can operate this camera. The photographer did not receive background training for this camera system, but he did see a demonstration of the camera system and image capture software.

There were four Broncolor HMI F 1200 lights, each of which had reflectors and a VWFL lens, used to light the scene indirectly by bouncing the light off of white walls and a 12' ceiling. These lights simulated daylight illumination. In his day-to-day imaging, the photographer does changes the positions of the lights for every object being imaged. Table LIII shows the CCT, chromaticity coordinates, and luminance of this illumination. Figure 96 shows the relative spectral power distribution of the HMI lights. These data were obtained by measuring the Halon , which was placed in the scene, with a calibrated PR650 spectroradiometer.

Table LIII Broncolor HMI F 1200 taking illuminant characteristics.

<b>Correlated Color Temperature</b>	5086K
<b>Chromaticity x (2° Observer)</b>	0.3429
<b>Chromaticity y (2° Observer)</b>	0.3528
<b>Luminance (2° Observer)</b>	552.2cd/m <sup>2</sup>

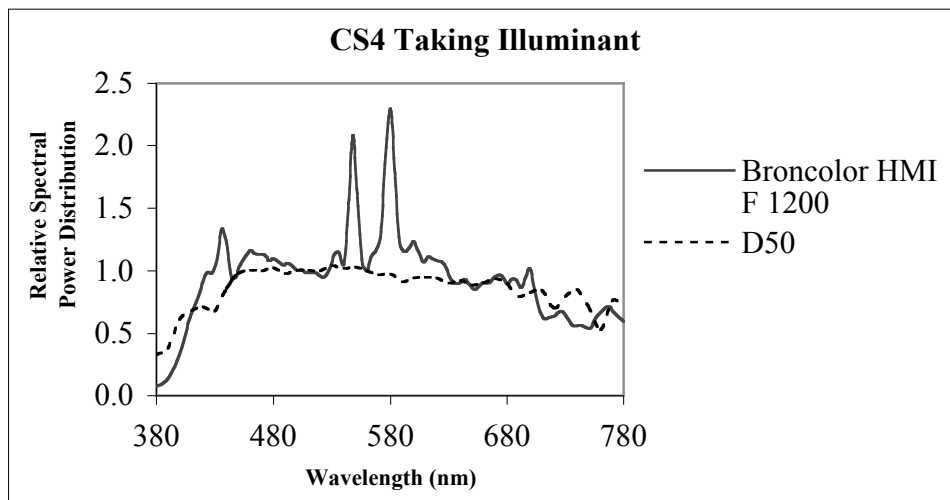


Figure 96. Relative spectral power distribution of the Broncolor HMI F 1200 lights that were used in the CS4 set-up. CIE illuminant D<sub>50</sub> is included for comparison.

The capture software used was Better Light ViewFinder 5.3.4. The monitor used was a Mitsubishi Diamond Pro 2060u monitor, on which visual corrections were made. This monitor was set so that it had a color depth of millions of colors, a resolution of 1152dpi x 870dpi at 75Hz, a gamma of 2.2 and a 6500K white point.

#### **4.6.2 Case Study Four: Imaging Procedure**

At the start of the case study on day one, a piece of black foam core board, which was used as the background during the imaging, was placed on the easel and taped there. Then the 26" x 22" image area was marked out and the Halon was centrally taped at the top, along with the case-study-imaging description label. Inside the marked-out area were also placed the two paintings (flower and fish). The photographer was asked to set up the camera, lights and easel in the same way that he would if he were imaging paintings in his usual everyday imaging at the museum. He was asked to light the entire marked-out image area. The camera, lights and easel were not set up from previous imaging, so he set everything up from scratch. The photographer used a level to make sure that the camera, which was set up on a monopod, was parallel to the easel. The illumination uniformity was not checked with a light meter. Figure 97 shows how the camera and lights were placed in relation to the easel during the imaging procedure. The labeled distances are approximate.

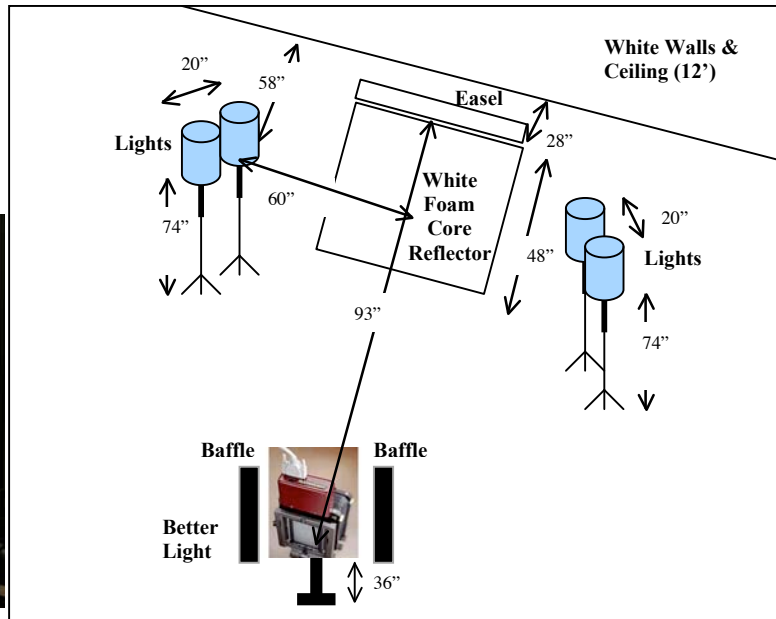


Figure 97. Image (left) and schematic (right) of the CS4-imaging set-up. The reflector had not yet been set up when the image on the left was taken.

After the camera, lights, and easel were set up, the photographer focused the camera on the paintings, manually at the camera, by looking through the ground glass. Then he placed a Macbeth ColorChecker target in front of the paintings. He prescanned the image and determined what the cropped image area would be in order to minimize the scanning time. Figure 98 shows approximately where the paintings image was cropped.

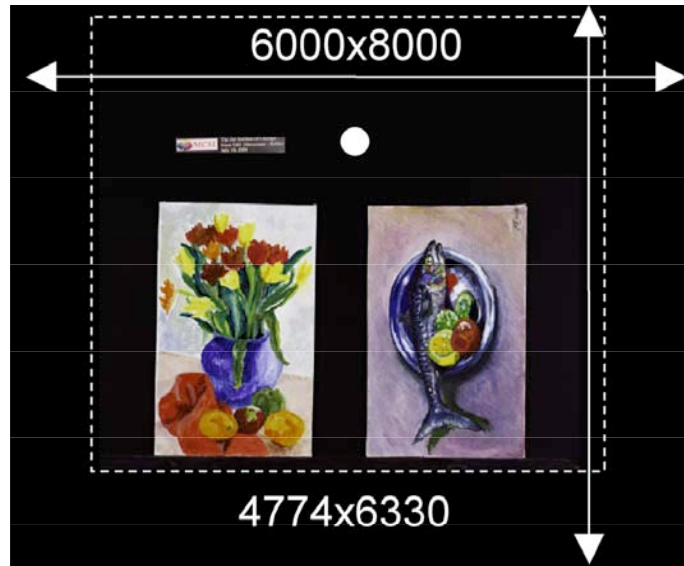


Figure 98. CS4 native resolution and cropped painting image area in pixels.

The aperture, which was continuous, was set to f/11. The photographer was asked to determine the nominal exposure time by making sure that the Halon was not clipped. He determined the exposure time, which was controlled in the image capture software, by adjusting the exposure time until the prescanned image had the correct exposure, which was when the Halon had digital count values that were maximum unclipped. The exposure time of 1/15s. and the aperture of f/11 became the nominal exposure settings of the case-study-imaging session. The ISO speed was set to 300. Still using the prescanned image, the photographer checked the spatial illumination uniformity by comparing the values across the even-toned black background in the image capture software. Then, in the prescanned image, the photographer used four patches of the ColorChecker grayscale to create a tone curve in the image capture software. Figure 99 illustrates this. The tone curve is shown on the right side of the screen shot.

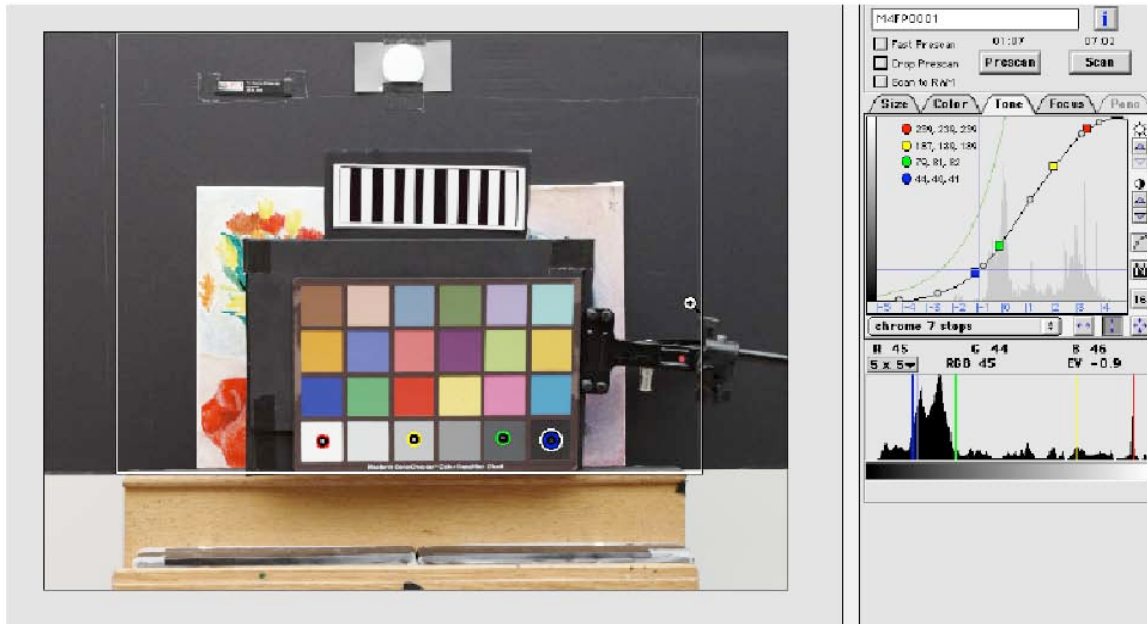


Figure 99. Screen shot of the prescanned image with the ColorChecker (left) and the tone curve that was created using four of the grayscale patches (right).

The photographer, in his usual imaging, sometimes uses the target consisting of black and white edges shown in Figure 99 as a guide when focusing. He did not use it during the case study.

The ColorChecker was then removed and the paintings image was then scanned at the nominal exposure settings. This image was automatically exported into Adobe Photoshop® where it was saved in the Macintosh byte order as an 8-bit RGB tiff file. This image was called the digital master. Figure 100 shows what was automatically applied to the digital master in the image capture software and in Adobe Photoshop® before it was saved. There was no camera profile assigned. The tone curve, shown in Figure 99 above, was applied and the image was converted to a working space profile. The digital master file had an effective resolution of 235ppi and the file size was 87MB.

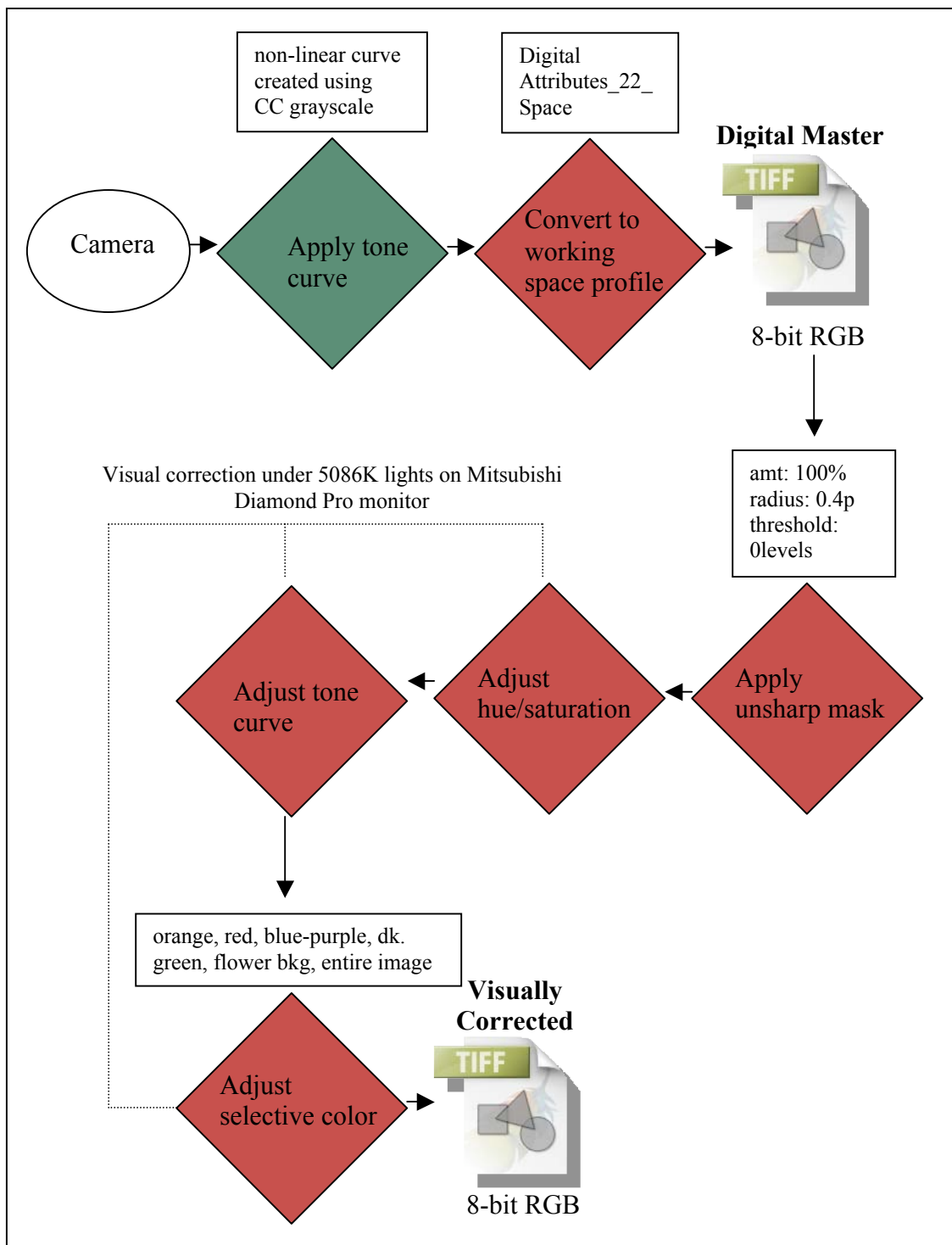


Figure 100. Flowchart of CS4 digital imaging workflow. A **green** background in the diamond means that the action was performed in the capture software. A **red** background in the diamond means that the action was performed in Adobe Photoshop®.

Because the photographer usually creates a visually corrected image, he was asked to visually correct the painting's digital master and save it. Figure 100 shows what processing the photographer did to the visually corrected image in Adobe Photoshop® before it was saved as an 8-bit tiff image file. When this image was visually corrected, both paintings were corrected as if they were one painting since they both contained the same pigments. When the photographer adjusted the selective color, for the most part, he selected parts of the flower painting and adjusted different colors separately. If the fish painting had the same colors that he selected in the flower painting, they were also adjusted simultaneously. It took the photographer approximately one hour to do the visual corrections. The photographer made the visual adjustments under the same Broncolor HMI F 1200 lights. He put a hood over himself and the monitor to avoid flare on the monitor when he was making his visual judgments. Figure 101 shows an image of the photographer making his visual adjustments.



Figure 101. Image of CS4 photographer making visual corrections to the paintings image.

This concluded the first part of the case study.

In the second part of the case study, the camera and lights set-up remained the same. Unless otherwise specified, the images taken in the second part were saved as digital master files with the same digital workflow as shown in Figure 100. The paintings were replaced by each of the three color-reproduction-accuracy targets (see Figures 25, 26, and 27) one at a time, which were each imaged once at the nominal exposure settings. The photographer refocused the camera before each image was taken. The cropped area remained the same as it was for the paintings image. The system-spatial-uniformity-gray-card target, shown in Figure 13, was imaged next, after the photographer refocused. It was imaged at the nominal exposure settings. It was imaged twice. For the second image, the two gray cards were each rotated 180°. In the same way, the spatial cross-talk target, shown in Figure 38, was imaged next, twice. In the second image, the spatial cross-talk target was rotated 180°. The next target that was imaged after refocusing by the photographer, this time using the frequency-based focusing tool in the image capture software, was the spatial-frequency-response target, which is shown on the left side of Figure 39. This target was also imaged at the nominal exposure settings and in the same cropped image area. The SFR target was then imaged a second time at the nominal exposure settings, but this time, the target was placed in the upper left corner of the cropped image area (see Figure 102 below). The photographer did not refocus the camera before imaging the SFR target again.

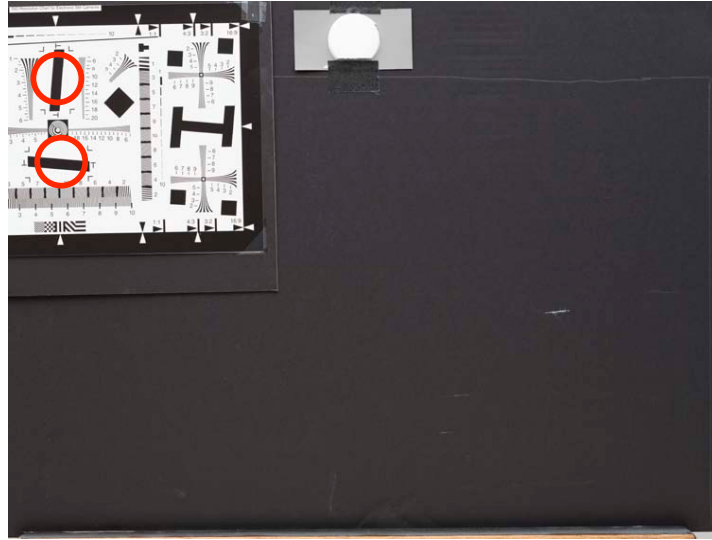


Figure 102. Placement of the SFR target in the CS4 cropped image area. The knife-edges used in the analysis are circled in red.

The next target that was imaged by the photographer was the noise target, which is shown in Figure 37. It was not necessary to refocus the camera before imaging this target because it was the same distance from the camera as the previous target. The cropped image scanning area was reduced in order to further decrease the camera's scanning time. It was imaged at the nominal exposure settings five times.

The OECF target, shown in Figure 16 was the next target to be imaged. Again, there was no need for the photographer to refocus before imaging this target. The cropped image scanning area was increased again to approximately what it was for the paintings image. This target was imaged three times. It was imaged once at the nominal exposure settings, a second time overexposed, by setting the exposure time to 1/8s. and keeping the aperture the same, and a third time underexposed, by, again, keeping the aperture the same and setting the exposure time to 1/30s. The OECF target was then imaged three more times at the same exposure settings as before. This time, prior to the image being taken, the color management was turned off so that the image was not

converted to the Digital Attributes working space profile. Also, the automatic tone corrections made in the image capture software were removed and replaced by a linear curve. These images were saved as 16-bit RGB tiff images. After the OECF target was imaged, the camera position was marked and the PR650 spectroradiometer, which was set up on a tripod, was put in its place and aimed at the OECF target. It was then moved closer to the target in order to fit the area to be measured by the spectroradiometer inside each of the twelve patches on the OECF chart. All twelve of the patches were measured from the darkest patch to the lightest patch. The Halon was also measured. While each patch was being measured by the spectroradiometer, the rest of the target was masked by placing a piece of opaque black cardboard over it. After all of the measurements were taken with the spectroradiometer, it was removed and the camera was put back into place. This concluded the imaging on the first day of the case study.

At the beginning of the second day of the case study, the depth of field target was set up on the easel. Before the depth of field target was imaged, the settings were returned to the same settings as the first set of OECF images, which is the same as the digital master file, shown in Figure 100. The photographer focused on the edge of the center square, the 3" high square, using the frequency-based focusing tool in the image capture software. This target was imaged at the nominal exposure settings, and cropped.

The monochromator instrument was the final thing to be imaged. The set-up for the monochromator imaging is shown in Figure 103.

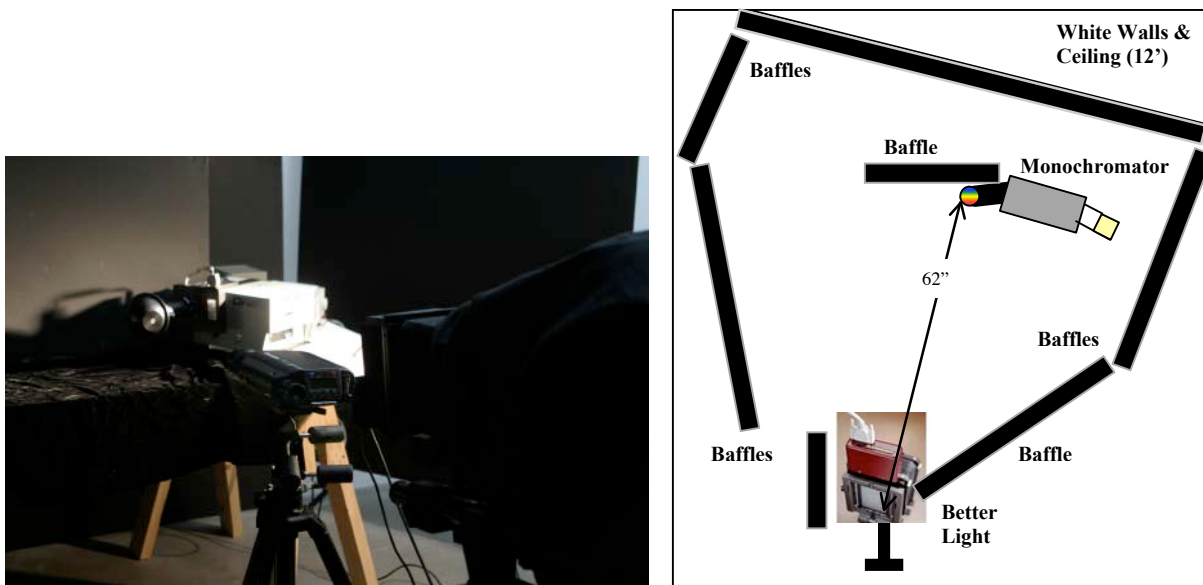


Figure 103. Image (left) and schematic (right) of the CS4 set-up for the monochromator instrument imaging.

There were no lights on when the monochromator was imaged. The photographer focused the camera so that the opening of the monochromator sphere was in focus. The aperture was opened all the way up to f/5.6 in order to maximize the amount of light being imaged by the camera. The ISO speed was changed from 300 to 424. The optimal exposure time was determined to be 1/8s. The PR650 spectroradiometer was also set up in front of the camera (see Figure 103) so that it could take measurements simultaneously as the camera was scanning the images. Because the scanned image area was cropped so that it was slightly larger than the spot of light coming out of the monochromator, the spectroradiometer did not interfere with the images. Prior to the monochromator imaging, the color management was turned off so that the image was not converted to the Digital Attributes working space profile. Also, the automatic tone corrections made in the image capture software were removed and replaced by a linear curve. This was done in order to obtain images that were as raw as possible. Thirty-six images and

spectroradiometer measurements were taken simultaneously as the monochromator bandpass peak settings ranged from 380nm to 730nm in 10nm increments. These images were saved as 16-bit RGB tiff images. This concluded the imaging procedure of case study four.

After the imaging procedure was finished, measurements were made off of the monitor with the PR650 spectroradiometer. First, the visually corrected paintings image was opened in Adobe Photoshop® with the embedded Digital Attributes profile used and the eleven uniform patches of pigment of each painting were zoomed in on and measured. Then the digital master image with the ColorChecker target in it was opened with the embedded ProPhoto RGB profile used and each of the 24 patches were measured. Next, the ColorChecker digital master image was cropped down and, using the paint bucket tool, was filled with red (255, 0, 0), green (0, 255, 0), blue (0, 0, 255), white (255, 255, 255), black (0, 0, 0), and grays with equal digital values of 24,48,90,180, and 224, consecutively. Each of these colors were measured with the PR650 spectroradiometer. Finally, the Halon was placed on the monitor and the ambient room light that was hitting the monitor was measured. Before the case study was ended, the photographer was asked to make his best possible visual match with the Davidson & Hemmendinger Color Rule under the Broncolor HMI F 1200 lights.

#### **4.6.3 Case Study Four: Results and Discussion**

##### Colorimetric Accuracy of Digital Imaging Workflow

Figure 104 shows the CIELAB error vector plots between the spectrophotometrically measured fish painting data and the lightness corrected digital

master fish painting image CIELAB data, between the lightness corrected digital master fish painting image CIELAB data and the lightness corrected visually corrected fish painting image CIELAB data, and between the spectrophotometrically measured fish painting data and the CIELAB data obtained from the CRT spectral radiance measurements of the non-lightness corrected visually corrected image. Table LIV shows the mean  $\Delta E_{00}$  of the fish and flower paintings between the spectrophotometrically measured data and the lightness corrected digital master paintings image CIELAB data, the lightness corrected visually corrected paintings image CIELAB data and the CRT spectral radiance measurement CIELAB data.

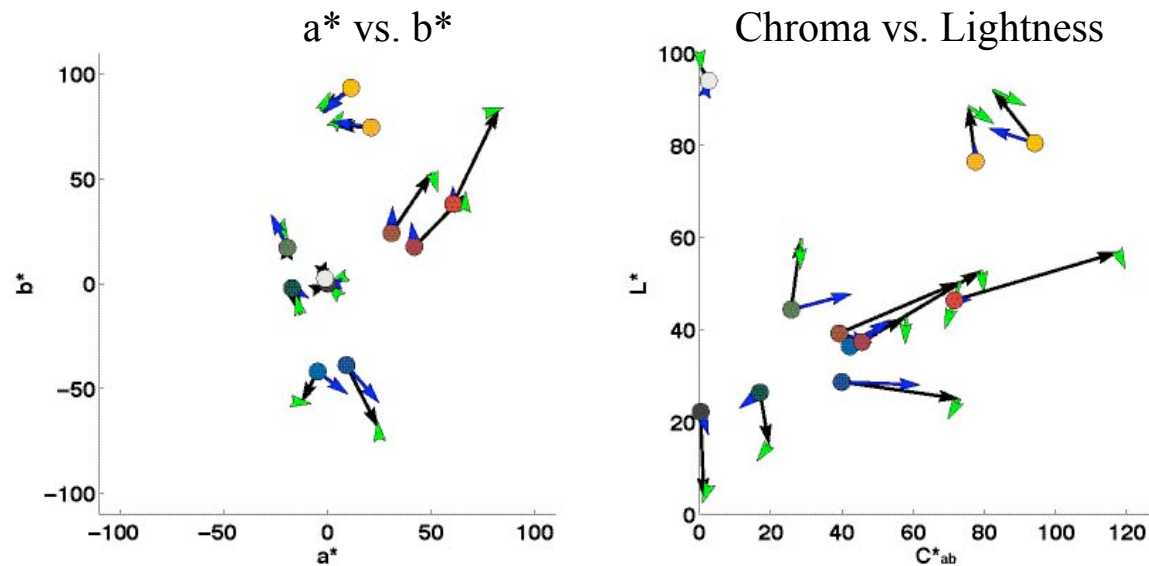


Figure 104. CS4 CIELAB  $a^*$  vs.  $b^*$  (left) and  $C^*_{ab}$  vs.  $L^*$  (right) error vector plots of the fish painting uniform patch areas between the measured patch data (dot) and the 1. Digital master image patch data (point of black vector arrow), 2. Visually corrected image patch data (point of green vector arrow), and 3. Spectroradiometric measurements of the CRT monitor of the non-lightness corrected visually corrected image patch data (point of blue vector arrow).

Table LIV. CS4 mean  $\Delta E_{00}$  of fish and flower paintings' 22 total uniform patch areas between the measured spectral reflectance and the CIELAB data of the digital master image, visually corrected image, and the CRT spectroradiometric measurements of the visually corrected image.

	<u>Lab Image Data</u>	<u>Lab Image Normalized to Halon L* = 100</u>
	<u><math>\Delta E_{00}</math></u>	
<b>Digital Master Image</b>	12.71	13.32
<b>Visually Corrected Image</b>	9.69	10.32
<b>CRT Measurements</b>	7.36	N/A

Since the purpose of visual editing the digital master image is to improve its color accuracy (make it appear more like the original), it would be expected that the  $\Delta E_{00}$  of the visually corrected image would be less than the digital master image. It would also be expected that the green error vectors would be the same length as, but in the exact opposite direction than the black vectors in Figure 104, that is, aiming back to the spectrophotometrically-measured values depicted by the colored dots. The results show that the  $\Delta E_{00}$  of the visually corrected image is smaller than that of the digital master image. The green vectors should point to the measured values (colored dots) in Figure 104, but, for the most part, they do not. The black error vectors are long for some of the colors, which means that these colors of the digital master image are very inaccurate. The green error vectors are short, which means that the photographer changed the color of the digital master very little. Also, it would be expected, if the monitor was calibrated accurately, that the CRT measurements blue error vectors would point to the same place as the visually corrected image green vectors, which means that the photographer would see the same colors on the monitor that are in the visually corrected image file. This is generally not the case, as can be seen in Figure 104. Even though there were inaccuracies

of the monitor calibration, the  $\Delta E_{00}$  of the CRT measurements were smaller than those of the digital master and the visually corrected image, which shows that the photographer did improve the color of the image on the monitor, but those improvements did not get stored in the visually edited image file itself, which will be viewed later on a different monitor.

The  $\Delta E_{00}$  values shown in Table LIV are large. There is an increase in the  $\Delta E_{00}$  value after the lightness correction for the digital master image and the visually corrected image. The causes of the color difference error can be seen in Figure 104. In general, the digital master image is more chromatic than the measured spectral reflectance data, and the visually corrected image is slightly darker than the digital master image.

#### System Spatial Uniformity

The results of the system spatial uniformity for CS4 are shown in Figure 105. A table of supplemental data, Table 7-IV, is in Appendix 7.1.

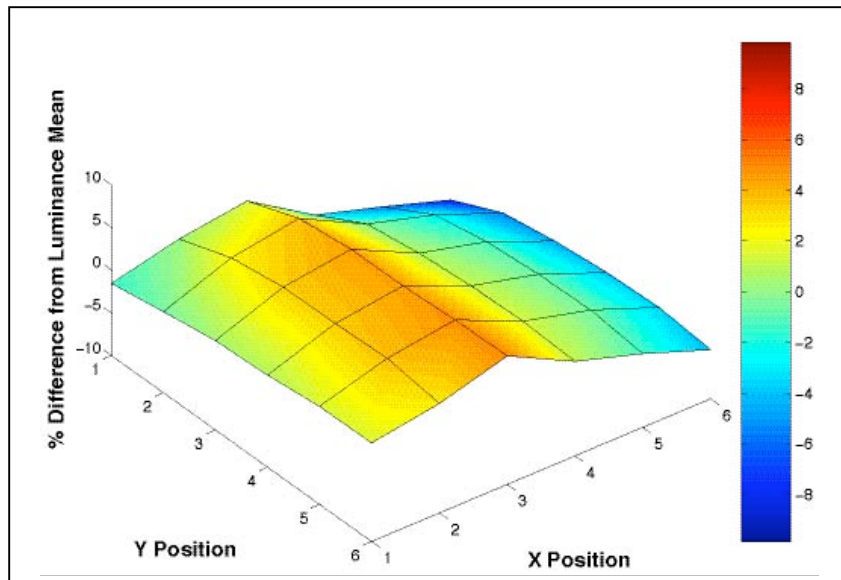


Figure 105. CS4 system spatial uniformity surface plot of % difference from luminance (Y) mean of gray card target.

In CS4, the photographer did not use a light meter during the set-up of the lights, but checked the uniformity of the digital counts of the image in the image capture software. Also, the lighting was indirect. The system spatial uniformity surface plot in Figure 105 shows that the left side of the gray card target image was of higher luminance than the right side.

### Tone Reproduction

The results of the tone reproduction for CS4 are shown in Figure 106. A table of supplemental data, Table 7-IX, is in Appendix 7.2.

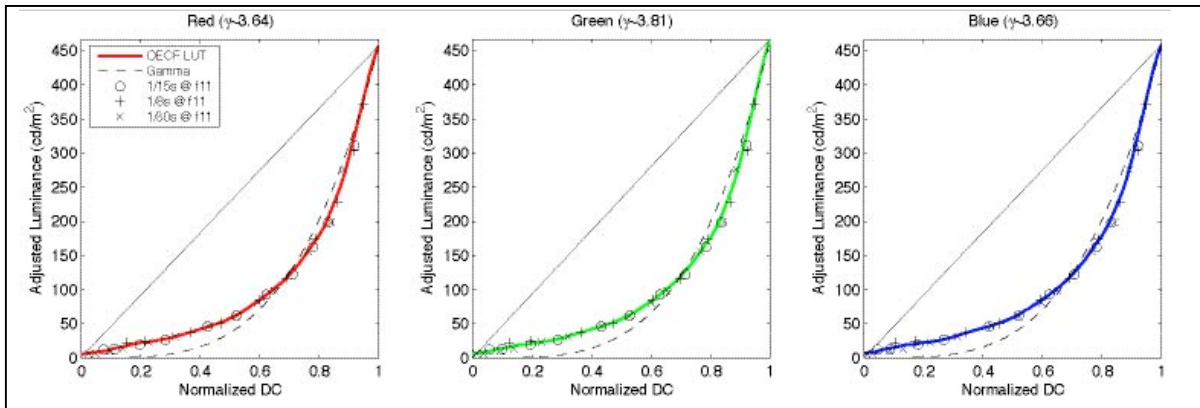


Figure 106. CS4 OECF curves.

The OECF curve for the green channel has a different gamma encoding than the red and blue channels. The working space profile, Digital Attributes\_22\_Space, which the CS4 images get converted to when opened, has a gamma encoding of 2.2 for all three channels. This means that the images will get interpreted with a gamma encoding that significantly different than the gamma encoding of the image.

### Color Reproduction Accuracy

#### *Spectral Sensitivity*

The relative spectral sensitivity results for CS4 are shown in the left plot of Figure 107 and the relative spectral sensitivity curves rotated to fit the CIE 2° observer color-matching functions are shown in the right plot. These relative spectral sensitivities are those of the camera combined with the Better Light daylight balancing/IR cut-off filter.

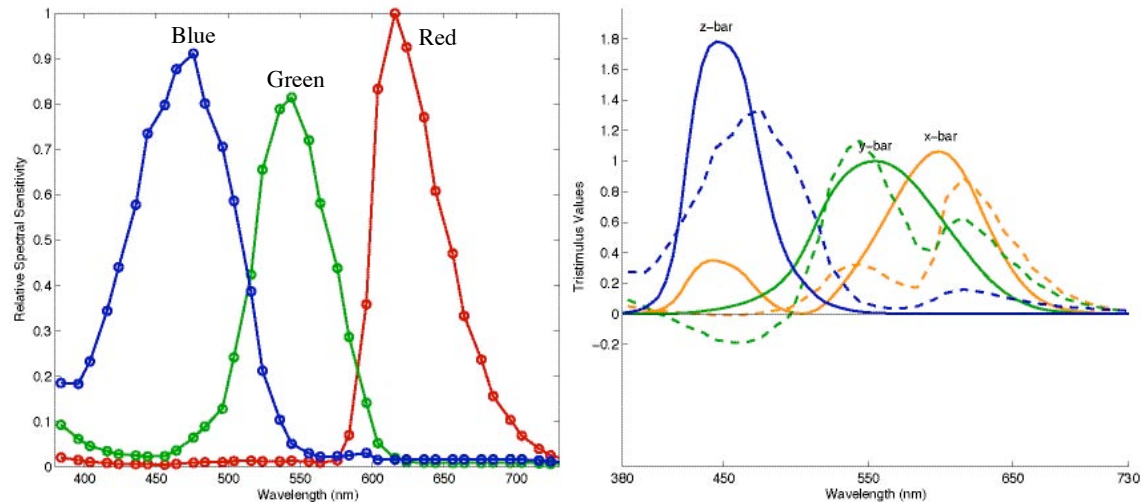


Figure 107. CS4 relative spectral sensitivities (left) and relative spectral sensitivities (dotted line) rotated to fit the CIE 2° observer (right).

The plots in Figure 107 show that there was a significant amount of UV radiation being imaged by the camera. The lack of fit of the relative spectral sensitivities to the CIE 2° observer color-matching functions (shown in the plot on the right of Figure 107) can be explained by the shifts in peak sensitivities, a weaker (red and blue channels) and stronger (green channel) peak sensitivity, and a negative lobe in the green channel.

The  $\mu$ -factor results for CS4 are shown in Table LV.

Table LV. CS4  $\mu$ -factor results.

<u>Detector</u>	<u>Color Matching Functions</u>	<u>Taking Illuminant (Measured CCT)</u>	<u>Viewing Illuminant</u>	<u><math>\mu</math>-Factor</u>
Camera	CIE 2° Observer	HMI (5086K)	D <sub>50</sub>	0.80
		D <sub>50</sub>		0.80
		HMI (5086K)		0.95
		D <sub>50</sub>		1.00
CIE 2° Observer				

The  $\mu$ -factor results in CS4 show that the digital imaging system as a whole, produced a  $\mu$ -factor of 0.80, which is less than the desired  $\mu$ -factor of 0.90. There is no improvement in the  $\mu$ -factor when the taking illuminant is not taken into account.

### *Target-based Color Reproduction Accuracy*

In Figure 108, the CIELAB error vector plots are shown between the measured patch data and the image patch data of the Macbeth ColorChecker for CS4 using the Lab image data, which was normalized so that the Halon L\* equaled 100. The camera images of the color targets were used for this analysis.

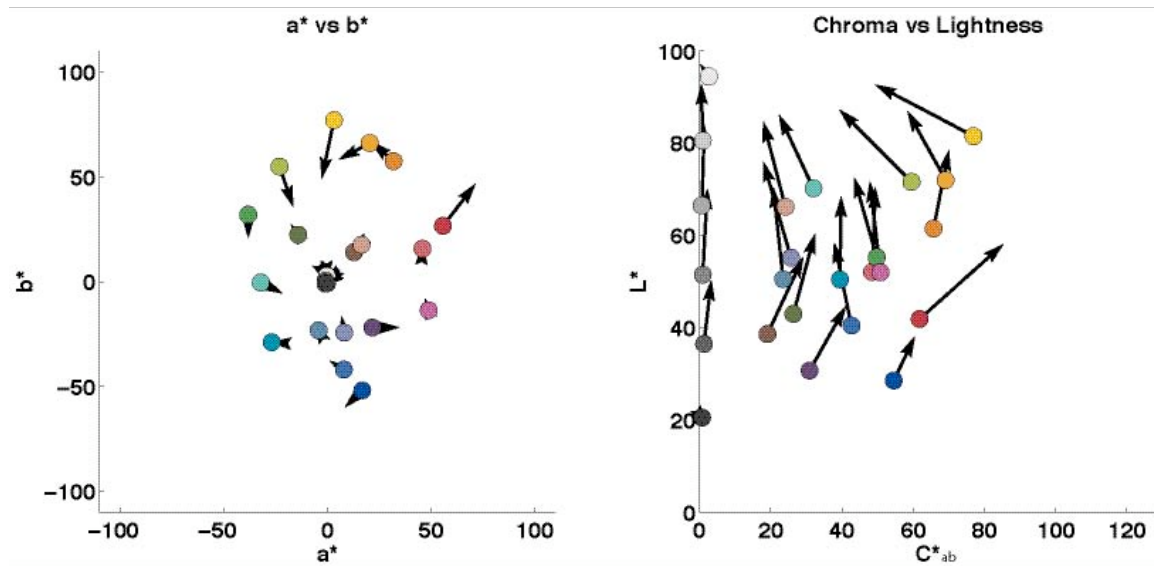


Figure 108. CS4 CIELAB a\* vs. b\* (left) and C\*<sub>ab</sub> vs. L\* (right) error vector plots of the Macbeth ColorChecker between the measured patch data (dot) and the lightness corrected Lab image patch data (point of vector arrow).

In CS4, the a\* vs. b\* plot in Figure 108 shows that the more chromatic colors had larger errors than the neutral colors. The a\* vs. b\* plot shows that the errors were both in hue

and chroma, depending on where the color lies in the CIELAB color space. The  $C^*_{ab}$  vs.  $L^*$  plot shows that most of the error was caused by the image data being systematically lighter than the measured data.

Figure 109 is a histogram of the  $\Delta E_{00}$  error distributions of the Macbeth ColorChecker for CS4, which was evaluated, again, using the lightness corrected Lab image data.

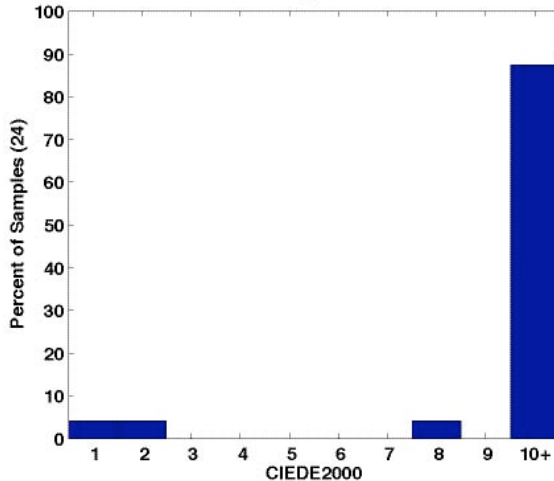


Figure 109. CS4 histogram of the  $\Delta E_{00}$  error distributions of the Macbeth ColorChecker between the measured patch data and the lightness corrected Lab image patch data.

This graph shows that, since most of the error bars are on the right side, the color difference errors were relatively high.

In Table LVI, the mean, standard deviation and the 90<sup>th</sup> percentile data are given for the  $\Delta E^*_{ab}$  and  $\Delta E_{00}$  data between the measured patch data and the image patch data for each color reproduction accuracy chart in CS4.

Table LVI. CS4 mean, standard deviation, and 90<sup>th</sup> percentile of the  $\Delta E^*_{ab}$  and  $\Delta E_{00}$  data between the measured patch data and the image patch data for each color reproduction accuracy chart.

Color Reproduction Accuracy Chart	Lab Image Data						Lab Image Normalized to Halon L* = 100					
	$\Delta E^*_{ab}$			$\Delta E_{00}$			$\Delta E^*_{ab}$			$\Delta E_{00}$		
	Mean	Std. Dev.	90 <sup>th</sup> Perc.	Mean	Std. Dev.	90 <sup>th</sup> Perc.	Mean	Std. Dev.	90 <sup>th</sup> Perc.	Mean	Std. Dev.	90 <sup>th</sup> Perc.
ColorChecker DC	16.59	8.00	23.72	11.89	5.46	17.12	17.71	8.08	24.53	12.72	5.65	18.20
ColorChecker	18.72	6.40	26.01	13.71	4.35	17.65	19.81	6.46	26.51	14.58	4.56	18.59
Esser	19.32	5.52	26.39	12.91	2.39	15.45	20.42	5.50	27.57	13.78	2.54	16.45
Esser Grayscale	11.70	4.50	16.39	9.11	3.95	13.64	12.79	4.82	17.81	9.88	4.20	14.64
BCRA	18.58	10.00	33.28	12.22	5.58	17.68	19.67	9.98	33.52	13.03	5.77	18.80
Blue Pigments	21.46	4.77	28.04	13.83	4.91	18.95	22.50	4.74	28.95	14.58	4.99	19.78
Pigment Target	22.51	11.65	43.65	12.20	3.43	16.10	23.38	11.90	45.23	12.82	3.54	16.86
Kodak Color Separation	16.54	7.62	26.64	9.49	3.25	11.70	17.37	7.49	27.86	10.04	3.34	12.56
Kodak Grayscale	10.67	4.66	15.53	8.22	3.56	12.66	11.30	4.84	16.64	8.68	3.81	13.66
IT8	15.61	5.44	20.41	10.46	2.93	13.99	16.71	5.61	21.60	11.24	3.16	15.00
IT8 Grayscale	10.72	4.24	16.34	8.55	3.72	14.22	11.58	4.75	17.73	9.16	4.08	15.22
Mean	16.58	6.62	25.13	11.14	3.96	15.38	17.57	6.74	26.18	11.86	4.15	16.34

What can be seen from this table is that the lightness corrected image data had higher  $\Delta E^*_{ab}$  and  $\Delta E_{00}$  values in comparison to the measured data than the non-lightness corrected image data. Also, when comparing the lightness corrected  $\Delta E_{00}$  values, the color reproduction accuracy of the Kodak Grayscale chart was the most accurate

followed by the IT8 Grayscale chart. The ColorChecker DC and Blue Pigment charts were reproduced the least accurately, followed by the Esser chart. It is preferred, since this testing procedure is geared toward imaging paintings, that the Macbeth ColorChecker DC, the Macbeth ColorChecker the Blue Pigments and the Pigment Target charts are reproduced the most accurately. In this case, the CCDC and Blue Pigment charts were reproduced very inaccurately and the ColorChecker and the Pigment Target charts were reproduced intermediary in accuracy compared to the other charts. Overall, this museum's digital imaging system reproduced neutrals the best. The mean  $\Delta E^*_{ab}$  values of all of the color charts were very poor compared to the desired value of 2.00.

Table LVII. CS4 mean, standard deviation, and 90<sup>th</sup> percentile of the  $\Delta E^*_{ab}$  and  $\Delta E_{00}$  data between the measured patch data and the image patch data for the Macbeth ColorChecker and ColorChecker DC charts using both the lightness corrected Lab image patch data and the RGB image patch data (CCDC characterization chart data used to build a linearized RGB to XYZ 3x3 transform) to determine the CIELAB data.

<b><u>Color Reproduction Accuracy</u></b> <b><u>Chart (Image Data/Transformation)</u></b>	<b><u><math>\Delta E^*_{ab}</math></u></b>			<b><u><math>\Delta E_{00}</math></u></b>		
	<b><u>Mean</u></b>	<b><u>Std. Dev.</u></b>	<b><u>90<sup>th</sup> Perc.</u></b>	<b><u>Mean</u></b>	<b><u>Std. Dev.</u></b>	<b><u>90<sup>th</sup> Perc.</u></b>
<b>ColorChecker DC (Lab/Profile)</b>	17.71	8.08	24.53	12.72	5.65	18.20
<b>ColorChecker DC (RGB/CCDC)</b>	3.89	4.06	8.85	2.27	1.57	4.35
<b>ColorChecker (Lab/Profile)</b>	19.81	6.46	26.51	14.58	4.56	18.59
<b>ColorChecker (RGB/CCDC)</b>	4.88	3.66	9.38	2.62	1.69	4.42

Table LVII compares the color differences between the image CIELAB data determined using an embedded profile in Adobe Photoshop® (the first evaluation method described in Section 3.4.2), which are listed in Table LVI above, and determined using an OECF linearization combined with a 3x3 RGB to XYZ transform created and optimized with the CCDC data (the second evaluation method described in Section 3.4.2). The data in

this table show that the simple 3x3 transformation performed significantly better for both charts. This means that there can be a great improvement in the embedded profile used at this museum.

### *Metamerism*

Table LVIII shows the D&H Color Rule metameric match data of CS4. The HMI taking illuminant was the illuminant for all three matches in this case study.

Table LVIII. CS4 D&H Color Rule metameric matches and the  $\Delta E^*_{ab}$  or  $\Delta E_{00}$  color differences of each metameric match as “seen” by the camera and CIE 2° observer under the HMI taking illuminant.

<u>Detector</u>	<u>Metameric Match</u>	<u>Camera</u>	<u>CIE 2° Observer</u>	<u>Camera</u>	<u>CIE 2° Observer</u>
		$\Delta E^*_{ab}$		$\Delta E_{00}$	
<b>Camera</b>	U-20	2.99	15.32	2.07	16.20
<b>CIE 2° Observer</b>	K-10	15.35	0.50	19.00	0.46
<b>Photographer</b>	I-9	16.04	2.51	19.78	2.69

What can be seen from Table LVIII is that none of the three detectors had the same match under the same illuminant, which means that the camera is not “seeing” the same colors of the D&H Color Rule as that of the photographer or the CIE 2° observer. The difference in the match between the CIE 2° observer and the photographer could be caused by the photographer having slightly different spectral sensitivities (color-matching functions), since the CIE 2° observer is only an average human observer response. The color differences of the CIE 2° observer and photographer’s metameric matches as “seen” by the camera are very large, which reiterates the fact that their spectral sensitivities

differ. The same is true for the CIE 2° observer as the detector of the camera match in CS4.

### Noise

#### *Image Noise*

Table LIX shows the image noise results of CS4 for each channel and the mean of all three channels.

Table LIX. CS4 image total, fixed pattern and temporal noise results.

	<u>Red Channel</u>	<u>Green Channel</u>	<u>Blue Channel</u>	<u>Mean of RGB Channels</u>
<b>Total Average Noise (DC)</b>	2.90	2.67	2.94	2.84
<b>Total Signal to Noise Ratio</b>	22.26	24.87	21.23	22.79
<b>Fixed Pattern Average Noise (DC)</b>	2.37	2.29	2.63	2.43
<b>Fixed Pattern Signal to Noise Ratio</b>	27.17	28.98	23.79	26.65
<b>Temporal Average Noise (DC)</b>	1.66	1.37	1.33	1.45
<b>Temporal Signal to Noise Ratio</b>	38.82	48.45	47.09	44.79
<b>Black Temporal Average Noise (DC)</b>	2.66	1.73	1.98	2.12

For CS4, the total average noise exceeds the desirable amount of noise limit of 1 digital count in all three channels. Table LIX shows that the blue channel had more total noise than the other two channels and the green channel had the least amount of total noise in CS4. The amount of temporal noise is less than the fixed pattern noise.

### *Color Noise*

Table LX shows the color noise results for CS4.

Table LX. CS4 color noise results of selected patches of the Macbeth ColorChecker.

<u>ColorChecker Patch</u>	<u>Mean Normalized DC</u>			<u>% Standard Deviation (Norm. DC)</u>			<u>MCDM</u>	
	<u>R</u>	<u>G</u>	<u>B</u>	<u>R</u>	<u>G</u>	<u>B</u>	<u><math>\Delta E^*_{ab}</math></u>	<u><math>\Delta E_{00}</math></u>
<b>Red (15)</b>	0.61	0.48	0.38	1.06	1.33	2.18	2.00	1.36
<b>Green (14)</b>	0.90	0.79	0.74	0.31	0.34	0.43	0.88	0.69
<b>Blue (13)</b>	0.61	0.68	0.80	1.09	0.50	0.40	1.21	0.94
<b>Cyan (18)</b>	0.51	0.59	0.40	1.49	0.64	2.00	1.83	1.01
<b>Magenta (17)</b>	0.74	0.72	0.84	0.52	0.47	0.34	0.99	0.84
<b>Yellow (16)</b>	0.72	0.88	0.88	0.67	0.23	0.30	0.94	0.59
<b>White (19)</b>	0.90	0.70	0.35	0.30	0.56	2.68	1.62	0.65
<b>Gray (22)</b>	0.49	0.55	0.78	1.58	1.04	0.46	1.53	0.94
<b>Black (24)</b>	0.89	0.55	0.56	0.24	0.95	0.86	1.20	0.62
<b>Mean</b>				0.81	0.67	1.07		
							<b>MMCDM</b>	1.36
								0.85

The data in Table LX show that there were small differences between the amounts of noise of each color patch. The % standard deviation results show that the green channel had the least amount of color noise and the blue channel had the most. The  $\Delta E_{00}$  color difference results show that the yellow patch and the black patch had the least amount of color noise and the red and cyan patches had the most amount of color noise.

### Dynamic Range

Table LXI shows the dynamic range results of CS4 for each channel and the mean of all three channels.

Table LXI. CS4 dynamic range results.

	<u>Red Channel</u>	<u>Green Channel</u>	<u>Blue Channel</u>	<u>Mean of RGB Channels</u>
<b>ISO Digital Still Camera Dynamic Range (Luminance Ratio)</b>	546.84	823.65	852.25	740.91
<b>ISO Digital Still Camera Dynamic Range (Density)</b>	2.74	2.92	2.93	2.87
<b>Theoretical Dynamic Range (Density)</b>	2.41	2.41	2.41	2.41

In CS4, the measured dynamic range was greater than the theoretical dynamic range in all three channels. The blue channel had the most amount of dynamic range of the three channels and the red channel had the least.

#### Spatial Cross-talk

Table LXII shows, for each channel, the mean linearized value of all 30 gray patch means, the percent relative maximum difference, and the percent relative standard deviation values for CS4.

Table LXII. CS4 summary of spatial cross-talk results.

	<u>Red Channel</u>	<u>Green Channel</u>	<u>Blue Channel</u>	<u>Mean of RGB Channels</u>
<b>Mean Linearized DC</b>	0.28	0.28	0.35	0.30
<b>Relative Maximum Difference (%)</b>	3.37	2.76	5.76	3.97
<b>Relative Standard Deviation (%)</b>	0.71	0.73	1.88	1.11

The data in Table 7-XIV for CS4 in Appendix 7.3 show that the mean digital count value of a gray patch that is surrounded by white in one image is always higher than the value of the patch in the same position surrounded by black in the other image. This shows that

spatial cross-talk is having an effect on the image. Table LXII shows that the spatial cross-talk affected the blue channel the most in CS4.

### Spatial Frequency Response (SFR)

The results of the SFR for CS4 are shown in Figure 110 and Table LXIII.

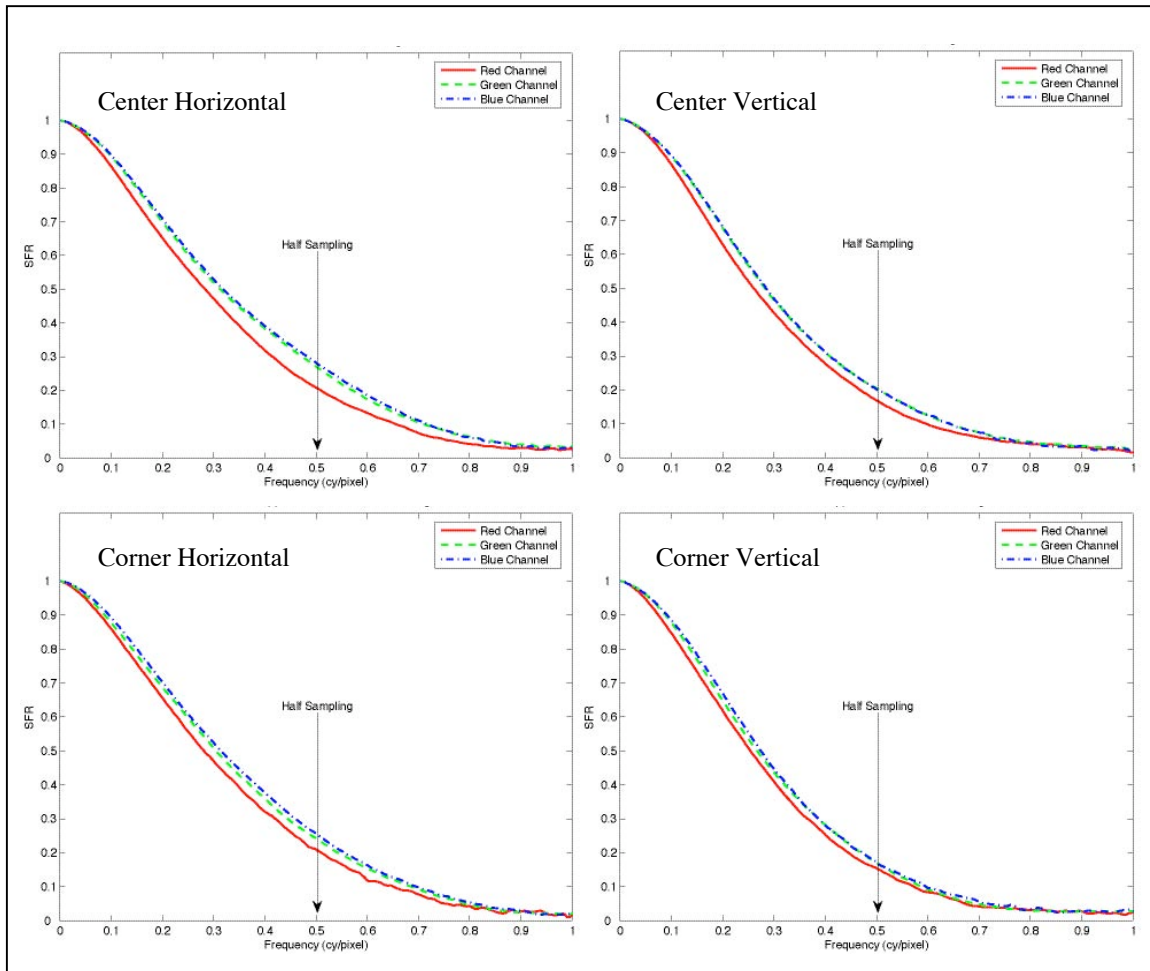


Figure 110. CS4 SFR of center horizontal edge (top left), center vertical edge (top right), upper left corner horizontal edge (bottom left), and upper left corner vertical edge (bottom right).

Table LXIII. CS4 SFR area results.

<u>Edge</u>	Area Under SFR Curve From Frequencies of 0.0 to 0.5cy/pixel			
	<u>Red Channel</u>	<u>Green Channel</u>	<u>Blue Channel</u>	<u>Mean of RGB Channels</u>
<b>Center Horizontal</b>	0.584	0.628	0.636	0.616
<b>Center Vertical</b>	0.559	0.591	0.593	0.581
<b>Corner Horizontal</b>	0.584	0.613	0.626	0.608
<b>Corner Vertical</b>	0.542	0.568	0.576	0.562
<b>Mean</b>				0.592

It is evident, from the data shown in Table LXIII and Figure 110, that the SFR in the horizontal direction was better than the SFR in the vertical direction. Since this camera is a scanning camera that scans horizontally (right to left), this implies that the SFR caused by the linear array itself was better than the SFR caused by the linear array's scanning. Secondly, the SFR in the center (on-axis) was slightly better than the SFR in the corner (off-axis) of the cropped image area. Thirdly, the green and blue channel SFRs, which were approximately the same, were higher than the red channel.

#### Color Channel Registration

Table LXIV shows the color channel registration results for CS4.

Table LXIV. CS4 color channel registration results.

<u>Edge</u>	Misregistration Shift (pixels)		
	<u>Red Channel</u>	<u>Green Channel</u>	<u>Blue Channel</u>
<b>Center Horizontal</b>	0.007	0.000	0.012
<b>Center Vertical</b>	0.025	0.000	0.051
<b>Corner Horizontal</b>	0.141	0.000	0.053
<b>Corner Vertical</b>	0.001	0.000	0.033
<b>Maximum</b>	0.141	0.000	0.053
<b>Mean</b>	0.043	0.000	0.037
<b>Mean of RGB Channels</b>			0.027
Note: Green channel used as reference			

It is evident, from the data in Table LXIV, that the red channel and blue channel misregistration errors were comparable in comparison to the green channel. The maximum amount of misregistration was less than 0.2 pixels. Out of the four edges, the corner horizontal edge had the most amount of misregistration shift in the red and blue color channels. The red channel's corner vertical edge had the least amount of misregistration error. The misregistration error on the horizontal knife-edge was comparable to that of the vertical edge in both the center and corner of the cropped image area.

### Depth of Field

Figure 111 shows the plot of the depth of field distance vs. area under the SFR curve for the horizontal edge of each color channel for CS4.

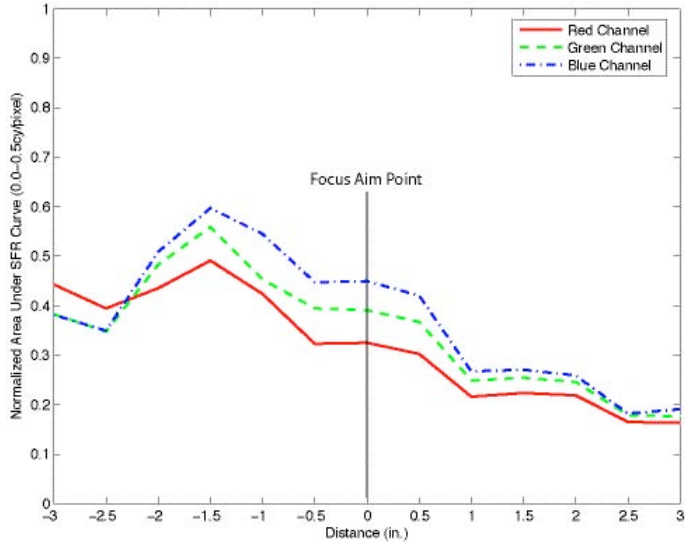


Figure 111. CS4 depth of field area under SFR curve vs. distance of horizontal edge.

Differences between the red, green and blue color channels in the plot in Figure 111 were caused by their misregistration shifts (see the Color Channel Registration part of this section). Two pieces of information can be obtained about the depth of field image of CS4 from this plot. One is that the sharpness, and therefore the depth of field, of the image decreased as the camera-to-subject distance changed. The other is that the focusing method (using a frequency tool in the image capture software), which was used to focus on the 3" high column during the imaging of the depth of field target, was not accurate. Instead of the focus being at the focus aim point, it was about 1.5" farther away from the camera. There appears to be a dependency of the SFR on the location of the 13 horizontal edges in the image, which is why the curve in Figure 111 is not smooth. Since the SFR results shown in Figure 110 and Table LXIII show that the effect of the location of an edge in the image on the SFR is very small, this was probably caused by the depth of field target not being completely parallel to the camera (from the left side to the right side) when it was imaged.

#### **4.7 Case Study Comparison**

The four museum case studies were performed on the digital camera systems used by each museum for their typical digital imaging of paintings for archiving. The photographer at each museum followed their typical imaging procedures. The cameras, lights and workflows were all different among the four museums. The museums were not chosen based on their differences, but because they were early adopters of digital imaging. The two sections that follow compare results of the four museums for each of

the two parts of the case studies. The first part analyzed each museum's digital imaging workflows. The second part characterized their camera systems.

#### 4.7.1 Paintings Comparison

Figure 112 shows the comparison of the digital master Lab images of the paintings between the four museum case studies. These images are not corrected for lightness to make the L\* of Halon equal to 100.



Figure 106. Digital master painting Lab images, from left to right, CS1, CS2, CS3, and CS4.

The painting images shown in Figure 112 are similar to a typical painting image that would be stored as the digital master in the digital archive. Without being able to compare it to the original, a scholar, for example, looking at any one of these images

would probably think that it is a true representation of the actual painting. Given the large color differences between these paintings, this thinking is not reality. The cobalt blue pigment, which, as mentioned before, is one of the hardest pigments to reproduce because it is seen as blue in color, but reflects a lot of red light in the longer wavelength part of the visible spectrum, is located on the left hand side of the vase in the flower painting. The effect of the long wavelength reflectance tail is most apparent in the flower painting image of CS4, causing the cobalt blue pigment to be reproduced as purple.

Figure 113 shows the comparison of the visually corrected Lab images of the paintings between the museum case studies CS2, CS3, and CS4 (CS1 did not create a visually corrected image). These images are also not corrected for lightness to make the L\* of Halon equal to 100.



Figure 107. Visually corrected painting Lab images, from left to right, CS2, CS3, CS4

Even though there is a noticeable change in the color of these images from the digital master images, there is still a large amount of color difference between the museums. The purple appearance of the cobalt blue in CS4 was improved after visual editing of the digital master image. Table LXV compares the mean  $\Delta E_{00}$  of the fish and flower paintings across the four museum case studies.

Table LXV. CS1, CS2, CS3, and CS4 mean  $\Delta E_{00}$  of fish and flower paintings' 22 total uniform patch areas between the measured spectral reflectance and the CIELAB data of the digital master image, visually corrected image, and the CRT spectroradiometric measurements of the visually corrected image.

	<u>Lab Image Data</u>		<u>Lab Image Normalized to Halon L* = 100</u>		<u>CRT Measurements</u>
	<u>Digital Master</u>	<u>Visually Corrected</u>	<u>Digital Master</u>	<u>Visually Corrected</u>	
	<u><math>\Delta E_{00}</math></u>				
<b>CS1</b>	12.26	N/A	12.22		N/A
<b>CS2</b>	6.87	6.94	4.01	7.58	5.75
<b>CS3</b>	10.54	10.56	6.78	8.41	9.79
<b>CS4</b>	12.71	9.69	13.32	10.32	7.36

The Lab Image Data columns correspond to the images in Figures 112 and 113 above. CS4 had the largest amount of color inaccuracies in the digital master, followed by CS1, then CS3, and CS2 had the least amount of color inaccuracies. After visual corrections of the digital master image, CS4's color inaccuracies improved the most. CS2 and CS3's color inaccuracies became slightly worse. In CS2, CS3 and CS4, the CRT measurements had a smaller mean  $\Delta E_{00}$  value, which means that in all three cases, the CRT monitor was not calibrated accurately and the photographer saw improvements in color on the monitor when he was making the visual corrections, but these improvements were not stored in the visually corrected image files. Table LXVI further explains the inaccuracies of the monitor calibrations. This table shows the mean and max

$\Delta E^*_{ab}$  and  $\Delta E_{00}$  between the CIELAB data calculated from the CRT monitor spectroradiometric measurements (in the same way as the CRT measurements of the painting uniform areas) of the digital master file of the Macbeth ColorChecker and the CIELAB data of the Lab image of the ColorChecker digital master file for CS2, CS3, and CS4. There was no visual editing in CS1, so these monitor measurements were not performed.

Table LXVI. CRT monitor calibration accuracy mean and maximum color differences of the Macbeth ColorChecker between CRT spectroradiometric measurements of the digital master file and digital master Lab image data of CS2, CS3, and CS4.

	$\Delta E^*_{ab}$		$\Delta E_{00}$	
	<u>Mean</u>	<u>Max</u>	<u>Mean</u>	<u>Max</u>
<b>CS2</b>	1.87	3.82	1.24	2.04
<b>CS3</b>	2.36	3.23	1.80	2.57
<b>CS4</b>	6.06	16.02	3.42	7.85

The color difference values in Table LXVI would be approximately 0.00 if the monitors were calibrated accurately. CS2 had the most accurately calibrated monitor and CS4 had the least.

There are numerous differences between the painting images shown in Figures 112 and 113 above. Color differences are the most obvious differences, but there are also spatial differences. The results and discussion sections (sections 4.3.3, 4.4.3, 4.5.3, and 4.6.3) explain the results of the digital master image characterizations for each museum case study. The next section, section 4.7.2, compares the characterization results between the four case studies.

The causes of the color and spatial differences in the digital master files can be attributed to the different camera systems and imaging procedures used by each museum.

The digital master images are visually edited by different photographers, causing the visually corrected images to also look different. Table LXVII lists other causes for the differences in appearance of the visually corrected images; the differences between the four case studies' viewing environments in which the visual editing was performed.

Table LXVII. Parameters of viewing illumination and monitor for CS2, CS3, and CS4 used for the visual correction of the paintings.

	<b><u>CS2</u></b>	<b><u>CS3</u></b>	<b><u>CS4</u></b>
<b><u>Viewing Illumination Type</u></b>	Fluorescent	Fluorescent	HMI
<b><u>Viewing Illumination Measured CCT</u></b>	4963K	5407K	5086K
<b><u>Viewing Illumination Measured Luminance</u></b>	401.7cd/m <sup>2</sup>	138.9cd/m <sup>2</sup>	552.2cd/m <sup>2</sup>
<b><u>Monitor Type</u></b>	Barco	Sony Artisan	Mitsubishi Diamond Pro
<b><u>Monitor Measured CCT</u></b>	6031K	5198K	6258K
<b><u>Monitor Measured Peak Luminance</u></b>	75.32cd/m <sup>2</sup>	67.5cd/m <sup>2</sup>	77.3cd/m <sup>2</sup>

In CS2, CS3, and CS4, both the correlated color temperatures and the luminance levels between the illumination under which the paintings were viewed and the monitor on which the paintings image was viewed are different for each case study. When comparing across the three case studies, all of the parameters listed in Table LXVII are different, further explaining the differences in the visually corrected paintings images among the museums.

The working space profiles embedded by each case study, that the paintings images get converted to when opened, had white points of 5000K for CS2, 5000K for CS3, and 6500K for CS4. This means that the images will get interpreted with white points at these correlated color temperatures, which are all different than the white points of the monitors used in each case study to color correct the paintings images.

#### **4.7.2 Characterization Comparison**

In this section, the results of the characterizations of the digital master images of the targets used in the testing procedure for CS1, CS2, CS3, and CS4 are compared. In CS2, the camera image is evaluated instead of the digital master image for some of the image quality parameters (see section 4.4.3 for which image is used for each image quality parameter). Keep in mind that this section does not just compare the camera systems themselves, but each museum's digital imaging workflow in creating a digital master image. Table LXVIII compares the mono-numeric metric values for each image quality parameter of the four museum case studies. A discussion of the table follows the table along with some supplemental tables and figures, which further illustrate the comparisons. The results below indicate that none of the museums' digital imaging workflows and digital camera systems performed the better than the others for every image quality parameter tested in the museum case studies.

Table LXVIII. Summarization of the characterization mono-numeric metrics for comparison of CS1, CS2, CS3, and CS4 results.

<b><u>Image Quality Parameter</u></b>	<b><u>Mono-numeric Metric Value</u></b>			
	<b>CS1</b>	<b>CS2</b>	<b>CS3</b>	<b>CS4</b>
<b>System Spatial Uniformity</b>				
Max $\Delta E_{00}$ from Mean of All Patches	2.04	3.90	1.16	2.01
<b>Tone Reproduction</b>				
Mean Gamma of RGB Channels	2.80	2.03	1.70	3.70
<b>Color Reproduction Accuracy – Spectral Sensitivity</b>				
$\mu$ -Factor (Camera – CIE 2° Observer, Taking Illuminant – D <sub>50</sub> )	0.68	0.79	0.81	0.80
<b>Color Reproduction Accuracy – Target-based</b>				
Mean $\Delta E_{00}$ 90 <sup>th</sup> Percentile of All Charts of Normalized CIELAB Image Data – Halon L* = 100	12.74	6.73	5.05	16.34
<b>Noise – Image</b>				
Mean of RGB Channels Total Signal to Noise Ratio	35.85	14.16	14.11	22.79
<b>Noise – Color</b>				
MMCDM	0.92	1.01	0.89	0.85
<b>Dynamic Range</b>				
Mean of RGB Channels ISO DSC Dynamic Range (Density)	2.86	2.81	2.65	2.87
<b>Spatial Cross-talk</b>				
Mean of RGB Channels of Relative Maximum Difference (%)	5.83	6.52	6.43	3.97
<b>Spatial Frequency Response</b>				
Mean of Mean of RGB Channels Across Four Edges - Area Under SFR Curve From Frequencies of 0.0 to 0.5 cy/pixel	0.484	0.616	0.862	0.592
<b>Color Channel Registration</b>				
Mean of RGB Channels Across Four Edges - Misregistration Shift (pixels)	0.130	0.136	0.035	0.027
<b>Depth of Field</b>				
Mean of Mean of RGB Channels Across 13 Distances Normalized by the Largest RGB Channel Mean – Area Under SFR Curve From Frequencies of 0.0 to 0.5 cy/pixel	0.645	0.531	0.967	0.630

### *System Spatial Uniformity*

Table LXVIII shows that CS3 had the lowest system spatial uniformity  $\Delta E_{00}$  and CS2 had the highest  $\Delta E_{00}$ . The lower the  $\Delta E_{00}$  value is, the better the system spatial uniformity. The system spatial uniformity surface plots of % difference from luminance (Y) mean of gray card target for the four case studies are plotted again in Figure 114 for comparison purposes.

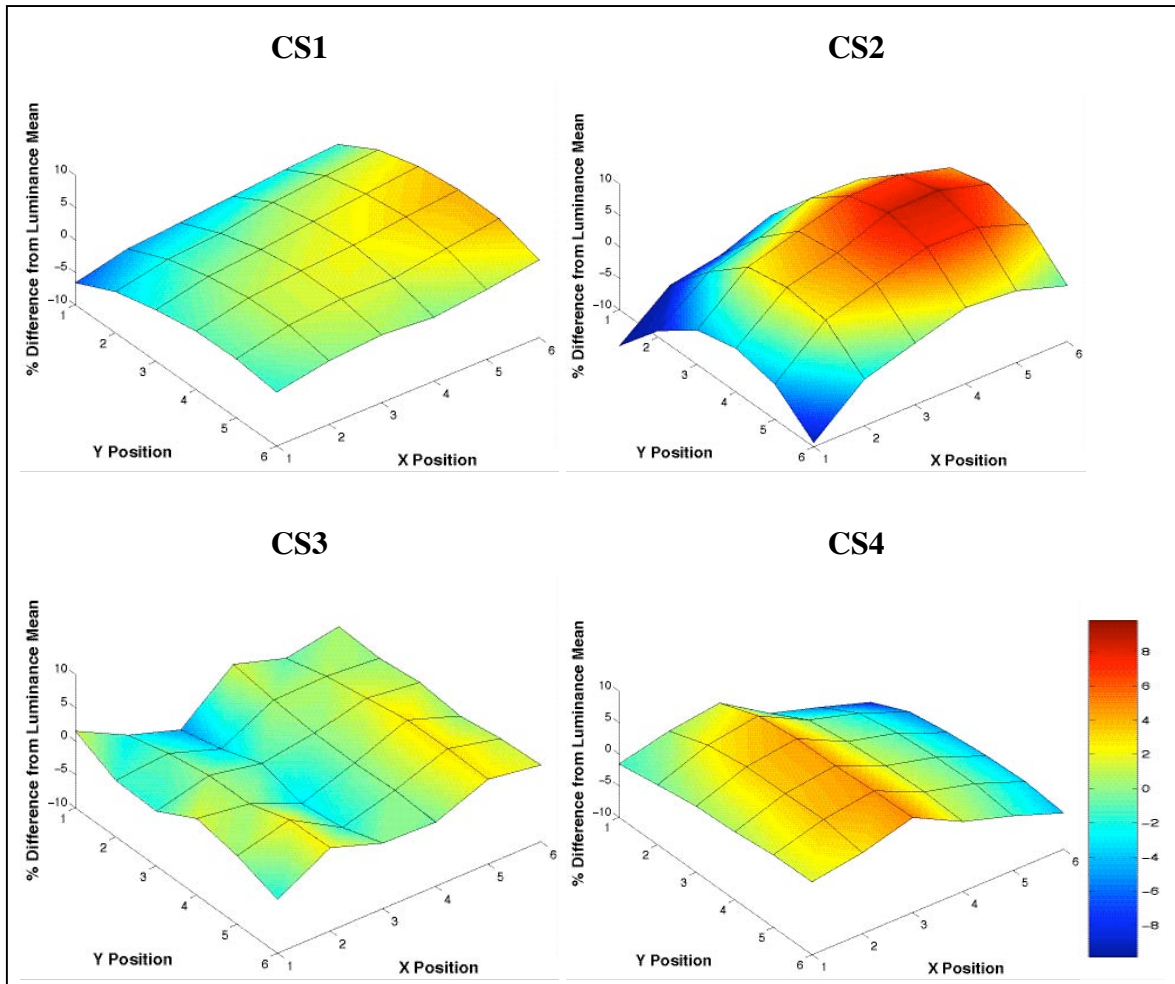


Figure 114. System spatial non-uniformity results comparison of the four case studies.

From these data, it can be concluded that metering of the entire image area or doing a correction of non-uniformities using the image capture software before imaging every painting helps to reduce system spatial non-uniformities.

### Tone Reproduction

Table LXVIII shows that all of the museums' images had a different gamma encoding that was greater than 1.0. The gamma encoding results from one museum is not necessarily better than that of any another museum. The gamma encoding can be imposed on an image by the camera's profile, the image software, or through post-processing, such as in Adobe Photoshop®. If the gamma encoding is known, it can show what the actual gamma encoding of each channel is and if there is any unwanted clipping. It is preferable that the gamma encoding of the image is interpreted at the same gamma encoding when it is converted to the working space profile so that the tonal relationships remain accurate when the image is opened in the future.

### Color Reproduction Accuracy

#### *Spectral Sensitivity*

Table LXVIII shows that the  $\mu$ -factors of the CS2 through CS4 digital imaging systems ranged from 0.68 to 0.81, with the  $\mu$ -factor of CS3 being the highest. The  $\mu$ -factor of CS1 was lower than the other case studies. The closer that the  $\mu$ -factor value is to unity, the better that the spectral sensitivities match the CIE 2° observer color-matching functions under the D<sub>50</sub> taking illuminant, or a linear combination of these color-matching functions. The  $\mu$ -factor results can be improved by using a taking light

source with its spectral power distribution closer to the rendering illuminant, D50 in this case, or a camera with better inherent spectral sensitivities.

#### *Target-based Color Reproduction Accuracy*

The lightness corrected (normalized Lab image data, where the Halon L\* was set equal to 100) image data were used in this section for the purpose of comparing across the four museum case studies' target-based color reproduction accuracy results. The 90<sup>th</sup> percentile of the mean  $\Delta E_{00}$  of all 11 of the color reproduction accuracy charts of this image data is compared in Table LXVIII. The 90<sup>th</sup> percentile was used rather than the average because in visual experiments evaluating color quality, maximum errors better correlate with perceived quality (Day, 2004). The lower this value is, the better the target-based color reproduction accuracy. The digital imaging system of CS4 (16.34) had the highest 90<sup>th</sup> percentile  $\Delta E_{00}$  and the digital imaging system of CS3 (5.05) had the lowest. The comparison of the target-based color reproduction results across the four case studies do not correlate exactly with the comparison of the spectral sensitivity results. This is because the target-based results were affected by the accuracy of the profile, which helps to overcome spectral sensitivity limitations. Overall, the target-based color errors were small when the  $\mu$ -factor was large, but there was a large range in the 90<sup>th</sup> percentile  $\Delta E_{00}$  values over the small range in  $\mu$ -factor values. Figures 115 and 116 below compare the mean and 90<sup>th</sup> percentile  $\Delta E_{00}$  values, respectively, for each chart across all four museum case studies.

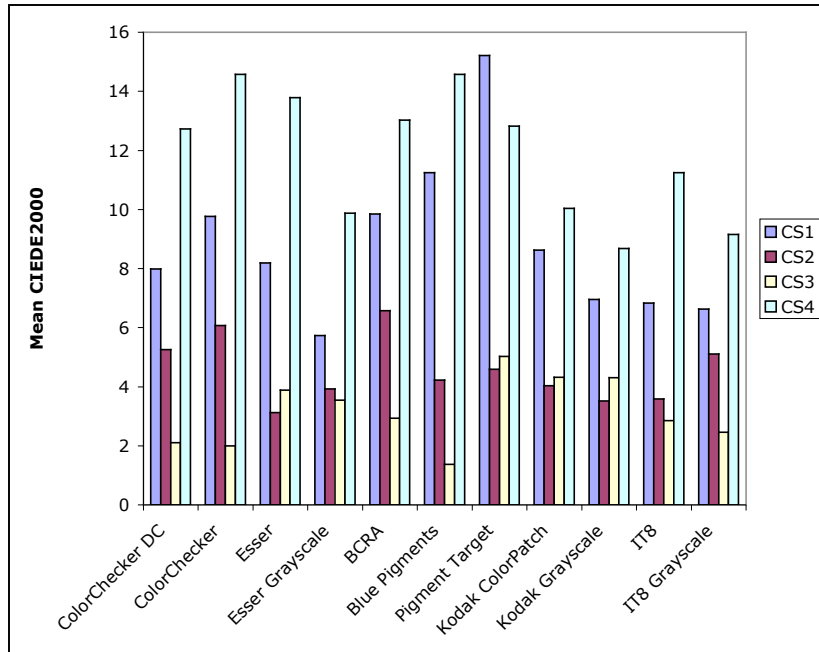


Figure 115. Color reproduction accuracy comparison of four museum case studies. The mean  $\Delta E_{00}$  of each color chart of the normalized Lab image data, where the Halon L\* was set equal to 100 (see Tables XVIII, XXXI, XLIV, and LVI), is plotted.

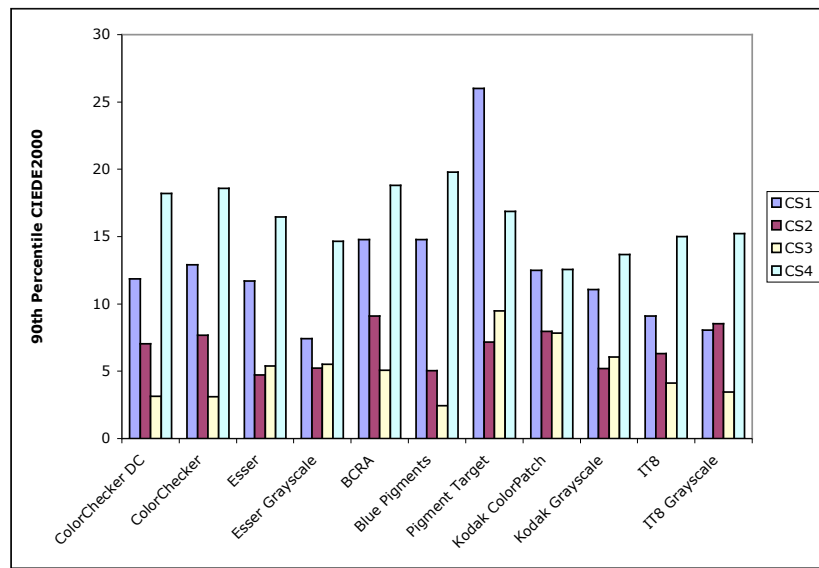


Figure 116. Color reproduction accuracy comparison of four museum case studies. The 90<sup>th</sup> percentile  $\Delta E_{00}$  of each color chart of the normalized Lab image data, where the Halon L\* was set equal to 100 (see Tables XVIII, XXXI, XLIV, and LVI), is plotted.

The shape of the bar plots in Figures 115 and 116 are basically the same. These figures show that the color difference errors of CS1 and CS4 are much larger than CS2 and CS3. These figures also show that there was no single chart that was always reproduced the most accurately or inaccurately by all four of the museum case studies. For example, the Blue Pigment chart was produced the most accurately by CS3, but the least accurately by CS4.

Figure 117 shows a visual comparison of the color differences of the Lab digital master images of the Macbeth ColorChecker without any lightness correction, which were converted into the sRGB color space. This was done by first, converting the Lab images to CIELAB images, second, converting the CIELAB values into XYZ tristimulus values, then using a chromatic-adaptation transform to transform the D<sub>50</sub> XYZ tristimulus values to D<sub>65</sub> XYZ tristimulus values, and finally, converting these values into the sRGB color space. The measured ColorChecker data's XYZ tristimulus values were calculated using the CIE 2° observer and CIE illuminant D<sub>50</sub>, and then also converted into the sRGB color space (after the same chromatic-adaptation transform was used). See standard IEC 61966-2-1 (1999) and IEC 61966-2-1 Amendment 1 (2003) for the details about the sRGB transformation calculation. The colors of the image in Figure 117 appear as if they would if the digital master files were all opened and displayed on the same device.

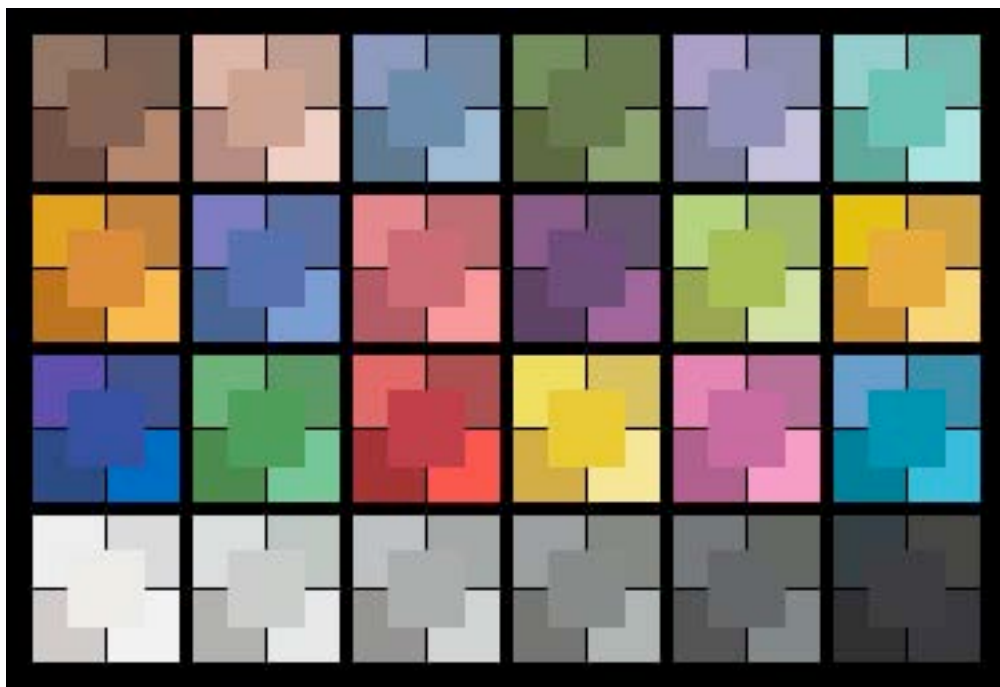


Figure 117. Color reproduction accuracy comparison of the CS1 (top left), CS2 (top right), CS3 (bottom left) and CS4 (bottom right) Macbeth ColorChecker Lab digital master images to the measured data (center) rendered using illuminant D<sub>50</sub>.

The CS2 and CS3 ColorChecker charts were reproduced more accurately than the CS1 and CS4 ColorChecker charts. There is a noticeable difference in hue, chroma and lightness of almost every patch of the ColorChecker in the four case studies in comparison to the measured ColorChecker, shown in Figure 117.

The amount of color difference errors resulting in all four case studies is mostly dependent on the spectral sensitivities of the camera system and the accuracy of the profiles used in each case study. Since the spectral sensitivities of the camera cannot be changed, except with the use of filters, it is easier to create a profile that is as accurate as possible. The profiles should be optimized using a target representing the pigments and materials being imaged with the camera. Any combination of the Macbeth ColorChecker, Macbeth ColorChecker DC, Blue Pigments, and Pigments Target charts

would be sufficient to use when optimizing the profiles. Figures 118 and 119 compare the mean and 90<sup>th</sup> percentile  $\Delta E_{00}$  color differences between the image CIELAB data determined using an embedded profile in Adobe Photoshop® (the first evaluation method described in Section 3.4.2), and determined using an OECF linearization combined with a 3x3 RGB to XYZ transform created and optimized with the CCDC data (the second evaluation method described in Section 3.4.2). The data in these figures show that the simple 3x3 transformation performed significantly better than the case study profiles for the Macbeth ColorChecker chart in CS1, CS2, and CS4.

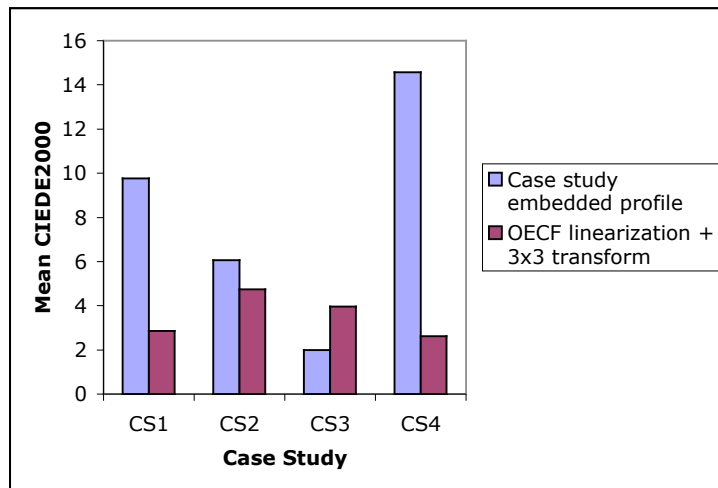


Figure 118. Comparison of the color accuracy, mean  $\Delta E_{00}$ , of the Macbeth ColorChecker chart between using each case study's embedded profile and using the OECF to linearize the RGB data followed by a simple 3x3 transform (optimized using the Macbeth ColorChecker DC) from RGB to XYZ tristimulus values to evaluate the color accuracy.

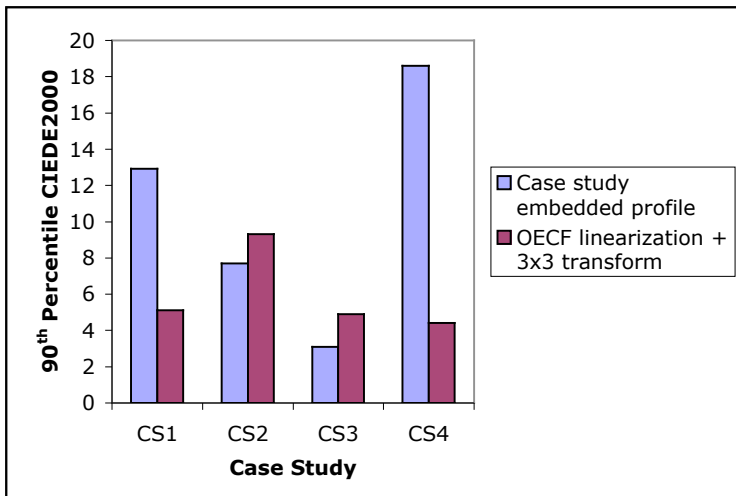


Figure 119. Comparison of the color accuracy, 90<sup>th</sup> percentile  $\Delta E_{00}$ , of the Macbeth ColorChecker chart between using each case study's embedded profile and using the OECF to linearize the RGB data followed by a simple 3x3 transform (optimized using the Macbeth ColorChecker DC) from RGB to XYZ tristimulus values to evaluate the color accuracy.

### *Metamerism*

The metameric matches of each museum case study cannot be compared to each other because the illuminant under which the matches were made by the camera, CIE 2° observer and photographer were different. The main purpose of including the D&H Color Rule in the testing procedure was to determine whether or not the photographer's spectral sensitivities (color-matching functions) were the same as the camera and the standard CIE 2° observer using a visual tool. In other words, this tool demonstrates how closely what the photographer sees resembles what the camera "sees," and what the standard CIE 2° observer would see. Figure 120 shows how the metameric matches, which were made using the D&H Color Rule by the camera and photographer, differed for each museum case study.

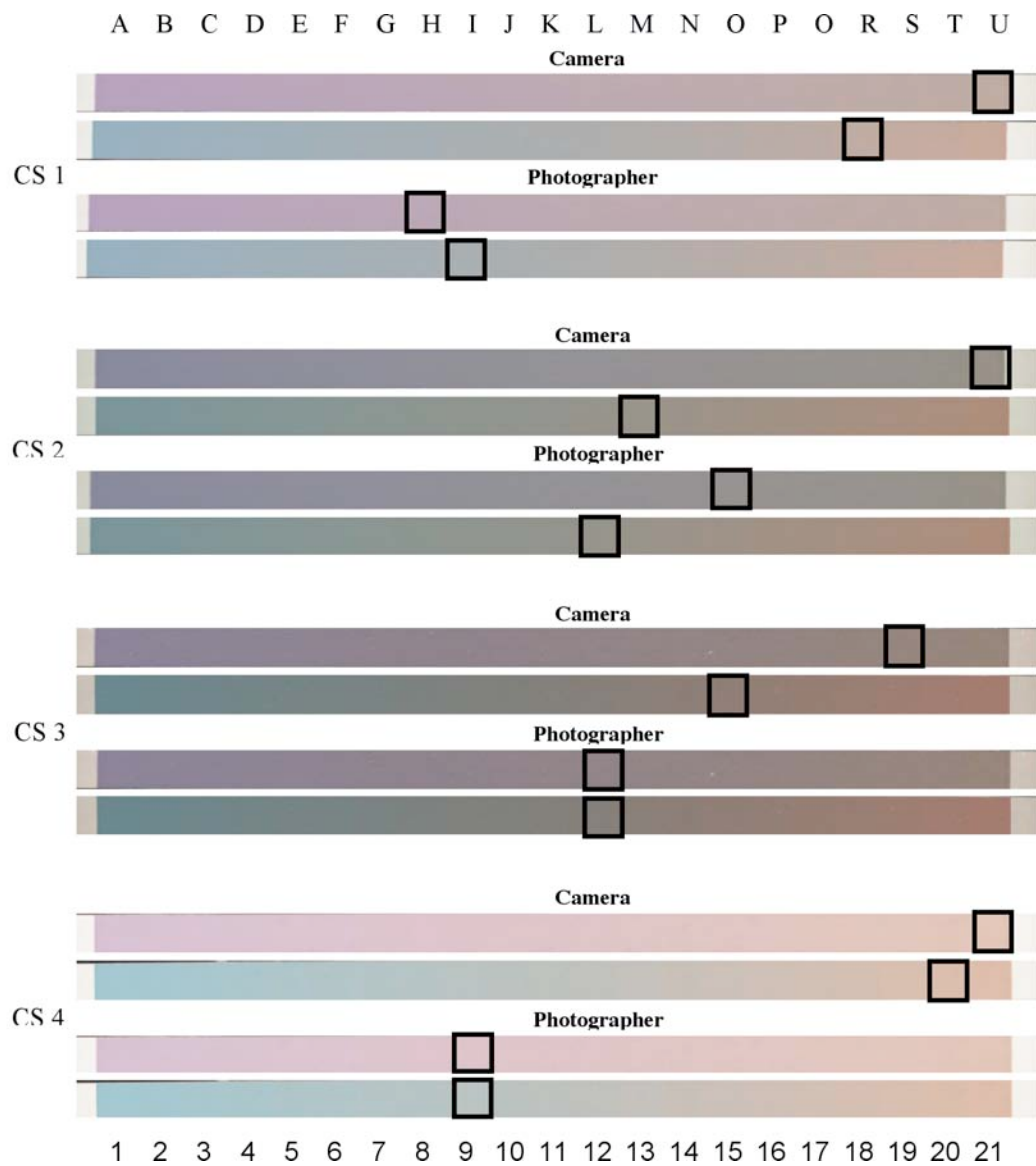


Figure 120. Davidson & Hemmendinger Color Rule matameric matches made by the photographer and camera in each of the four museum case studies.

The images in Figure 120 are the digital master Lab images of the D&H Color Rule, which were cut out of the target images and rotated. The CS3 camera and photographer were each viewing the match under different illuminations. There is no “correct” metameristic match that can be made using the D&H Color Rule. The match depends on the light source under which the match is made and the inherent spectral sensitivities of the detector. If the metameristic matches were the same for the camera and the photographer in each case study, then this would indicate that there would be no or a small amount of visual corrections to the images after digital capture, because the image would appear and have CIELAB values that were similar or the same as the original painting.

### Noise

#### *Image Noise*

The results in Table LXVIII compare the signal-to-noise ratios of the four museum case studies. The higher this value is, the less noise the images have. CS1 had the least amount of noise, followed by CS4. CS2 and CS3 had the largest amount of noise in comparison to the other case studies. There are a few trends, with a couple of exceptions, in the image noise data among the four museum case studies discussed in the CS Results and Discussion sections. The green channel had the least amount of total image noise. The blue channel had the most amount of total image noise. Since noise is inevitable in almost any digital camera system, it would be expected that the noise would be reduced by the camera manufacturer as much as possible in the green channel, since the average human visual system is most sensitive to that channel. More noise in the blue

channel is preferable, since the average human visual system is the least sensitive to noise in this channel. However, the absolute sensitivity of the blue channel is usually the lowest because blue filters used in color cameras have low transmittance and CCD sensors have low quantum efficiency in the blue range.

CS3 was the only case study that had a digital camera system that automatically subtracted a dark correction image in order to reduce fixed pattern and total noise. Although this is preferred, the reason that it had the lowest SNR compared to the other three case studies was probably because of the un-sharp masking that was applied to the digital master image. Other than dark correction image subtraction, using a low ISO speed and short exposure time when imaging will also help in the reduction of the image noise level. However, this may not be possible depending on the luminance of the lighting.

### *Color Noise*

The MMCDM results in Table LXVIII are similar among the four museum case studies. The smaller the MMCDM value, the less color noise a digital camera has. The color noise MMCDMs of the four museum case studies were small. CS4 had the least amount of color noise and CS2 had the most. The comparison of the results in Table LXVIII between the four museums are not correlated with the comparison of the color reproduction accuracy or the image noise results. There are a few trends, with a couple of exceptions, in the color noise data among the four museum case studies discussed in the CS Results and Discussion sections. Similar to the trends discussed in the Image Noise part of this section above, the green channel had the least amount of color noise

and the blue channel had the most amount of color noise. The black and yellow patches had the least amount of noise. The red patch had the most amount of noise.

### *Dynamic Range*

The results in Table LXVIII comparing the dynamic ranges of the four museum case studies show that they are very similar to each other. The higher the dynamic range of the imaging system, the better the potential tonal range of the images. The CS4 images were 8-bit, so the ISO 15739 dynamic range calculation was less accurate than when the 16-bit images were used in CS1-CS3, because there was less precision in this calculation. A trend found in the dynamic range data among the four museum case studies discussed in the CS Results and Discussion sections was that the red channel had the most dynamic range in comparison to the green and blue channels.

In order to obtain the most dynamic range achievable by a digital imaging system, the amount of spatial cross-talk or flare should be reduced as much as possible. Depending on the tonal range of the paintings being imaged by the photographers in their day-to-day imaging at the museum, the maximum dynamic range achievable by their imaging system may not always be necessary in order to reproduce the tonal range of painting accurately.

### *Spatial Cross-talk*

The results in Table LXVIII comparing the spatial cross-talk of the four museum case studies show that CS2 had the highest mean relative maximum percent difference of the RGB channels and CS4 had the lowest. The higher the relative maximum difference

of the gray patches, the more spatial cross-talk. A trend found in the spatial cross-talk data among the four museum case studies discussed in the CS Results and Discussion sections was that the blue channel had the most spatial cross-talk in comparison to the red and green channels. In order to reduce the amount of spatial cross-talk, or image flare, in a digital image, the image area surrounding the painting being imaged should be as dark as possible.

### *Spatial Frequency Response (SFR)*

The SFR results in Table LXVIII comparing the four museum case studies show that CS3 had the highest SFR, which is mostly caused by the unsharp masking that was applied to the digital master files by the photographer. CS1 had the lowest SFR value of the four museum case studies. The closer that this value is to unity, the better the preservation of detail of the original object that the image has, or the sharper it is. The SFR data among the four museum case studies discussed in the CS Results and Discussion sections showed that for the scanning linear array cameras (CS1, CS2, and CS4), the SFR caused by the linear array itself was better than the SFR caused by the linear array's scanning. The area array Sinar Sinarback 54H camera used in CS3 had an SFR that was better in the horizontal direction than the vertical direction. In the museum case studies, the SFR in the centers of the images were not always better than in the corners of the cropped or uncropped image areas.

The SFR results of the case studies could have been affected by the tool used for focusing the images before capture. In CS1, the photographer focused by looking

through the ground glass, whereas in CS2, CS3, and CS4, a magnification tool or frequency focusing tool in the image capture software was used to focus the images.

### Color Channel Registration

The results in Table LXVIII comparing the mean amount of misregistration shift across the four edges and three channels show that all of the misregistration errors were acceptably less than 0.5 pixels. The closer the misregistration is to zero the better the color channel registration. The results show that CS4 had the least amount of misregistration error, followed by CS3. CS2 had the most amount of misregistration error. It would have been expected that CS3 would have the least amount of misregistration error, since it is an area array camera, but the digital imaging system in CS4 had very small misregistration errors for a scanning linear array camera. Similar to the SFR results in the SFR part of this section above, in the museum case studies, the color channel registration in the centers of the images were not always better than in the corners of the cropped or uncropped image areas.

### Depth of Field

The depth of field results in Table LXVIII are the means of the red, green, and blue channels of the mean SFR area value of the area under SFR curve vs. distance plots, in the CS Results and Discussion sections (also shown in Figure 121 below), normalized by the maximum mean SFR area of the RGB channels (see Tables 7-XV to 7-XIX in Appendix 7.4) in the area under the SFR curve vs. distance plots. This value can range from zero to unity. The closer this value is to unity, the more depth of field the image

had. If this value had a value of one, the curve in the area under the SFR curve vs. distance plots would be a straight horizontal line. The values in Table LXVIII show that CS3 had the largest depth of field over the 6" distance range. CS2 had the smallest depth of field.

The mono-numeric depth of field values in Table LXVIII summarize the depth of field of the four case studies reasonably accurately, but because none of the focus points coincided with the focus aim points and they were located at different distances for each case study, this mono-numeric metric does not tell the whole story. For this reason, the area under the SFR curve vs. distance plots are plotted again in Figure 121 for comparison purposes.

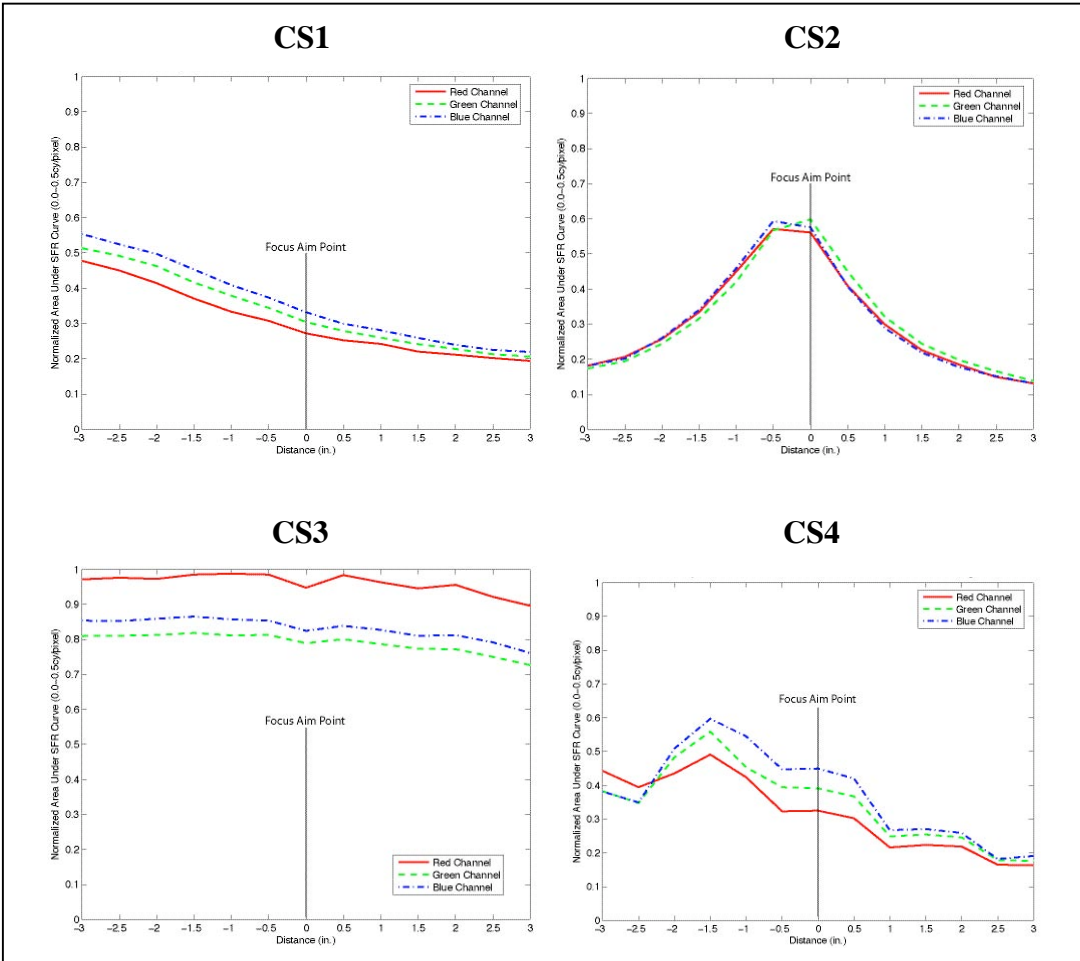


Figure 121. Depth of field results comparison of the four case studies.

Table LXIX lists the characteristics of the parameters that have a significant effect on each museum case study's depth of field results. In order for a painting image to have an adequate depth of field, the f-number should be high (small aperture), the lens should have a short focal length, and the camera-to-subject distance should be large.

Table LXIX. Factors that influenced the depth of field results of CS1, CS2, CS3, and CS4.

	<u>CS1</u>	<u>CS2</u>	<u>CS3</u>	<u>CS4</u>
<b>Lens Manufacturer</b>	Leica	Schneider	Rodenstock	Sinar
<b>Lens Focal Length</b>	100mm	150mm	100mm	210mm
<b>Lens Aperture</b>	f/8	f/11	f/17.8	f/11
<b>Camera-to-Subject Distance</b>	81"	41"	72"	79"

The data in Table LXIX show that CS3, which had the largest depth of field, used the shortest focal length lens and the smallest lens aperture and had a large camera-to-subject distance, whereas CS2, which had the smallest depth of field of the four museum case studies, used a larger focal length lens and a larger aperture and had the smallest camera-to-subject distance of the four case studies.

## **5. Conclusions**

The testing procedure described in this thesis can be used to provide objective measures of a range of performance characteristics of digital-camera systems and workflows, which are used in cultural heritage institutions to document archival quality digital master reproductions of their painting collections. Cultural heritage institutions can store future characterization data as metadata with their images. Also, digital camera manufacturers can use this characterization data to see where imaging systems need improvements for cultural heritage applications.

This testing procedure was used to perform four benchmarking case studies in American museums, which were all early adopters of digital-image archiving. As a result of these case studies, many differences were discovered among their current digital-imaging practices, which points out the need for standardization in American museums.

Ideally, a raw digital image should be captured and stored as a digital master with the characterization metadata of the digital-imaging system and the targets themselves. This way, the digital information is as accurate as possible and if, in the future, there is an improvement in the way digital data are interpreted, the raw data and the information about the means by which it was formed can be retrieved. Cultural heritage institutions should also document their digital-imaging workflows. When a painting is digitized, an accurate archival quality reproduction of the painting should be the goal of the photographer. In other words, the photographer should not image the painting with a specific reproduction purpose in mind. After a painting is imaged and the raw data stored, derivatives can then be made in the form of reproductions.

## **6. References**

### **A**

ANSI IT8.7/2: 1993, *Graphic Technology - Color reflection target for input scanner calibration.* 1<sup>st</sup> Edition.

ANSI Website. <http://www.ansi.org>.

### **B**

Berns, R. S., “Billmeyer and Saltzman’s Principles of Color Technology”; Third Edition, John Wiley & Sons, NY, 2000.

Berns, R.S., Taplin, L.A., Nezamabadi, M., Modifications of a Sinarback 54 Digital Camera for Spectral and High-Accuracy Colorimetric Imaging: Simulations and Experiments, June 2004. <http://www.art-si.org>.

Besser, H., Trant, J., Introduction to Imaging. Getty Art History Information Program, 1996.

Burns, P., Slanted-Edge MTF for Digital Camera and Scanner Analysis. Proc. IS&T PICS, 2000: p. 135-138.

Burns, P., Williams, D., Using Slanted-Edge Analysis for Color Registration Measurement. Proc. IS&T PICS, 1999: p. 51-53.

### **C**

CIE Publication No. 15.2, 1986, *Colorimetry*. 2<sup>nd</sup> Edition.

CIE Publication No. 51, 1981, *A method for assessing the quality of daylight simulators for colorimetry*. 1<sup>st</sup> Edition.

CIE Website. <http://members.eunet.at/cie>.

Conway, P., Overview: Rationale for Digitization and Preservation. Handbook for Digital Projects: A Management Tool for Preservation and Access; First Edition, 2000: Ch.2.

### **D**

D’Amato, D., Imaging Systems: the Range of Factors Affecting Image Quality. Guides to Quality in Visual Resource Imaging, 2000. <http://www.rlg.org/visguides/visguide3.html>.

Day, E. A., Berns, R. S., Taplin, L. A., Imai, F. H., A psychophysical experiment evaluating the color and spatial-image quality of several multi-spectral image capture techniques, *J. Imag. Sci. Tech.*, 2004: 48, p. 99-110.

## E

## F

Frey, F., Measuring Quality of Digital Masters. Guides to Quality in Visual Resource Imaging, 2000. <http://www.rlg.org/visguides/visguide4.html>.

Frey, F., Reilly, J., Digital Imaging for Photographic Collections: Foundations for Technical Standards. Image Permanence Institute, 1999.  
[http://www.rit.edu/~661www1/sub\\_pages/8page3g.htm](http://www.rit.edu/~661www1/sub_pages/8page3g.htm).

Frey, F., Susstrunk, S., Color Issues to Consider in Pictorial Image Data Bases. Technology, 1996; SPIE Vol. CR61: p. 120-152.

## G

## H

Harold, R., McDowell, D., Standard Viewing Conditions for the Graphic Arts. GATF World, January/February 1999; Vol. II No.1: p. 7-13.

## I

IEC 61966-2-1: 1999, *Multimedia systems and equipment - Colour measurement and management - Part 2-1: Colour management - Default RGB colour space – sRGB*. 1<sup>st</sup> Edition.

IEC 61966-2-1 Amendment 1: 2003, *Multimedia systems and equipment - Colour measurement and management - Part 2-1: Colour management - Default RGB colour space – sRGB*. 1<sup>st</sup> Edition.

IEC 61966-8: 2001, *Multimedia systems and equipment - Colour measurement and management - Part 8: Multimedia colour scanners*. 1<sup>st</sup> Edition.

IEC 61966-9: 2000, *Multimedia systems and equipment - Colour measurement and management - Part 9: Digital cameras*. 1<sup>st</sup> Edition.

IEC Website. <http://www.iec.ch>.

IFLA/ICA Working Group, Guidelines for Digitization Projects: for collections and holdings in the public domain, particularly those held by libraries and archives. March 2002. <http://www.ifla.org/VII/s19/pubs/digit-guide.pdf>.

ISO 3664: 2002, *Viewing conditions - Graphic technology and photography*. 2<sup>nd</sup> Edition.

ISO 7589: 2000, *Photography - Illuminants for sensitometry - Specifications for daylight, incandescent tungsten and printer*. 2<sup>nd</sup> Edition.

ISO 12231: 1997, *Photography - Electronic still-picture cameras - Terminology*. 1<sup>st</sup> Edition.

ISO 12232: 1998, *Photography - Electronic still-picture cameras - Determination of ISO speed*. 1<sup>st</sup> Edition.

ISO 12233: 2000, *Photography - Electronic still-picture cameras - Resolution measurements*. 1<sup>st</sup> Edition.

ISO 12646: 2002, *Graphic Technology - Displays for color proofing - Characteristics and viewing conditions*. DIS.

ISO 14524: 1999, *Photography - Electronic still-picture cameras - Methods for measuring opto-electronic conversion functions (OECFs)*. 1<sup>st</sup> Edition.

ISO 15739: 2003, *Photography - Electronic still-picture imaging - Noise measurements*. 1<sup>st</sup> Edition.

ISO 17321-1: 2003, *Graphic technology and photography - Colour characterisation of digital still cameras (DSCs) - Part 1: Stimuli, metrology, and test procedures*. WD.

ISO 17321-2: 2003, *Graphic technology and photography - Colour characterization of digital still cameras (DSCs) - Part 2: Methods for determining transforms from raw DSC to scene-referred data*. WD.

ISO 22028-1: 2002, *Photography and Graphic Technology - Extended color encodings for digital image storage, manipulation and interchange - Part 1: Architecture and requirements*. DIS.

ISO Website. <http://www.iso.org>.

## J

## K

Kenney, A., Digital Benchmarking for Conversion and Access. Moving Theory into Practice: Digital Imaging for Libraries and Archives, 2000: Ch.3: p. 24-60.

## L

Luo, M. R., Cui, G., Rigg, B., The Development of the CIE 2000 Colour Difference Formula: CIEDE2000. Col. Res. Appl., 26, 2001.

## M

McDowell, D., Standards Update: What? by Whom? with Whom? And How Does It All Fit Together? IPA Bulletin, July/August 2002: p. 20-29.

Myers, R. D., Gray Card Selection. Better Light, Inc., March 2002.

## N

NISO, *Data Dictionary - Technical Metadata for Digital Still Images*. 2002, DIS.

NISO Website. <http://www.niso.org>.

## O

## P

Price-Wilkin, J., Access to Digital Image Collections: System Building and Image Processing. Moving Theory into Practice: Digital Imaging for Libraries and Archives, 2000: Ch.6: p. 101-118.

Puglia, S., Reed, J., Rhodes, E., Technical Guidelines for Digitizing Archival Materials for Electronic Access: Creation of Production Master Files – Raster Images. U.S. National Archives and Records Administration (NARA), June, 2004.

## Q

Quan, S., Evaluation and Optimal Design of Spectral Sensitivities for Digital Color Imaging, 2002.

## R

Rhodes, E., et al., Colorado Digitization Project: General Guidelines for Scanning. 1999. <http://coloradodigital.coalliance.org/scanning.html>.

Rhyne, C., Scholar Commentary: An End-User Speaks Up. Handbook for Digital Projects: A Management Tool for Preservation and Access; First Edition, 2000: Ch.10.

Rosen, M. R., and Frey, F. S., RIT American Museums Survey on Digital Imaging for Direct Capture of Artwork. Proc. IS&T Second Archiving Conference, 2005: p. xx-xx (in press).

## S

Song, T., and Luo, M. R., Testing Colour Difference Images Using a CRT Monitor, The eighth Color Imaging SID, 2000: p. 44-48.

Stokes, M., "Colorimetric Tolerances of Digital Images", MSc Thesis, College of Graphic Arts and Photography, Rochester Institute of Technology, Rochester, New York, U.S., 1991.

## T

## U

Uroz, J., Luo, M. R., and Morovic, J., Perception of Colour Difference Between Printed Images, "Colour Science: Exploiting Digital Media", John Wiley & Sons, Ltd, 2001.

## V

Vogt-O'Connor, D., Selection of Materials for Scanning. Handbook for Digital Projects: A Management Tool for Preservation and Access; First Edition, 2000: Ch.4.

Vora, P. L., and Trussell, H. J., Measure of Goodness of a Set of Color Scanning Filters, J. Opt. Soc. Am. A, 1993: 10, p 8-23.

## W

Waibel, G., To Preserve or to Present? Spectra, Fall 2000: 6.

Weidner, V. R., Hsia, J. J., Reflection Properties of Pressed Polytetrafluoroethylene Powder, J. Opt. Soc. Am., 1981: Vol. 71 No. 7, p. 856-861.

Williams, D., Burns, P. Diagnostics for Digital Capture using MTF. Proc. IS&T PICS, 2001: p. 227-232.

Wrotniak, J. A., Photo tidbits: Depth of Field and Your Digital Camera. 2003,  
<http://www.wrotniak.net/photo/dof/>.

**X**

**Y**

**Z**

## **7. Appendices**

The appendices below contain some supplemental tables and graphs that list and describe meaningful data resulting from CS0 through CS4, which were in too large of amounts to include in the body of this thesis.

### **Appendix 7.1: System Spatial Uniformity Supplemental Data**

Tables 7-I through 7-IV include supplemental data for the analysis of the CS1 through CS4 system spatial uniformity, respectively. The procedure that was used to determine these data for all of the case studies is described in section 3.2. Plots of the percent difference of each patch from the luminance mean of all 36 patches are used to summarize these data in the Results and Discussion section of each case study (see Figures 56, 73, 89, and 105 in the System Spatial Uniformity part of sections 4.3.3, 4.4.3, 4.5.3, and 4.6.3, respectively). The maximum  $\Delta E_{00}$  between the patches and the mean of all the patches is a mono-numeric metric that summarizes each case study's system spatial uniformity results and is listed in Table LXVIII in section 4.7.2 for CS1 through CS4 as a metric of comparison between the four case studies. At the bottom of each table in this Appendix are the digital camera ISO speed and exposure settings used by the photographer in each case study for the gray card images that were evaluated for system spatial uniformity.

Table 7-I. CS1 system spatial uniformity luminance (Y) and CIELAB results of differences between each of 36 evenly spaced patches and the mean of all 36 patches.

<u>Patch #</u>	<u>% Difference From Luminance (Y) Mean of All Patches</u>	<u>CIELAB Data From Mean of All Patches</u>					
		<u><math>\Delta L^*</math></u>	<u><math>\Delta a^*</math></u>	<u><math>\Delta b^*</math></u>	<u><math>\Delta C^*_{ab}</math></u>	<u><math>\Delta E^*_{ab}</math></u>	<u><math>\Delta E_{00}</math></u>
1	-1.7	-0.51	-0.72	0.31	-0.48	0.93	0.96
2	-0.2	-0.05	-0.59	0.27	-0.42	0.65	0.72
3	0.5	0.15	-0.05	-0.29	0.26	0.33	0.25
4	-0.2	-0.04	0.45	-0.42	0.53	0.62	0.54
5	0.8	0.23	0.66	-0.58	0.74	0.90	0.79
6	2.0	0.59	0.35	-0.11	0.20	0.70	0.60
7	-0.9	-0.27	-0.75	0.41	-0.58	0.89	0.93
8	0.9	0.28	-0.58	0.38	-0.51	0.75	0.73
9	1.6	0.49	0.03	-0.23	0.22	0.54	0.39
10	1.5	0.45	0.53	-0.37	0.51	0.78	0.70
11	2.7	0.82	0.79	-0.56	0.76	1.26	1.10
12	4.0	1.19	0.46	-0.11	0.23	1.28	1.03
13	-1.0	-0.30	-0.80	0.47	-0.65	0.97	1.00
14	0.8	0.24	-0.60	0.40	-0.54	0.76	0.75
15	1.6	0.49	0.03	-0.24	0.24	0.55	0.39
16	2.2	0.67	0.56	-0.38	0.53	0.95	0.82
17	3.3	0.98	0.80	-0.60	0.81	1.40	1.18
18	4.1	1.22	0.44	-0.12	0.24	1.30	1.04
19	-2.1	-0.62	-0.86	0.56	-0.75	1.19	1.14
20	-0.3	-0.07	-0.66	0.46	-0.61	0.81	0.81
21	0.5	0.17	0.01	-0.17	0.17	0.24	0.17
22	1.5	0.46	0.57	-0.35	0.50	0.81	0.75
23	2.4	0.73	0.81	-0.57	0.78	1.24	1.09
24	3.3	1.00	0.45	-0.11	0.23	1.10	0.91
25	-3.6	-1.09	-0.93	0.63	-0.84	1.56	1.40
26	-2.0	-0.59	-0.72	0.52	-0.68	1.06	0.98
27	-1.3	-0.39	-0.07	-0.11	0.09	0.41	0.32
28	0.1	0.04	0.48	-0.24	0.37	0.54	0.57
29	0.9	0.27	0.75	-0.46	0.66	0.92	0.90
30	1.5	0.46	0.38	0.00	0.10	0.60	0.59
31	-6.6	-2.02	-1.10	0.83	-1.07	2.45	2.04
32	-4.7	-1.43	-0.89	0.73	-0.93	1.84	1.54
33	-4.0	-1.22	-0.24	0.13	-0.19	1.25	0.95
34	-3.3	-0.99	0.31	-0.01	0.10	1.04	0.83
35	-2.5	-0.76	0.57	-0.25	0.40	0.98	0.88
36	-2.0	-0.59	0.15	0.17	-0.12	0.63	0.51
<b>Maximum</b>						<b>2.45</b>	<b>2.04</b>
<i>ISO: N/A, Exposure Time: 0.1160119s., Integration Time: 0.1160119s., F-stop: 8</i>							

Table 7-II. CS2 system spatial uniformity luminance (Y) and CIELAB results of differences between each of 36 evenly spaced patches and the mean of all 36 patches.

<u>Patch #</u>	<u>% Difference From Luminance (Y) Mean of All Patches</u>	<u>CIELAB Data From Mean of All Patches</u>					
		<u><math>\Delta L^*</math></u>	<u><math>\Delta a^*</math></u>	<u><math>\Delta b^*</math></u>	<u><math>\Delta C^*_{ab}</math></u>	<u><math>\Delta E^*_{ab}</math></u>	<u><math>\Delta E_{00}</math></u>
1	-9.3	-2.58	-0.06	-0.19	0.17	2.58	2.16
2	-2.6	-0.68	0.75	-0.12	0.29	1.02	1.16
3	-0.2	-0.02	0.80	-0.51	0.68	0.94	1.07
4	2.1	0.59	0.77	0.07	0.12	0.97	1.17
5	1.4	0.41	0.31	0.03	0.04	0.52	0.55
6	-1.1	-0.27	-0.26	0.75	-0.78	0.84	0.65
7	-4.4	-1.18	-0.42	-0.12	0.05	1.26	1.15
8	2.4	0.68	0.45	-0.13	0.22	0.83	0.83
9	4.8	1.32	0.70	-0.65	0.80	1.63	1.46
10	7.3	1.96	0.72	-0.01	0.18	2.09	1.87
11	7.1	1.92	0.28	-0.04	0.10	1.94	1.60
12	4.3	1.18	-0.26	0.60	-0.64	1.35	1.09
13	-3.1	-0.81	-0.56	-0.25	0.16	1.01	1.06
14	3.3	0.91	0.35	-0.23	0.30	1.00	0.88
15	5.4	1.46	0.58	-0.63	0.74	1.70	1.46
16	8.5	2.26	0.66	0.01	0.15	2.35	2.04
17	8.6	2.30	0.17	0.01	0.03	2.31	1.88
18	6.3	1.70	-0.47	0.56	-0.63	1.85	1.55
19	-4.5	-1.21	-0.71	-0.13	0.01	1.41	1.42
20	2.1	0.60	0.06	-0.21	0.22	0.64	0.52
21	4.5	1.23	0.31	-0.61	0.66	1.40	1.14
22	6.8	1.82	0.36	-0.09	0.17	1.86	1.56
23	6.8	1.83	-0.08	-0.09	0.07	1.83	1.49
24	4.6	1.25	-0.75	0.65	-0.77	1.59	1.49
25	-9.0	-2.48	-0.72	-0.08	-0.03	2.58	2.30
26	-3.0	-0.78	0.00	-0.02	0.02	0.78	0.64
27	-0.9	-0.20	0.13	-0.51	0.53	0.57	0.42
28	2.0	0.57	0.14	0.07	-0.04	0.59	0.51
29	1.7	0.50	-0.25	0.03	-0.08	0.56	0.54
30	-0.6	-0.14	-0.86	0.76	-0.89	1.16	1.26
31	-15.7	-4.46	-0.72	0.05	-0.17	4.52	3.90
32	-9.4	-2.61	-0.04	0.14	-0.14	2.61	2.18
33	-8.0	-2.19	0.04	-0.38	0.38	2.23	1.85
34	-5.0	-1.35	0.02	0.26	-0.25	1.37	1.13
35	-5.2	-1.39	-0.38	0.15	-0.22	1.45	1.27
36	-7.8	-2.14	-1.04	0.87	-1.02	2.54	2.34
<b>Maximum</b>						<b>4.52</b>	<b>3.90</b>
<i>ISO: 200, Exposure Time: 1/20s., Integration Time: 1/20s., F-stop: 11</i>							

Table 7-III. CS3 system spatial uniformity luminance (Y) and CIELAB results of differences between each of 36 evenly spaced patches and the mean of all 36 patches.

<u>Patch #</u>	<u>% Difference From Luminance (Y) Mean of All Patches</u>	<u>CIELAB Data From Mean of All Patches</u>					
		<u><math>\Delta L^*</math></u>	<u><math>\Delta a^*</math></u>	<u><math>\Delta b^*</math></u>	<u><math>\Delta C^*_{ab}</math></u>	<u><math>\Delta E^*_{ab}</math></u>	<u><math>\Delta E_{00}</math></u>
1	-1.9	-0.47	0.06	-0.06	0.08	0.48	0.44
2	2.5	0.60	0.12	-0.12	0.16	0.62	0.56
3	-0.2	-0.04	0.08	0.00	0.04	0.09	0.10
4	-0.4	-0.10	0.03	-0.11	0.11	0.15	0.12
5	2.7	0.66	0.06	-0.15	0.16	0.68	0.61
6	1.5	0.36	-0.09	-0.13	0.07	0.40	0.37
7	0.3	0.07	0.05	-0.01	0.03	0.09	0.09
8	2.3	0.55	0.15	0.00	0.08	0.57	0.53
9	-2.2	-0.54	0.08	0.11	-0.05	0.56	0.52
10	0.0	0.01	0.07	-0.06	0.09	0.09	0.08
11	2.9	0.71	0.00	-0.13	0.11	0.73	0.66
12	1.1	0.27	-0.08	-0.09	0.03	0.29	0.28
13	1.5	0.36	0.07	-0.01	0.04	0.37	0.34
14	0.3	0.08	0.07	0.07	-0.02	0.13	0.14
15	-3.0	-0.74	0.03	0.13	-0.10	0.75	0.68
16	-0.2	-0.05	0.05	-0.03	0.05	0.08	0.08
17	2.9	0.70	0.00	-0.07	0.05	0.70	0.63
18	0.1	0.03	-0.14	-0.01	-0.06	0.14	0.17
19	-1.8	-0.44	0.02	0.07	-0.05	0.44	0.40
20	0.2	0.06	0.07	0.04	0.00	0.10	0.11
21	-1.3	-0.32	0.00	0.10	-0.08	0.34	0.30
22	-0.1	-0.02	0.04	-0.06	0.07	0.07	0.06
23	1.8	0.43	0.00	-0.06	0.05	0.44	0.40
24	0.8	0.19	-0.14	-0.03	-0.04	0.24	0.24
25	-1.5	-0.37	-0.03	0.11	-0.11	0.39	0.35
26	-0.8	-0.20	0.04	0.11	-0.08	0.23	0.21
27	-3.5	-0.86	-0.01	0.12	-0.11	0.87	0.80
28	0.5	0.13	0.01	-0.09	0.09	0.16	0.14
29	0.7	0.18	-0.06	-0.04	0.01	0.19	0.18
30	0.1	0.02	-0.13	0.04	-0.10	0.14	0.15
31	1.5	0.36	-0.02	0.06	-0.06	0.37	0.33
32	-2.5	-0.61	-0.04	0.06	-0.07	0.61	0.56
33	-5.0	-1.24	-0.12	0.19	-0.23	1.26	1.16
34	1.5	0.36	-0.02	-0.06	0.04	0.37	0.33
35	-1.0	-0.23	-0.08	0.01	-0.04	0.24	0.23
36	0.4	0.11	-0.15	0.09	-0.15	0.20	0.20
						<b>Maximum</b>	1.26
							1.16
ISO: 25, Exposure Time: 1/15s., Integration Time: 1/15s. , F-stop: 17.8							

Table 7-IV. CS4 system spatial uniformity luminance (Y) and CIELAB results of differences between each of 36 evenly spaced patches and the mean of all 36 patches.

<u><b>Patch #</b></u>	<u><b>% Difference From Luminance (Y) Mean of All Patches</b></u>	<u><b>CIELAB Data From Mean of All Patches</b></u>					
		<u><b><math>\Delta L^*</math></b></u>	<u><b><math>\Delta a^*</math></b></u>	<u><b><math>\Delta b^*</math></b></u>	<u><b><math>\Delta C^*_{ab}</math></b></u>	<u><b><math>\Delta E^*_{ab}</math></b></u>	<u><b><math>\Delta E_{00}</math></b></u>
1	1.5	0.53	-0.05	-0.49	0.46	0.72	0.50
2	2.8	0.95	0.08	-0.52	0.52	1.08	0.70
3	5.0	1.68	0.04	-0.63	0.61	1.80	1.17
4	1.1	0.37	0.08	-0.12	0.14	0.40	0.26
5	-1.4	-0.45	-0.01	0.04	-0.04	0.45	0.30
6	-4.2	-1.43	-0.29	0.09	-0.16	1.47	1.01
7	1.5	0.50	-0.05	-0.32	0.30	0.60	0.42
8	3.8	1.26	0.09	-0.40	0.41	1.33	0.86
9	4.9	1.64	0.04	-0.44	0.43	1.70	1.11
10	1.4	0.49	0.07	0.03	0.00	0.50	0.34
11	-0.6	-0.20	0.00	0.18	-0.17	0.27	0.18
12	-3.6	-1.22	-0.30	0.23	-0.30	1.28	0.88
13	0.8	0.27	-0.01	-0.21	0.20	0.34	0.23
14	3.5	1.17	0.15	-0.33	0.36	1.23	0.80
15	4.5	1.52	0.10	-0.34	0.35	1.56	1.01
16	1.2	0.42	0.16	0.10	-0.05	0.46	0.36
17	-0.8	-0.26	0.04	0.24	-0.22	0.35	0.25
18	-3.9	-1.33	-0.24	0.27	-0.33	1.37	0.92
19	0.5	0.17	0.05	-0.17	0.17	0.24	0.15
20	3.4	1.14	0.16	-0.26	0.29	1.18	0.77
21	4.5	1.50	0.11	-0.29	0.31	1.53	1.00
22	0.7	0.24	0.22	0.24	-0.17	0.40	0.39
23	-1.3	-0.43	0.07	0.31	-0.27	0.53	0.38
24	-4.6	-1.55	-0.24	0.37	-0.42	1.61	1.08
25	-0.5	-0.16	0.00	-0.04	0.04	0.17	0.11
26	2.5	0.83	0.10	-0.20	0.21	0.86	0.56
27	3.7	1.25	0.10	-0.22	0.24	1.28	0.83
28	-0.3	-0.08	0.22	0.35	-0.27	0.42	0.43
29	-2.5	-0.84	-0.01	0.47	-0.45	0.97	0.64
30	-5.6	-1.92	-0.28	0.53	-0.59	2.01	1.34
31	-1.5	-0.51	-0.01	0.00	-0.01	0.51	0.34
32	0.3	0.12	0.00	-0.06	0.06	0.13	0.09
33	1.4	0.48	0.00	-0.11	0.11	0.50	0.33
34	-3.6	-1.20	0.12	0.51	-0.46	1.31	0.90
35	-5.9	-2.02	-0.16	0.61	-0.63	2.12	1.40
36	-8.5	-2.92	-0.35	0.58	-0.65	3.00	2.01
<b>Maximum</b>						3.00	2.01
ISO: 300, Exposure Time: 1/15s., Integration Time: 1/15s., F-stop: 11							

## Appendix 7.2: Tone Reproduction Supplemental Data

Tables 7-V through 7-IX include supplemental data for the analysis of the CS0 through CS4 tone reproduction, respectively. These tables list the mean digital counts of the OECF target 12 patches and Halon for each exposure. They also list the measured luminances of each patch and the Halon, which were measured with a PR650 spectroradiometer. The procedure that was used to collect these data is described in section 3.3. The legend in Figure 17, which is a plot of the CS0 OECF curves, shows the exposure times and aperture settings for the OECF images taken in CS0. The legends in similar plots of the OECF curves for CS1 through CS4, which are in the Results and Discussion section of each case study (see Figures 57, 74, 90, and 106 in the Tone Reproduction part of sections 4.3.3, 4.4.3, 4.5.3, and 4.6.3, respectively), show the exposure times and aperture settings for the OECF images taken in these four case studies.

Table 7-V. CS0 tone reproduction measured luminance of each of 12 OECF target patches and Halon and the mean digital counts of each of the 12 patches and the Halon of four exposure levels used to capture each image.

Patch #	Measured Luminance (cd/m <sup>2</sup> ) CIE 2° observer	Nominal Exposure			Overexposed			Underexposed 1			Underexposed 2		
		Mean DC <sub>R</sub>	Mean DC <sub>G</sub>	Mean DC <sub>B</sub>	Mean DC <sub>R</sub>	Mean DC <sub>G</sub>	Mean DC <sub>B</sub>	Mean DC <sub>R</sub>	Mean DC <sub>G</sub>	Mean DC <sub>B</sub>	Mean DC <sub>R</sub>	Mean DC <sub>G</sub>	Mean DC <sub>B</sub>
1	32.65	2319.1	2973.7	2592.0	3927.1	4961.5	4476.6	1439.9	1647.6	1512.5	998.8	1034.7	1006.7
2	51.74	3589.4	4819.6	4572.8	5850.3	7593.2	7153.3	2069.2	2843.3	2629.6	1317.7	1584.1	1511.6
3	101.70	6078.9	8092.5	7845.4	9032.1	11848.0	11452.0	3742.7	5241.1	5030.0	2217.1	3097.6	2985.3
4	143.90	7347.1	9967.3	9680.7	11231.0	14424.0	14012.0	4870.7	6708.6	6460.8	2939.3	4144.5	4002.7
5	234.90	10231.0	13353.0	13072.0	14680.0	18978.0	18576.0	6553.7	9233.5	8944.1	4299.1	6102.4	5909.2
6	315.60	12055.0	15684.0	15327.0	17267.0	22084.0	21658.0	8051.2	10906.0	10651.0	5403.3	7379.5	7214.3
7	461.60	14605.0	18946.0	18586.0	20655.0	26488.0	26025.0	10172.0	13341.0	13076.0	6504.2	9192.2	8906.0
8	595.20	17013.0	21826.0	21485.0	23990.0	30363.0	29908.0	11902.0	15521.0	15225.0	7897.5	10738.0	10517.0
9	811.90	19461.0	25091.0	24686.0	27255.0	34748.0	34195.0	13717.0	17917.0	17613.0	9428.8	12522.0	12296.0
10	975.00	21285.0	27216.0	26807.0	29714.0	37609.0	37056.0	15094.0	19526.0	19190.0	10494.0	13729.0	13467.0
11	1498.00	26028.0	33273.0	32816.0	36069.0	45724.0	45146.0	18521.0	24036.0	23661.0	13034.0	17078.0	16777.0
12	2047.00	29958.0	38106.0	37627.0	41336.0	52224.0	51632.0	21529.0	27638.0	27253.0	15184.0	19765.0	19446.0
Halon	2231.00	31380.0	39441.0	38884.0	43254.0	54032.0	53286.0	22643.0	28636.0	28204.0	15968.0	20502.0	20139.0

Table 7-VI. CS1 tone reproduction measured luminance of each of 12 OECF target patches and Halon and the mean digital counts of each of the 12 patches and the Halon of three exposure levels used to capture each image.

Patch #	<u>Measured Luminance (cd/m<sup>2</sup>) CIE 2° observer</u>	Nominal Exposure			Overexposed			Underexposed		
		Mean DC <sub>R</sub>	Mean DC <sub>G</sub>	Mean DC <sub>B</sub>	Mean DC <sub>R</sub>	Mean DC <sub>G</sub>	Mean DC <sub>B</sub>	Mean DC <sub>R</sub>	Mean DC <sub>G</sub>	Mean DC <sub>B</sub>
		2.94	3519.9	2910.6	3064.5	6551.1	5314.3	4640.4	2062.6	1850.2
1	2.94	3519.9	2910.6	3064.5	6551.1	5314.3	4640.4	2062.6	1850.2	2056.5
2	6.09	5680.0	4950.2	5108.1	10433.0	9843.4	9206.1	2238.8	2063.1	2272.1
3	13.00	11208.0	10823.0	11112.0	17888.0	17721.0	17530.0	2728.4	2585.3	2843.2
4	19.20	14733.0	14604.0	14772.0	21934.0	21989.0	21828.0	3292.0	3065.2	3606.9
5	34.40	20934.0	20932.0	21186.0	29620.0	29753.0	29821.0	6249.8	6050.4	6793.6
6	46.80	24408.0	24491.0	24567.0	34410.0	34623.0	34495.0	8453.2	8347.5	8922.3
7	71.90	30437.0	30453.0	30796.0	42581.0	42714.0	43007.0	12517.0	12468.0	13087.0
8	96.10	35004.0	35073.0	35188.0	48783.0	48982.0	48984.0	15412.0	15422.0	15793.0
9	134.00	40947.0	40810.0	41329.0	56029.0	55991.0	56400.0	18847.0	18778.0	19268.0
10	159.00	44600.0	44587.0	44988.0	59406.0	59478.0	59679.0	20832.0	20834.0	21229.0
11	249.00	55000.0	55004.0	55415.0	65259.0	64955.0	65267.0	26491.0	26528.0	26871.0
12	337.00	60479.0	60555.0	60713.0	65259.0	64955.0	65267.0	30922.0	31048.0	31277.0
Halon	393.00	61694.0	61687.0	63491.0	65259.0	64955.0	65267.0	32503.0	32566.0	33264.0

Table 7-VII. CS2 tone reproduction measured luminance of each of 12 OECF target patches and Halon and the mean digital counts of each of the 12 patches and the Halon of three exposure levels used to capture each image.

Patch #	<u>Measured Luminance (cd/m<sup>2</sup>) CIE 2° observer</u>	Nominal Exposure			Overexposed			Underexposed		
		Mean DC <sub>R</sub>	Mean DC <sub>G</sub>	Mean DC <sub>B</sub>	Mean DC <sub>R</sub>	Mean DC <sub>G</sub>	Mean DC <sub>B</sub>	Mean DC <sub>R</sub>	Mean DC <sub>G</sub>	Mean DC <sub>B</sub>
		10.60	10475.0	10011.0	9167.5	12215.0	11603.0	10470.0	9179.5	8813.9
1	10.60	10475.0	10011.0	9167.5	12215.0	11603.0	10470.0	9179.5	8813.9	8197.5
2	19.50	11569.0	11211.0	10322.0	14053.0	13673.0	12478.0	9625.2	9288.3	8641.2
3	43.30	14244.0	14079.0	13076.0	18276.0	18195.0	16898.0	10697.0	10453.0	9732.9
4	63.50	16144.0	16105.0	15106.0	21193.0	21300.0	20041.0	11570.0	11388.0	10650.0
5	114.00	20268.0	20344.0	19188.0	27162.0	27447.0	26051.0	13572.0	13455.0	12614.0
6	158.00	23004.0	23221.0	22182.0	31094.0	31586.0	30386.0	15032.0	14981.0	14183.0
7	242.00	27845.0	28113.0	26872.0	37829.0	38372.0	36918.0	17614.0	17606.0	16658.0
8	325.00	31451.0	31882.0	30827.0	42843.0	43589.0	42427.0	19661.0	19727.0	18856.0
9	438.00	36405.0	36832.0	35516.0	49574.0	50267.0	48827.0	22508.0	22578.0	21550.0
10	543.00	39353.0	39900.0	38789.0	53594.0	54427.0	53311.0	24250.0	24400.0	23453.0
11	842.00	48308.0	48943.0	47666.0	62827.0	57005.0	65216.0	29603.0	29842.0	28714.0
12	1140.00	55146.0	55862.0	54835.0	63193.0	57041.0	65239.0	33832.0	34206.0	33092.0
Halon	1270.00	56791.0	56229.0	57883.0	63193.0	57041.0	65239.0	35089.0	35366.0	34648.0

Table 7-VIII. CS3 tone reproduction measured luminance of each of 12 OECF target patches and Halon and the mean digital counts of each of the 12 patches and the Halon of three exposure levels used to capture each image.

Patch #	<u>Relative Luminance (cd/m<sup>2</sup>) CIE 2° observer</u>	Nominal Exposure			Overexposed			Underexposed		
		<u>Mean DC<sub>R</sub></u>	<u>Mean DC<sub>G</sub></u>	<u>Mean DC<sub>B</sub></u>	<u>Mean DC<sub>R</sub></u>	<u>Mean DC<sub>G</sub></u>	<u>Mean DC<sub>B</sub></u>	<u>Mean DC<sub>R</sub></u>	<u>Mean DC<sub>G</sub></u>	<u>Mean DC<sub>B</sub></u>
		1	2	3	4	5	6	7	8	9
1	1.18	4194.2	3692.3	3411.8	8528.0	7876.3	6876.1	2213.1	1850.7	1764.3
2	1.77	5619.2	5357.3	5057.1	11605.0	11404.0	10382.0	2713.5	2440.8	2353.8
3	3.67	7974.9	7954.9	7719.6	16906.0	17223.0	16192.0	3693.3	3518.7	3473.2
4	5.33	9831.3	9900.3	9709.5	20902.0	21400.0	20347.0	4419.7	4333.5	4248.8
5	8.75	13596.0	13726.0	13579.0	28835.0	29621.0	28395.0	5948.6	5958.7	5869.2
6	12.31	16428.0	16539.0	16493.0	34554.0	35402.0	34198.0	7104.2	7140.0	7072.7
7	18.54	20338.0	20463.0	20434.0	43009.0	44036.0	42599.0	8806.3	8876.6	8812.6
8	24.81	23864.0	23948.0	23992.0	50366.0	51547.0	50014.0	10352.0	10426.0	10385.0
9	32.93	28591.0	28655.0	28798.0	60300.0	59746.0	59942.0	12397.0	12456.0	12442.0
10	39.57	31442.0	31469.0	31674.0	65051.0	59844.0	61340.0	13695.0	13741.0	13750.0
11	61.06	40688.0	40702.0	41080.0	65134.0	59846.0	61354.0	17718.0	17764.0	17821.0
12	82.58	47940.0	48010.0	48429.0	65134.0	59846.0	61354.0	20939.0	20996.0	21087.0
Halon	100.00	52500.0	52128.0	52764.0	65134.0	59846.0	61354.0	22943.0	22793.0	22976.0

Table 7-IX. CS4 tone reproduction measured luminance of each of 12 OECF target patches and Halon and the mean digital counts of each of the 12 patches and the Halon of three exposure levels used to capture each image.

Patch #	<u>Measured Luminance (cd/m<sup>2</sup>) CIE 2° observer</u>	Nominal Exposure			Overexposed			Underexposed		
		<u>Mean DC<sub>R</sub></u>	<u>Mean DC<sub>G</sub></u>	<u>Mean DC<sub>B</sub></u>	<u>Mean DC<sub>R</sub></u>	<u>Mean DC<sub>G</sub></u>	<u>Mean DC<sub>B</sub></u>	<u>Mean DC<sub>R</sub></u>	<u>Mean DC<sub>G</sub></u>	<u>Mean DC<sub>B</sub></u>
		1	2	3	4	5	6	7	8	9
1	12.00	19.4	14.7	11.3	39.1	31.5	26.3	6.5	3.5	2.4
2	13.30	28.7	25.7	22.4	54.9	49.5	43.7	12.0	9.5	7.5
3	19.80	50.3	49.8	46.2	94.0	92.7	86.8	24.9	23.8	22.0
4	26.90	72.2	72.8	68.7	119.8	120.4	116.0	36.0	35.5	33.6
5	45.70	108.3	110.1	107.0	152.9	154.5	151.9	58.0	59.1	56.8
6	62.30	133.3	134.7	132.5	176.0	177.5	175.4	80.7	82.1	79.9
7	92.70	158.8	160.3	158.6	200.7	202.0	200.5	109.3	110.7	109.1
8	122.00	181.3	182.4	180.7	220.0	221.0	219.9	133.0	134.1	132.9
9	162.00	198.9	200.0	199.0	234.3	235.1	234.4	151.8	152.9	152.0
10	198.00	212.1	212.8	211.9	241.6	242.1	241.7	165.6	166.7	165.9
11	311.00	234.3	234.9	234.6	251.8	252.0	251.9	194.5	195.6	195.2
12	397.00	245.0	245.5	245.2	255.0	255.0	255.0	214.1	215.1	214.8
Halon	552.00	249.3	249.7	250.0	255.0	255.0	255.0	225.1	226.0	227.3

### Appendix 7.3: Spatial Cross-talk Supplemental Data

Figure 7-1 shows the target, also shown in Figure 38, imaged in the testing procedure to evaluate spatial cross-talk. The 15 equally spaced gray squares in the target oriented at 0° are labeled with the same number in Figure 7-1a as the corresponding gray patch in Figure 7-1b (target is oriented at 180°), which it was compared to (see section 3.7 for the description of this comparison in the testing procedure).

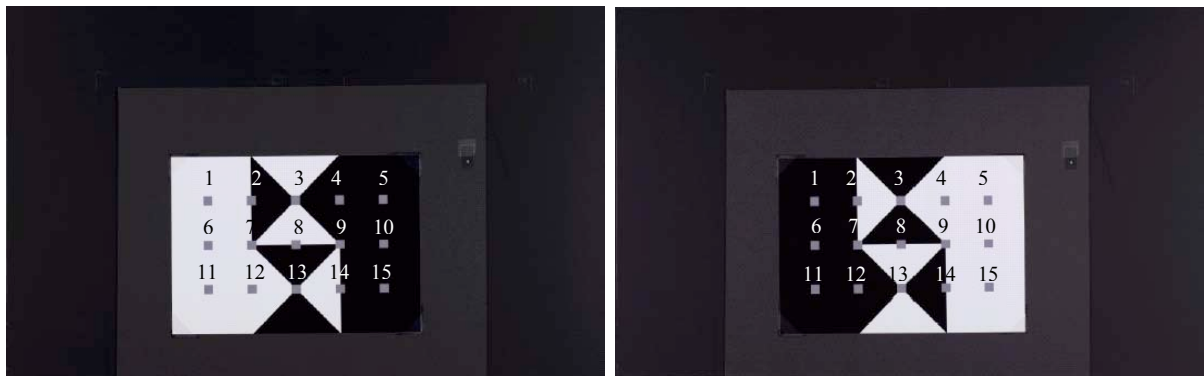


Figure 7-1 a, b. Spatial Cross-talk target oriented at 0° (left) and Spatial Cross-talk target oriented at 180° (right).

Tables 7-X through 7-XIV include supplemental data for the analysis of the CS0 through CS4 spatial cross-talk, respectively. The data listed in these tables are the linearized (inverse OECF applied) normalized (DC / maxDC) mean RGB image data of the 15 gray patches of each of the two images (oriented at 0° and 180°). The procedure that was used to analyze these data for all of the case studies is described in section 3.7.

Table 7-X. CS0 spatial cross-talk linearized normalized mean digital counts of 15 gray patches obtained from images of target oriented at 0° and 180°.

Patch #	Mean DC at 0°			Mean DC at 180°		
	R	G	B	R	G	B
1	0.1605	0.1664	0.1963	0.1542	0.1597	0.1839
2	0.1553	0.1624	0.1873	0.1570	0.1645	0.1878
3	0.1546	0.1632	0.1859	0.1571	0.1654	0.1886
4	0.1502	0.1594	0.1815	0.1568	0.1667	0.1912
5	0.1485	0.1584	0.1801	0.1528	0.1629	0.1892
6	0.1649	0.1692	0.2006	0.1583	0.1624	0.1875
7	0.1608	0.1670	0.1923	0.1583	0.1641	0.1877
8	0.1590	0.1653	0.1890	0.1591	0.1655	0.1892
9	0.1550	0.1625	0.1848	0.1581	0.1659	0.1904
10	0.1505	0.1584	0.1805	0.1580	0.1661	0.1934
11	0.1654	0.1686	0.1987	0.1590	0.1624	0.1873
12	0.1637	0.1693	0.1961	0.1562	0.1607	0.1850
13	0.1607	0.1664	0.1908	0.1577	0.1635	0.1878
14	0.1573	0.1639	0.1875	0.1558	0.1621	0.1885
15	0.1519	0.1588	0.1823	0.1569	0.1636	0.1923

Table 7-XI. CS1 spatial cross-talk linearized normalized mean digital counts of 15 gray patches obtained from images of target oriented at 0° and 180°.

Patch #	Mean DC at 0°			Mean DC at 180°		
	R	G	B	R	G	B
1	0.1924	0.1920	0.3176	0.1936	0.1930	0.3081
2	0.1917	0.1925	0.3087	0.1981	0.1984	0.3153
3	0.1943	0.1963	0.3106	0.2017	0.2024	0.3253
4	0.1923	0.1923	0.3070	0.2009	0.2000	0.3298
5	0.1924	0.1926	0.3055	0.2001	0.1983	0.3306
6	0.1910	0.1906	0.3148	0.1927	0.1917	0.3042
7	0.1922	0.1937	0.3086	0.1952	0.1952	0.3083
8	0.1950	0.1969	0.3110	0.1998	0.2003	0.3195
9	0.1919	0.1921	0.3056	0.1990	0.1979	0.3234
10	0.1921	0.1921	0.3031	0.2004	0.1987	0.3312
11	0.1870	0.1861	0.3055	0.1891	0.1879	0.2985
12	0.1913	0.1922	0.3066	0.1917	0.1910	0.3015
13	0.1941	0.1958	0.3081	0.1953	0.1958	0.3098
14	0.1916	0.1913	0.3038	0.1948	0.1929	0.3136
15	0.1893	0.1891	0.2983	0.1980	0.1958	0.3248

Table 7-XII. CS2 spatial cross-talk linearized normalized mean digital counts of 15 gray patches obtained from images of target oriented at 0° and 180°.

Patch #	Mean DC at 0°			Mean DC at 180°		
	R	G	B	R	G	B
1	0.2356	0.3593	0.3339	0.2235	0.3412	0.3077
2	0.2314	0.3529	0.3239	0.2341	0.3561	0.3224
3	0.2345	0.3565	0.3220	0.2389	0.3619	0.3263
4	0.2298	0.3497	0.3137	0.2428	0.3687	0.3337
5	0.2279	0.3479	0.3085	0.2392	0.3637	0.3324
6	0.2349	0.3593	0.3319	0.2229	0.3408	0.3047
7	0.2337	0.3578	0.3260	0.2280	0.3487	0.3139
8	0.2354	0.3580	0.3225	0.2351	0.3571	0.3218
9	0.2303	0.3514	0.3137	0.2365	0.3612	0.3268
10	0.2268	0.3461	0.3062	0.2380	0.3638	0.3332
11	0.2286	0.3498	0.3234	0.2171	0.3331	0.2990
12	0.2323	0.3562	0.3251	0.2209	0.3372	0.3044
13	0.2316	0.3529	0.3172	0.2279	0.3478	0.3131
14	0.2300	0.3504	0.3123	0.2289	0.3488	0.3162
15	0.2225	0.3399	0.3002	0.2343	0.3582	0.3266

Table 7-XIII. CS3 spatial cross-talk linearized normalized mean digital counts of 15 gray patches obtained from images of target oriented at 0° and 180°.

Patch #	Mean DC at 0°			Mean DC at 180°		
	R	G	B	R	G	B
1	0.1598	0.1705	0.2026	0.1585	0.1688	0.2008
2	0.1578	0.1687	0.1988	0.1628	0.1734	0.2050
3	0.1605	0.1714	0.1998	0.1666	0.1770	0.2101
4	0.1595	0.1706	0.1989	0.1677	0.1791	0.2135
5	0.1583	0.1699	0.1971	0.1655	0.1764	0.2129
6	0.1603	0.1712	0.2025	0.1596	0.1698	0.2007
7	0.1595	0.1708	0.1998	0.1611	0.1715	0.2035
8	0.1621	0.1726	0.2004	0.1658	0.1757	0.2085
9	0.1609	0.1726	0.1992	0.1663	0.1779	0.2113
10	0.1573	0.1679	0.1946	0.1656	0.1763	0.2134
11	0.1603	0.1707	0.2026	0.1600	0.1704	0.2023
12	0.1582	0.1690	0.1989	0.1572	0.1668	0.2001
13	0.1634	0.1738	0.2024	0.1634	0.1739	0.2074
14	0.1663	0.1777	0.2055	0.1668	0.1775	0.2141
15	0.1575	0.1683	0.1960	0.1652	0.1752	0.2131

Table 7-XIV. CS4 spatial cross-talk linearized normalized mean digital counts of 15 gray patches obtained from images of target oriented at 0° and 180°.

Patch #	<u>Mean DC at 0°</u>			<u>Mean DC at 180°</u>		
	<u>R</u>	<u>G</u>	<u>B</u>	<u>R</u>	<u>G</u>	<u>B</u>
1	0.2806	0.2787	0.3583	0.2721	0.2719	0.3390
2	0.2793	0.2784	0.3542	0.2836	0.2811	0.3508
3	0.2808	0.2795	0.3515	0.2857	0.2821	0.3540
4	0.2732	0.2734	0.3439	0.2811	0.2799	0.3541
5	0.2642	0.2646	0.3327	0.2705	0.2707	0.3475
6	0.2783	0.2777	0.3564	0.2723	0.2710	0.3364
7	0.2807	0.2799	0.3532	0.2779	0.2776	0.3456
8	0.2828	0.2797	0.3509	0.2857	0.2821	0.3536
9	0.2738	0.2742	0.3426	0.2781	0.2783	0.3507
10	0.2652	0.2643	0.3305	0.2700	0.2710	0.3473
11	0.2742	0.2736	0.3502	0.2667	0.2671	0.3335
12	0.2834	0.2815	0.3565	0.2741	0.2741	0.3434
13	0.2855	0.2816	0.3543	0.2780	0.2769	0.3474
14	0.2767	0.2757	0.3445	0.2715	0.2724	0.3456
15	0.2633	0.2629	0.3308	0.2696	0.2705	0.3473

#### **Appendix 7.4: Depth of Field Supplemental Data**

Tables 7-XV through 7-XIX include supplemental data for the analysis of the CS0 through CS4 depth of field, respectively. These data are the areas under the SFR curve from frequencies of 0.0 to 0.5 cy/pixel of the SFR curves for each distance on the depth of field target, which are plotted in the figure that goes along with each table (Figures 7-2 through 7-6, respectively). The SFR data used to describe the depth of field at each distance were either obtained, in each case study, from the horizontal or vertical edges, whichever had the best SFR results from the SFR analysis.

The procedure that was used to determine these data for all of the case studies is described in section 3.10. A plot of the SFR area data shown in Tables 7-XV through 7-XIX versus their corresponding distance on the depth of field target was used to summarize these data in the Results and Discussion section of each case study (see Figures 62, 79, 95, and 111 in the Depth of Field part of sections 4.3.3, 4.4.3, 4.5.3, and 4.6.3, respectively). For CS0, this plot is shown in Figure 44 in section 3.10. The mean of the mean areas under the SFR curves of the RGB channels across the 13 distances, included in the tables below, which were normalized by the maximum SFR area in each table below, is a mono-numeric metric that summarizes each case study's depth of field, which was used in Table LXVIII in Section 4.7.2 for CS1 through CS4 to compare the depth of field across the four museum case studies.

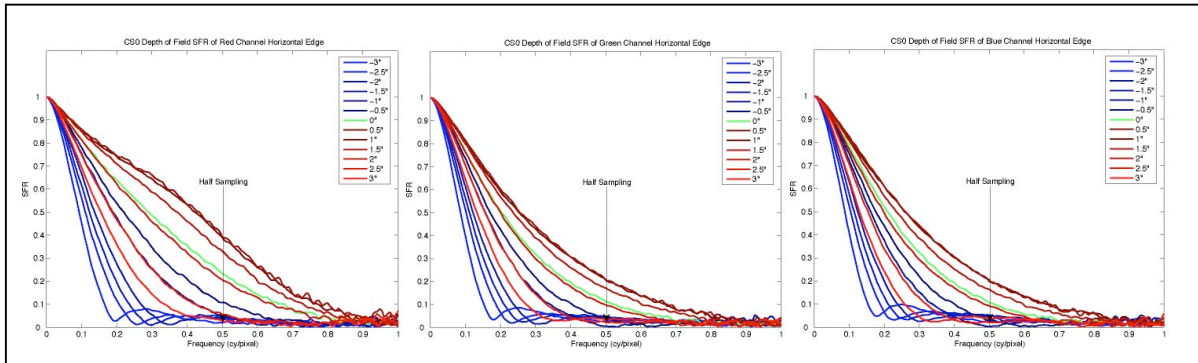


Figure 7-2. CS0 depth of field SFR of horizontal edges of depth of field target image for red, green and blue channels (from left to right).

Table 7-XV. CS0 depth of field areas under the SFR curves (from 0.0 to 0.5 cy/pixel) shown in Figure 7-2 for each distance on the depth of field target for the red, green and blue channels.

<b>Distance From Center 3" Square (in.)</b>	<b>Area Under SFR Curve From Frequencies of 0.0 to 0.5cy/pixel</b>			
	<b>Red Channel</b>	<b>Green Channel</b>	<b>Blue Channel</b>	<b>Mean of RGB Channels</b>
-3	0.225	0.215	0.222	0.221
-2.5	0.256	0.241	0.249	0.249
-2.0	0.282	0.262	0.270	0.271
-1.5	0.309	0.280	0.288	0.292
-1.0	0.428	0.356	0.360	0.381
-0.5	0.486	0.400	0.405	0.430
0	0.583	0.470	0.476	0.509
0.5	0.694	0.548	0.554	0.598
1.0	0.703	0.556	0.558	0.606
1.5	0.656	0.522	0.520	0.566
2.0	0.566	0.459	0.456	0.493
2.5	0.424	0.354	0.344	0.374
3.0	0.355	0.306	0.297	0.319
			<b>Mean</b>	<b>0.409</b>

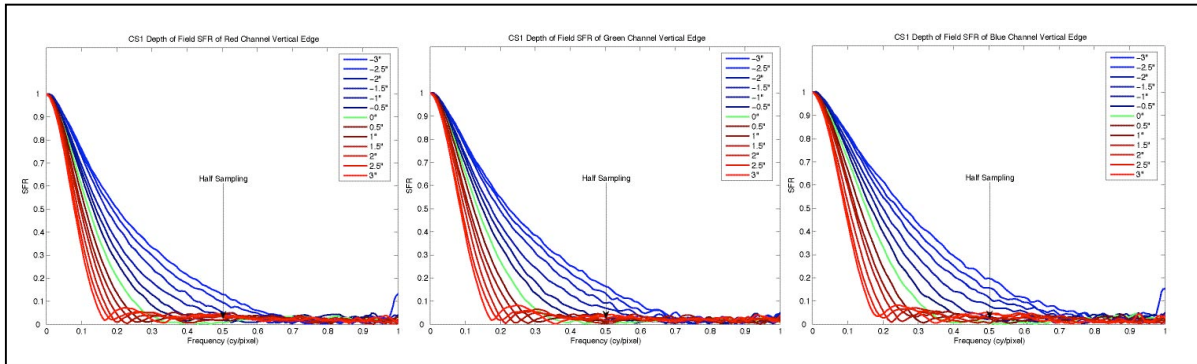


Figure 7-3. CS1 depth of field SFR of vertical edges of depth of field target image for red, green and blue channels (from left to right).

Table 7-XVI. CS1 depth of field areas under the SFR curves (from 0.0 to 0.5 cy/pixel) shown in Figure 7-3 for each distance on the depth of field target for the red, green and blue channels.

<u>Distance From Center 3" Square (in.)</u>	<u>Area Under SFR Curve From Frequencies of 0.0 to 0.5cy/pixel</u>			
	<u>Red Channel</u>	<u>Green Channel</u>	<u>Blue Channel</u>	<u>Mean of RGB Channels</u>
-3	0.478	0.513	0.553	0.515
-2.5	0.450	0.492	0.525	0.489
-2.0	0.414	0.463	0.497	0.458
-1.5	0.371	0.416	0.453	0.413
-1.0	0.333	0.379	0.409	0.373
-0.5	0.308	0.344	0.373	0.342
0	0.272	0.304	0.332	0.303
0.5	0.252	0.278	0.299	0.277
1.0	0.242	0.259	0.281	0.261
1.5	0.220	0.241	0.259	0.240
2.0	0.211	0.228	0.239	0.226
2.5	0.202	0.213	0.225	0.213
3.0	0.194	0.206	0.219	0.206
			<b>Mean</b>	0.332

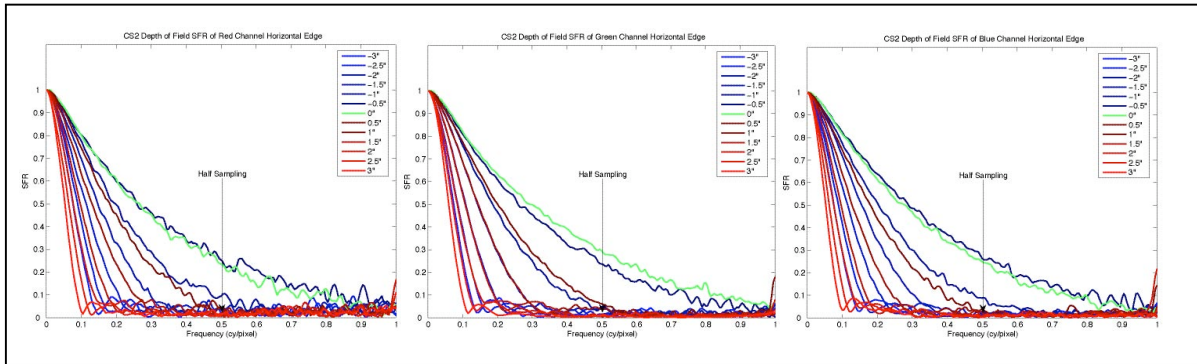


Figure 7-4. CS2 depth of field SFR of horizontal edges of depth of field target image for red, green and blue channels (from left to right).

Table 7-XVII. CS2 depth of field areas under the SFR curves (from 0.0 to 0.5 cy/pixel) shown in Figure 7-4 for each distance on the depth of field target for the red, green and blue channels.

<u><b>Distance From Center 3" Square (in.)</b></u>	<u><b>Area Under SFR Curve From Frequencies of 0.0 to 0.5cy/pixel</b></u>			
	<u><b>Red Channel</b></u>	<u><b>Green Channel</b></u>	<u><b>Blue Channel</b></u>	<u><b>Mean of RGB Channels</b></u>
-3	0.181	0.173	0.181	0.179
-2.5	0.206	0.194	0.202	0.201
-2.0	0.258	0.244	0.260	0.254
-1.5	0.334	0.316	0.341	0.330
-1.0	0.450	0.420	0.459	0.443
-0.5	0.572	0.568	0.594	0.578
0	0.561	0.599	0.575	0.578
0.5	0.410	0.451	0.408	0.423
1.0	0.299	0.321	0.289	0.303
1.5	0.226	0.244	0.219	0.230
2.0	0.185	0.198	0.178	0.187
2.5	0.150	0.166	0.151	0.156
3.0	0.131	0.138	0.131	0.133
			<b>Mean</b>	<b>0.307</b>

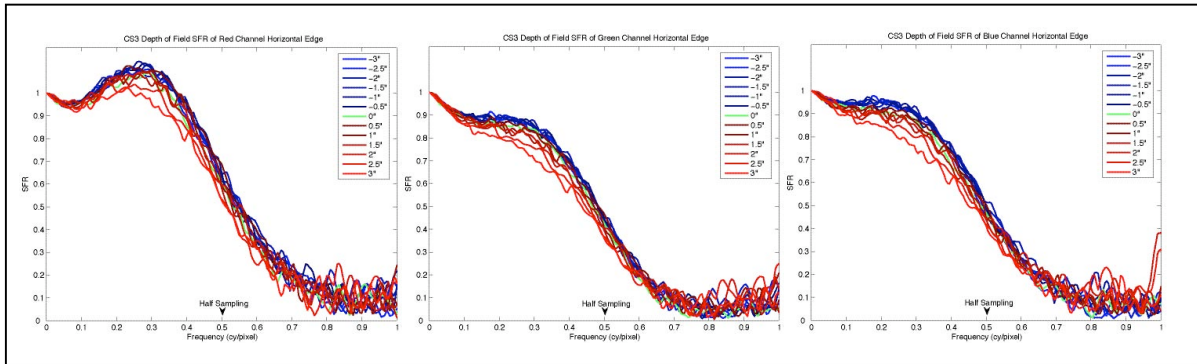


Figure 7-5. CS3 depth of field SFR of horizontal edges of depth of field target image for red, green and blue channels (from left to right).

Table 7-XVIII. CS3 depth of field areas under the SFR curves (from 0.0 to 0.5 cy/pixel) shown in Figure 7-5 for each distance on the depth of field target for the red, green and blue channels.

<u><b>Distance From Center 3" Square (in.)</b></u>	<u><b>Area Under SFR Curve From Frequencies of 0.0 to 0.5cy/pixel</b></u>			
	<u><b>Red Channel</b></u>	<u><b>Green Channel</b></u>	<u><b>Blue Channel</b></u>	<u><b>Mean of RGB Channels</b></u>
-3	0.972	0.810	0.854	0.879
-2.5	0.977	0.810	0.852	0.880
-2.0	0.973	0.813	0.859	0.882
-1.5	0.985	0.819	0.866	0.890
-1.0	0.988	0.812	0.858	0.886
-0.5	0.985	0.813	0.854	0.884
0	0.948	0.789	0.825	0.854
0.5	0.984	0.801	0.839	0.875
1.0	0.964	0.787	0.827	0.859
1.5	0.946	0.774	0.810	0.843
2.0	0.956	0.772	0.812	0.847
2.5	0.922	0.750	0.792	0.821
3.0	0.896	0.727	0.761	0.795
			<b>Mean</b>	<b>0.861</b>

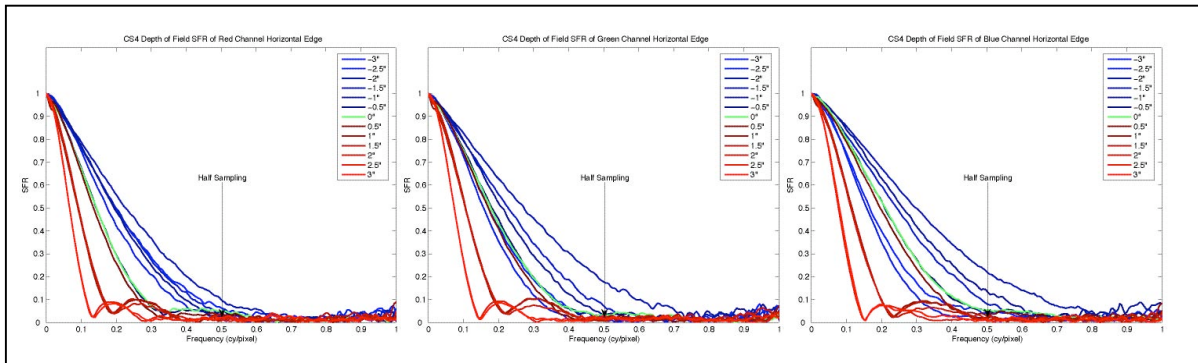


Figure 7-6. CS4 depth of field SFR of horizontal edges of depth of field target image for red, green and blue channels (from left to right).

Table 7-XIX. CS4 depth of field areas under the SFR curves (from 0.0 to 0.5 cy/pixel) shown in Figure 7-6 for each distance on the depth of field target for the red, green and blue channels.

<u><b>Distance From Center 3" Square (in.)</b></u>	<u><b>Area Under SFR Curve From Frequencies of 0.0 to 0.5cy/pixel</b></u>			
	<u><b>Red Channel</b></u>	<u><b>Green Channel</b></u>	<u><b>Blue Channel</b></u>	<u><b>Mean of RGB Channels</b></u>
-3	0.443	0.383	0.382	0.403
-2.5	0.395	0.347	0.349	0.364
-2.0	0.435	0.483	0.509	0.476
-1.5	0.491	0.559	0.597	0.549
-1.0	0.424	0.453	0.545	0.474
-0.5	0.323	0.395	0.448	0.388
0	0.325	0.391	0.450	0.389
0.5	0.303	0.368	0.421	0.364
1.0	0.216	0.249	0.267	0.244
1.5	0.223	0.255	0.270	0.249
2.0	0.219	0.246	0.259	0.241
2.5	0.165	0.179	0.182	0.176
3.0	0.163	0.176	0.191	0.177
			<b>Mean</b>	0.346